Design and realization of a piezoelectric mobile for cooperative use

Hassan Hariri

UNIVERSITÉ PARIS SUD

Comprendre le monde, construire l'avenir®

UNIVERSITE PARIS-SUD

ÉCOLE DOCTORALE : "Sciences et Technologies de l'Information, des Télécommunications et des Systèmes" (STITS)
Laboratoire de Génie Electrique de Paris (LGEP)

***DISCIPLINE** Physique*

THÈSE DE DOCTORAT

Soutenue le 28/11/2012

Par

Hassan HARIRI

Conception et réalisation d'un mobile piézoélectrique pour utilisation coopérative

Directeur de thèse :	Adel RAZEK	Directeur de recherche (CNRS)
Co-encadrant :	Yves BERNARD	Professeur des Universités (université Paris 11)
<u>Composition du jury</u> :		
Président du jury :		
Rapporteurs :	Lionel PETIT	Professeur des Universités (INSA de Lyon)
	Dejan VASIC	Maitre de Conférence-HDR (ENS de Cachan)
Examinateurs :	Bruno DEHEZ	Professeur des Universités (Université Catholique de Louvain)
	Marc LETHIECQ	Professeur des Universités (Université de Tours)

REMERCIEMENTS

Les travaux présentés dans ce mémoire ont été réalisés au laboratoire de génie électrique de Paris (LGEP).

- Je veux remercier mes encadrants de thèse Adel RAZEK et Yves BERNARD d'avoir accepté ma candidature sur ce sujet de thèse. Je l'ai choisi pour construire mon profil de recherche dans ce domaine.
  Je remercie monsieur Yves BERNARD, mon co-encadrant de thèse, professeur à l'université paris 11, qui a consacré son temps pour encadrer ces travaux. Je le remercie pour sa patience et sa pédagogie d'encadrement. Je le remercie également pour sa gentillesse. J'ai beaucoup appris de sa méthodologie de travail et de sa créativité.
  Je remercie monsieur Adel RAZEK, mon directeur de thèse et directeur de recherche émérite au CNRS. J'ai beaucoup profité de ses années d'expériences et je les ai aussi senties lors des réunions, quand il me faisait des remarques ou qu'il me posait des questions. Je le remercie également pour sa disponibilité à m'aider à régler les problèmes administratifs qui concernent la recherche ainsi que ceux hors de la recherche.
- Je remercie mon ami Camilo HERNANDEZ, un maitre de conférences à l'université de Savoie, ancien doctorant au LGEP pour toutes les discussions et les partages d'idées ensembles.
- Je remercie Romain CORCOLLE, maître de conférences à l'université Paris 11 de m'avoir donné le code éléments finis qu'il a fait pendant son MASTER 2 au LGEP et pour toutes les discussions avec lui.
- Je remercie Laurent DANIEL, maître de conférences, HDR à l'université Paris 11 pour ses conseils et ses discussions utiles où j'ai profité de son expérience en mécanique des matériaux.
- Je tiens à remercier mon ami Mohamed BOUTCHICH maitre de conférences au LGEP pour toutes les discussions intéressantes qu'on a eu ensemble au niveau ses travaux de recherche et concernant la miniaturisation du prototype expérimental ainsi qu'au niveau humain.
- Je tiens à remercier Laurent SANTANDREA de m'avoir aidé à comprendre la méthode des éléments finis au début de ma thèse.
- Je remercie tous les membres du thème ''multiphysique'' au laboratoire pour les discussions utiles qu'on a eues pendant les réunions du thème.
- Je tiens à remercier Hussein HUSSEIN, stagiaire en MASTER 2 qui a travaillé dans la perspective de ma thèse sur la conception et la réalisation d'un minirobot piézoélectrique aquatique.

Je veux remercier mon laboratoire d'accueil le Laboratoire de Génie Electrique de Paris (LGEP). Je veux remercier tous les membres du laboratoire ainsi que tous les membres de l'IUT de Cachan où j'étais enseignant pendant la thèse.

- Je commence par remercier le directeur du laboratoire Frédéric BOUILLAULT qui donne de son temps pour la direction et la responsabilité du laboratoire.
- Je veux remercier vivement tous les enseignants à l'IUT de Cachan et en particulier au département GEII1. L'enseignement, c'est le métier que j'adore. Je veux vous remercier pour les moments qu'on a passé ensemble avec les étudiants. Ça m'a fait plaisir de donner avec vous aux étudiants.
  Je veux remercier les deux chefs de département GEII1de l'IUT de Cachan, professeur gilles RAYNAUD et professeur Francisco ALVES mon responsable pédagogique à l'IUT. Je veux remercier en particulier monsieur Philippe COSTE, madame Agnès PRIOU, monsieur Didier BOILEVIN et monsieur Nicolas GAC.
- Je remercie également, professeur Claude MARCHAND conseiller aux thèses et chef de département MOCOSEM (MOdélisation et COntrôle de Systèmes

ElectroMagnétiques) et le professeur Demba DIALLO chef de l'équipe COCODI (COnception, COmmande, DIagnostic) pour ses conseils utiles sur la vie au laboratoire. Je remercie également tous les membres de l'équipe COCODI pour les discussions à propos de ces travaux lors de réunions.

- Je remercie l'équipe administrative du laboratoire pour leur gentillesse et leur disponibilité : Brigitte VINCENT, Alexandra STABE, Christine SOULAT, Christine SAFAKHAH,Françoise RICHARD et Françoise JUBIN.
- Je remercie le personnel informatique au LGEP : Olivier HUBERT et Greg CHALVIGNAC pour leur disponibilité et leurs interventions sur les problèmes informatiques.
- Je remercie Eric BERTHELOT, ingénieur de recherche au LGEP pour toutes les discussions utiles qu'on eux ensemble concernant la partie électronique de mes expérimentations.
- Je remercie les techniciens de l'atelier électronique et mécanique pour leur disponibilité lors de mes demandes concernant la réalisation des prototypes expérimentaux: Michel POLICE, Richard ANDLAUER et Philippe SPRUYT.
- Je présente aussi mes remerciements à tous les membres du laboratoire, en particulier à mes collègues doctorants et post-doctorants qui m'ont donné leur confiance pour être leur représentant au conseil de laboratoire. J'espère avoir réussi ma mission.

Cher LGEP, je tiens à vous remercier tout particulièrement pour la chaleur de votre accueil, votre convivialité et votre professionnalisme.
J'ai passé auprès de vous, trois ans dans une ambiance de travail très agréable et enrichissante à tous niveaux.
J'espère un jour pouvoir de nouveau croiser votre route.
Avec encore tous mes remerciements.

Durant ma thèse, j'ai discuté avec des chercheurs à l'international par échange d'emails. Je voudrais remercier :

- Qing-Ming WANG professeur à l'université de Pittsburgh, USA.
- Nima MAHMOODI maître de conférences à l'université d'Alabama, USA.
- Nader JALILI professeur à l'université de Northeastern, USA.
- Metin SITTI professeur à l'université de Carnegie Mellon, USA.
- Andrew FLEMING chercheur et maitre de conférences à l'université de Newcastle, Australia.
- Lothar GAUL professeur à l'université de Stuttgart, Germany.
- Kwon Joong SON maitre de conférences à l'AUD (American university in Dubai), UAE.
- Mohammad TAWFIK professeur à l'université de Cairo, Egypte.

Je voudrais remercier les membres du jury (extérieur au LGEP) :

- Monsieur Marc LETHIECQ professeur des universités à l'université de Tours pour l'honneur qu'il m'a fait en acceptant d'être le président du jury de cette thèse.
- Monsieur Lionel PETIT professeur des universités à L'INSA de Lyon d'avoir accepté d'être rapporteur de cette thèse.
- Monsieur Dejan VASIC maitre de conférences HDR à l'ENS de Cachan d'avoir accepté d'être rapporteur de cette thèse.
- Monsieur Bruno DEHEZ professeur des universités à l'université Catholique de Louvain d'avoir accepté d'être examinateur de cette thèse.

Je veux remercier les responsables de mes formations pendant la thèse : Marc LEGR, Stéphanie MARQUIS, Pierre BELLE, Sylvie SALAMITOU, Alain SARFATI, Bruno DUVAL, Michèle LE-CAM et Pascale THIEBAUT.

Je veux remercier aussi l'école doctorale STITS en particulier les secrétaires Dominique MARTIN et Laurence STEPHEN ainsi que la directrice de l'école doctorale Véronique VEQUE.

Je veux avant tous remercier mes amis au LGEP et à l'extérieur de m'avoir assisté à ma soutenance et de m'aider dans l'organisation de cette journée. La journée n'a pas été gérée sans vous. Je teins également à vous remercier pour le diner qu'on a passé ensemble le soir de la soutenance et pour le cadeau qui vous m'avez offert.

Je veux remercier mes parents grâce à qui j'ai pu venir en France pour faire mon MASTER 2 et grâce à leurs soutiens j'ai pu également continuer ma thèse de doctorat au laboratoire de génie électrique de Paris (LGEP).

Je veux remercier la France de m'avoir accepté afin de continuer mes études supérieures. Je veux remercier la France, le pays dans lequel j'ai obtenu mes deux plus hauts diplômes, le diplôme de MASTER 2 et le diplôme de doctorat. Le pays dans quel j'ai commencé à construire ma personnalité et à me poser la question de mon projet professionnel. Le pays dans lequel j'ai commencé à penser à mon avenir. Le pays dans lequel j'ai appris beaucoup des choses au niveau scientifique, au niveau humain, au niveau culturel et en terme d'organisation ainsi qu'au niveau politique et au niveau de la société en générale.
J'étais très content de découvrir la France à travers Paris, la ville dans laquelle j'ai vécu trois ans pendant mon doctorat.

A mon arrivée en France en septembre 2008 pour faire mon MASTER de Génie Electrique Génie des Procédés (GEGP) à Lyon, mon ami Ali MAKKEE m'a attendu à la station Part-Dieu, le terminus de la navette de l'aéroport et m'a hébergé jusqu'à ce que je trouve un logement. Merci Ali pour l'aide que tu m'as apportée pendant mon année de MASTER à Lyon. Je veux remercier également mes amis de Lyon Alaa HIJAZI et Wael HOURANI.

Le premier jour de mon arrivée à Paris au début de ma thèse, j'étais accueilli par mon ami Hassan CHOUIB. Je veux le remercier pour l'aide qu'il m'a apportée. Je veux remercier tous mes amis à Orsay-Ville, en particulier Bilal KANSO et Kassem MOGRABIE. Je tiens à remercier aussi tous les membres de notre équipe de football à Gif sur Yvette et mes amis de combat libre à Orsay-Ville. L'ambiance était parfaite grâce à vous.

Sujet de thèse : Conception et réalisation d'un mobile piézoélectrique pour utilisation coopérative

Résumé

L'objectif de cette thèse est de concevoir et de réaliser un mobile piézoélectrique pour utilisation coopérative. Le terme mobile piézoélectrique est utilisé dans cette thèse pour décrire un robot piézoélectrique miniature. Ce robot miniature mobile est actionné par des matériaux piézoélectriques. L'objectif de la thèse est donc la conception et la réalisation d'un robot pouvant être miniaturisé et qui pourrait donc être utilisé dans le cadre du mimétisme des essaims biologiques (fourmis, abeilles…) pour un fonctionnement coopératif.

Le robot réalisé est constitué d'un support mince et de patchs piézoélectriques. Les patchs piézoélectriques sont collés sur le support de façon intelligente afin de déplacer le support en milieu terrestre. Dans ce contexte, la thèse est divisée en trois parties.

La première partie est consacrée à la modélisation d'un tel système (support mince avec des patches piézoélectriques sur une seule de ses faces). Une modélisation par la méthode des éléments finis est développée pour ce système en se basant sur le principe variationnel d'Hamilton et en considérant l'hypothèse de Love-Kirchhoff. L'originalité de cette modélisation réside dans l'utilisation de la notion du plan neutre pour modéliser ce système asymétrique. Cela permet de ne modéliser le système étudié que par un modèle éléments finis à deux dimensions (2D) tout en tenant compte de la troisième dimension dans le calcul.

La deuxième partie présente le principe de fonctionnement du robot qui est inspiré des moteurs linéaire ultrasoniques à ondes progressive. Cette partie présente toutes les étapes de la conception optimale afin de créer les mouvements nécessaires. La conception optimale est étudiée en utilisant la modélisation par éléments finis obtenue dans la première partie.

La troisième partie de cette thèse est dédiée à la réalisation d'un prototype expérimental. Le processus de fabrication ainsi que l'électronique associée au robot sont présentés dans cette partie. Le robot est caractérisé expérimentalement en mesurant la vitesse en fonction de la tension appliquée, la vitesse en fonction de masses embarquées par le robot et la vitesse en fonction de la force fournie par le robot. Ce robot est, par ailleurs, comparé avec d'autres systèmes de même nature.

Mots clés : Robot piézoélectrique miniature, mimétisme des essaims biologiques (swarms), modélisation par la méthode des éléments finis, théorie des plaques minces asymétriques, moteurs linéaire ultrasoniques à ondes progressive.

Thesis subject: Design and realization of a piezoelectric mobile for cooperative use

Abstract

The objective of this thesis is to design and realize a piezoelectric mobile for cooperative use. The term piezoelectric mobile is used in this thesis to describe a piezoelectric miniature robot. This mobile miniature robot is actuated by piezoelectric materials. The aim of the thesis is the design and the realization of a robot that can be miniaturized and could therefore be used in the context of biological mimicry swarms (ants, bees ...) for a cooperative operation.

The realized robot consists of a thin support and piezoelectric patches. Piezoelectric patches are bonded on the support on an intelligent manner in order to move the support on land. In this context, the thesis is divided into three parts.

The first part is devoted to the modeling of such a system (thin support with piezoelectric patches on one of its faces). Modeling by the finite element method is developed for this system based on the variational principle of Hamilton and considering the Love-Kirchhoff hypothesis. The originality of this model lies in the use of the concept of the neutral plane to model this asymmetric system. This allows modeling the system studied by a finite element model in two dimensions (2D), taking into account the third dimension in the calculation.

The second part presents the operating principle of the robot which is inspired by the linear traveling wave ultrasonic motors. This section presents all the stages of the optimal design to create the necessary movements. The optimal design is investigated using finite element modeling obtained in the first part.

The third part of this thesis is devoted to the realization of an experimental prototype. The manufacturing process and the associated electronics for the robot are presented in this section. The robot is characterized experimentally by measuring the speed according to the applied voltage, the speed versus mass loaded by the robot and the speed according to the force provided by the robot. This robot is also compared with other similar systems.

Keywords: Piezoelectric miniature robot, mimicking biological swarms, modeling by the finite element method, the theory of thin plates asymmetric, linear traveling wave ultrasonic motors.

SUJET DE THESE

CONCEPTION ET REALISATION D'UN MOBILE PIEZOELECTRIQUE POUR UTILISATION COOPERATIVE

Une synthèse longue en français de la thèse

Conception et réalisation d'un mobile piézoélectrique pour utilisation coopérative

Une synthèse longue en français de la thèse

Sommaire

1. Introduction

Ma thèse est intitulée conception et réalisation d'un mobile piézoélectrique pour utilisation coopérative. Commençons par expliquer le terme ‘’mobile piézoélectrique’’, puis nous expliquerons pourquoi nous avons choisi d'en concevoir pour une utilisation coopérative.

Le terme ‘’mobile piézoélectrique’’ signifie robot piézoélectrique miniature. Ce sont des robots miniatures mobiles actionnés par des matériaux piézoélectriques.

Dans ce manuscrit, je présenterai la conception et la réalisation de petits robots conçus pour une utilisation coopérative future.

Ces robots sont constitués d'un support mince et de patchs piézoélectriques. Les patchs piézoélectriques sont collés sur le support de façon intelligente afin de permettre le déplacement du support avec plusieurs degrés de liberté.

L'idée du projet est de déplacer le support mince dans les trois milieux (terre, air et liquide), elle est inspirée du poisson raie Manta. Le milieu de vie de la raie Manta est l'eau mais ce poisson est capable de voler sur une courte période (figure ci-dessous). Si l'on applique le principe de locomotion de cette raie Manta aux robots, nous pouvons réaliser des robots capables de se déplacer dans trois milieux car le déplacement sur terre peut être réalisé en utilisant le principe de locomotion aquatique de la raie Manta (ceci est montré dans la thèse).

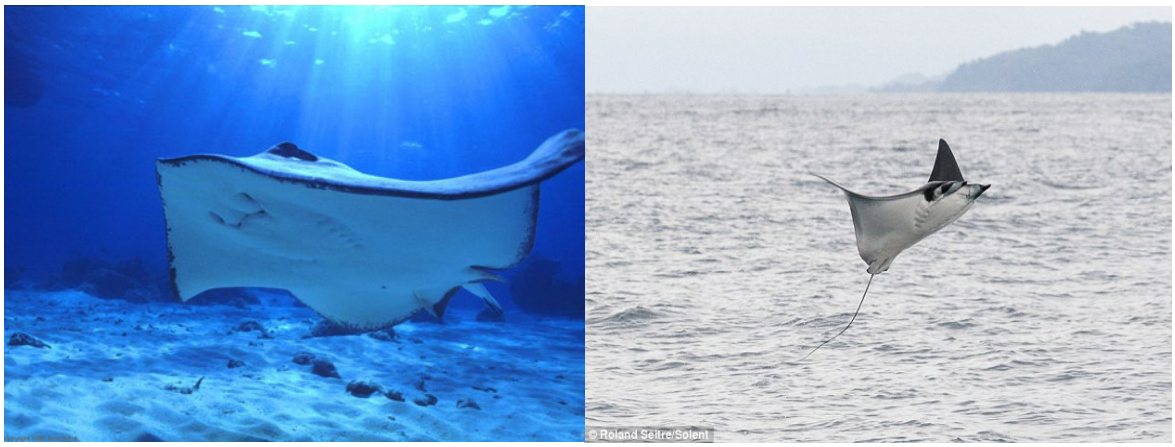

Manta ray fish inside and outside the water

[http://animals.desktopnexus.com/wallpaper/209676/, http://picinpic.blogspot.fr/2011/07/manta-ray-fish.html]

Ainsi, le projet consiste à concevoir et réaliser un robot miniature piézoélectrique capable de se déplacer dans les trois milieux (terre, air et liquide) pour une utilisation coopérative future.

Mon travail dans ce projet consiste à vérifier la faisabilité d'un déplacement mimant la Manta raie sur la terre en utilisant des matériaux piézoélectriques, de concevoir et de réaliser un prototype pour démontrer cette faisabilité sur la terre. Nous accompagnons ce travail d'une étude préliminaire et de perspectives pour le déplacement aquatique et aérien basé sur le prototype terrestre.

Mon travail a pour objectif de répondre aux questions suivantes:

Est-il possible en utilisant des matériaux piézoélectriques de déplacer un avatar de raie Manta (la forme de la raie Manta est considérée comme une plaque mince), avec plusieurs degrés de liberté sur la terre en générant une onde progressive dans la plaque mince?

Ce robot terrestre peut il être étendu pour provoquer des déplacements dans les milieux aquatique et aérien comme dans le cas de la raie Manta?

L'intérêt de ce projet est plus marqué quand les robots piézoélectriques sont petits et qu'ils peuvent se déplacer dans différents milieux (sol, air, liquide). Les robots que nous envisageons pourraient être miniaturisés.

Les essaims de robots sont aujourd'hui considérés comme une nouvelle solution pour surmonter les limites de la robotique traditionnelle. L'opération conjointe et coopérative de robots est inspirée de l'organisation collective des êtres vivants, qui émergent des formes d'intelligence et de contrôle de groupe au-delà de la capacité des organismes individuels impliqués (figure ci-dessous).

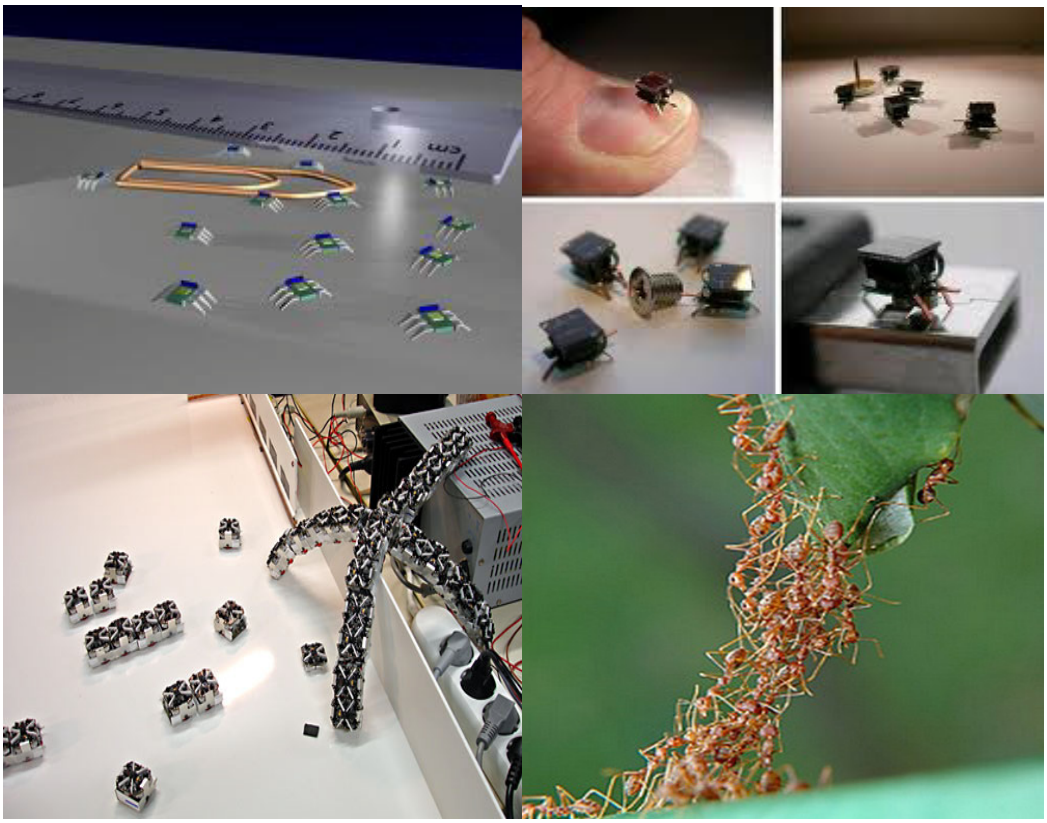

Swarms behavior

[

http://www.ipvs.uni-stuttgart.de/abteilungen/bv/forschung/projekte/I-Swarm/print_view,
http://www.hizook.com/blog/2009/08/29/i-swarm-micro-robots-realized-impressive-full-system-integration,
http://blog.autoworld.com.my/index.php/2009/02/26/swarm-technology-the-biggest-contribution-to-eco-tech/

]

Les robots essaims pourraient être utilisés dans de nombreuses applications, telles que stockage des cellules, la recherche des objets dans les zones étroites ou sur le comportement des essaims, la surveillance de la sécurité, les applications médicales, etc.

Selon un rapport publié récemment par l'IRAP, Inc, ''ET112: Piezoelectric Actuators and Motors–Types, Applications, New Developments, Industry Structure and Global Markets,'' le marché mondial des matériaux piézoélectrique exploités en actionneurs et en moteurs a été estimé à 6,6 milliards de dollars en 2009 et devrait atteindre 12,3 milliards de dollars en 2014, représentant un taux de croissance annuel moyen (TCAM) de 13,2% par an. Le tableau ci-dessous tiré de l'IRAP Inc, présente le marché mondial taille/pourcentage de la part des actionneurs piézoélectriques et des moteurs par application d'ici à 2014.

Applications	2009 ($ Mil.)	2009 (%)	2014 ($ Mil.)	2014 (%)	AAGR (%) 2009-14
Ultra-small scale motion related applications	3,200	48.6	6,000	48.9	13.4
Cameras, microscope lenses, mirrors and optics.	2,800	42.5	5,200	42.4	13.1
Others – e.g., auto fuel injectors, micro-pumps, micro-blowers, piezo ink cartridges, surgery instruments, mini-robots	587	8.9	1090	8.7	13.1
Total	**6,587**	**100**	**12,290**	**100**	**13.2**

Global share for piezoelectric actuators and motors by application, through 2014

L'investissement des Etats (USA, Japon, Europe, Corée et Chine) dans la R&D dans le domaine des robots essaim est énorme étant donné la quantité de publications annuelles. Les

mêmes idées de conception de robots sont mises en œuvre dans les pays qui tentent d'améliorer la maniabilité, le contrôle, la fonctionnalité, la vitesse et l'autonomie.

L'investissement américain est énorme dans ce domaine et en particulier dans le cas des robots essaims à base de matériaux piézoélectriques (mon domaine d'intérêt dans cette recherche) et c'est pourquoi beaucoup d'idées nouvelles viennent d'eux.

Je citerai ci-dessous quelques projets de recherche européens importants et récents dans le domaine des robots essaims (certains d'entre eux ont utilisé les matériaux piézoélectriques et d'autres non).

Le projet I-SWARM est un projet européen (Allemagne, Suède, Suisse, Autriche, Grèce, Royaume-Uni, Italie et Espagne). Il a eu lieu entre 2004 et 2008. Cela a été un grand succès et a donné une remarquable présence de l'Europe dans le domaine de minirobots essaims.

Le projet SYMBRION est un projet financé par la Commission européenne (Allemagne, Autriche, Pays-Bas, Belgique, Royaume-Uni et la France). Il a commencé à partir du développement et de la recherche précédente du projet I-SWARM et les projets open-source SWARMROBOT. La durée du projet est de 2008 à 2013. Une grande partie des développements au sein de SYMBRION est open-source et open-matériel aussi.

Le projet E-SWARM contribuera à l'élaboration d'une méthodologie d'ingénierie pour la construction de systèmes d'intelligence en artificielle essaim fondée sur des bases scientifiques rigoureuses. Le projet a démarré en 2010 pour une période de 5 ans. Son investigateur principal est le professeur Marco Dorigo (IRIDIA laboratoire de l'université libre de Bruxelles), l'un des fondateurs de l'intelligence en essaim et des champs de recherche essaim robotique.

En France, plusieurs projets sont parrainés par l'ANR, l'ONERA et le CNRS.

REMANTA projet (2002-2006) a été inspiré par la nature pour la conception des drones à ailes battantes, ANR / ELESA OVMI projet (2007-2011) met l'accent sur l'élaboration de lois de commande pour actionner les ailes d'un robot piézoélectrique biomimétique volant. Le projet d'action PEA (2007-2014) a pour objectif de démontrer scientifiquement la coopération de plusieurs véhicules autonomes fonctionnant dans des environnements différents, ANCRES un projet ANR (2012-2015) étudie également la coopération de plusieurs véhicules autonomes hétérogènes (air et terre) dans un contexte de gestion des crises, notamment dans le domaine du nucléaire ...

La recherche dans le domaine de la microrobotique essaims s'intéresse et se poursuit aujourd'hui avec un investissement de plus en plus d'états en raison des applications dans divers domaines et du faible coût de fabrication. Il est remarquable en Angleterre cette année,

que la recherche pour développer des machines intelligentes a reçu un coup de pouce de 16 millions de livres par un partenariat entre le gouvernement et l'industrie dans des domaines tels que: la surveillance dans des environnements dangereux tels que les installations en eau profonde, les centrales nucléaires et les nursebots pour les hôpitaux et les avions.

Permettez-moi maintenant de vous présenter la constitution du manuscrit:

1. Comme nous l'avons vu plus haut, le robot piézoélectrique miniature conçu devrait être en mesure in fine de se déplacer dans trois mileix. Pour cela, nous avons commencé l'étude en consultant la littérature pour les robots piézoélectriques miniatures dans les trois milieux de déplacement (terre, liquide et air) afin d'éviter la répétition d'un travail antérieur inspiré du poisson raie Manta et actionné par des patchs piézoélectriques. Dans le premier chapitre de ce manuscrit, nous trouvons une classification des robots miniatures piézoélectriques selon les milieux de déplacement. En particulier, nous nous sommes intéressés aux principes de locomotion de ces robots, car le but de notre projet est d'utiliser un principe de locomotion afin de générer de déplacement (principe de locomotion de la raie Manta ou d'un mouvement ondulatoire).
2. Après avoir comparé les principes de locomotion des robots piézoélectriques miniatures existants avec celui que nous avons proposé, nous étudierons dans le prochain chapitre la modélisation de notre système qui est composé d'une structure fine avec des pastilles piézoélectriques collé sur la structure. Le deuxième chapitre comprend une introduction à la modélisation des structures minces avec des pastilles piézoélectriques.
3. Le troisième chapitre est consacré à la modélisation d'un tel système (patchs piézoélectriques collés sur des structures minces). À la fin de ce chapitre, nous pourrons en utilisant l'équation numérique obtenue, calculer les fréquences de résonance et déterminer les modes de résonance. Nous pouvons calculer les déplacements transversaux du système, les contraintes et les déformations obtenues en appliquant des forces sur le système ou en appliquant des tensions électriques sur certains patchs piézoélectriques. Nous pouvons également déterminer les tensions obtenues sur des patchs piézoélectriques déformés. Ainsi, nous pouvons calculer les valeurs des courants et les charges électriques des pastilles piézoélectriques.
4. Dans le chapitre 4, des dispositifs expérimentaux seront construits et testés pour valider les modèles obtenus à partir du chapitre 3.

5. Le chapitre 5 est intitulé ‘’traveling wave piezoelectric beam robot’’. Dans ce chapitre, nous présentons la conception et le principe de fonctionnement du robot piézoélectrique à onde progressive de type poutre. La conception optimale sera étudiée en utilisant l'équation numérique obtenue dans le chapitre 3.
6. Le processus de fabrication sera présenté dans le chapitre 6 et l’onde progressive sera démontrée expérimentalement par la caractérisation du robot (vitesse, masses embarquées, forces mécaniques, ...). A la fin, les avantages de ce robot par rapport aux autres existants seront présentés.
7. Le principe de fonctionnement d’un robot de type plaque, ses dimensions, sa conception, ses procédés de fabrication, les résultats théoriques et expérimentaux ont été déposés pour un brevet. Le chapitre 7 est intitulé ‘’overview’’ et dans ce chapitre, nous allons parler brièvement de certains points, parmi lesquels:

- Modélisation analytique du robot et comparaison à la modélisation par éléments finis.
- La structure du robot (cas d’une plaque) sera présentée sous forme d’un transformateur piézoélectrique.
- L’amortissement des vibrations des poutres et des plaques minces sera présenté brièvement avec quelques résultats théoriques et expérimentaux utilisant le modèle développé pour les applications robotiques.
- Une équation matricielle dans l’espace d'état sera construite à partir de l'équation des éléments finis. L'équation dans l'espace d'état est très utile en automatique. Dans notre cas, elle peut être utilisée pour contrôler la vibration de la poutre/plaque de manière à amortir les vibrations, ou pour générer une onde progressive sans utiliser de circuits passifs.
- A la fin, on donne un exemple de la façon dont nous pouvons utiliser notre modèle dans la théorie du traitement du signal afin de détecter des dommages dans des structures comme poutre / plaque minces.

Enfin, une conclusion générale et des perspectives sont données. Dans les perspectives nous allons parler d’un futur modèle pour la poutre-plaque robot piézoélectrique en milieu aquatique. Quelques idées sont proposées pour le milieu aérien, ainsi que pour la miniaturisation.

2. Chapitre 1

Le chapitre 1 concerne les principes de locomotion des robots piézoélectriques miniatures. Nous commençons par définir ce que signifie robot piézoélectrique miniature, puis, nous abordons les matériaux piézoélectriques et les actionneurs piézoélectriques. Enfin nous étudions les principes de locomotion des robots piézoélectriques miniatures qui sont classés en fonction de leurs déplacements dans un milieu fluidique (liquide et air) ou sur un support solide. Des robots piézoélectriques miniatures sont pris comme exemples.

La recherche faite dans le premier chapitre ne tient pas compte de tous les principes de locomotion des robots. Elle était seulement dédiée aux principes de locomotion des robots piézoélectriques miniatures existants.

Après la lecture de cette recherche portant en particulier sur la locomotion sur un substrat solide, on va remarquer que la forme de la plaque que nous avons proposée utilise la locomotion ‘’resonant drive’’. En principe de locomotion ‘’resonant drive’’, les actionneurs piézoélectriques sont utilisés à leurs fréquences de résonance pour produire une déformation maximale. Ce mouvement est défini par la génération de glissement avec une variation de la force de contact [(Driesen, 2008)]. Le mouvement se produit lorsque la force d'inertie devient supérieure à la force de frottement maximale. Ce principe est fréquemment utilisé dans les moteurs ultrasonores à ondes progressives et stationnaires. Comme nous volons à générer une onde progressive dans la plaque (raie Manta forme), notre modèle sera inspiré des moteurs ultrasonores à onde progressive.

La recherche bibliographique montre que le poisson raie Manta utilise les nageoires médiane et/ou couplées (**M**edian and/or **P**aired **F**in : **MBF**) pour la propulsion. Plus précisément, il utilise le mode Rajiform pour générer la poussée nécessaire pour se déplacer. En dehors de l'eau, le poisson raie Manta utilise les ailes battantes (battement des nageoires pectorales qui sont flexibles et longues) pour produire la poussée nécessaire pour voler à l’extérieur de l'eau.

La plupart des poissons robots piézoélectriques miniatures dans la littérature utilisent la nageoire caudale (**B**ody and/or **C**audal **F**in : **BCF**) pour générer des mouvements de propulsion car cela est plus facile à concevoir, fabriquer et contrôler. La conception et le contrôle de la propulsion **MPF** pour créer l'ondulation nécessaire à la propulsion sont plus compliqués.

La réponse à la question : ‘’Pouvons-nous proposer à la fin de cette thèse une conception créant la propulsion ondulatoire de notre robot piézoélectrique miniature terrestre (comme le raie Manta)?’’ est dans les perspectives de ce manuscrit.

3. Chapitre 2

Notre robot sera inspiré des moteurs ultrasonores à onde progressive. Ces moteurs sont connus par la théorie des poutres en flexion, c'est pourquoi nous avons divisé l'étude en théorie des poutres en flexion et théorie des plaques en flexion. Dans le manuscrit, l'onde est générée sur une poutre premièrement, puis dans une plaque.

Le chapitre 2, présente brièvement l'élasticité linéaire, les équations de la mécanique et de la piézoélectricité sous forme matricielle 3D complète où toutes les contraintes et les déformations sont représentées pour des matériaux isotropes sous l'hypothèse d'élasticité linéaire. Dans certains cas particuliers, les équations mécaniques et piézoélectriques peuvent être écrites en 2D (cas d'une plaque mince) ou 1D (cas d'une poutre mince). Ces cas pratiques sont présentés dans le chapitre 3. On a présenté brièvement la théorie d'Euler-Bernoulli et de Love-Kirchhoff dans le cas de la théorie des poutres et des plaques respectivement.

Nous avons discuté dans le chapitre 2, le champ de déplacement dans le cas des vibrations de flexion des poutres et des plaques. Le champ de déplacement a été, sans prendre en considération les pastilles piézoélectriques. Le champ de déplacement avec des pastilles piézoélectriques collées sur la poutre et la plaque est traité dans le chapitre 3.

Les équations numériques statiques et dynamiques dans le cas général d'un système contenant des matériaux élastiques et piézoélectriques sont présentées. Ces équations sont dérivées du principe variationnel, qui est détaillé. La discrétisation temporelle en utilisant la méthode de Newmark est aussi brièvement présentée à la fin.

4. Chapitre 3

Les structures minces contenant des matériaux piézoélectriques sont largement utilisées pour contrôler les vibrations [(Hariri, et al., 2011), (Yasin, et al., 2010)], pour détecter des dommages dans la structure [(Qu, et al., 2006), (Yan, et al., 2002)], pour réaliser des micropompes [(Hernandez, et al., 2010)], des vannes [(Bernard, et al., 2011)] et des robots miniatures [(Hariri, et al., 2010)]. Deux grosses branches sont étudiées dans la littérature pour des structures minces contenant des matériaux piézoélectriques en fonction de leur domaine d'application : des structures de types poutre et des structures de types plaque. Ces systèmes peuvent être symétriques ou asymétriques si les matériaux piézoélectriques sont placés sur une ou les deux faces.

Dans un système symétrique les matériaux piézoélectriques sont collés face à face de part et d'autre de la poutre/plaque (colocalisés) alors que dans un système asymétrique les matériaux piézoélectriques sont collés seulement sur une face (non-colocalisés). Il convient de noter qu'il existe un autre type de structure renfermant des matériaux piézoélectriques où les matériaux piézoélectriques sont intégrés dans la poutre/plaque, ce type de structure n'est pas abordé dans notre étude.

Pour des structures symétriques ou asymétriques de type poutre avec respectivement des patchs piézoélectriques colocalisés ou non-colocalisés, un modèle 1D analytique ou numérique peut être utilisé pour modéliser un tel système. Dans le premier cas l'axe neutre est pris comme axe de symétrie du système tandis que, dans le cas des systèmes asymétriques, il est nécessaire de déterminer l'axe neutre.

Dans le cas des structures de type plaque, une méthode par éléments finis 2D ou 3D peut être utilisée pour modéliser le système. Dans l'approche 3D, des éléments de volume sont utilisés tandis que dans l'approche 2D des éléments de surface sont utilisés. La 3ème dimension est introduite dans les équations du modèle. Il est évident que la seconde approche est plus rapide, mais un peu plus compliquée dans la formulation du modèle.

Dans la littérature plusieurs articles sont consacrés à la modélisation des structures fines avec des pastilles piézoélectriques en utilisant l'approche 2D dans le cas où la symétrie du système est maintenue par la disposition de patchs. L'approche 2D est plus difficile pour une structure asymétrique, où des patchs piézoélectriques ne sont pas, en raison du fait que le plan neutre de la structure n'est pas confondu avec le plan médian.

Le but du chapitre 3 est de développer une méthode éléments finis 2D (et 1D respectivement) pour modéliser un système asymétrique où les patchs piézoélectriques non-colocalisées sont collés sur une plaque mince (et une poutre mince respectivement), en utilisant la notion de plan neutre (et axe neutre, respectivement). Ce n'est pas une méthode standard 2D, puisque le calcul est effectué sur une structure qui n'a pas de symétrie qui permette de telles hypothèses simples. En fait, sans déterminer le plan neutre pour ce système asymétrique, nous ne pouvons pas le modéliser en 2D et la modélisation devrait être faite en modélisation éléments finis 3D [(Hariri, et al., 2012)].

L'équation générale qui représente tout système mécanique et/ou piézoélectrique déterminée en utilisant le principe variationnel dans le chapitre 2 est utilisée dans le chapitre 3 pour déterminer l'équation numérique des patchs piézoélectriques non-colocalisées collés sur des structures fines.

Deux cas particuliers sont traités à la fin de chapitre 3, le premier cas est celui dit" actionneur-capteur" où certains patchs sont utilisés comme capteurs et d'autres comme actionneurs, tandis que le second est le cas de "actionneur actionneur", où tous les patchs sont utilisés comme actionneurs.

5. Chapitre 4

Un dispositif expérimental a été construit. Il est décrit dans le chapitre 4 et sert à valider notre modèle du chapitre 3. Dans le chapitre 4, nous avons présenté le dispositif expérimental, puis nous avons commencé le processus de validation en comparant les résultats du modèle avec les données expérimentales dans le cas d'une poutre et d'une plaque (figures ci-dessous). La comparaison est effectuée aux fréquences de résonance et concerne les déplacements du système pour une tension appliquée aux patchs piézoélectriques actionneurs, ainsi que la tension obtenue aux patchs piézoélectriques capteurs.

Après validation du modèle dans le chapitre 4, les deux chapitres suivants (chapitres 5 et 6) parlent de la génération d'une onde progressive dans la poutre tandis que la génération d'une onde progressive dans la plaque a fait l'objet d'un brevet.

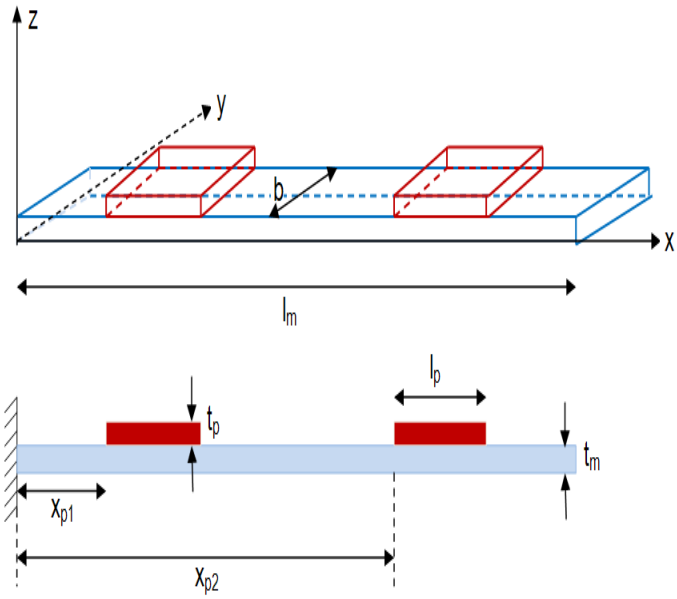

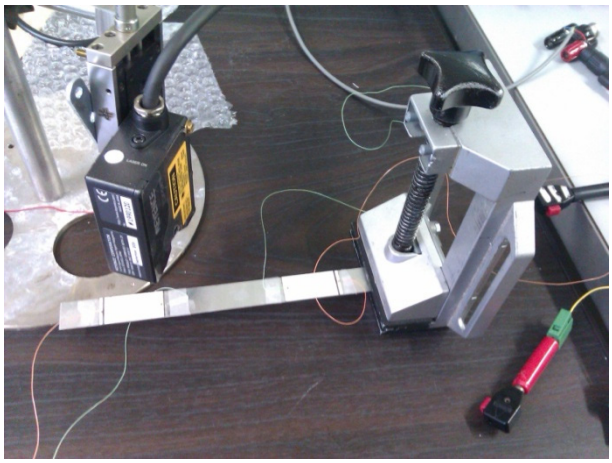

Beam experimented device

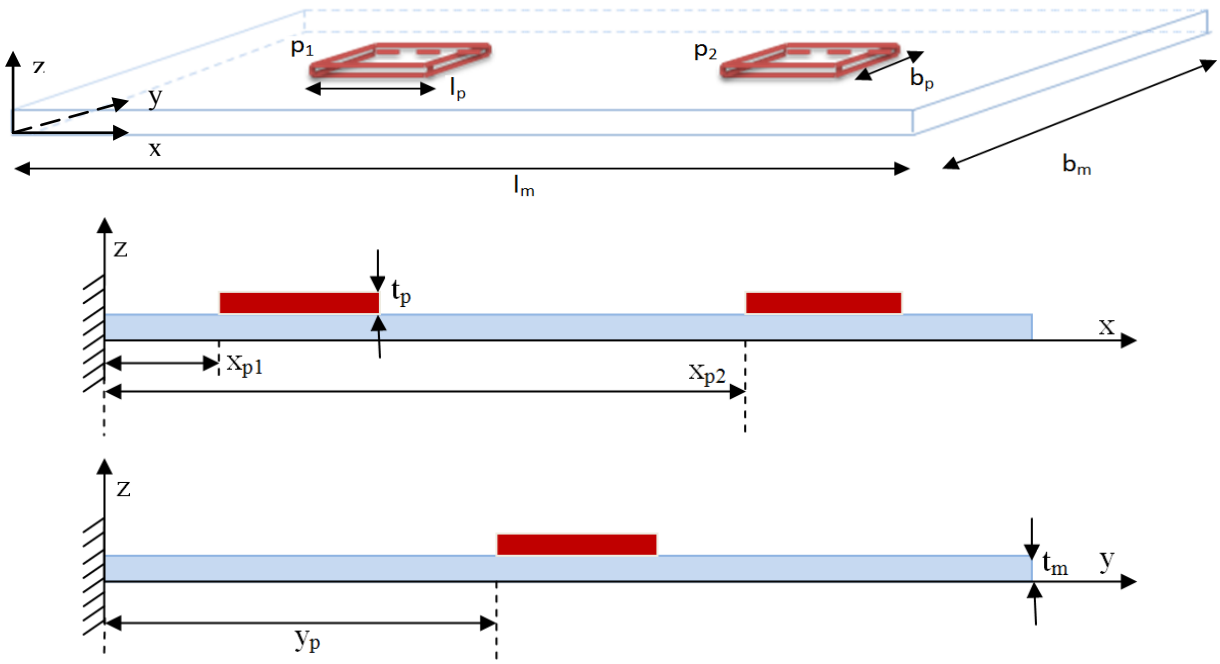

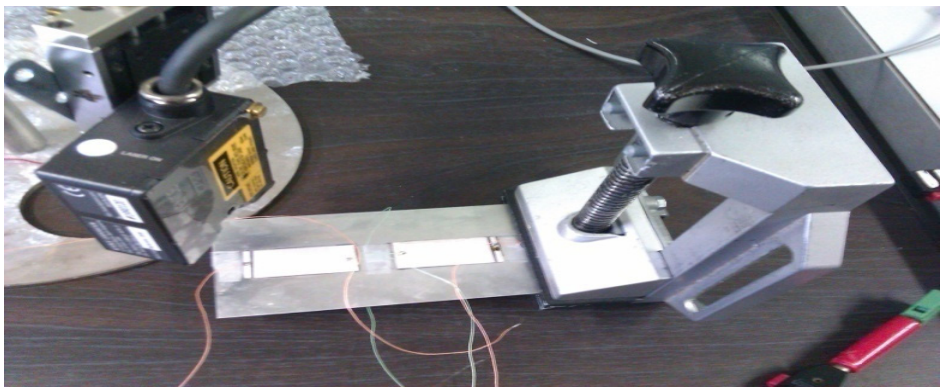

Plate experimented device

6. Chapitre 5

Le chapitre 5 est l'aboutissement de notre projet, nous avons appliqué le modèle développé dans le chapitre 3 et validé dans le chapitre 4 pour démontrer théoriquement la génération d'une onde progressive sur une structure de type poutre mince. Ensuite, un prototype expérimental pour valider les résultats théoriques est présenté dans le chapitre 6.

Comme nous le savons maintenant, le principe de fonctionnement de notre robot est inspiré de moteurs linéaires ultrasons à ondes progressives. Ainsi, au début du chapitre 5, nous avons introduit le principe de fonctionnement de notre robot piézoélectrique à onde progressive (figures ci-dessous) en l'illustrant une brève revue sur les moteurs linéaires ultrasonique à onde progressive pour être en mesure de voir les différences entre notre robot et les autres.

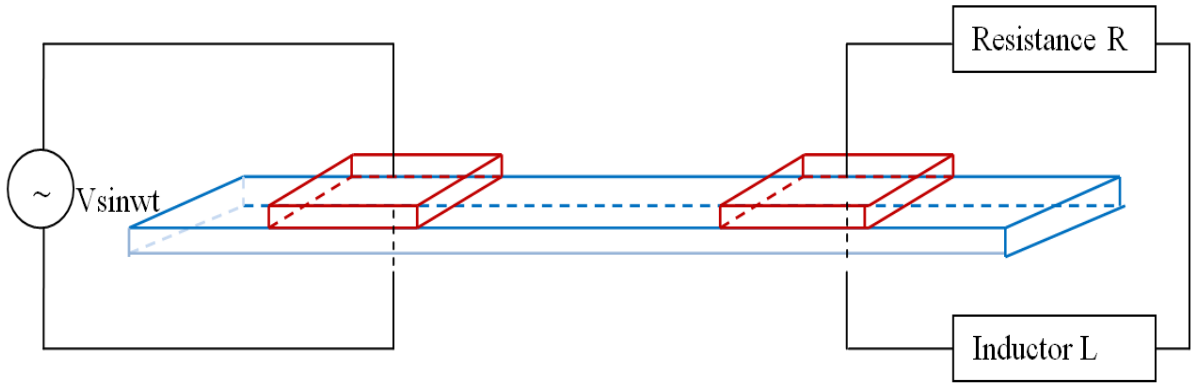

Schematic figure of the one mode excitation: 1ME

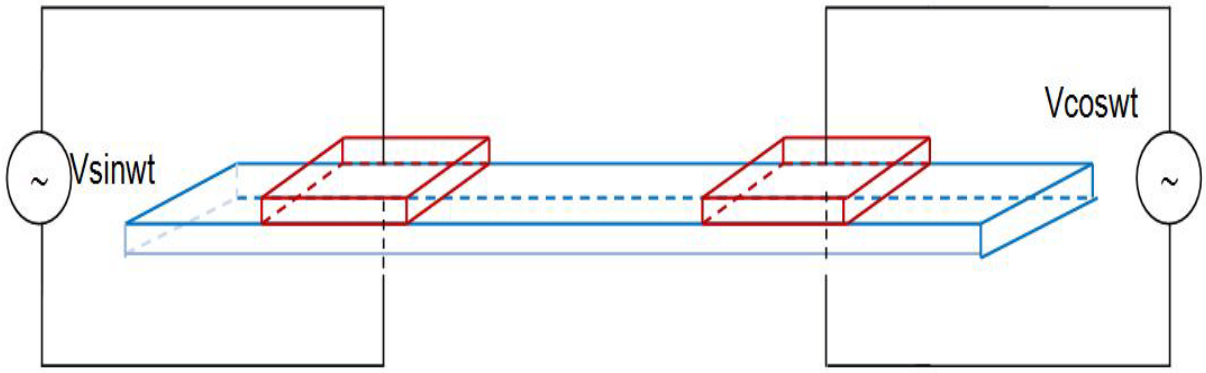

Schematic figure of the two modes excitation: 2ME

Après avoir introduit le principe de fonctionnement de notre robot piézoélectrique à onde progressive, la modélisation du robot piézoélectrique est présentée en utilisant l'équation

matricielle obtenue dans le chapitre 3 à notre cas d'application. La conception optimale est étudiée en détail, intégrant les dimensions du robot, les positions des patchs piézoélectriques, la fréquence de fonctionnement optimal et les performances des ondes progressives du robot.
Une poutre en aluminium a été choisie avec des dimensions données (180 mm × 17 mm × 0,5 mm). Les dimensions des patchs piézoélectriques ont été déterminées (32 mm × 17 mm × 0,27 mm). Deux positions des patchs piézoélectriques près des extrémités de la poutre ont été étudiées pour le robot à ‘’un mode d’excitation : 1ME’’ et le robot à ‘’deux modes d’excitation : 2ME’’.
Deux échantillons avec des positions Xp des patchs différentes, échantillon 1 (Xp1 = 24 mm, Xp2 = 124 mm) et échantillon 2 (Xp1 = 14 mm, Xp2 = 134 mm). L’échantillon 1 a montré les meilleures performances dans le 1ME et le 2ME à la fois (les performances de l'onde dépendent de la forme d'onde [voir chapitre 5] et le déplacement transversal). Selon le tableau ci-dessous, les performances de l’onde sont, dans l'ordre décroissant: 2ME position 1, 2ME position 2, 1ME position 1 et 1ME position 2.
Dans la technique à deux modes d'excitation, on excite les deux patchs à une fréquence entre deux modes de résonance alors que dans la technique à un mode d'excitation, un patch est excité à la fréquence de résonance et l'autre est utilisé pour absorber l’énergie mécanique afin d'éviter la réflexion de l’onde. Cela explique pourquoi les déplacements transversaux dans la technique à deux modes d'excitation sont plus grands que dans la technique à un mode d'excitation, même si dans cette dernière nous excitons à la fréquence de résonance (tableau ci-dessous). La propagation des ondes dans la poutre générées par la technique à deux modes d'excitation est moins homogène que dans le cas d'une mode d’excitation. Les figures montrent que dans le cas de la technique à un mode d’excitation, l'amplitude a le même niveau au milieu de la poutre alors que dans le cas de la technique à deux modes d’excitation, l'amplitude n’a pas le même niveau au milieu de la poutre.

One mode excitation	
(1) Position 1 at f_{17}	**(2) Position 2 at f_{16}**
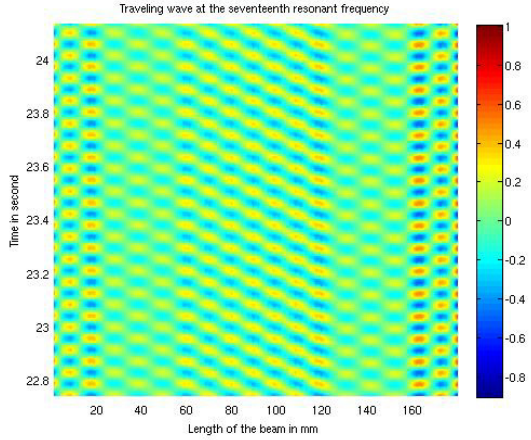	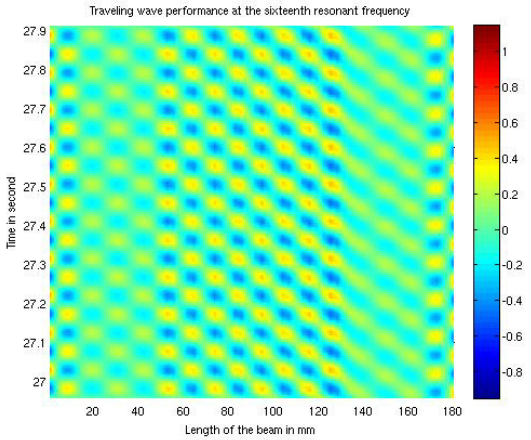
Two modes excitation	
(3) Position 1 at f_{16*17}	**(4) Position 2 at f_{16*17}**
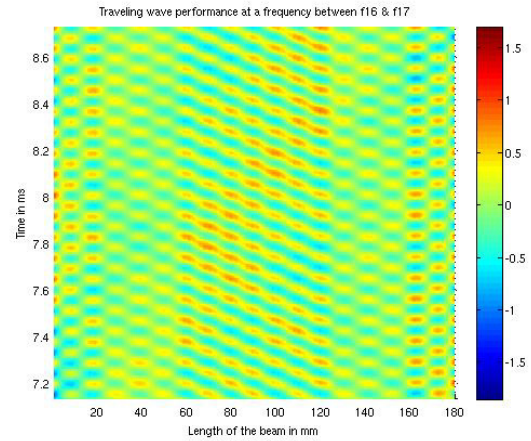	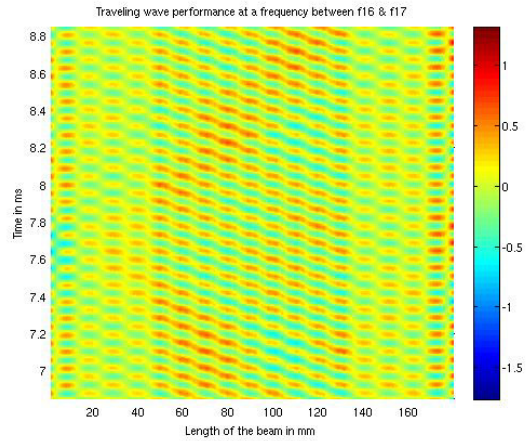

Table: Optimal traveling wave performances for both modes at each position

7. Chapitre 6

Le chapitre 6 est consacré à la fabrication et à la validation expérimentale du robot. Deux robots ont été fabriqués dans le chapitre 6. Le robot 1 correspond à l'échantillon 1 et le robot 2 correspond à l'échantillon 2 (voir figures ci-dessous).

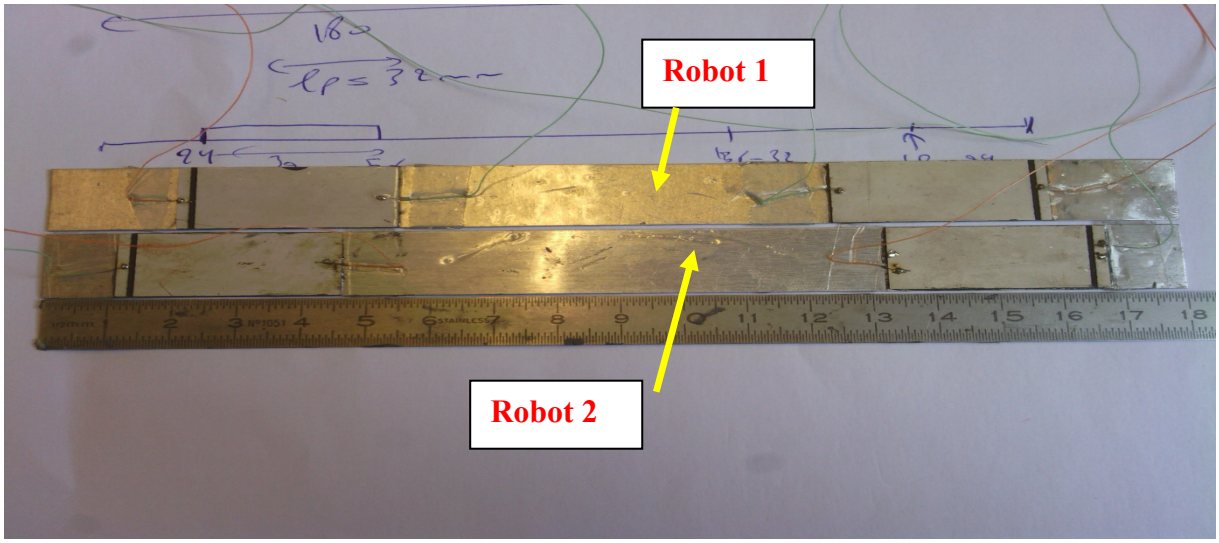

Robot 1 where piezoelectric patches are located at position 1 & Robot 2 where piezoelectric patches are located at position 2

Un circuit supplémentaire constitué d'une résistance et d'une inductance en série (RL série) est connecté à l'un des deux patchs piézoélectriques dans le cas de la technique à un mode d'excitation. Pour le robot 1, le circuit RL série a été calculé à la 17ème fréquence de résonance (R_{17} = 9.75Ω, L_{17} = 9 mH). Pour le robot 2, le circuit RL série a été calculé à la 16ème fréquence de résonance (R_{16} = 23.75 Ω, L_{16} = 11.4 mH).

Des circuits électroniques pour alimenter les actionneurs piézoélectriques ont été conçus et des circuits RL série pour les capteurs piézoélectriques ont été réalisés (figures ci-dessous). Les deux robots ont été testés expérimentalement dans la technique à 'un mode d'excitation'' et la technique à ''deux modes d'excitation'' afin de valider nos résultats de simulation donnés dans le chapitre 5.

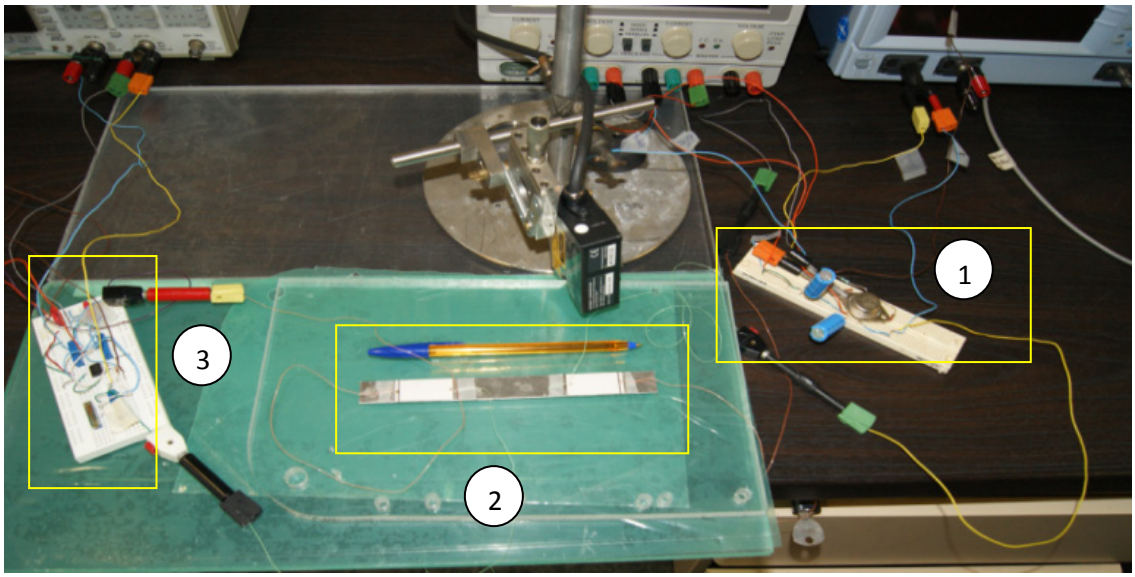

Robot structure for the one mode excitation operating principle (1: power amplifier, 2: robot body, 3: series RL synthetic inductor)

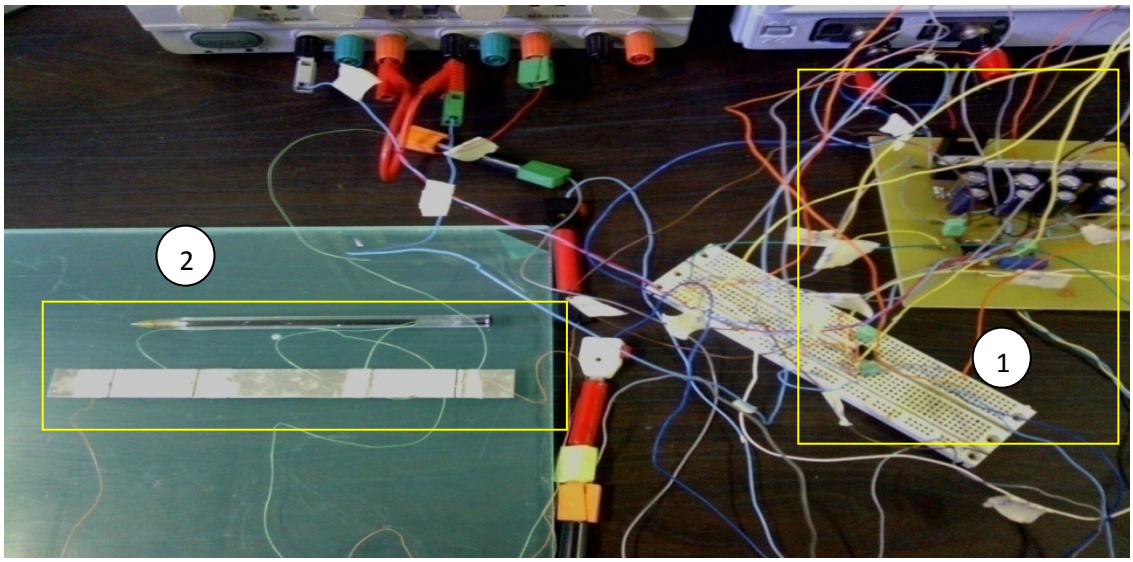

Robot structure for the two modes excitation operating principle (1: Power amplifiers, 2: robot body)

Le robot 1 qui montre une meilleure vitesse dans les deux modes de fonctionnement a été choisi pour mener un caractérisation complète. La vitesse en fonction de la tension appliquée, la vitesse en fonction de masse embarquée et la vitesse en fonction de la force mécanique fournie ont été mesurées sur une surface lisse en verre.

Le robot 1 a une fréquence de fonctionnement optimale égale à 11,3 kHz. Il se déplace à 131.5 mm/s sous 30V d'amplitude sans masse embarquée dans le cas de la technique à ‘’deux modes d'excitation’’. Sous la même tension, ce robot peut fournir 432 μW (7.2 mN, 60 mm/s).

Dans le cas de la technique à ‘’un mode d’excitation’’, il a une fréquence de fonctionnement optimale égale à 11,6 kHz. Il se déplace à 81.19 mm/s sous 30V d'amplitude sans masse embarquée. Sous la même tension, ce robot peut fournir 360 μW à son point de fonctionnement nominal 9 mN, 40 mm/s).

A la fin du chapitre 6, une comparaison entre nos robots et des robots existants similaires (chapitre 5) et quelques moteurs linéaires ultrasonores à onde progressive est faite.

8. Chapitre 7

L'objectif de ce travail était de créer une onde progressive sur une plaque mince pour la déplacer suivant plusieurs degrés de liberté en utilisant des patchs piézoélectriques (Figure ci-dessous).

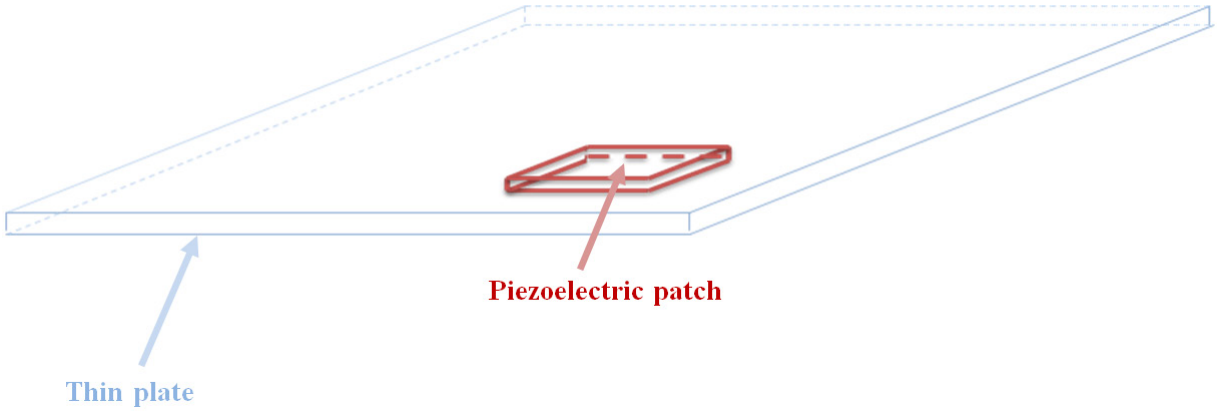

One piezoelectric patch bonded on thin plate

La création d'une onde progressive sur une poutre mince a été présentée dans le chapitre 5 et le chapitre 6 (figure ci-dessous).

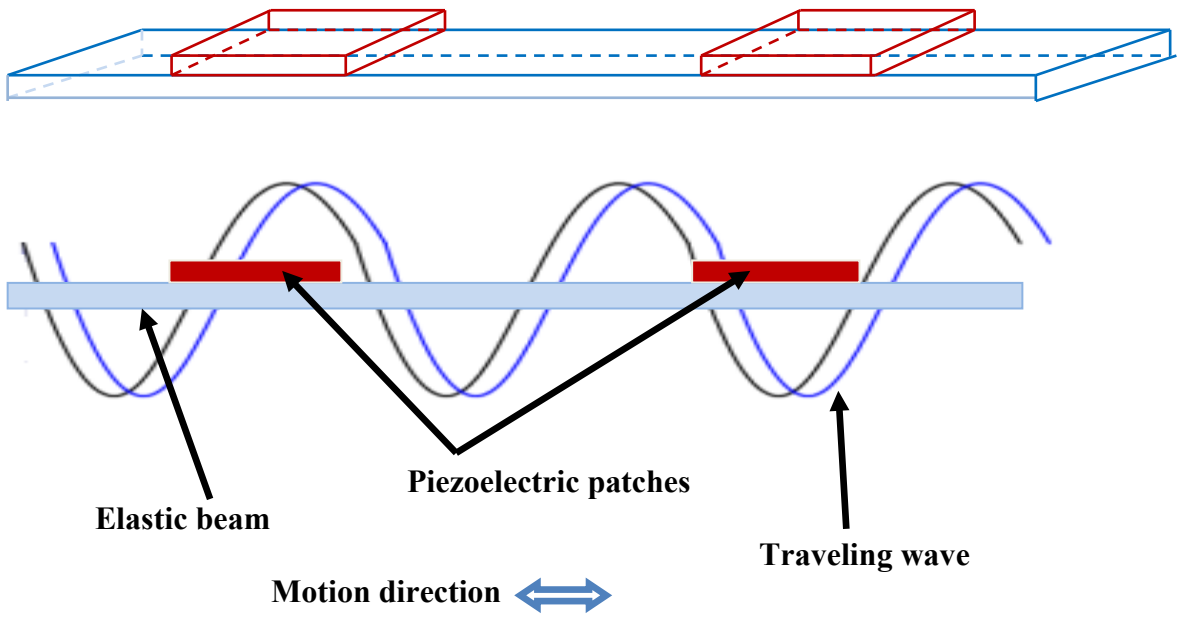

Schematic diagram of the traveling wave piezoelectric beam robot. 3D view on the top and side view on the bottom

Deux principes de fonctionnement sont présentés et utilisés pour déplacer la poutre mince en utilisant des patchs piézoélectriques : La technique ‘’un mode d'excitation’’ et la technique ‘’deux modes d’excitation’’. La conception optimale et le processus de fabrication ont également été présentés dans les chapitres précédents.

La création d'une onde progressive sur une plaque mince en utilisant des pastilles piézoélectriques n'a pas encore été présentée. Les dimensions, la conception, les procédés de fabrication, la simulation et les résultats expérimentaux ont été déposés pour un brevet et ne seront pas détaillés dans cette thèse.

Le chapitre 7 est intitulé ‘’overview’’ et montre toutes les autres applications qui pourrait être faites en utilisant le modèle par éléments finis développé.

Tout d'abord, nous avons présenté la possibilité de concevoir des transformateurs piézoélectriques en utilisant notre modèle et un prototype est présenté à cet effet.

Deuxièmement, l’amortissement de vibrations d’une poutre mince et plaque mince en utilisant notre modèle est présenté et est vérifié expérimentalement.

Troisièmement, le contrôle actif de structures flexibles est examiné sous peu, alors le principe de contrôle actif en utilisant notre modèle éléments finis est présenté par transformation de notre modèle éléments finis en espace modal, puis en espace d'état. A la fin de cette section, les fonctions de transfert sont déterminées.

Ensuite, la détection de défauts dans des structures par l'emploi de matériaux piézoélectriques est présentée et des papiers sont cités.

Nous avons ensuite parlé de la nécessité d'une optimisation topologique telle que des algorithmes stochastiques dans le cas de structures complexes, certains articles sont pris comme exemples.

Enfin des modèles analytiques sont comparés à notre modèle éléments finis (en citant quelques articles analytiques pour des structures minces avec des pastilles piézoélectriques). Une analogie électrique est donnée à partir de notre modèle éléments finis. Nous sommes donc en mesure de représenter une structure mince avec des patchs piézoélectriques actionneurs/capteurs par un circuit électrique équivalent. Cette analogie électrique est donnée dans la littérature en utilisant des modèles analytiques, on peut le mettre en œuvre à partir du modèle par éléments finis.

9. Perspectives

Dans les perspectives de ce manuscrit, nous vous avons proposé un futur état de l'art des systèmes intelligents utilisant des matériaux piézoélectriques. Nous avons parlé de la façon dont d'améliorer notre modèle éléments finis pour décrire notre robot, de la façon d'augmenter les degrés de liberté de notre robot et de la façon d'améliorer l'efficacité du robot en utilisant d'autres circuits passifs. Un asservissement est proposé comme perspectives pour augmenter l'autonomie du robot. A la fin, un prototype est proposé pour le déplacement aquatique et terrestre à la fois. Enfin, nous avons essayé de répondre à la question de la miniaturisation.

10.Originalité de travail

En fait, la théorie de 1ME a été démontrée en 1993 par Sashida et al. [(Sashida, et al., 1993)], ainsi qu'en 1985 par Kuribayashi et al. [(Kuribayashi, et al., 1985)]. Celle de 2ME a été introduite par Loh et al. [(Loh, et al., 2000)] en 2000.

En outre, la génération d'une onde progressive sur une poutre à l'aide de ces deux principes de fonctionnement (1ME et 2ME) a été réalisée expérimentalement par Hernandez [(Hernandez, 2010)] dans sa thèse de doctorat dans notre laboratoire.

Il a utilisé ces deux principes pour générer une onde progressive sur une poutre pour application au micro-pompage et son travail a été breveté.

Le concept de notre système est différent. Dans notre cas, l'onde progressive générée doit déplacer tout le système (application robot) et pas seulement objet posé sur la poutre.

L'originalité est dans la conception proposée pour ce système. Notre robot, comme montré dans la bibliographie du chapitre 1 est le premier dans la littérature qui se déplace au moyen de deux pastilles piézoélectriques collées sur la même face d'une structure de type poutre.

Ainsi, l'originalité était dans le design. Derrière cette fabrication facile, se cache une conception optimale complexe. Le but de mon travail consistait à trouver cette conception optimale afin de créer une onde capable de déplacer tout le système (2 patchs collées sur la poutre), puis à valider et prouver expérimentalement le déplacement de l'ensemble.

Qui est plus, dans le cas de la plaque, c'est non seulement le design qui est nouveau, mais aussi le principe de fonctionnement.

La modélisation 2D par éléments finis pour des structures minces avec des patchs piézoélectriques colocalisés (structures symétriques) a été faite dans la littérature. Pour des structures asymétriques (structures minces avec des patchs piézoélectriques non-colocalisées), nous sommes les premiers a avoir proposé une modélisation par éléments finis 2D pour ces structures grâce à la détermination du plan neutre [(Hariri, et al., 2012)]. La résolution de ce genre de structures en 2D permet d'économiser du temps de calcul. Cela est intéressant si une conception optimale est nécessaire.

11.Historique de travail

Dans ce paragraphe, je voudrais vous présenter mon travail de doctorat durant ces trois années comme un bref historique.

J'ai d'abord commencé par une recherche bibliographique sur la locomotion des animaux [(Biewener, 2003)] dans les trois milieux des déplacements (terre, eau et air) et sur les robots piézoélectriques miniatures existants dans la littérature [(Hariri, et al., 2010), chapitre 1].

Après avoir vu qu'il n'y a pas de robot ayant la même structure que celle que nous avons proposée, nous avons commencé à travailler sur notre idée. L'idée de départ était de coller astucieusement des pastilles piézoélectriques sur une plaque mince dont les oscillations (induites par l'actionnement piézoélectrique) créaient un mouvement adapté à l'environnement terrestre.

Le système proposé m'a forcé à faire une autre recherche bibliographie sur les structures similaires (systèmes intelligents utilisant des matériaux piézoélectriques) comme les systèmes unimorphse, bimorphes, matériaux piézoélectriques intégrés dans des poutres, poutres avec des pastilles piézoélectriques (colocalisées ou non-colocalisées), des systèmes de type plaque avec des pastilles piézoélectriques, des plaques circulaires, etc.

Nous avons constaté qu'il y a beaucoup de systèmes intelligents utilisant des matériaux piézoélectriques (systèmes de type plaque/poutre fine avec des pastilles piézoélectriques) dans la littérature pour des applications telles que l'amortissement des vibrations, récupération d'énergie, détection des défauts causés aux structures [chapitre 7] et quelques moteurs piézoélectriques ultrasonores à onde progressive. Différentes manières sont utilisées pour décrire ces systèmes, tels que des modèles analytiques, des modèles par circuit équivalent (poutre, plaque) [chapitre 7] et des modèles par éléments finis [chapitre 3].

Pour avoir une conception optimale pour une application donnée, les modèles ont été combinés avec des techniques d'optimisation (déterministes ou stochastiques) [chapitre 7].

Dans le chapitre 7, nous avons justifié le choix d'un modèle éléments finis pour décrire notre système. Un modèle par éléments finis 1D pour une poutre avec des pastilles piézoélectriques localisées pour une application d'amortissement avait été developpé par Romain CORCOLLE lors de son stage de MASTER 2 au laboratoire. Nous n'avons donc pas commencé de zéro. Ensuite, la décision a été prise de diviser notre travail en deux parties : robot piézoélectrique à onde progressive de type poutre et robot piézoélectrique à onde progressive de type plaque.

La modélisation des deux cas d'étude (modèles de poutres et de plaques) a été comparée aux modèles avec un logiciel par éléments finis commercial (COMSOL 3.5a). Après validation, une conception optimale a été faite en utilisant la stratégie de modélisation développée dans cette thèse, puis des prototypes expérimentaux ont été fabriqués, et nos modèles ont été comparés avec les résultats expérimentaux cette fois-ci (chapitre 4).

Les modèles éléments finis développés ont l'avantage d'avoir une dimension en moins par rapport à ceux des logiciels par éléments finis commerciaux. Par exemple une poutre avec des patchs piézoélectriques (colocalisés ou non-colocalisés) est modélisée en 2D à l'aide du logiciel commercial par éléments finis, alors qu'elle est modélisée en 1D par notre modèle éléments finis.

Après une étude de conception optimale afin de générer l'onde progressive dans la poutre [chapitre 5], les prototypes de type poutre ont été testés et les résultats sont donnés dans le chapitre 6.

Le prototype de type plaque, ses simulations et ses résultats expérimentaux ont été déposés pour un brevet.

12.Références

Bernard Y. et Razek A. Piezoelectric valve modeling and design [Revue] // AC2011. - 2011. - pp. pp.124-131..

Biewener A. Animal locomotion [Livre]. - [s.l.] : Oxford university press, 2003.

Driesen W Concept, modeing and experimental characterization of the modulated fric-tion inertial drive (MFID), Locomotion principle: Application to mobile microrobots [Livre]. - Lausanne : Swiss Federal Institue of Technology, 2008.

Hariri H., Bernard Y. et Razek A. A New Efficient Modeling Concept of Non-Collocated Piezoelectric Patches Bonded on thin Structure [Revue]. - [s.l.] : Submitted in Journal of mathematics and computers in simulations, 2012.

Hariri H., Bernard Y. et Razek A. Finite element model of a beam structure with piezoelectric, patches using RL shunt circuits [Revue] // AC2011, 14th International Conference on active systems for dynamics markets. - 2011. - pp. pp.124-13.

Hariri H., Bernard Y. et Razek A. Locomotion principles for piezoelectric miniature robots [Revue] // Proceedings on actuator 10. - 2010. - pp. pp. 1015-1020..

Hernandez C., Bernard Y. et Razek , A. A global assessment of piezoelectric actuated micro-pumps [Revue] // European. Physical Journal Applied Physics. - 2010. - pp. Vol. 51, Issue: 2,1-8..

Kuribayashi M., Ueha S. et Mori E. Excitaion conditions of a flexural traveling waves for a reversible ultrasonic linear motor [Revue] // Journal of the acoustical society od America 77. - 1985. - pp. 1431-1435.

Loh B.G. et Ro P.I. An object transport system using flexural ultrasonic progressive waves generated by two modes excitation [Revue] // IEEE transaction on ultrasonic, ferroelectrics, and frequency control. - 2000. - pp. 994-999.

Qu G.M. [et al.] analysis of a piezoelectric composite plate with cracks [Revue] // Journal of composite structures. - 2006. - pp. vol. 72, no1,111-118..

Sashida T. et Kenjo T. An introduction to ultrasonic motors [Livre]. - Oxford : Clarendon Press, 1993.

Yan Y.J. et Yam L.H. Online detection of crack damage in composite plates using embedded piezoelectric actuators/sensors and wavelet analysis [Revue] // Journal of Composite Structures. - 2002. - pp. Vol 58, Issue 1,29-38..

Yasin M. Y., Ahmad N. et Alam M.N. Finite element analysis of actively controlled smart plate with patched actuators and sensors [Revue] // Latin American Journal of Solids and Structures. - 2010. - pp. Vol 7, No 3,227-247.

DESIGN AND REALIZATION OF A PIEZOELECTRIC MOBILE FOR COOPERATIVE USE

Thesis subject

DESIGN AND REALIZATION OF A PIEZOELECTRIC MOBILE FOR COOPERATIVE USE

- **Forward and motivation of this work**

- **Table of contents**

    1. **Chapter 1: Locomotion principle for piezoelectric miniature robots**

    2. **Chapter 2: Introduction to the numerical modeling of thin structures with piezoelectric patches**

    3. **Chapter 3: Modeling of non-collocated piezoelectric patches bonded on thin structures**

    4. **Chapter 4: Experimental validation of models**

    5. **Chapter 5: Traveling wave piezoelectric beam robot**

    6. **Chapter 6: Robot manufacturing and experimental measurements**

    7. **Chapter 7: Overview**

- **Conclusion and perspectives**

FORWARD AND MOTIVATION OF THIS WORK

Forward and motivation of this work

My project thesis is entitled design and realization of a piezoelectric mobile for cooperative use. So let start by explaining the term piezoelectric mobiles and then to answer the question about why we chose to design it for a cooperative use.

The term piezoelectric mobile here means piezoelectric miniature robots. These are mobile miniature robots actuated by piezoelectric materials.

In this manuscript I will present the design and realization of small robots designed for future cooperative use.

These robots consist of a thin support and piezoelectric patches. The piezoelectric patches are bonded on the support in a clever way in order to move the support with multi degree of freedom.

The idea of the project is to move the thin support in the three mediums (earth, liquid and air) and it is inspired from the Manta ray fish. As we know the living environment for the Manta ray is the water but, this fish is able to fly also for a short time (figure below). If we apply the locomotion principle of this Manta ray to robots we can realize robots able to move in three mediums because moving in earth could be done using the liquid locomotion principle for the Manta ray. The flapping of wings of the Manta ray is used for the air environment.

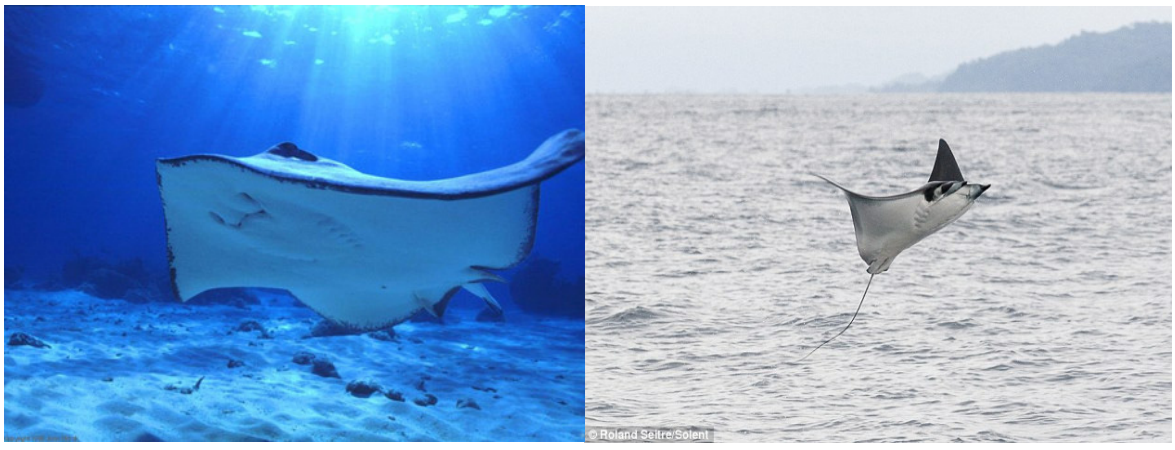

Manta ray fish inside and outside the water
[http://animals.desktopnexus.com/wallpaper/209676/,
http://picinpic.blogspot.fr/2011/07/manta-ray-fish.html]

So, the project consists of design and realizes a piezoelectric miniature robot able to move in the three mediums (earth, liquid and air) for future cooperative use.

My work in the project consists to verify the feasibility of the displacement of a mimetic Manta ray on earth using piezoelectric materials, design and realize a prototype to

demonstrate this feasibility on earth. Then make a preliminary design and perspective for liquid and air displacement based on the same prototype as in earth, in order to be able to move in the three mediums of displacement in a future work.

My work aims to answer these following questions:

Is it possible using piezoelectric materials to move a mimetic Manta ray (Manta ray shape is considered as a thin plate) with multi degree of freedom on the earth by generating a traveling wave motion on the thin plate?

Is this robot can be extended based on the same prototype as in earth to create displacement on liquid and air environments like Manta ray fishes?

The interest of this project lies especially when the piezoelectric robots are small and they can move in various media (soil, air, liquid). Robots we envision are inspired from the locomotion of Manta ray and they could be miniaturized, so they can be placed within the scope of mimetic biological swarms.

Robot swarms are considered today as a new solution to overcome the limitations of traditional robotics. The joint and cooperative operation of robots are inspired from the collective organizing of living beings, which emerge forms of intelligence and group control beyond the capacity of individual organisms involved (figure below).

Swarms behavior

[

http://www.ipvs.uni-stuttgart.de/abteilungen/bv/forschung/projekte/I-Swarm/print_view,
http://www.hizook.com/blog/2009/08/29/i-swarm-micro-robots-realized-impressive-full-system-integration,
http://blog.autoworld.com.my/index.php/2009/02/26/swarm-technology-the-biggest-contribution-to-eco-tech/

]

Swarms robots could be used in many applications, such as cell storing, research objects in narrow areas or on swarm behavior, surveillance for security, medical applications & etc.

According to a recently published report from IRAP, Inc., ‘’ET112: Piezoelectric Actuators and Motors–Types, Applications, New Developments, Industry Structure and Global Markets,’’ the global market for piezoelectric-operated actuators and motors was estimated to be $6.6 billion in 2009 and is estimated to reach $12.3 billion by 2014, showing an average annual growth rate (AAGR) of 13.2% per year. Below a table taken from IRAP Inc., presents global market size/percentage share for piezoelectric actuators and motors by application through 2014.

Applications	2009 ($ Mil.)	2009 (%)	2014 ($ Mil.)	2014 (%)	AAGR (%) 2009-14
Ultra-small scale motion related applications	3,200	48.6	6,000	48.9	13.4
Cameras, microscope lenses, mirrors and optics.	2,800	42.5	5,200	42.4	13.1
Others – e.g., auto fuel injectors, micro-pumps, micro-blowers, piezo ink cartridges, surgery instruments, mini-robots	587	8.9	1090	8.7	13.1
Total	**6,587**	**100**	**12,290**	**100**	**13.2**

Global share for piezoelectric actuators and motors by application, through 2014

The Investment of states (USA, Japan, Europe, Korea, and China) in R&D in the area of swarm robots is enormous given the amount of annual publications. The same design ideas of robots are repeated between countries trying to improve maneuverability, control, functionality, speed, autonomy...

The U.S. investment is huge in this area and in particular in the case of swarms robots based on piezoelectric materials (my field of interested in this research) and this is why many new

ideas come from them. More detailed about the U.S., piezoelectric swarms robots can be seen in chapter one.

I will cite below some important and recent European research projects in the field of swarm robots (some of them have used the piezoelectric materials and some of them not) and in particular the case of France.

The I-SWARM project is a European project (Germany, Sweden, Switzerland, Austria, Greece, United Kingdom, Italy, and Spain), it took place between 2004 and 2008. It was a great success and gave a remarkable presence of Europe in the field of swarms minirobotics. Then the SYMBRION project is a project funded by European Commissions (Germany, Austria, Netherlands, Belgium, United Kingdom and France), started from previous development and research from project I-SWARM and the open-source SWARMROBOT projects. The project duration is between 2008 and 2013. A large part of the developments within SYMBRION is open-source and open-hardware also.

The E-SWARM project will contribute to the development of an engineering methodology for the construction of artificial swarm intelligence systems based on rigorous scientific foundations. The project started in 2010 for a period of 5 years. Its principal investigator is Professor Marco Dorigo (IRIDIA lab at the university libre de Bruxelles), one of the founders of the swarm intelligence and swarm robotics research fields.

In France, several projects are sponsored with ANR, ONERA and CNRS.

REMANTA project (2002-2006) was inspired by nature to design UAVs with flapping wings, ANR/ELESA OVMI project (2007-2011) focuses on the development of control laws for actuating the wings of a biomimetic piezoelectric flying robot. PEA Action project (2007-2014) aims to scientifically demonstrate the cooperation of multiple autonomous vehicles operating in different environments, ANCHORS ANR project (2012-2015) is also studying the cooperation of several heterogeneous autonomous vehicles (air and earth) in a context of crisis management, especially in the nuclear ...

Research in the field of swarms microrobotics takes interest and continues nowadays with more and more investment of states due to its applications in various fields and low manufacturing cost. It was remarkable in England this year that, research to develop intelligent machines has received a boost of 16 million pounds through a partnership between government and industry in areas such as: monitoring in hazardous environments such as water facilities deep and nuclear power plants, nursebots for hospitals and aircraft.

Let me now introduce the constitution of the manuscript:

1. As we have seen above, the piezoelectric miniature robot designed should be able at the final stage to move in the three mediums displacement. For that, we began the study by looking on the literature to piezoelectric miniature robots in the three mediums displacement (earth, liquid and air) to avoid repetition of work if there is any robot based on the inspiration from the Manta ray fish and actuated by piezoelectric patches like what we have proposed. In the first chapter of this manuscript, we find a classification of piezoelectric miniature robots by medium displacement. In particular, we were interested in the locomotion principles of these robots because the goal of our project is to use a locomotion principle to generate displacement (Manta ray locomotion principle or undulatory traveling wave motion).
2. After comparing the existing locomotion principles for piezoelectric miniature robots with our proposed one, we will study in the next the modeling of our system which is composed of thin structure with piezoelectric patches bonded on it. The second chapter includes an introduction to modeling of thin structures with piezoelectric patches.
3. The third chapter is dedicated to modeling of such system (non-collocated piezoelectric patches bonded on thin structures). At the end of this chapter, we will be able by using the obtained numerical equation to calculate the resonance frequencies and determining the mode shapes. We can compute the transverse displacements of the system, stresses, and strains obtained by applying forces on the system or by applying electrical voltages on some piezoelectric patches; we can also determine the obtained voltages for others piezoelectric batches. Also we can compute the currents values and the electric charges of piezoelectric patches.
4. In chapter 4, an experimental device will be built and tested to validate the model obtained from chapter 3.
5. Chapter 5 is entitled traveling wave piezoelectric beam robot. In this chapter we will present the design and the operation principle for this traveling wave piezoelectric beam robot. The optimal design will be studied using the numerical equation obtained in chapter 3. This numerical equation will be readapted with the operation principle of the robot in order to demonstrate the generation of the traveling wave.
6. Fabrication process will be presented in chapter 6 and traveling wave will be demonstrated experimentally by characterization of the robot (velocity, embedded masses, mechanical forces,…). At the end significance and benefits for this robot compared to others will be presented.

7. No discussion in chapter 7 about piezoelectric plate robot. Actually, the operation principle of this robot, dimensions, design, fabrication processes, theoretical and experimental results have been filed for a patent. This chapter is entitled overview and in this chapter we will talk shortly about some points, among them:
    - Analytical modeling versus finite element modeling for this robot.
    - The robot structure (plate case) will be presented as a piezoelectric transformer. The piezoelectric transformer design, theoretical and experimental results are presented briefly by using our developed model.
    - Damping vibration of thin beams and plates will be presented briefly with some theoretical and experimental results using the same model developed for robotics applications.
    - A state space matrix equation will be represented from the finite element equation. The state space equation is very useful in automatic. Particularly in our case, it can be used to control the vibration of the beam/plate in order to damp the vibration for example or to generate a traveling wave instead of the use of passive circuits.
    - At the end, an example is given for how we can use our model in the theory of signal processing in order to detect damage in structures like beam/plate.
    - …….
    -

Finally, a general conclusion and perspective are given. In the perspective we will talk shortly about a future design for the piezoelectric beam-plate robot in aquatic medium. Some ideas are proposed for flying beam-plate robot. Also we will talk about miniaturization.

TABLE OF CONTENTS

Chapter 1: locomotion principle for piezoelectric miniature robots

Chapter 2: Introduction to the numerical modeling of thin structures with piezoelectric patches

Chapter 3: Modeling of non-collocated piezoelectric patches bonded on thin structures

Chapter 4: Experimental validation of models

Chapter 5: traveling wave piezoelectric beam robot

Chapter 6: Robot manufacturing and experimental measurements

Chapter 7: Overview

CHAPTER 1

LOCOMOTION PRINCIPLE FOR PIEZOELECTRIC MINIATURE ROBOTS

Chapter 1: locomotion principle for piezoelectric miniature robots

List of figures

List of Tables

1.1. Introduction

The locomotion principle proposed in our project is the Manta ray locomotion as we have seen in the forward and motivation of this work. This locomotion principle consists of generating a travelling wave on a plate in order to move it in multi degree of freedom by using piezoelectric patches.

This chapter presents a big review of existing works on piezoelectric miniature robots. They are classified by medium displacement and we are interested on the locomotion principle of these robots in order to see the similarities and differences between the existing locomotion principles and those we have proposed.

This chapter concerns locomotion principle for piezoelectric miniature robots, we begin by defining what means piezoelectric miniature robot, then, I give a bit of background about the definition of piezoelectric materials and piezoelectric actuators, and then we will study the locomotion principles of piezoelectric miniature robots which are classified by their displacement through a fluid medium or on a solid substrate. Some piezoelectric miniature robots are taken as examples.

1.2. Piezoelectric miniature robot

A general definition of robots does not exist in literature because there is no one satisfies everyone. Some definition can be found in [(ISO), (Lee, et al., 2006)]. Furthermore, a possible one is to define a robot as an electromechanical system designed for a given application. Miniature robots are either defined on a basis of the task they are performing either on their size [(Dario, et al., 1992), (Caprari, 2003)]. However, henceforth in this chapter, the term mobile miniature robots will represent robots with a size of less than 1 dm^3 and a motion range of at least several times the robots body length [(Driesen, 2008)]. Then piezoelectric miniature robots are mobile miniature robots actuated by piezoelectric materials. Mobile miniature robots could be used in many applications, such as cell storing, research objects in narrow areas or on swarm behavior, surveillance for security, medical applications &c.

1.3. Piezoelectric actuators

Many actuators types are used in mobile miniature robots to convert electrical to mechanical energy. The choice of an actuator depends in the application. A comparison of some actuation types are given in (Penella, 2005). The piezoelectric actuators are piezoelectric materials

using the indirect effect. In piezoelectric materials, an electric potential is produced when a stress is applied. This is known as the direct piezoelectric effect. Conversely the application of an electric field results in the development of a strain and/or stress in the materials. This is known as the indirect piezoelectric effect. Later in chapter 2, we will describe in more details the modeling concept of piezoelectric materials.

The piezoelectric actuators are able to interact in different medium displacement. In comparison with other types of actuation, the piezoelectric actuators have low displacement range and a low strain but high displacement accuracy and high response speed. In addition, they are suitable for miniaturization [(Uchino, 2006)] and do not generate electromagnetic noise. Manufacturing of multilayer piezoelectric actuators and bending piezoelectric actuators have the potential to eliminate the drawbacks of piezoelectric materials and make them among the most commonly used in mobile miniature robots. Piezoelectric actuators are responsible for motion in mobile miniature robots and are characterized by two energy transformations. The first conversion is the electrical to mechanical conversion and the second is the mechanical to mechanical conversion. The first conversion reflects the reverse piezoelectric effect, which generates small motion of mobile miniature robots. The second conversion containing specific locomotion principles amplifies the motion of mobile miniature robots. Locomotion principles for mobile miniature robots are mostly inspired from animal locomotion and are classified by their displacement through a fluid medium or on a solid substrate. In this chapter, we will study these locomotion principles and some piezoelectric miniature robots are taken as examples.

1.4. Locomotion on a solid substrate

The forces related to motion on land are the force of gravity, the normal reaction, the friction force, which depends on friction coefficient, contact force and the active force that generates the motion. Locomotion on a solid substrate for mobile miniature robots includes wheeled locomotion, walking, inchworm, inertial drive, resonant drive and friction drive. We will describe in this section, these locomotion principles.

1.4.1. Wheeled locomotion

The principle is based on small engines powering wheels. These engines can be DC motors, step motors, electromagnetic motors or piezomotors. Rolling motion with wheels for miniature robots is characterised by great motion velocities due to the low friction between

wheels and substrate. However it is not very effective in terms of resolution because the efficiency of motors drives decreases with decreasing scale, moreover at small scale the integration of efficient rotary bearings is very complicated [(Driesen, 2008)]. As examples for wheeled locomotion in miniature robots driven by piezoelectric materials, we can count:

1-The world-smallest 4W vehicle [(Uchino, 2006)] driven by two metal tube USM's in the Penn State university (Figure 1. 1);

2-A miniature robot called Jemmy has been developed at EPFL driven by rotating piezomotors [(Driesen, 2008)];

3-Epson Micro Robot System presented a miniature robot called Monsieur II-P driven by two ultra thin ultrasonic motors [(Epson, 2010)].

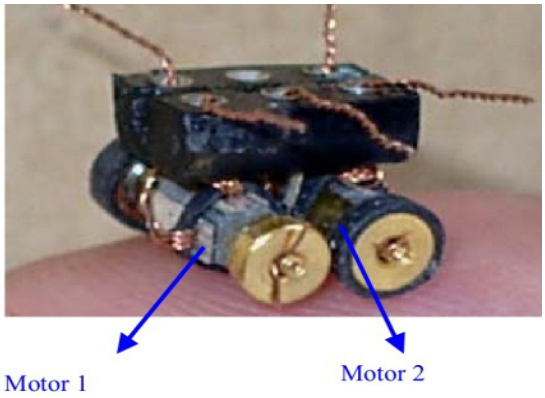

Figure 1. 1: The world-smallest 4W vehicle [(Uchino, 2006)]

1.4.2. Walking locomotion

The principle of this locomotion is based on legs which are the drive units, to achieve a walking similar to the biological organism. The legs are either fixed on a robot (Figure 1.2) or in a stationary element (Figure 1.3) where the slider moves. The second case is not considered for mobile miniature robots. In walking mechanisms, the legs are divided into two sets, where each set alone can maintain the equilibrium of robot or slider. The legs maybe thermal, polymer, electrostatic or piezoelectric drives units. The piezoelectric actuators are generally multilayer benders or monolithic multilayer. The control signals are a square wave [(Ebefors, et al., 2005)], sinusoidal or trapezoidal waves like in reference [(Simu, et al., 2006)]. Walking is essentially a quasistatic locomotion. At high frequency, the control of drive unit can cause motion instabilities, for this reason it is advisable to work in quasi static mode and the goal of high speed can achieve by using other locomotion principles. We can count as examples for walking locomotion in piezoelectric miniature robots:

1- A piezoelectric walking robot called SPIDER-II actuated by 9 piezoelectric bimorph is present in [(Rembold, et al., 1997)]
2- Within the scope of MINIMAN project [(MINIMAN, 2010)], the MINIMAN V robot consists of two monolithic piezoelectric drive units put together back to back [(Simu & Johansson, 2002)]. The top drive unit is intended for locomotion whiles the button for manipulating. Each drive unit has six monolithic piezoelectric legs.
3- Within the scope of MiCRoN project [(MiCRoN, 2010)], a walking locomotion is demonstrated in [(Snis, et al., 2004)]. The module consists of four feet actuated by monolithic multilayer piezoelectric benders. Some examples are taken in Figure 1. 4.

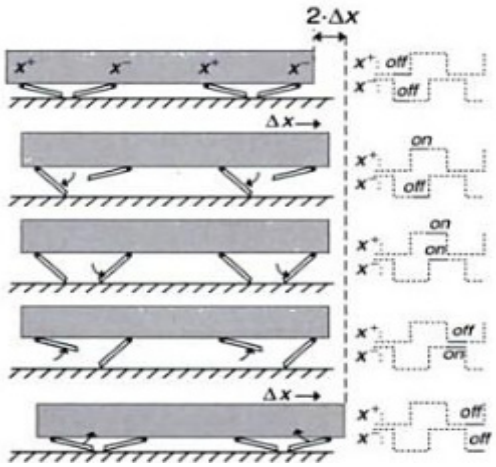

Figure 1.2 : *mechanisms (Robot motion) [*(Ebefors, et al., 2005)*]*

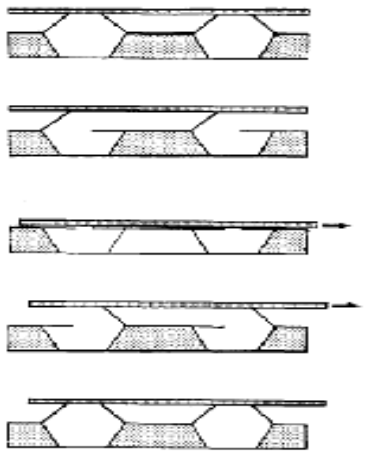

Figure 1.3 : *Walking mechanisms (Slider motion) [*(Driesen, 2008)*]*

Jumping is one of solution to overcome the difficulty of locomotion in rough terrain for small size system. The jumping locomotion idea is to store energy and release it quickly to jump. In order to be able to perform repetitive jumps in a given direction, it is important to be able to

upright after landing, steer and jump gain. A review of the uprighting and steering principles of existing jumping miniature robots is present in [(Kovac, 2010)]. Figure 1.5 describes the basic principle of locomotion for one miniature robot actuated by 3 piezoelectric drive units. As we can remark, the control signal is based on smooth contraction (store energy) and rapid elongation (release it quickly).

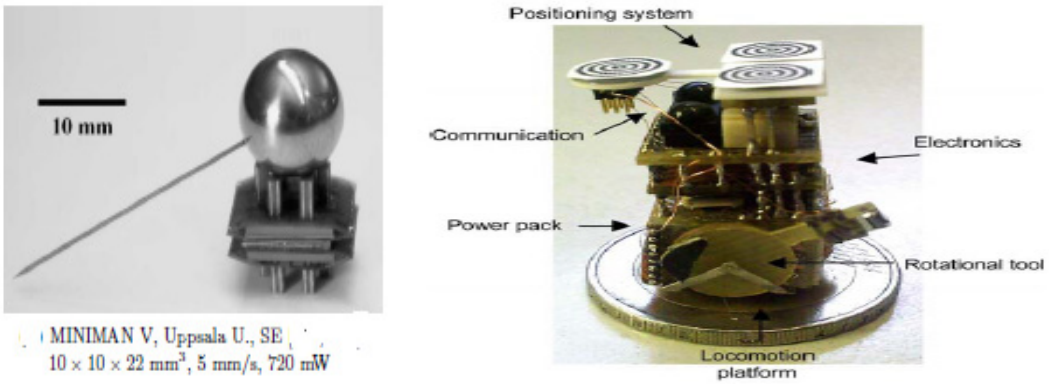

Figure 1. 4: walking locomotion examples [(J.B.Penella, 2005)]

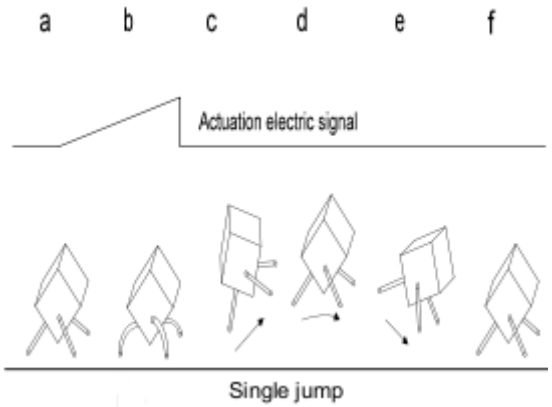

Figure 1.5 *: Basic principle of locomotion, a. initial position, b. combined forces from the legs and the floor, c .robot is lifted, d. robot loosing contact with the floor, e. robot is falling down, f. robot is back on the floor. The deflection amplitudes of the legs are exaggerated here for clarity [*(Nguyen, et al., 2006)*].*

1.4.3. Inchworm locomotion

An inchworm device consists of 3 actuators, two clampers and one extensor actuators. Always, the extensor is situated between the two clampers .The clamper is used to clamp the device into the slider (Figure 1.6) or into the substrate (Figure 1.7 & Figure 1.8) while the extensor generate the stroke required for the displacement. As examples for inchworm locomotion in piezoelectric miniature robots, we can count:

1- A two mobile mini- and microrobots with inchworm locomotion driven by piezoelectric actuators and electromagnetic clamps are presented in [(Aoyama, et al., 2001), (Fuchiwaki, et al., 2002)].

2- A three mobile minirobot driven by three, triangularly arranged piezoelectric stack actuators are presented in [(Codourey, et al., 1995), (Koyanagi, et al., 2000), (Torii, et al., 2001)] as we can show in Figure 1. 9.

3- A minirobot consists of one piezoelectric stack actuator and four electromagnetic clamps are presented in [(Yan, et al., 2006)].

4- A biomimetic micro crawling robot built using smart composite microstructures (SCM) is made of articulated microstructures integrated with piezoelectric actuators, wiring, and sensors [(J.Wood, 2008), (Wood, et al., 2008)]. Many bio inspired device like worm miniature robot operates in inchworm principles not based on piezoactuator exist in literature [(Phee, et al., 2002),(Lim, et al., 2008), (Carrozza, et al., 1997), (Asari, et al., 2000),(Menciassi, et al.)].

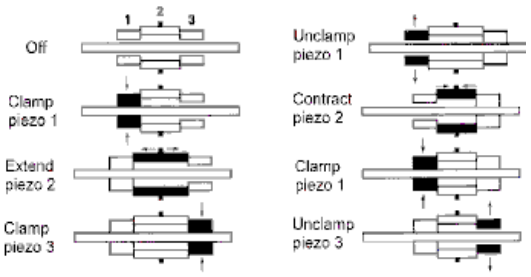

Figure 1.6 : *Inchworm principle (slider motion) [*(May, 1975.)*]*

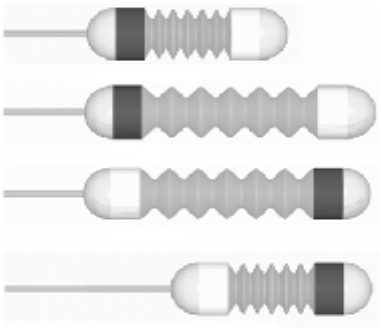

Figure 1.7 *: Inchworm principle (robot colonoscopy motion) [*(Phee, et al., 2002)*]*

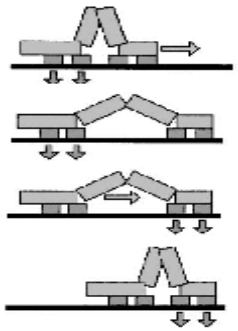

Figure 1.8 : *Inchworm principle (robot motion) [(*Kotay & D.Rrus, 2000) *]*

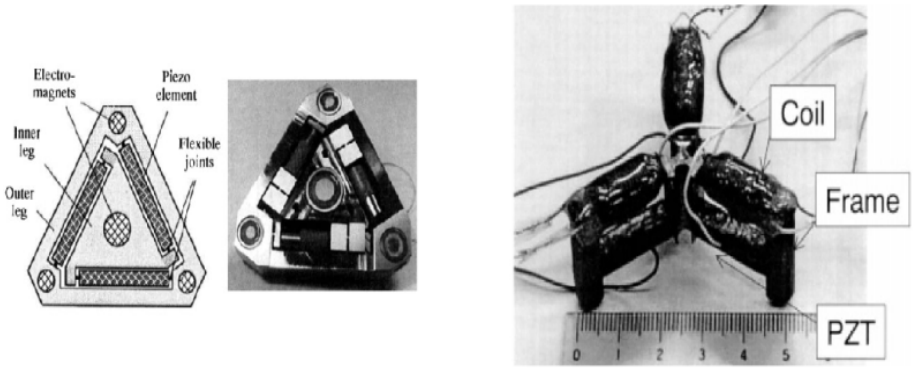

Figure 1.9: Inchworm locomotion examples [(Codourey, et al., 1995) & (Torii, et al., 2001)]

1.4.4. Inertial drive

The inertial drive principle is generated in the case of asymmetric actuation, i.e. in the case of rapid extension (or contraction) and slow contraction (or extension) of the actuator; for this reason, the most of miniature robots based on inertial drive principles are actuated by piezoelectric actuators, because of their high bandwith. Two types of inertial drive principles can be distinguished: the stick-slip principle and the impact drive principle. This distinction is due to the difference in the design of the device (Figure 1.10). A stick-slip design consists of: an inertial mass which is the main body; legs which are the piezoelectric drive units, they are either fixed in the inertial mass (robot motion), either fixed on the substrate (slider motion) and a contact surface which is fixed in the legs. An impact drive design consists of an inertial mass connected to the main body via a piezoelectric element, due to its design, the impact drives are typically driven by a sawtooth signal with a quadratic ramp phase to enable store a maximum amount of kinetic energy in the motion of the inertial mass, resulting in the maximum step displacement of the body of the robot [(Driesen, 2008)]. The steps of motion for each device are shown in Figure 1.11 & Figure 1.12

Many miniature robots based on the inertial drive principles, as examples we can take:

1- A cybernetic in-pipe impact drive actuator based on impact drive principle and actuated by two piezo stacks [(Ikuta, et al., 1991)].
2- A miniature robot called SPIDER-I based on stick-slip principle and actuated by 3 times 2 piezoelectric bimorph actuators connected in series [(Rembold, et al., 1997)].
3- The MINIMAN V and the MiCRoN miniature robots, already presented in walking locomotion are also able to do the stick-slip motion as discussed in [(Simu & Johansson, 2006)].

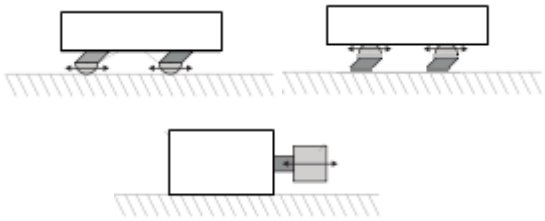

Figure 1.10: *inertial drive design*

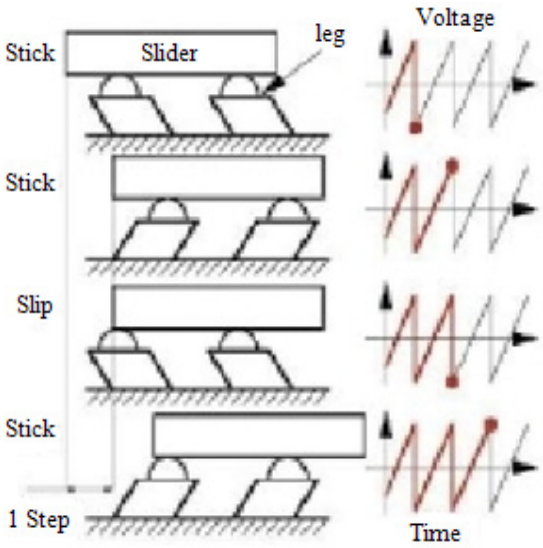

Figure 1.11: *stick-slip principle [* (Stepping principles, 2010)*]*

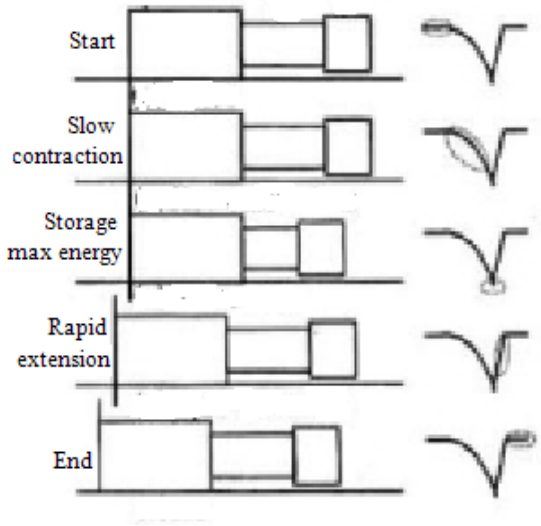

Figure 1.12 : *impact drive principle [* (Stepping principles, 2010)*]*

1.4.5. Resonant drive

Resonant drive mechanisms are frequently used in the field of ultrasonic motors (USM) and it is defined by inertial slip generation with contact force variation [(Driesen, 2008)]. According to this definition, the motion is generated by variation of the contact force, where the contact force variation is the inertial effect of a vertical vibration, which results from the back-and-forth motion of the robot body. Therefore to increase the inertial force, one must increase the horizontal vibration and consequently the frequency of feet vibration. Motion occurs when this inertial force becomes larger than the maximum friction force between feet and substrate. So we must increase the frequency until a threshold where motion occurs. As examples for piezoelectric mobile miniature robot:

1- Based on the configuration of inclined vibrating legs, two miniature robots are developed at the Uppsala University. The first one is actuated by multilayer piezoceramic legs and the second is developed within the scope of I-Swarm project [(SWARMS, 2010)], it is named I-Swarm robot and it is actuated by a monolithic structure of a piezoelectric polymer (P(VDF-TrFE)) [(Edqvist, et al., 2008)].
2- A minirobot based on SWUSM is presented in [(Ferreira, et al., 1997)], The SWUM consists of a piezoelectric plate assembled to the metallic resonator.
3- A minirobot based on bidirectional SWUSM is proposed in [(Son, et al., 2006)]. The bidirectional SWUSM consists of two piezoelectric-metal composite beams vibrating in resonance mode (Figure 1. 13).

4- A mobile minirobot developed at EPFL [(Cimprich, et al., 2006)], actuated in the resonance mode by 3 monolithic piezoelectric push-pull actuators (Figure 1.13).

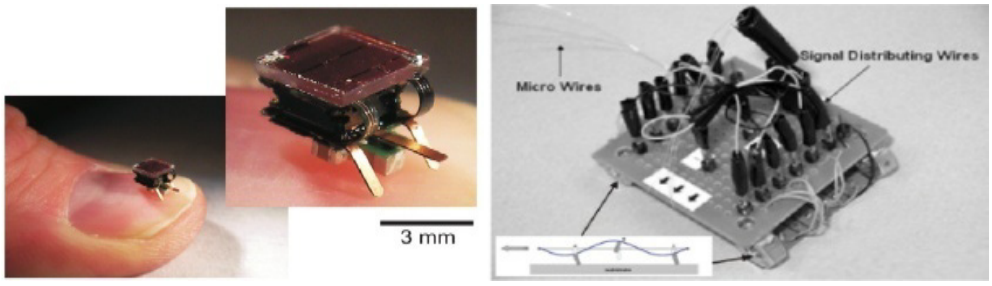

Figure 1. 13: Resonant drive examples

1.4.6. Friction drive

In this case, the generation of motion is due to the change of friction coefficient during horizontal vibration of robot body. The change of friction coefficient results from a no-perpendicular contact angle between robot feet and substrate. It differs from the resonant drive by the fact that, in the resonant drive the horizontal vibration generates the inertial vibration, that in turn generates the motion of the robot; in the friction drive, no inertial force vibration occurs during horizontal vibration but a change in the friction coefficient, which causes a motion in the direction of low friction without intervention of the inertial force. As examples for piezoelectric miniature robots using this mode, we can take:

1- A mobile tube wall miniature robot consists of piezoelectric bimorph actuator with four flexible fins attached to it [(Aoshima, et al., 1993)] as shown Figure 1.14.
2- A microrobot based on the friction drive, driven by piezoelectric actuators is presented in [(Ishihara, et al., 1995)].
3- A microrobot proposed in [(Matsuoka, et al., 1993)] actuated by two piezoelectric unimorph disk actuators.

A novel type of locomotion proposed by Driesen et al. [(Driesen, Breguet, & Clavel, 2006)], can be classified as a mix between resonant and friction drive, it based on the superposition of a variation of the contact force and a horizontal vibration generating a periodic slip at the interface between robot and work floor. In the same manner, we can classified the miniature robots taken in example 1, presented in the section inertial drive as a mix between resonant and friction drive due to the use of inclined vibrating legs.

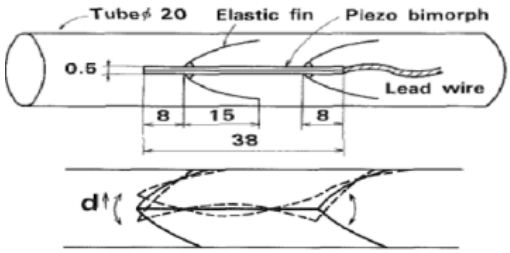

Figure 1. 14: Friction drive examples [(Aoshima, et al., 1993)]

1.4.7. Summary of miniature robots on a solid substrate

Find below a summarized table (Table 1. 1) for piezoelectric miniature robots on a solid substrate.

Institution	Brief description	Reference
Penn state university, USA	The world-smallest 4W vehicle driven by two metal tube USM	[(Uchino, 2006)]
EPFL, Switzerland	A miniature robot called Jemmy driven by rotating piezomotors	[(Driesen, 2008)]
Seiko Epson Corporation, Japan	a miniature robot called Monsieur II-P driven by two ultra thin ultrasonic motors	[(Epson, 2010)]
Karlsruhe Institute of Technology (KIT), Germany	A piezoelectric walking robot called SPIDER-II actuated by 9 piezoelectric bimorph	[(Rembold, et al., 1997)]
Department of Materials Science, Uppsala University, Sweden	MINIMAN V robot consists of two monolithic piezoelectric drive units put together back to back. The top drive unit is intended for locomotion whiles the button for manipulating. Each drive unit has six monolithic piezoelectric legs.	[(Simu & Johansson, 2002)]

Institution	Brief description	Reference
Uppsala University, Department of Engineering Sciences Department of Physics and Materials Science, Sweeden	The module consists of four feet actuated by monolithic multilayer piezoelectric benders	[(MiCRoN, 2010)]
NanoRobotics Laboratory, Department of Computer Engineering and Institute of Biomedical Engineering, École Polytechnique de Montréal (EPM), Campus of the Université de Montréal, Montréal (Québec) Canada	one jumping miniature robot actuated by 3 piezoelectric drive units	[(Nguyen, et al., 2006)]
Dept. of Mech. Eng. & Intelligent Syst., Univ. of Electro-Commun., Chofu, Japan	A two mobile mini- and microrobots with inchworm locomotion driven by piezoelectric actuators and electromagnetic clamps	[(Aoyama, et al., 2001), (Fuchiwaki, et al., 2002)]
Inst. of Robotics, Eidgenossische Tech. Hochschule, Zurich	A mobile minirobot driven by three, triangularly arranged piezoelectric stack actuators	[(Codourey, et al., 1995)]
Aichi Institute of Technology, Toyota, Japan	A mobile minirobot driven by three, triangularly arranged piezoelectric stack actuators	[(Koyanagi, et al., 2000), (Torii, et al., 2001)]
Department of Precision Instruments and Mechanology, Tsinghua University, China	minirobot consists of one piezoelectric stack actuator and four electromagnetic clamps	[(Yan, et al., 2006)]
School of Engineering & Appied Sciences, Harvard University, Cambridge, UK. Department of Electrical Engineering & Computer Sciences, University of California, Berkeley, USA.	A biomimetic micro crawling robot built using smart composite microstructures (SCM) is made of articulated microstructures integrated with piezoelectric actuators, wiring, and sensors	[(J.Wood, 2008), (Wood, et al., 2008)]

Institution	Brief description	Reference
Dept. of Mech. Syst. Eng., Kyushu Inst. of Technol., Fukuoka, Japan	A cybernetic in-pipe impact drive actuator based on impact drive principle and actuated by two piezo stacks	[(Ikuta, et al., 1991)]
Karlsruhe Institute of Technology (KIT), Germany	A miniature robot called SPIDER-I based on stick-slip principle and actuated by 3 times 2 piezoelectric bimorph actuators connected in series	[(Rembold, et al., 1997)]
Uppsala University, Sweden	I-swarm robot is based on the configuration of inclined vibrating legs and actuated by a monolithic structure of a piezoelectric polymer	[(Edqvist, et al., 2008)]
Electrotechnical Laboratory, Intelligent Systems Division, Autonomous Systems Section, Tsukuba,Japan. Laboratoire de Mécanique Appliquée, Besançon, France	A minirobot based on SWUSM, consists of a piezoelectric plate assembled to the metallic resonator	[(Ferreira, et al., 1997)]
Department of Mechanical Engineering, Carnegie Mellon University, Pittsburgh,USA	A minirobot based on bidirectional SWUSM consists of two piezoelectric-metal composite beams vibrating in resonance mode	[(Son, et al., 2006)]
EPFL, Switzerland	A mobile minirobot actuated in the resonance mode by 3 monolithic piezoelectric push-pull actuators	[(Cimprich, et al., 2006)]
NTT Transmission Systems Laboratories, Ibaraki-Ken, Japan	A mobile tube wall miniature robot consists of piezoelectric bimorph actuator with four flexible fins attached to it	[(Aoshima, et al., 1993)]
Dept. of Micro Syst. Eng., Nagoya Univ., Japan	A microrobot based on the friction drive, driven by piezoelectric actuators	[(Ishihara, et al., 1995)]

Institution	Brief description	Reference
MEITEC Corp., Nagoya, Japan	A microrobot actuated by two piezoelectric unimorph disk actuators	[(Matsuoka, et al., 1993)]

Table 1. 1: Piezoelectric miniature robot on a solid substrate

1.5. Locomotion in liquid

The movement in liquid is totally inspired from animal locomotion and is divided into locomotion inside liquid and locomotion at the liquid surface. The design of miniature robots in aquatic medium depends on the liquid properties; the forces were acting on and some factors influencing the locomotion. The forces acting on miniature robots inside liquid are thrust, drag, weight buoyancy and hydrodynamic lift (Figure 1.15).

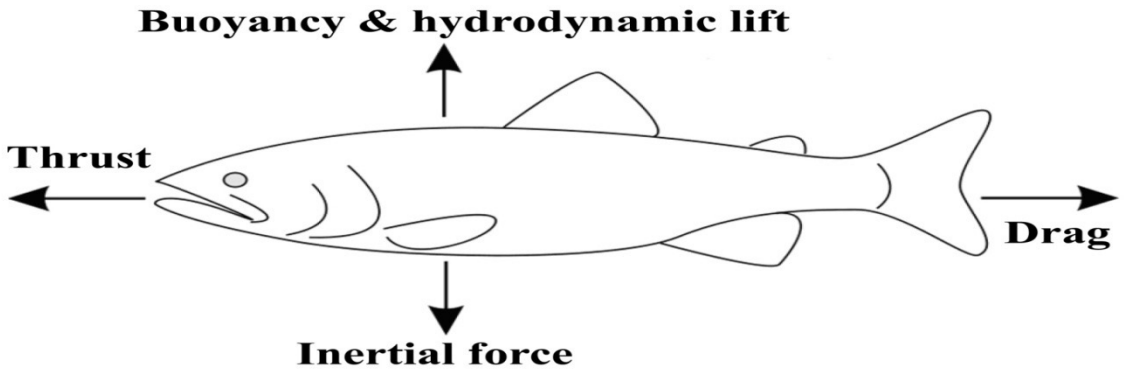

Figure 1.15 : *The forces acting on a swimming fish*

The thrust here is defined as the force generated by moving portions of the miniature robot body on the fluid surrounding it, to move miniature robot forward. The inertial force depends on the body mass while the buoyancy force is generated by fins and it depends on the mass of fluid displaced. The hydrodynamic lift is generated by fins to supplement buoyancy and balance the vertical forces when horizontal motion is demanded. The drag is the resistive force exerted by the fluid on its body and it consists of viscous drag and pressure drag. Viscous drag is skin friction between the miniature robot and boundary layer of water. The pressure drag exerted by distortions of flow around miniature robot body and energy lost in the vortices formed by the fins as they generate lift or thrust. At the liquid surface, the forces acting on miniature robots are the same but in this case the miniature robots use the surface

tension of liquid which represents the work required to deform a liquid over a unit area [(BIEWENER, 2003)] to generate lift, buoyancy and thrust, or they use the mass density of liquid to generate these forces. An important factor influencing the locomotion for miniature robots in liquid is the Reynolds number (Re) that describes the viscous versus inertial forces. At low Re viscous forces reign, but at high Re inertial forces dominate. This has important consequences for the propulsive mechanisms and design for locomotion at low and high Re [(BIEWENER, 2003)]. The Froude number (Fr) is also an important factor that describes the propulsive efficiency of the miniature robots. It is the ratio of the useful propulsive power over the total power expended by the mobile miniature robots. As already mentioned the design of miniature robots in aquatic medium depends on surface tension of liquid, density of liquid, Reynolds number and the forces were acting on, locomotion principles itself are not influenced by the type of liquid. So, the study of locomotion principles in any type of liquid is the same, we then consider the case of water in the following. As the movement in liquid for mobile miniature robots is totally inspired from animal locomotion, a study of animal locomotion in water is given in this section, with some applications in the field of piezoelectric miniature robots.

1.5.1. Locomotion inside water

Locomotion inside water includes swimming or non-swimming locomotion. The latter includes specialized actions such as flying and gliding, as well as jet propulsion. In this section, we will describe only the swimming locomotion because it is the most used in the field of miniature robot and it is divided into fish swimming mechanisms (at high and moderate Re) and micro-organisms swimming mechanisms (at low Re).

1.5.1.1. Fish swimming mechanisms

To aid in the description of fish swimming mechanisms; Figure 1.16 identifies the elements of fish. The fish swims either by body and/or caudal fin (BCF) movements or using median and/or paired fin (MPF) propulsion.

The BCF propulsion has been classified into five swimming modes: Anguilliform, subcarangiform, carangiform, thurnniform and ostraciform. The latter is the only oscillatory BCF mode; it is characterized by the pendulum oscillation of the caudal fin, while the body remains essentially rigid. The others are undulatory BCF modes. In anguilliform mode, ondulations of large amplitude are obtained by whole body.

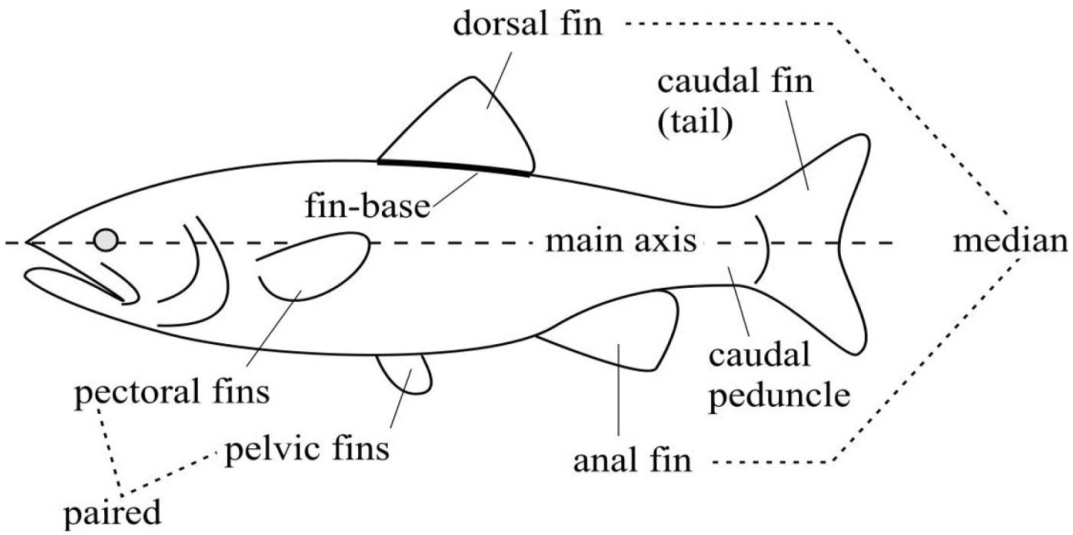

Figure 1.16 : Elements of fish [(Sfakiotakis, et al., 1999)]

Similarly for subcarangiform mode, but the amplitude of undulations is limited in front and increased in the latter half of the body. For carangiform mode, the amplitude of the undulations is limited to the last third of the body. In thunniform mode, the thrust is generated by the caudal fin only.

The MBF propulsion has been classified into seven swimming modes: Rajiform, diodontiform, amiiform, gymnotiform, balistiform, labriform and tetraodontiform. The two latter modes are classified into undulatory fin motions, while the five remaining are classified into oscillatory fin motions. In rajiform mode, the most of the body length undulate vertically along the pectorals that are flexible and very long. Similarly, in diodontiform mode, thrust is generated by the pectoral fins but they are not in the same level and the same shape as that in mode Rajiform. In amiiform mode, propulsion is obtained by undulations of a long-based dorsal fin. Contrary, in gymnotiform mode, propulsion is obtained by undulations of a long-based anal fin. In balistiform mode, both the anal and dorsal fins undulate to generate thrust. In labriform mode, thrust is generated by oscillatory movements of the pectoral fins. In tetraodontiform mode, the dorsal and anal fins beat together, either in phase or alternating phase to generate thrust. Figure 1.17 describes fish swimming modes.

Some piezoelectric miniature robots like swimming fishes are developed in [(Fukuda, et al., 1994),(Tzeranis, et al., 2003), (Borgen, et al., 2003),(Deng, et al., ICRA 2005), (Kodati, et al., 2007), (Wiguna, et al., 2006),(Hu, et al., 2006)], where piezoelectric actuators are used for producing the movements of BCF and MPF for miniature robots. The choice between swimming modes in liquid depends on the application expected. For example the design of thunniform swimmers miniature robots is optimized for high speed swimming in calm waters

and is not well suited to other actions such as slow swimming, turning maneuvers and rapid acceleration from stationary and turbulent water [(Sfakiotakis, et al., 1999)]. Example is given in Figure 1.18.

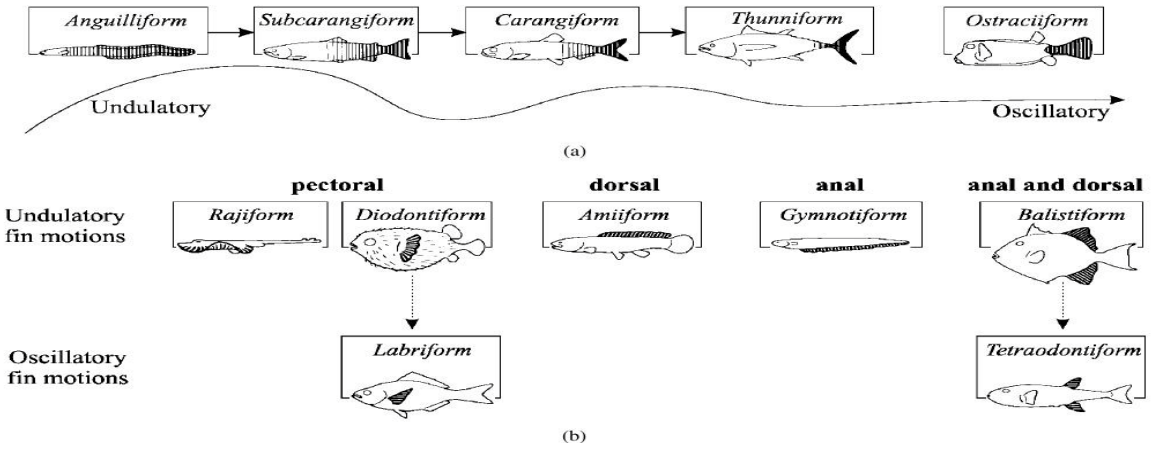

Figure 1.17 : *Swimming modes associated with (a) BCF propulsion and (b) MPF propulsion. Shaded areas contribute to thrust generation [*(Sfakiotakis, et al., 1999)*]*

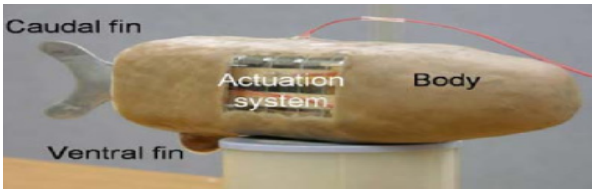

Figure 1. 18: Fish swimming locomotion example

1.4.1.2. Micro-organisms swimming mechanisms

All the micro swimming mechanics such as flagella, spermatozoa, cilia, and amoeba crate in one way or another traveling wave, advanced in the opposite direction of the micro organisms locomotion. The swimming mechanics of micro-organisms are divided into flagellar and ciliary swimming.

Flagellar swimming is the simplest swimming method for micro system and is produced by a sinusoidal or helical wave in an elastic tail. In contrast of flagella, cilia beat in asymmetrical fashion i.e. by orienting the cilia parallel to the flow during the recovery stroke much lower drag is produced than when they beat in a more perpendicular orientation during the propulsive stroke [(BIEWENER, 2003)].

Piezoelectric actuators are used in [(Kosa, et al., 2007), (Kosa, et al., 2008)] for creating the travelling wave needed for the movements of swimming micro organisms (Figure 1. 19).

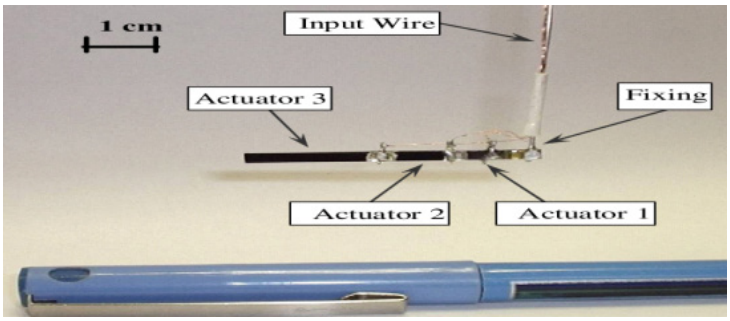

Figure 1. 19: Micro-organisms locomotion example

1.5.2. Locomotion at the water surface

Locomotion at the water surface is divided into two different locomotion principles: striding on the water surface like water striders and running on the water surface like a basilisk lizard. Water striders take advantage of their size by using the surface tension of water to generate forces in order to step over the surface of water. These forces increase with the depth of the unwetted limb of the water striders [(BIEWENER, 2003)]. Basilisk lizard have a weight which is larger than the surface tension can support, it takes advantage of the mass density of the water, which exerts a reactive force when running rapidly with its webbed feet [(BIEWENER, 2003)]. As example we take the water strider miniature robot walking on water describes in [(Suhr, et al., 2005)] (Figure 1.20).

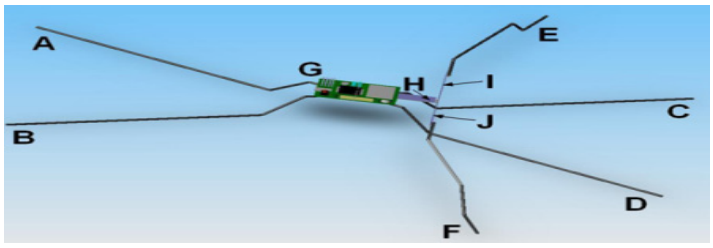

Figure 1. 20: Locomotion example at the water surface

1.5.3. Summary of piezoelectric miniature robots inside and on liquid

Find below a summarized table (Table 1.2) for piezoelectric miniature robots inside and on liquid.

Institution	Locomotion principles	Reference
Nagoya University in Japan	Micro-mobile robot in water, which possesses a pair of fins and moves them symmetrically (pectoral).	[(Fukuda, et al., 1994), (Fukuda, Kawamoto, Arai, & Matsuura, 1995)]
National Technical University of Athens, Greece.	A small autonomous robotic vehicle driven by an oscillating foil (ostraciiform).	[(Tzeranis, et al., 2003)]
Dept. of Mech. Eng., Ohio State Univ., Columbus, OH, USA	A miniature swimming vehicle that propels itself through oscillations of a flexible fin mounted in the stern (ostraciiform).	[(Borgen, et al., 2003)]
Dept. Mechatronics Engineering, Incek, Ankara, Turkey	Fish-like swimming mini robot, that propels by oscillating its tail fin(ostraciiform).	[(Tunçdemir, et al., 2004)]
Robotics and Intelligent Machines Laboratory University of California, Berkeley	Micro underwater vehicle mimicking a boxfish , with rigid body propelled by a oscillating tail fin (ostraciiform) and steered by a pair of independent side fins (tetraodontiform)	[(Deng, et al., ICRA 2005)]
NanoRobotica Lab at Carnegie Mellon University, Pittsburgh, USA	Miniature water strider miniature robot walking on water, biologically inspired from water strider	[(Suhr, et al., 2005), (Song, et al., 2007)]

Institution	Locomotion principles	Reference
Konkuk University, Korea	Biomimetic fish miniature robot uses subcarangiform, ostraciiform and thunniform caudal fins as swimming modes.	[(Wiguna, et al., 2006), (Heo, et al., 2007), (Wiguna, Heo, Park, & Goo, 2009), (Nguyen, et al., 2010)]
Inst. of Autom., National Univ. of Defense Technol., Changsha,China.	An underwater bio-robot inspired by Rhinecanthus aculeatus, which belongs to median and/or paired fin (MPF) propulsion fish and impresses researchers with agility by cooperative undulation of the dorsal-and-anal fins (balistiform)	[(Hu, et al., 2006)]
Dept. of Mech. Eng., Technion - Israel Inst. of Technol., Haifa	Microrobot powered by traveling waves in elastic tails, for maneuvering inside the human body(flagellar swimming)	[(Kosa, Shoham, & Zaaroor, 2007)]
Delaware Univ., Newark, USA	Micro autonomous robotic uses Ostraciiform mechanism as swimming mode.	[(Kodati, et al., 2007)]
Dept. of Inf. Technol. & Electr. Eng., ETH Zurich, Swiss	Medical micro robot using flagellar swimming method.	[(Kosa, et al., 2008)]

Table 1.2 : Piezoelectric miniature robots in liquid

1.6. Locomotion in air

The movement in air for mobile robots is classified into two groups: active air vehicle and passive air vehicle. The first group is divided into three different locomotion principles: flapping, rotary and fixed wing. The passive air vehicle consists of one locomotion principle, the gliding flight. Like in liquid locomotion, the Reynolds number (Re) is an important parameter in the design of flight vehicles, and it is defined in the same manner. The Re varies linearly with air vehicle weight [(Mueller, 1999)], so miniature air vehicles (MAVs) operate at low Re where the viscous forces dominate. The flapping wing method is the most efficient way for MAVs because it generates the greatest thrust with the same power expended, among the other methods and it is the most used in the field of piezoelectric miniature robots, for this reason, it is the only method described here.

1.6.1. Flapping wing MAV

Unsteady state flow aerodynamics is obtained in the case of flapping wing MAV, because leading-edge vortices (LEV) are formed during downstroke wing (Figure 1.22) and are shed at the start of the upstroke and so on. LEV helps to generate a high lift coefficient during flight and according to the movements of wings and wind, forward thrust is generated during downstroke movement and drag is generated during upstroke (Figure 1.23). As examples for piezoelectric flapping wings MAV, see references [(Sitti, 2001), (Campolo, et al., 2003), (Park, et al., 2006), (Nguyen, et al., 2007), (Ming, et al., 2008)] as shown Figure 1. 21. Below some piezoelectric flapping wing MAVs are given.

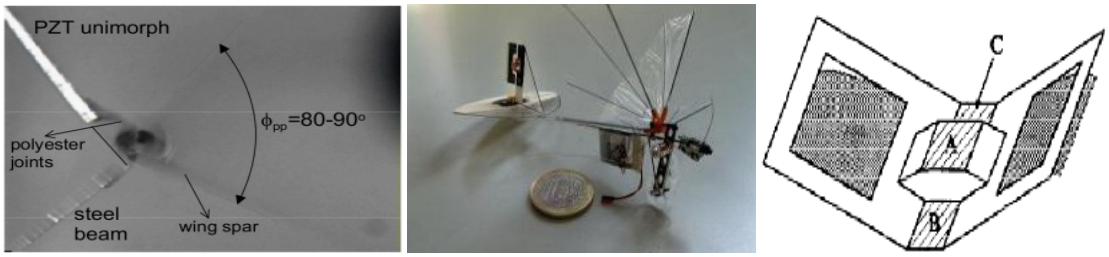

Figure 1. 21: Flapping wing MAV examples

Figure 1.22 : LEV are formed during downstroke

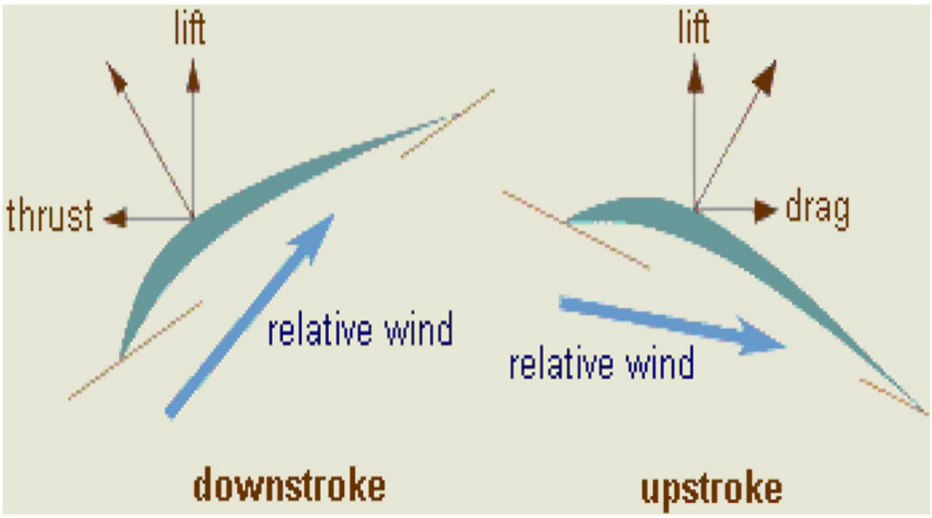

Figure 1.23 : Forces acting on wings during up and down movement

Institution	Brief description	Reference
Dept. of Electr. Eng. & Comput. Sci., California Univ., Berkeley, CA, USA	Inspired by biological insect flight, an autonomous flight microrobot is developed using 2 flapping wings	[(Yan, et al., 2001)]
Dept. of Electr. Eng. & Comput. Sci., California Univ., Berkeley, CA, USA	PZT actuated four-bar mechanism with two flexible links for micromechanical flying insect thorax	[(Sitti, 2001)]
Department of Mechanical Engineering, Vanderbilt University, Nashville, TN, USA	Development of Elastodynamic Components for Piezoelectrically Actuated Flapping Micro-Air Vehicle	[(Cox, et al., 2002)]
Dept. of Electr. Eng. & Comput. Sci., California Univ., Berkeley, CA, USA	Two types of biomimetic gyroscopes have been constructed using foils of stainless steel	[(Wu, et al., 2002)]
Dept. of Electr. Eng. & Comput. Sci., California Univ., Berkeley, CA, USA	Inspired by biological insect, design of a microrobot using wing rotation at the end to increase maneuverability for flying flapping wings	[(Yan, et al., 2002)]

Institution	Brief description	Reference
Dept. of Electr. Eng. & Comput. Sci., California Univ., Berkeley, CA, USA	Development of piezoelectric bending actuators for micromechanical flapping mechanisms	[(Campolo, et al., 2003)]
Artificial Muscle Research Center, Department of Aerospace Engineering, Konkuk University, 1 Hwayang, Korea	An Insect-Mimicking Flapping System	[(Park, Syaifuddin, Goo, Byun, & Yoon, 2006)]
Harvard Univ., Cambridge, USA	Flight of an insect-sized robotic fly	[(Wood, 2007)]
Dept. of Adv. Technol. Fusion, Konkuk Univ., Seoul, South Korea	Flying insect-like flapper actuated by a compressed LIPCA	[(Nguyen, et al., 2007)]
Dept. of Mech. Eng. & Intell. Syst., Univ. of Electro-Commun., Chofu,Tokyo	Develop flapping robots using a new type of piezoelectric material, (piezoelectric fiber composites)	[(Ming, et al., 2008)]
Dept. of Mater., Cranfield Univ., Bedford, UK	Coupled piezoelectric fans with two degree of freedom motion for the application of flapping wing micro aerial	[(Chung1, et al., 2008)]
Institut Polytechnique de Grenoble, France	Modeling and control of a piezoelectric flapping wing biomimetic robot	[(Rifai, 2008)]
Army Research Laboratory, USA	Bio-Mimetic Millimeter-Scale Flapping Wings for Micro Air Vehicles	[(Kroninger, et al., 2009)]

Table 1.3 : piezoelectric flapping wing MAVs

1.7. Conclusion and discussion

At the beginning, it is useful to remind that our goal in this thesis is to realize a terrestrial piezoelectric miniature robot by generating a traveling wave on the plate taken as the shape of the Manta ray fish and to propose at the end a design for aquatic locomotion based on the same plate shape (Manta ray form).

This review does not include all locomotion principles for robots. It was dedicated on locomotion principles for the existing piezoelectric miniature robots only.

After reading this review and looking in particular at the locomotion on a solid substrate, we can notice that the plate shape that we have proposed uses resonant drive locomotion. As we have seen in this chapter, section 1.4.5, in resonant drive principle the piezoelectric actuators

are used at their resonant frequency to produce maximal deformation and it is defined in [(Driesen, 2008)] by inertial slip generation with contact force variation, so motion occurs when the inertial force becomes larger than the maximum friction force. This principle is frequently used in standing wave and traveling wave type ultrasonic motors. As we are interested to generate a traveling wave on the plate (Manta ray shape), our design will be inspired from traveling wave motors and it will be for robotics application.

we can note that the Manta ray fish uses inside water the Median and/or Paired Fin (MPF) for propulsion, more precisely it uses the Rajiform mode (most of the body length undulate vertically along the pectorals that are flexible and very long) to generate the thrust needed to move. Outside the water, the Manta ray fish uses the flapping wings (flapping pectorals fins that are flexible and very long) to generate the thrust needed to fly over water. The most of piezoelectric miniature robots fishes in literature use Body and/or Caudal Fin (BCF) propulsion to generate movements because it is easy to design, manufacture and control it while, the design and the control of MPF propulsion to create the undulation needed for propulsion are more complicated. The question arises now is can we propose at the end of this thesis a design for undulatory propulsion piezoelectric miniature robot in water for our earth piezoelectric miniature robot?

Our conclusion is that, the operation principle of traveling wave ultrasonic motors (resonant drive locomotion) will be used to generate the traveling wave on the plate (Manta ray shape), we should begin now to study the modeling of our system that is composed of thin structure with piezoelectric patches bonded on it.

The second chapter includes an introduction to modeling thin structures with piezoelectric patches in the general case while the third is dedicated to modeling of non-collocated piezoelectric patches bonded on thin structures taking a particular case of study.

1.8. References

Aoshima S.-I., Tsujimura T. et Yabuta T. Miniature mobile robot using piezo vibration for mobility in a thin tube [Revue] // Journal of Dynamic Systems, Measurement and Control, Transactions of the ASME, vol. 115, no. 2 A. - 1993. - pp. pp. 270–278.

Aoyama H. et Fuchiwaki O. Flexible micro-processing by multiple micro robots in SEM [Revue] // IEEE Int. Conf. on Robotics and Automation, ICRA '01, vol. 4. - 2001. - pp. 3429–3434.

Asari V.K., Kumar S. et Kassim I.M. A Fully Autonomous Microrobotic Endoscopy System [Revue] // Journal of Intelligent and Robotic Systems 28. - 2000. - pp. pp. 325–341.

BIEWENER A. Animal locomotion [Livre]. - [s.l.] : Oxford university press, 2003.

Borgen M.G., Washington G.N. et Kinzel G.L. Design and evolution of a piezoelectrically actuated miniature swimming vehicle [Revue] // IEEE/ASME transactions on mechatronics, volume 8. - 2003. - pp. pp. 66 -76.

Campolo D., Sahai R. et Fearing R. Development of piezoelectric bending actuators with embedded piezoelectric sensors for micromechanical flapping mechanisms [Revue] // in IEEE International Conference on Robotics and Automation, vol. 3. - 2003. - pp. pp. 3339–3346.
Caprari G. Autonomous Micro-Robots: Applications and limitations [Livre]. - Lausanne : Swiss Federal Institue of Technology Lausann, 2003.
Carrozza M.C., Lencioni L. et Magnani B. The Development of a Microrobot System for Colonoscopy [Revue] // Proceedings Conference on Computer Vision, Virtual Reality and Robotics in Medicine and Medial Robotics and Computer-Assisted Surgery. - 1997. - pp. pp. 779-788.
Chung1 Hsien Chun [et al.] Coupled pie-zoelectric fans with two degree of freedom motion for the application of flapping wing micro aerial ve-hicles [Revue] // Sensors and Actuators A (Physical). - 2008.
Cimprich T. [et al.] Ultrasonic monolithic piezoelectric multi DOF actuators for mobile microrobots [Revue] // in Proc. Int. Conf.on New Actuators, ACTUATOR ’06. - 2006. - pp. pp. 114–117.
Codourey A. [et al.] A robot system for automated handling in micro-world [Revue] // Proc. IEEE/RSJ Int. Conf. on Intelligent Robots and Systems, IROS ’95, vol. 3. - 1995. - pp. pp. 185–190.
Cox A. [et al.] The Development of Elastodynamic Com-ponents for Piezoelectrically Actuated Flapping Micro-Air Vehicles [Revue] // Journal of Intelligent Material Systems and Structures, Vol. 13, No. 9. - 2002. - pp. 611-615 .
Dario P. [et al.] Microactuators for microrobots: a critical survey [Revue] // Journal of Micromechanics and Microengineering, vol. 2, no. 3. - 1992. - pp. 141–157.
Deng X. et Avadhanula S. Biomimetic Micro Underwater Vehicle with Oscillating Fin Propulsion: System Design and Force Measurement [Revue] // Proceedings of the 2005 IEEE International Conference on Robotics and Automation. - ICRA 2005. - pp. pp. 3312 – 3317.
Driesen W. Concept modeing and experimental characterization of the modulated fric-tion inertial drive (MFID) Locomotion principle Application to mobile microrobots [Livre]. - Lausanne : Swiss Federal Institue of Technology, 2008.
Ebefors T. et Stemme G. Microrobotics [Section du livre] // MEMS Handbook / auteur du livre Hak M. Gad-el. - Boca Raton : FL: CRC Press, 2005.
Edqvist E. [et al.] The assembly of millimetre sized mass producible autonomous robots [Revue] // in Proc. Int. Conf. on New Actuators, ACTUATOR ’08. - 2008. - pp. pp. 304–307.
Epson News Release: Epson to Unveil a Prototype Microrobot with Ultra-thin, Ultrasonic Motor and Power-Saving Bluetooth Module [En ligne]. - 2010. - http://global.epson.com/newsroom/news_2003_03_10.htm.
Ferreira A. et Minotti P. Control of a multidegree of freedom standing wave ultrasonic motor driven precise positioning system [Revue] // Review of Scientific Instruments,vol. 68, no. 4. - 1997. - pp. pp. 1779–1786.
Fuchiwaki O. et Aoyama H. Piezo based micro robot for microscope instrument [Revue] // Proc. Int. Conf. on Mechatronics Technology, ICMT ’02. - 2002. - pp. pp. 499–503.
Fukuda T. [et al.] Mechanism and swimming experiment of micro mobile robot in water [Revue] // proceedings of 1994 IEEE International Conference on Robotics and Automation, volume 1. - 1994. - pp. pp. 814-819.
Heo S. [et al.] Effect of an Artificial Caudal Fin on the Performance of a Bio-mimetic Fish Robot Propelled by Piezoelectric Actuators [Revue] // Journal of Bionic Engineering 4. - 2007. - p. pp. 151−158.
Hu T. [et al.] A Novel Conceptual Fish-like Robot Inspired by Rhinecanthus Aculea-tus [Revue] // ’’, 9th International Conference on Control, Automation, Robotics and Vision. - 2006. - pp. pp. 1 – 5.
Ikuta K., Kawahara A. et Yamazumi S. Miniature cybernetic actuators using piezoelectric device [Revue] // in Proc. IEEE Micro Electro Mechanical Systems, MEMS ’91. - 1991. - pp. pp. 131–136.
Ishihara H. [et al.] Approach to distributed micro robotic system development of micro line trace robot and autonomous micro robotic system [Revue] // in Proc. IEEE Int. Conf. on Robotics and Automation, ICRA’95, vol. 1. - 1995. - pp. pp. 375–380.
ISO 8373 // International Organisation of Standarisation ISO.

J.Wood R The first takeoff of a Biologically Inspried At-Scale Robotic Insect [Revue] // Trans. On Robotics, Vol. 24, No. 2. - 2008. - pp. pp.341-347.
Kodati P., Hinkle J. et Deng X. Micro Autonomous Robotic Ostraciiform (MARCO): Design and Fabrication [Revue] // IEEE International Conference on Robotics and Automation. - 2007. - pp. pp. 960 – 965.
Kosa G. [et al.] Flagellar swimming for medical micro robots: Theory, experiments and application [Revue] // 2nd IEEE RAS & EMBS International Conference on Biomedical Robotics and Biomechatronics. - 2008. - p. pp. .
Kosa G., Shoham M. et Zaaroor M. Propulsion Method for Swimming Microrobots [Revue] // IEEE Transactions on Robotics. - 2007. - pp. pp. 137 -150.
Kovac M. Bioinspired Jumping Locomotion for Miniature Robotics. - Lausane : EPFL, 09 07 2010.
Koyanagi T. [et al.] Miniature robots with three degrees of freedom [Revue] // Proc. IEEE Int. Symp. On Micromechatronics and Human Science, MHS'00,. - 2000. - pp. pp. 207–212.
Kroninger Christopher [et al.] Bio-Mimetic Millimeter-Scale Flapping Wings for Micro Air Vehicles [Revue]. - 2009.
Lee D.G. et suh N.P. axiomatic design and fabrication of composite structures applications in robots machine tools and automobiles [Livre]. - Oxford : Oxford university Press, 2006.
Lim J. [et al.] One pneumatic line based inchworm-like micro robot for half-inch pipe inspection [Revue] // Mechatronics 18. - 2008. - pp. pp. 315–322.
Matsuoka T. [et al.] Mechanical analysis of micro mobile machine with piezoelectric element [Revue] // in Proc.IEEE/RSJ Int. Conf. on Intelligent Robots and Systems, IROS '93. - 1993. - pp. pp. 1685–1690.
May W. G. [Brevet] : 3,902,084. - Piezoelectric Electromechanical Translation Apparatus. U.S. Patent, 1975..
Menciassi A. [et al.] Development of a biomimetic miniature robotic crawler [Revue] // Autonomous Robot 21. - pp. pp. 155–163.
MiCRoN Miniaturised Co-operative Robots advancing towards the Nanorange MiCRoN [En ligne]. - 2010. - http://lsro.epfl.ch/page66048.html.
Ming Aiguo [et al.] Development of an active flapping wing using Piezoelectric Fiber Composites' [Revue] // IEEE International Conference on Robotics and Biomimetics. - 2008. - pp. pp. 2144-2149.
MINIMAN Miniaturised Robot for Micro Manipulation:MINIMAN [En ligne]. - 2010. - http://rob.ipr.kit.edu/projekte_649.php.
Mueller T. J. Aerodynamic Measurements at Low Reynolds Numbers for Fixed Wing Micro-Air Vehicles [Revue] // Hessert Center for Aerospace Research, University of Notre Dame. - 1999.
Nguyen A.T. et Martel S. Embedded piezo-actuation system for automatic motion control of a fleet of miniature robots operating on a synchronized vibrating platform [Revue] // Sixth World Congress on Intelligent Control and Automation. - 2006.
Nguyen Q.S. [et al.] Performance evaluation of an improved fish robot ac-tuated by piezoceramic actuators [Revue] // Journal of Smart Materials and Structures, Volume 19, Number 3. - 2010.
Nguyen Quoc-Viet [et al.] A flying insect-like flapper actuated by a com-pressed LIPCA [Revue] // IEEE International Conference on Robotics and Biomimetics. - 2007. - pp. pp. 19 – 24.
Park H. Cheol [et al.] An Insect-Mimicking Flapping System Actuated by A Piezoceramic Actuator [Revue] // IEEE International Conference on Robotics and Biomimetics. - 2006. - pp. pp.451-456.
Penella Jordi Brufau Smart materials for micro robotics motion control and power harvesting [Rapport]. - Barcelona : [s.n.], 2005.
Phee L. [et al.] Analysis and Development of Locomotion Devices for the Gastrointestinal Tract [Revue] // IEEE transactions on biomedical engineering, vol. 49, no. 6. - 2002.
Rembold U. et Fatikow S. Autonomous Microrobots [Revue] // Journal of Intelligent and Robotic Systems, vol. 19, no. 4. - 1997. - pp. pp. 375–391.
Rifai Hala Modelisation et commande d'un robot biomimetique volant [Rapport]. - France : Institut polytechnique de Grenoble , 2008.

Sfakiotakis M., Lane D.M. et Davies JBC Review of fish swimming modes for aquatic locomotion [Revue] // IEEE Journal of Oceanic Engineering 24-2. - 1999. - pp. 237–252.
Simu U. et Johansson S. Analysis of static and dynamic motion mechanisms for piezoelectric miniature robots. [Revue] // journal of Sensors and actuators. - 2006.
Sitti M. PZT actuated four-bar mechanism with two flexible links for micromechanical flying insect thorax [Revue] // Proceedings ICRA. IEEE International Conference on Robotics and Automation, vol.4. - 2001. - pp. pp. 3893 – 3900.
Snis N., Simu U. et Johansson S. Piezoelectric drive platform for cm3 sized autonomous robot [Revue] // ACTUATOR 04. - 2004. - pp. pp. 106–109.
Son K. J. [et al.] An ultrasonic standing-wave-actuated nano-positioning walking robot: Piezoelectric-metal composite beam modelling [Revue] // Journal of Vibration and Control, vol. 12, no. 12. - 2006. - pp. pp. 1293–1309.
Song Y. S. et Sitti M. STRIDE: A Highly Maneuverable and Non-Tethered Water Strider Robot [Revue] // Proc. IEEE Robotics and Automation Conference, Rome, Italy, April . - 2007.
Stepping principles [En ligne]. - 2010. - http://lsro.epfl.ch/page65366.html.
Suhr S. H. [et al.] Biologically Inspired Miniature Water Strider Robot [Revue] // Pro-ceedings of the Robotics: Science and Systems I, Boston, U.S.A.. - 2005. - pp. pp. 319–325 .
Torii A., Kato H. et Ueda A. A miniature actuator with electromagnetic elements [Revue] // Electrical Engineering in Japan (English translation of Denki Gakkai Ronbunshi), vol. 134, no. 4,. - 2001. - pp. pp. 70–75.
Tunçdemir Ş., Koç B. et Erden A. Design of a swimming mini robot [Revue] // the 9th Mechatronics Forum International Conference. - 2004.
Tzeranis D. et Papadopoulos E. on the design of an autonomous robot fish [Revue] // proceedings of 11th Mediterranean Conference on Control and Automation. - 2003. - pp. pp. 17-20.
Uchino K. Expansion from IT/Robotics to ecological/energy applications [Revue] // ACTUATOR 2006. - 2006. - p. p.48.
Wiguna T. [et al.] Mechanical Design of Biomimetic Fish Robot Using LIPCA as Artificial Muscle [Revue] // in Key Engineering Materials, volume: Experimental Mechanics in Nano and Biotech-nology. - 2006. - pp. pp. 1443-1446.
Wood R. J. [et al.] Microrobot Design Using Fiber Rein-forced Composites [Revue] // Journal of Mechanical Design, Vol. 130, No. 5. - 2008. - pp. pp. 052304.1-052304.11.
Wood R.J., the first flight of an insect-sized robotic fly [Revue] // IEEE/RSJ International Conference on Intelli-gent Robots and Systems. - 2007.
Wu W.C., Wood R.J. et Fearing R.S. Halteres for the micromechanical flying insect [Revue] // Proceedings IEEE International Conference on Robotics and Automation. - 2002.
Yan J. [et al.] Thorax design and wing control for a mi-cromechanical flying insect [Revue]. - 2001.
Yan J.1 [et al.] Wing transmission for a micromechanical flying insect [Revue] // J. Micromechatronics (Netherlands). - 2002.
Yan S. [et al.] A 3-DOFs mobile robot driven by a piezoelectric actuator [Revue] // Smart Materials and Structures, vol. 15, no. 1. - 2006.

CHAPTER 2

INTRODUCTION TO THE NUMERICAL MODELING OF THIN STRUCTURES WITH PIEZOELECTRIC PATCHES

Chapter 2: Introduction to the numerical modeling of thin structures with piezoelectric patches

List of figures

2.1. Introduction

As we said in chapter one, the traveling wave generated on the plate will be based on the operation principle of linear traveling wave ultrasonic motors (resonant drive locomotion). These motors are known by the bending beam theory, that is why we will divide the study into bending beam theory and bending plate theory. Later in the manuscript the traveling wave will be generated on the beam first, and then we will take the case of the plate.

Here in this chapter we will present briefly the linear elasticity, mechanical and piezoelectric equations, and then theory of Euler-Bernoulli and Love-Kirchhoff in the case of bending beam and bending plate theory respectively.

We will speak about modeling of thin structures (beams and plates) with piezoelectric patches in the general case, which means without taking a particular case of study. We will talk first about the static and dynamic equations in the case of thin structures with piezoelectric patches in general. Then, we will talk about the numerical modeling of bending vibrations of beams and bending vibrations of plates, also in the general case. These numerical equations of beams and plates are obtained using the variational principle, which is detailed in this chapter. At the end the time discretization using Newmark method is briefly presented.

Many books in literature are talking about piezoelectricity, beams and plates multilayer theory, metal-piezoelectric composite, ultrasonic motors and finite element modeling [(Jaouen, 2005), (Chevalier, 1996), (Brissaud, 2007), (Decolon, 2000), (Gay, 2005), (Sashida, et al., 1993), (Senturia, 2002), (Dhatt, et al., 2005)]. Readers can refer to these books for more details.

Our work can be classified in the case of intelligent structures where smart structures integrated with piezoelectric actuators and/or sensors. Also to be short, I direct readers to [(Chopra, 2002)] where a big review of state of art of smart structures and integrated systems in particularly integrated piezoelectric materials.

2.2. Mechanical equations

It is necessary to use the mechanics of deformable solids to know the static and dynamic behavior of a plate/beam (Figure 2.1).

The state of a deformable solid is characterized by:

- Its strains ε (unitless),
- And stresses σ (N m^{-2}).

Assume also be in the case of linear elasticity.

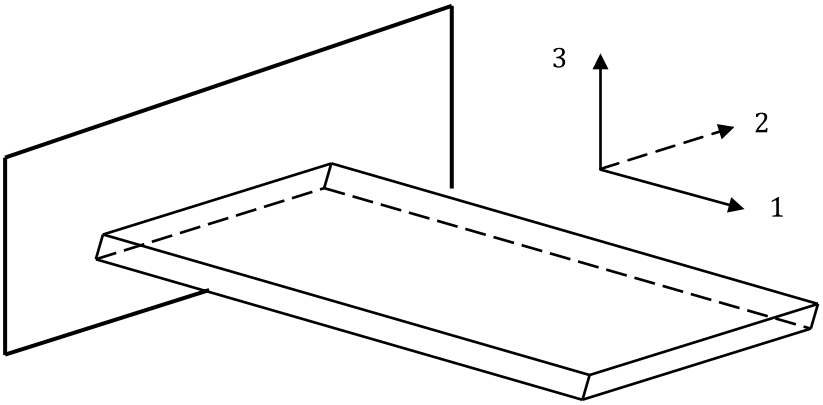

Figure 2.1 : Plate/Beam fixed at one end

2.2.1 Strains

Strains can be represented by a 3×3 tensor.

$$\{\varepsilon\ (\mathrm{M})\} = \begin{bmatrix} \varepsilon_{11} & \varepsilon_{12} & \varepsilon_{13} \\ \varepsilon_{21} & \varepsilon_{22} & \varepsilon_{23} \\ \varepsilon_{31} & \varepsilon_{32} & \varepsilon_{33} \end{bmatrix}$$

2. 1

Assumes that a deformable solid in a 3D orthonormal basis $(1, 2, 3)$ and whose movements along these three axes are u_1, u_2, u_3. So, assuming small strain, the strain tensor is related to the spatial derivatives of displacements as follows:

$$\{\varepsilon\ (\mathrm{M})\} = \begin{bmatrix} \frac{\partial u_1}{\partial x} & \frac{1}{2}\left(\frac{\partial u_1}{\partial y} + \frac{\partial u_2}{\partial x}\right) & \frac{1}{2}\left(\frac{\partial u_1}{\partial z} + \frac{\partial u_3}{\partial x}\right) \\ \frac{1}{2}\left(\frac{\partial u_1}{\partial y} + \frac{\partial u_2}{\partial x}\right) & \frac{\partial u_2}{\partial y} & \frac{1}{2}\left(\frac{\partial u_2}{\partial z} + \frac{\partial u_3}{\partial y}\right) \\ \frac{1}{2}\left(\frac{\partial u_1}{\partial z} + \frac{\partial u_3}{\partial x}\right) & \frac{1}{2}\left(\frac{\partial u_2}{\partial z} + \frac{\partial u_3}{\partial y}\right) & \frac{\partial u_3}{\partial z} \end{bmatrix}$$

2. 2

Note that the tensor $\{\ \varepsilon\ \}$ is symmetric.

Interpretation of various $\boldsymbol{\varepsilon_{ij}}$ on a 2D case is shown in Figure 2.2.

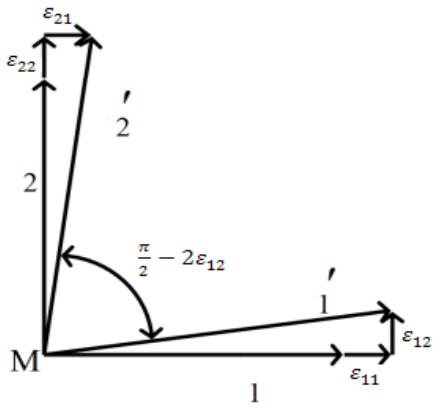

Figure 2.2: Applied strain in 2 direction (uniaaxial and shear strains)

It appears that the diagonal elements ε_{11}, ε_{22} and ε_{33} represent the relative elongations, while the non-diagonal terms ε_{12}, ε_{13} and ε_{23} represent the angular distortions. Moreover, it is noteworthy that $\Delta\theta_{ij}$ = -2ε_{ij} (for i ≠ j), as shown Figure 2.2. Therefore it is preferable to calculate 2ε_{ij} (for i ≠ j) rather than ε_{ij} to keep a physical meaning.

2.2.2 Stresses

As strains, stresses can be expressed as a 3x3 tensor.

$$\{\sigma\ (\mathrm{M})\} = \begin{bmatrix} \sigma_{11} & \sigma_{12} & \sigma_{13} \\ \sigma_{21} & \sigma_{22} & \sigma_{23} \\ \sigma_{31} & \sigma_{32} & \sigma_{33} \end{bmatrix}$$

2. 3

For equilibrium reasons: $\sigma_{ij} = \sigma_{ji}$. So the tensor $\{\sigma\}$ is symmetric too as the strain tensor. Interpretation of different $\boldsymbol{\sigma_{ij}}$ is shown in Figure 2. 3.

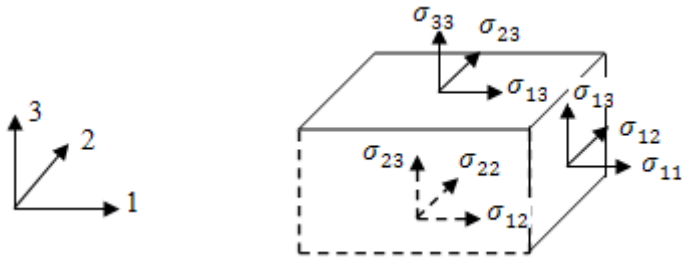

Figure 2. 3: Stresses applied to an elementary volume around a point M

The diagonal terms σ_{11}, σ_{22}, σ_{33} are the uniaxail stresses while the non-diagonal terms are the shear stresses.

2.2.3 Linear elasticity

The linear elastic behavior is characterized by a linear relationship between stress and strain (equation 2. 4).

$$\{\sigma\} = [C]\ \{\varepsilon\}$$

2. 4

Where $[C]$ is the stiffness tensor (4th order thus 81 coefficients). This equation can be rewritten in another form reporting the 4th order of $[C]$.

$$\sigma_{ij} = C_{ijkl}\ \varepsilon_{kl}$$

2. 5

As the strain tensor and the stress tensor are symmetric, the stiffness tensor has only 36 coefficients. Hence the idea to condense all these tensors:

- The strain tensor is condensed in a 6x1 tensor : $\{\varepsilon\} = \begin{Bmatrix} \varepsilon_{11} = \varepsilon_1 \\ \varepsilon_{22} = \varepsilon_2 \\ \varepsilon_{33} = \varepsilon_3 \\ 2\varepsilon_{23} = \varepsilon_4 \\ 2\varepsilon_{13} = \varepsilon_5 \\ 2\varepsilon_{12} = \varepsilon_6 \end{Bmatrix}$
- The stress tensor is condensed in a 6x1 tensor : $\{\sigma\} = \begin{Bmatrix} \sigma_{11} = \sigma_1 \\ \sigma_{22} = \sigma_2 \\ \sigma_{33} = \sigma_3 \\ \sigma_{23} = \sigma_4 \\ \sigma_{13} = \sigma_5 \\ \sigma_{12} = \sigma_6 \end{Bmatrix}$
- The stiffness tensor is condensed in a 6x6 tensor.

The factor 2 in the condensed strain tensor ensures the coherence energy for the product $\{\sigma\}^t\{\varepsilon\}$.

In the case of an isotropic material (independent behavior in all directions), the condensed stiffness tensor is expressed in terms of only two independent coefficients:

$$\begin{pmatrix} \sigma_1 \\ \sigma_2 \\ \sigma_3 \\ \sigma_4 \\ \sigma_5 \\ \sigma_6 \end{pmatrix} = \frac{Y}{(1+\upsilon)(1-2\upsilon)} \begin{bmatrix} 1-\upsilon & \upsilon & \upsilon & 0 & 0 & 0 \\ \upsilon & 1-\upsilon & \upsilon & 0 & 0 & 0 \\ \upsilon & \upsilon & 1-\upsilon & 0 & 0 & 0 \\ 0 & 0 & 0 & \frac{1-2\upsilon}{2} & 0 & 0 \\ 0 & 0 & 0 & 0 & \frac{1-2\upsilon}{2} & 0 \\ 0 & 0 & 0 & 0 & 0 & \frac{1-2\upsilon}{2} \end{bmatrix} \begin{pmatrix} \varepsilon_1 \\ \varepsilon_2 \\ \varepsilon_3 \\ \varepsilon_4 \\ \varepsilon_5 \\ \varepsilon_6 \end{pmatrix} \quad \text{2. 6}$$

Where Y is the Young's modulus of the material (N m^{-2}) and υ is the Poisson's ratio (unitless). The inverse relation may be written as

$$\begin{pmatrix} \varepsilon_1 \\ \varepsilon_2 \\ \varepsilon_3 \\ \varepsilon_4 \\ \varepsilon_5 \\ \varepsilon_6 \end{pmatrix} = \frac{1}{Y} \begin{bmatrix} 1 & -\upsilon & -\upsilon & 0 & 0 & 0 \\ -\upsilon & 1 & -\upsilon & 0 & 0 & 0 \\ -\upsilon & -\upsilon & 1 & 0 & 0 & 0 \\ 0 & 0 & 0 & 2(1+\upsilon) & 0 & 0 \\ 0 & 0 & 0 & 0 & 2(1+\upsilon) & 0 \\ 0 & 0 & 0 & 0 & 0 & 2(1+\upsilon) \end{bmatrix} \begin{pmatrix} \sigma_1 \\ \sigma_2 \\ \sigma_3 \\ \sigma_4 \\ \sigma_5 \\ \sigma_6 \end{pmatrix} \quad \text{2. 7}$$

2.3. Piezoelectricity

The constitutive equations of linear piezoelectricity can be given by the coupling (ε, E) as the following:

$$\{\sigma\} = [c^E]\{\varepsilon\} - [e]^t\{\mathrm{E}\}$$
$$\{D\} = [\mathrm{e}]\{\varepsilon\} + [\epsilon^\varepsilon]\{\mathrm{E}\}$$

2. 8

These two equations are tensor equations like the equation of linear elasticity (equation 2. 4), involving two new variables: {E} the electric field (Vm^{-1}, 3 component vector) and {D} the electric displacement (in Cm^{-2} or $NV^{-1}m^{-1}$, 3 component vector). $[c^E]$, [e] & $[\epsilon^\varepsilon]$ denote respectively the condensed tensors of elastic stiffness at constant electric field, piezoelectric constants and dielectric permittivities at constant strain.

With the simplifications due to the symmetries of crystals and in the case of PZT isotropic material, the tensors are:

$$\begin{pmatrix}\sigma_1\\ \sigma_2\\ \sigma_3\\ \sigma_4\\ \sigma_5\\ \sigma_6\\ D_1\\ D_2\\ D_3\end{pmatrix} = \left[\begin{array}{cccccc|ccc} c_{11}^E & c_{12}^E & c_{13}^E & 0 & 0 & 0 & 0 & 0 & -e_{31}\\ c_{12}^E & c_{11}^E & c_{13}^E & 0 & 0 & 0 & 0 & 0 & -e_{31}\\ c_{13}^E & c_{13}^E & c_{33}^E & 0 & 0 & 0 & 0 & 0 & -e_{33}\\ 0 & 0 & 0 & c_{44}^E & 0 & 0 & 0 & -e_{15} & 0\\ 0 & 0 & 0 & 0 & c_{44}^E & 0 & -e_{15} & 0 & 0\\ 0 & 0 & 0 & 0 & 0 & 2(c_{11}^E - c_{12}^E) & 0 & 0 & 0\\ \hline 0 & 0 & 0 & 0 & e_{15} & 0 & \epsilon_{11}^\varepsilon & 0 & 0\\ 0 & 0 & 0 & e_{15} & 0 & 0 & 0 & \epsilon_{11}^\varepsilon & 0\\ e_{31} & e_{31} & e_{33} & 0 & 0 & 0 & 0 & 0 & \epsilon_{33}^\varepsilon \end{array}\right] \begin{pmatrix}\varepsilon_1\\ \varepsilon_2\\ \varepsilon_3\\ \varepsilon_4\\ \varepsilon_5\\ \varepsilon_6\\ E_1\\ E_2\\ E_3\end{pmatrix}$$

2. 9

Another coupling that should be used in our study is the (σ, E) coupling

$$\{\varepsilon\} = [s^E]\{\sigma\} + [\mathrm{d}]^t\{\mathrm{E}\}$$
$$\{D\} = [\mathrm{d}]\{\sigma\} + [\epsilon^\sigma]\{\mathrm{E}\}$$

2. 10

In its extension form for crystals and in the case of PZT isotropic material, the tensors are:

$$\begin{pmatrix}\varepsilon_1\\ \varepsilon_2\\ \varepsilon_3\\ \varepsilon_4\\ \varepsilon_5\\ \varepsilon_6\\ D_1\\ D_2\\ D_3\end{pmatrix} = \left[\begin{array}{cccccc|ccc} s_{11}^E & s_{12}^E & s_{13}^E & 0 & 0 & 0 & 0 & 0 & d_{31}\\ s_{12}^E & s_{11}^E & s_{13}^E & 0 & 0 & 0 & 0 & 0 & d_{31}\\ s_{13}^E & s_{13}^E & s_{33}^E & 0 & 0 & 0 & 0 & 0 & d_{33}\\ 0 & 0 & 0 & 2s_{44}^E & 0 & 0 & 0 & d_{15} & 0\\ 0 & 0 & 0 & 0 & 2s_{44}^E & 0 & d_{15} & 0 & 0\\ 0 & 0 & 0 & 0 & 0 & 2\times 2(s_{11}^E - s_{12}^E) & 0 & 0 & 0\\ \hline 0 & 0 & 0 & 0 & d_{15} & 0 & \epsilon_{11}^\sigma & 0 & 0\\ 0 & 0 & 0 & d_{15} & 0 & 0 & 0 & \epsilon_{11}^\sigma & 0\\ d_{31} & d_{31} & d_{33} & 0 & 0 & 0 & 0 & 0 & \epsilon_{33}^\sigma \end{array}\right] \begin{pmatrix}\sigma_1\\ \sigma_2\\ \sigma_3\\ \sigma_4\\ \sigma_5\\ \sigma_6\\ E_1\\ E_2\\ E_3\end{pmatrix}$$

2. 11

2.4. Unknowns to be determined

Given the device geometry (thin beam/plate), only the bending will be considered. Twists and pulls-compression are therefore neglected.

The displacement field to be determined to know the status of the device is:

$$\{u\} = \begin{Bmatrix} u_1(x,y,z,t) \\ u_2(x,y,z,t) \\ u_3(x,y,z,t) \end{Bmatrix} \quad \text{2. 12}$$

With simplifying assumptions, this displacement field can be expressed using the single function w(x, y) (case of bending vibrations of plates) or w(x) (case of bending vibration of beams), which represents the deflection of the plate/beam along the z axis (

Figure 2.4) [(Jaouen, 2005)].

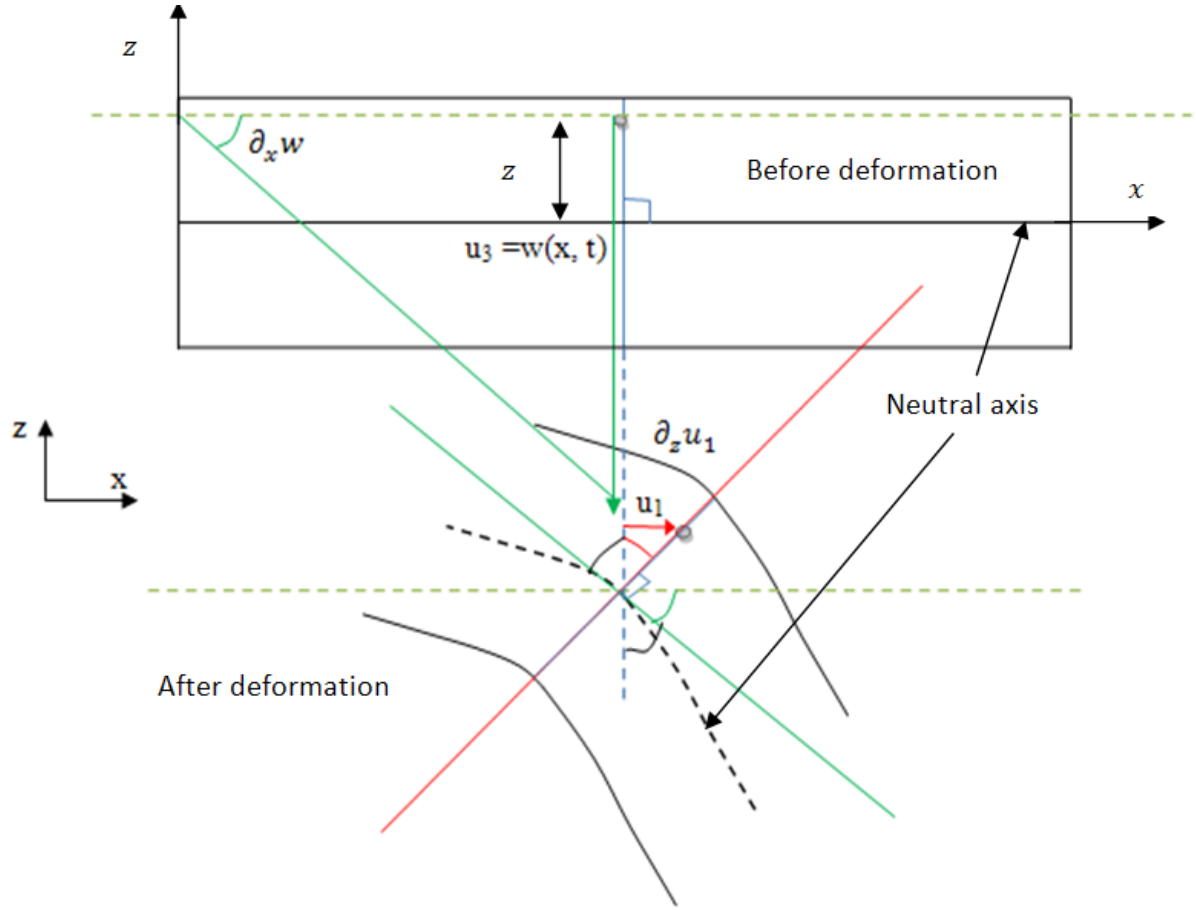

Figure 2.4: Kinematics of the deformation of an Euler-Bernoulli beam

2.4.1. Bending vibrations of beams

We call beam, a continuous medium having a very large dimension (x) with respect to the others two.

To simplify the displacement field, a Taylor series development of $u_i(x,y,z)$ with respect to y and z is made:

$$u_i(x,y,z) = u_i(x,0,0) + \mathrm{y}\frac{\partial u_i}{\partial y}(x,0,0) + \mathrm{z}\frac{\partial u_i}{\partial z}(x,0,0) + \frac{y^2}{2}\frac{\partial^2 u_i}{\partial y^2}(x,0,0) + \frac{z^2}{2}\frac{\partial^2 u_i}{\partial z^2}(x,0,0) + \mathrm{yz}\frac{\partial^2 u_i}{\partial y \partial z}(x,0,0) + \dots \quad \text{2. 13}$$

Theory of thin beam consists to neglect the terms of 2nd order and higher orders in this development.

$$u_i(x,y,z) \approx u_i(x,0,0) + \mathrm{y}\partial_y u_i(x,0,0) + \mathrm{z}\partial_z u_i(x,0,0) \quad \text{2. 14}$$

In the case of bending in the plane (x, z), displacements along y are zero ($u_2 = 0$).

According to Timoshenko assumptions [(Timoshenko, 1921), (Timoshenko, 1922)], the only unknowns are the deflection w and the rotation of the cross sections $\partial_z u_1$. So, the displacement field is:

$$\{u\} = \begin{cases} u_1(x,y,z,t) \approx z\partial_z u_1(x,t) \\ u_2(x,y,z,t) = 0 \\ u_3(x,y,z,t) \approx w(x,t) \end{cases} \quad \text{2. 15}$$

Moreover, the assumption of Bernoulli imposes the additional condition that the cross sections remain perpendicular to the neutral axis after deformation:

$$\partial_z u_1(x,t) = -\partial_x w(x,t) \quad \text{2. 16}$$

This assumption of Bernoulli returns to neglecting the transverse shear ε_{12} of the cross sections. This assumption is legitimate for a homogeneous material and for the first modes of vibration. All these assumptions lead to the following displacement field:

$$\{u\} = \begin{cases} u_1(x,y,z,t) \approx -z\partial_x w(x,t) \\ u_2(x,y,z,t) = 0 \\ u_3(x,y,z,t) \approx w(x,t) \end{cases} \quad \text{2. 17}$$

This displacement field is a good approximation for small deformations, which is supposed to be the case here.

2.4.2. Bending vibrations of plates

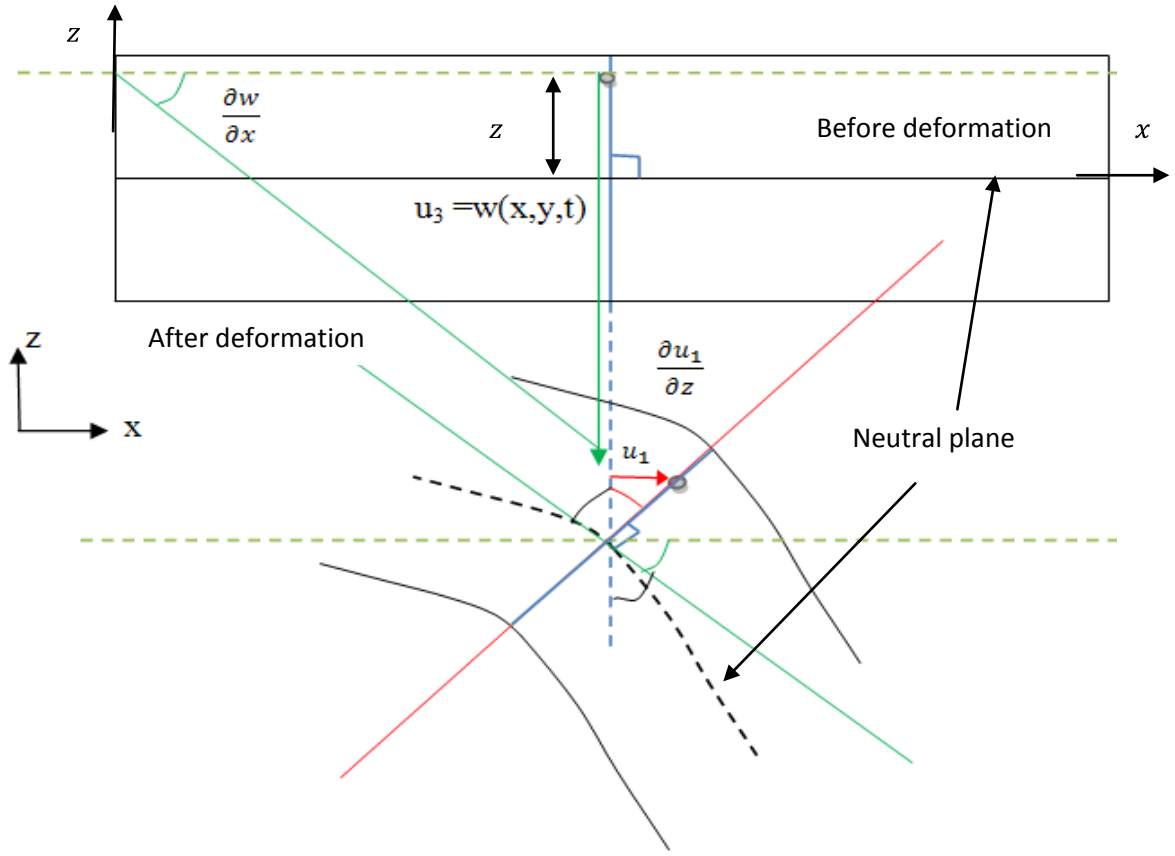

Figure 2. 5: Kinematics of the deformation of a Love-Kirchhoff plate

To determine the displacement field, the same process as in the case of beam bending is performed. This time, the plate having its two most important dimensions in the plane (x, y), the Taylor series development is made only with respect to z.

$$u_i(x,y,z) = u_i(x,y,0) + z\frac{\partial u_i}{\partial z}(x,y,0) + \frac{z^2}{2}\frac{\partial^2 u_i}{\partial z^2}(x,y,0) + \dots$$

2. 18

Always neglecting terms of order 2 or more (thin plate theory), the equation becomes:

$$u_i(x,y,z) \approx u_i(x,y,0) + z\frac{\partial u_i}{\partial z}(x,y,0)$$

2. 19

Therefore, bending is defined by three independent functions: the deflection w and the terms of rotation $\partial_z u_1$ and $\partial_z u_2$. The Kirchhoff-Love hypotheses are those of Timoshenko transposed to the case of plate and indicates that the deformed cross sections should remain

normal to the neutral plane of the plate. This imposes additional assumptions on the terms of rotation $\partial_z u_1$ and $\partial_z u_2$. So, the displacement field is:

$$\{u\} = \begin{cases} u_1(x,y,z,t) \approx -z\,\partial_x w(x,y,t) \\ u_2(x,y,z,t) \approx -z\partial_y w(x,y,t) \\ u_3(x,y,z,t) \approx w(x,y,t) \end{cases}$$

2. 20

As in the case of beam, this displacement field is a good approximation in the case of small displacements.

2.5. Static equation

For the system studied, the unknowns are:

- the deflection w (displacement along z-axis) and its spatial derivatives (∂w),
- and the voltage V on the piezoelectric elements

External actions are:

- forces (F) and moments (M) applied to the beam / plate,
- the electric charge Q applied to the electrodes.

The charge Q is related to the electrical displacement vector $\vec{D}$ by the equation:

$$Q = \int_S \vec{D}.d\vec{S}$$

2. 21

Similarly, the external mechanical actions (forces and moments) are related to the stress tensor; so in static, the system studied can be written as an equation like this:

$$\begin{bmatrix} K_{mm} & K_{mv} \\ K_{vm} & K_{vv} \end{bmatrix} \left\{ \frac{w \,\&\, \partial w}{V} \right\} = \left\{ \frac{F \,\&\, M}{Q} \right\}$$

2. 22

2.6. Dynamic equation

In dynamics, it must be added to the last equation the terms of inertia and friction. Assume that only the elastic friction occurs and that the electrical inertia does not take place to be taken into account.

The above equation becomes:

$$\begin{bmatrix} M & 0 \\ 0 & 0 \end{bmatrix} \frac{\partial^2}{\partial t^2} \left\{ \frac{w \,\&\, \partial w}{V} \right\} + \begin{bmatrix} C & 0 \\ 0 & 0 \end{bmatrix} \frac{\partial}{\partial t} \left\{ \frac{w \,\&\, \partial w}{V} \right\} + \begin{bmatrix} K_{mm} & K_{mv} \\ K_{vm} & K_{vv} \end{bmatrix} \left\{ \frac{w \,\&\, \partial w}{V} \right\} = \left\{ \frac{F \,\&\, M}{Q} \right\}$$

2. 23

For some particular circuits, circuit equation may involve time derivatives of V. It is then possible to use this equation and adding to the matrices [M], [C] and [K] the terms due to the circuit. Sometimes it is better to use a formulation with the time derivatives of Q; it will

therefore make a change of variable to have as unknowns the vector $\left\{\frac{w\ \&\ \partial w}{Q}\right\}$ and as external action$\left\{\frac{F\ \&\ M}{V}\right\}$.

2.7. Numerical modeling

Piezoelectric and mechanical equations for system like plate/beam with piezoelectric patches are difficult to solve analytically. Numerical modeling is recommended in these types of systems. This requires spatially discretizing of the plate/beam but also discretizing the time for time response analyses; the same for frequency, in case of frequency response analyses. For systems like bending vibrations of plates/beams as the case here, Hermite elements must be used to ensure the continuity of the solution w and its spatial derivatives [(Dhatt, et al., 2005)].

2.7.1. Bending vibrations of beams

The elements in the case of bending of beam (1D) are segments oriented along x-axis with two unknowns at each node: the deflection w and its spatial derivative $\partial_x w$.

The numerical equation for N discretization points of the beam becomes (in static):

$$\begin{bmatrix} K_{mm} & K_{mv} \\ K_{vm} & K_{vv} \end{bmatrix} \begin{Bmatrix} w_1 \\ \partial_x w_1 \\ w_2 \\ \partial_x w_2 \\ \vdots \\ w_N \\ \partial_x w_N \\ V \end{Bmatrix} = \begin{Bmatrix} F_{z1} \\ M_{y1} \\ F_{z2} \\ M_{y2} \\ \vdots \\ F_{zN} \\ M_{yN} \\ Q \end{Bmatrix} \quad 2.24$$

Where $[K_{mm}]$ has dimension 2N×2N, $[K_{mv}] = [K_{vm}]^t$ has dimension 2N×1 and $[K_{vv}]$ has dimension 1×1. The forces applied to the various nodes are carried by the z-axis while the moments are carried by the y-axis to be placed in the case of flexion.

These are the same unknowns in dynamic.

2.7.2. Bending vibrations of plates

The elements in the case of bending of plate (2D) are triangles (or quadrangles) in the plane (x, y) with unknowns in each node: the deflection w, its derivative $\partial_x w$ and $\partial_y w$.

The numerical equation for N discretization points of the plate becomes (in static):

$$\begin{bmatrix} K_{mm} & K_{mv} \\ K_{vm} & K_{vv} \end{bmatrix} \begin{Bmatrix} w_1 \\ \partial_x w_1 \\ \partial_y w_1 \\ w_2 \\ \partial_x w_2 \\ \partial_y w_2 \\ \vdots \\ w_N \\ \partial_x w_N \\ \partial_y w_N \\ V \end{Bmatrix} = \begin{Bmatrix} F_{z1} \\ M_{y1} \\ M_{x1} \\ F_{z2} \\ M_{y2} \\ M_{x2} \\ \vdots \\ F_{zN} \\ M_{yN} \\ M_{xN} \\ Q \end{Bmatrix}$$

2. 25

Where $[K_{mm}]$ has dimension 3N×3N, $[K_{mv}] = [K_{vm}]^t$ has dimension 3N×1 and $[K_{vv}]$ has dimension 1×1. The forces applied to the various nodes are carried by the z-axis while the moments are carried by the y-axis or x-axis to be placed in the case of flexion.

These are the same unknowns in dynamic.

2.7.3. Variational principle

To obtain the matrices [M], [C] and [K], we can express the energy balance of the system studied as a function: it is the variational formulation. The real trajectory is the one that makes this function stationary with respect to any arbitrary variation of displacement.

The most widely used variational principle in dynamic structures is the Hamilton principle, which sets that the sum of variations of kinetic energy and potential energy and the variation of work done by non-conservative forces, taken during any time interval t_1 to t_2 are zero.

$$\delta \int_{t_1}^{t_2} (\mathcal{L} + W) \mathrm{dt} = 0$$

2. 26

Where $\mathcal{L}$ is the Lagrangian ($\mathcal{L}$ = J - H with J the kinetic energy and H the global enthalpy) and W is the virtual work of external mechanical and electric forces.

The kinetic energy is equal to

$$\mathrm{J} = \int_V \frac{1}{2} \rho \left[\left(\frac{\partial u_1}{\partial t} \right)^2 + \left(\frac{\partial u_2}{\partial t} \right)^2 + \left(\frac{\partial u_3}{\partial t} \right)^2 \right] dV$$

$$J = \int_V \frac{1}{2} \rho \{\dot{u}\}^t \{\dot{u}\} \mathrm{dV}$$

2. 27

Where ρ is the volume density (kg m^{-3}).

The global enthalpy is equal to

$$\mathrm{H} = \int_V \frac{1}{2} (\{\varepsilon\}^t \{\sigma\} - \{\mathrm{E}\}^t \{D\}) \mathrm{dV}$$

2. 28

And finally, the virtual work of external mechanical and electrical forces is equal to

$$W = \int_V \{u\}^t \{F_V\} dV + t_p \{E\} Q$$

2. 29

Where $\{F_V\}$ represents the body applied forces and t_p the thickness of piezoelectric layer.

By applying Hamilton principle (2. 26) and replacing $\{\sigma\}$ and {D} by their equation (2. 8), we obtain:

$$\int_{t_1}^{t_2} [\int (\rho \{\delta \dot{u}\}^t \{\dot{u}\} - \{\delta\varepsilon\}^t [c] \{\varepsilon\} + \{\delta\varepsilon\}^t [e]^t \{E\} + \{\delta E\}^t [e] \{\varepsilon\} + \{\delta E\}^t [\epsilon^\varepsilon] \{E\} + \{u\}^t \{F_V\}) dV + t_p \{\delta E\} Q] dt = 0$$

2. 30

Integrating by parts the kinetic energy (2. 27), we obtain:

$$\int_{t_1}^{t_2} \rho \{\delta \dot{u}\}^t \{\dot{u}\} dt = [\rho \{\delta u\}^t \{\dot{u}\}]_{t_1}^{t_2} - \int_{t_1}^{t_2} \rho \{\delta u\}^t \{\ddot{u}\} dt$$

2. 31

$\{\delta u\}$ is zero at $t=t_1$ and $t=t_2$, the first term is zero.

Equation (2. 30) must be verified for any time interval thus the term to integrate temporally must be zero. Finally:

$$\int_V (-\rho \{\delta u\}^t \{\ddot{u}\} - \{\delta\varepsilon\}^t [c] \{\varepsilon\} + \{\delta\varepsilon\}^t [e]^t \{E\} + \{\delta E\}^t [e] \{\varepsilon\} + \{\delta E\}^t [\epsilon^\varepsilon] \{E\} + \{\delta u\}^t \{F_v\}) dV + t_p \{\delta E\} Q = 0$$

2. 32

This equation is representative of any mechanical and / or piezoelectric system.

Thanks to this equation, the creation of matrices [M], [C] and [K] will be easier as they will be built from elementary matrices for each element.

2.7.4. Time discretization: Newmark method

In dynamic, the equation is of order 2 in time and it looks like:

$$[M]\{\ddot{U}\} + [C]\{\dot{U}\} + [K]\{U\} = \{F\}$$

2. 33

To numerically solve this problem, there are several methods which one of the most common is the Newmark method [(Dhatt, et al., 2005)].

This method is called implicit, it can construct the vectors {U}, $\{\dot{U}\}$ and $\{\ddot{U}\}$ at time t from the same known vectors at time t-τ. For this, the following expansions are used (a and b are two coefficients between 0 and 1):

$$\{U_t\} = \{U_{t-\tau}\} + \tau\{\dot{U}_{t-\tau}\} + \frac{\tau^2}{2}((1\text{-b})\{\ddot{U}_{t-\tau}\} + b\{\ddot{U}_t\})$$

$$\{\dot{U}_t\} = \{\dot{U}_{t-\tau}\} + \tau((1\text{-a})\{\ddot{U}_{t-\tau}\} + a)\{\ddot{U}_t\})$$

2. 34

The solution at time t can be calculated; with,

$$\{U_t\} = [\overline{K}]^{-1}\{RT_t\}$$

2. 35

Where

$$[\overline{K}] = [M] + a\tau[C] + b\frac{\tau^2}{2}[K]$$

$$\{RT_t\} = b\frac{\tau^2}{2}\{F_t\} + [M](\{U_{t-\tau}\} + \{\dot{U}_{t-\tau}\} + (1\text{-b})\frac{\tau^2}{2}\{\ddot{U}_{t-\tau}\})$$

$$+ [C](a\tau\{U_{t-\tau}\} + (2a\text{-b})\frac{\tau^2}{2}\{\dot{U}_{t-\tau}\} + (a\text{-b})\frac{\tau^3}{2}\{\ddot{U}_{t-\tau}\})$$

2. 36

Then, the velocity and acceleration at time t must also be determined to calculate the solution to the next iteration. To do this, the expansions (equation 2. 34) should be used.

The convergence and stability of the method depends on the choice of the coefficients a and b. The most frequently used values are: a = b = ½ because it is a sufficient condition for stability, which assumes constant acceleration during time interval $t - \tau$, t.

2.8. Conclusion and discussion

In this chapter, we have briefly presented the definition of strains and stresses, and then we have seen shortly the mechanical and piezoelectric equations in matrix 3D complete form where all stresses and strains are represented for isotropic materials under the linear elasticity assumption. In some particular cases of study, mechanical and piezoelectric equations can be written in 2D (case of thin plate) or 1D (case of thin beam) matrix form. These practical cases are represented in the next chapter.

We have discussed the displacement field case of bending vibrations of beams and plates. The displacement field was determined in the case of beam and plate only without taking piezoelectric patches into consideration. The displacement field cases of piezoelectric patches bonded on the beam and the plate will be considered in the next chapter.

Static and dynamic numerical equations in the general case of a system containing elastic and piezoelectric materials are presented. These equations are derived from the variational principle, which is detailed in this chapter.

Our interest is to study the case of piezoelectric patches bonded on thin beam and thin plate structures on the same face, which we call non-collocated piezoelectric patches bonded on thin structure (beam and plate). This case of study will be done in the next chapter.

2.9. References

Brissaud Michel Matériaux piézoélectriques: Caractérisation, modélisation et vibration [Livre]. - Lausanne : Presses polytechniques et universitaires romandes, 2007.

Chevalier Luc Mécanique des systèmes et des milieux déformables [Livre]. - Cachan : ellipses, 1996.

Chopra Inderjit Review of state of art of smart structures and integrated systems [Revue] // AIAA Journal. - 2002. - pp. 2145-2187.

Decolon Christian Structures composites: Calcul des plaques et des poutres multicouches [Livre]. - Paris : Hermes Science publications, 2000.

Dhatt Gouri, Touzot Gilbert et Lefrancois Emmanuel Méthode des éléments finis [Livre]. - Paris : Lavoisier, 2005.

Gay Daniel Matériaux composites [Livre]. - Paris : Lavoisier , 2005.

Jaouen Luc Vibrations des milieux dscrets et continus [Livre]. - 2005.

Sashida Toshllku et Kenjo Takashi An introduction to ultrasonic motors [Livre]. - Japan : Oxford scien publication, 1993.

Senturia Stephen Microsystem Design [Livre]. - [s.l.] : Kluwer academic publishers , 2002.

Timoshenko S.P. On the correction factor for shear of the differential equation for transverse vibrations of bars of uniform cross-section [Revue] // Philosophical Magazine. - 1921. - p. pp. 744..

Timoshenko S.P. On the transverse vibrations of bars of uniform cross-section [Revue] // Philosophical Magazine. - 1922. - p. pp. 125.

CHAPTER 3

MODELING OF NON-COLLOCATED PIEZOELECTRIC PATCHES BONDED ON THIN STRUCTURES

Chapter 3: Modeling of non-collocated piezoelectric patches bonded on thin structures

List of figures

3.1. Introduction

Thin structures containing piezoelectric materials are widely used to control vibrations [(Hariri, et al., 2011), (Yasin, et al., 2010)], for detecting damage in the structure [(Qu, et al., 2006), (Yan, et al., 2002)], in micropumps [(Hernandez, et al., 2010)], in valves [(Bernard, et al., 2011)] and in miniature robots [(Hariri, et al., 2010)]. Two large branches are studied in the literature for thin structures containing piezoelectric materials due to their domain of applications, namely beam structures and plate structures. On the other hand, these systems may be symmetrical or asymmetrical where the piezoelectric materials are collocated or not on the thin beam/plate structures. In a symmetrical system the piezoelectric materials are bonded face-to-face on both sides of the beam/plate structure while in an asymmetrical one the piezoelectric materials are bonded only on one side surface of the structure. It may be noted that there is another type of structure containing piezoelectric materials where the piezoelectric materials are embedded in the beam/plate structure [(Yan, et al., 2002)], this type of structure is not concerned in this research study.

For symmetrical or asymmetrical beam structures with respectively collocated or non-collocated piezoelectric materials, a 1D analytical or numerical model can be used to model such system; examples for modeling symmetrical systems can be found in [(Corcolle, et al., 2008), (de Abreu, et al., 2004), (Jalili, 2009), (Lin, et al., 1999), (Nguyen, et al., 2006), (Park, 2003), (Varadan, 1996), (Yasin, et al., 2010)] and for asymmetrical ones in [(Chen, et al., 2007), (Hariri, Bernard, & Razek, 2011), (Jalili, 2009), (Kayacik, et al., 2008), (Son, et al., 2006)]. In the first case the neutral axis is taken as the symmetry axis (mid plane) of the system while in the case of asymmetrical systems it is necessary to determine such neutral axis.

In the case of plate structures, 2D or 3D Finite Element Method (FEM) can be used to model the system. In the 3D approach volume elements are used while in the 2D case surface elements are used, the 3rd dimension is introduced in the model equations. It is obvious that the second approach is faster but a little more complicated in model formulation.

Several papers in literature are devoted for modeling thin structure with piezoelectric patches using the 2D approach in the case where the symmetry of the system is maintained at the disposal of patches [(Corcolle, et al., 2008), (de Abreu, et al., 2004), (Jalili, 2009), (Liu, 1999), (Wang, 2003), (Yasin, et al., 2010)]. The 2D approach is more difficult for an asymmetrical structure, where piezoelectric patches are not collocated (patches bonded on

only one side of structure surface), due to the fact that the neutral plane of the structure is not confused with the mid plane as in the case of a symmetrical structure.

The aim of this chapter is to develop a 2D (and 1D respectively) Finit Element Model (FEM) to model an asymmetrical system where non-collocated piezoelectric patches are bonded on a thin plate (and thin beam respectively), using the notion of neutral plane (and neutral axis respectively). It is not a standard 2D model, since the calculation is performed on a structure that does not have symmetries that allow such easy assumptions. Actually without determining the neutral plane for such asymmetric system, we can't model it in 2D and the modeling should be done in 3D FEM.

In chapter 2, we have seen the mechanical and piezoelectric equations (constitutive equations) for isotropic materials under linear elasticity condition in matrix 3D complete form where all stresses and strains are represented. Cases of thin beams and thin plates stresses can be represented in 1D and 2D matrix form. These cases are treated in this chapter.

The displacement field was determined in the case of beam and plate without taking piezoelectric patches into consideration in the last chapter. Here the displacement field will be readapted in the case of asymmetric systems (non-collocated piezoelectric patches bonded on thin structures) by determining the neutral plane and the neutral axis of thin plate and thin beam respectively.

The general variational equation that represents any mechanical and / or piezoelectric system determined using the variational principle in the last chapter section 2.7.3 will be used here to determine the numerical equation of non-collocated piezoelectric patches bonded on thin structures.

Two cases are treated at the end, the first is the case said ‘’actuator-sensor’’ where some patches are used as sensors and others as actuators, while the second is the case of ’'actuator-actuator’’, where all patches are used as actuators (refer to the definition of piezoelectricity in chapter 1, section 1.3).

3.2. Constitutive equations

The constitutive equations in mechanics as in piezoelectricity (equation (2.6), (2.7), (2.9) & (2.11)) are valid in the general case i.e. in 3D. The approximations made to move in 1D or 2D leads to use new constitutive equations extracting from the general constitutive equations.

For thin components e.g., web or flange of an I-beam, automobile door panel, airplane skin, etc (Figure 3. 1), the in-plane stresses are much higher than out-of-plane stresses: (σ_1, σ_2, σ_6)

>> (σ_3, σ_4, σ_5). It is convenient to assume the out-of-plane stresses equal zero. This is called a state of plane stress.

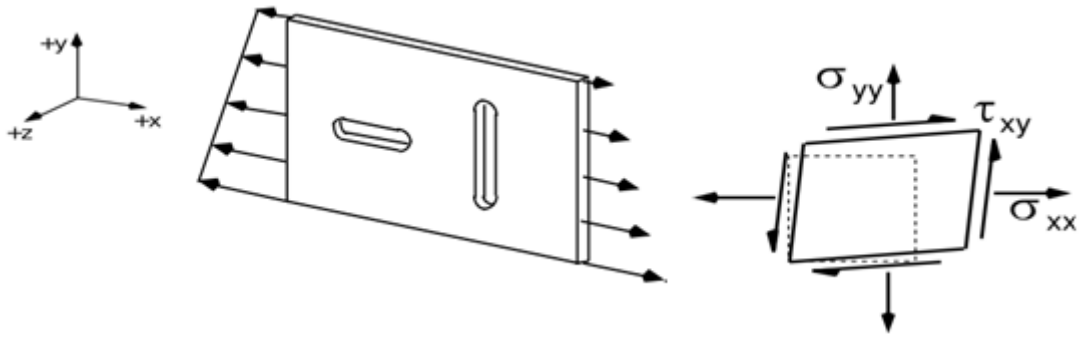

Figure 3. 1: Plane stress example [(Tuttle, 2009)]

For thick or very long components e.g., thick-walled pressure vessels, buried pipe, etc (Figure 3. 2), the in-plane strains are much higher than out-of-plane strains: (ε_1, ε_2, ε_6) >> (ε_3, ε_4, ε_5). It is convenient to assume the out-of-plane strains equal zero. This is called a state of plane strain.

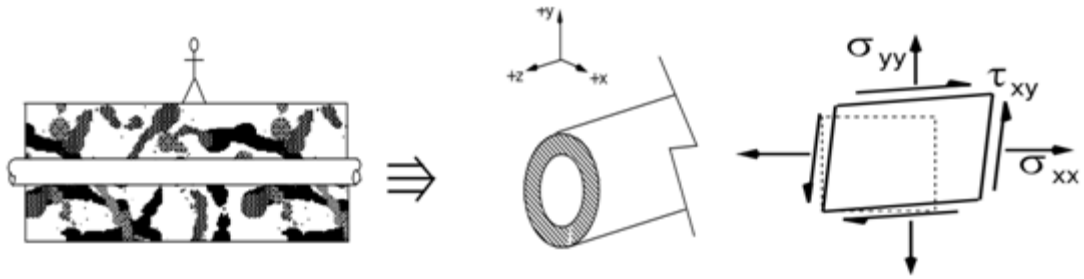

Figure 3. 2: plane strain example [(Tuttle, 2009)]

In the case of uniaxial load eg. truss members (Figure 3. 3), σ_1 is the only non zero stress.

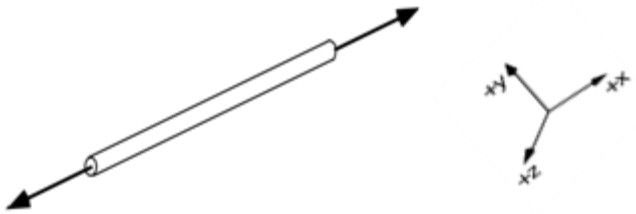

Figure 3. 3: Uniaxial stress example [(Tuttle, 2009)]

3.2.1 Case of piezoelectric patches bonded on a beam

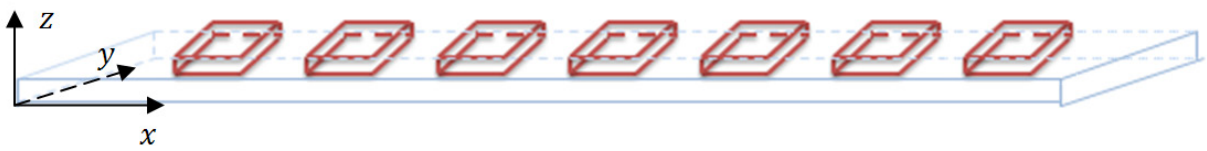

Figure 3. 4: non-collocated piezoelectric patches bonded on a beam of the same width

Our system studied is composed of non-collocated piezoelectric patches bonded on a thin beam (having a very large dimension (x) with respect to the two others) has the same width as the piezoelectric patches, as shown in Figure 3. 4. Electric field and electric displacement are uniform across the piezoelectric thicknesses and aligned on the normal to the mid-plane (z-direction), also the piezoelectric patches are polarized in z-direction.

$$\{E\} = \begin{Bmatrix} 0 \\ 0 \\ E_3 \end{Bmatrix}, \quad \{D\} = \begin{Bmatrix} 0 \\ 0 \\ D_3 \end{Bmatrix} \tag{3. 1}$$

In this case, when polarization and applied electric field have the same direction, transversal mode variation occurs in the piezoelectric patches; results in a variation along x-axis and y-axis. Case of thin beam, only x-direction is considered; therefore variation along y-axis is vanished (σ_1 is the only non zero stress). Figure 3.5 shows moments result from the uniaxial stresses distribution along x-axis, to produce the bending of the beam.

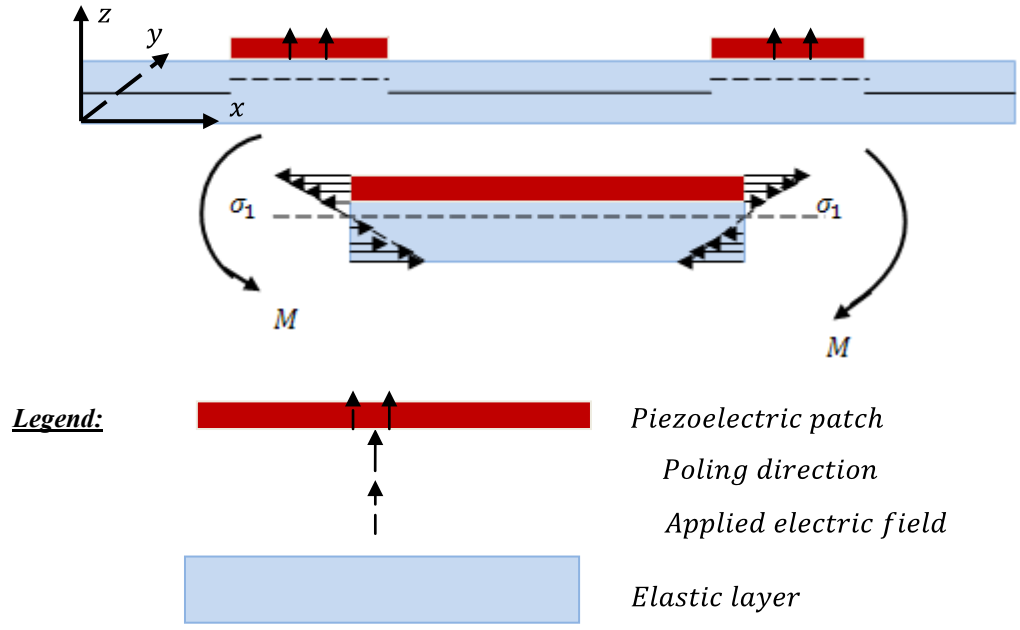

Figure 3. 5: Schematic of moment and normal stress distribution

3.2.1. 1 Mechanical constitutive equations

As we said before, in this case we considered that σ_1 is the only non zero stress. Using the compliance matrix of equation (2.7) we obtain according to Hook's law uniaxial stress [(Tuttle, 2009)]:

$$\sigma_1^m = Y\varepsilon_1 = c_m\,\varepsilon_1 \tag{3. 2}$$

Where σ_1^m and c_m represent respectively, the uniaxial stress in the x-direction and the Young modulus for the elastic layer.

3.2.1. 2 Piezoelectric constitutive equations

The formulation used is that of the coupling (ε, E) of equation 2.8 shown again below:

$$\begin{aligned}\{\sigma\} &= [c^E]\{\varepsilon\} - [e]^t\{E\}\\ \{D\} &= [e]\{\varepsilon\} + [\epsilon^\varepsilon]\{E\}\end{aligned} \tag{3. 3}$$

By using equation (2.11) and taking into account the assumption of equation (3. 1), we get:

$$\begin{cases} \varepsilon_1 = s_{11}^E\,\sigma_1 + d_{31}E_3 \\ D_3 = d_{31}\sigma_1 + \epsilon_{33}^\sigma E_3 \end{cases} \tag{3. 4}$$

Then, equation 3. 4 is transformed to (ε, E) coupling and we obtained:

$$\begin{cases} \sigma_1^p = \dfrac{1}{s_{11}^E}\,\varepsilon_1 - \dfrac{d_{31}}{s_{11}^E}E_3 \\ D_3 = \dfrac{d_{31}}{s_{11}^E}\varepsilon_1 + \left(\epsilon_{33}^\sigma - \dfrac{d_{31}^2}{s_{11}^E}\right)E_3 \end{cases} \tag{3. 5}$$

Where σ_1^p represents the uniaxial stress in the x-direction for the piezoelectric layer. Using the same notation as in equation 3. 3, we can write equation 3. 5 as the following:

$$\begin{cases} \sigma_1^p = c_p^E\,\varepsilon_1 - e_pE_3 \\ D_3 = e_p\varepsilon_1 + \epsilon_p^\varepsilon E_3 \end{cases} \tag{3. 6}$$

3.2.2 Case of piezoelectric patches bonded on a plate

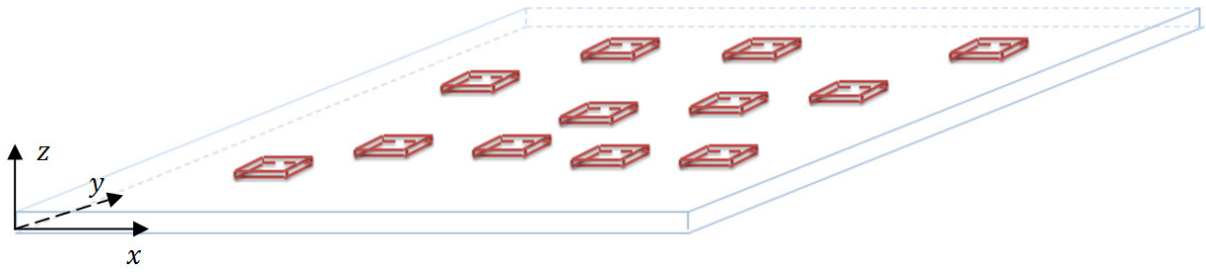

Figure 3. 6: Non-collocated piezoelectric patches bonded on a plate

The system studied in this case is composed of non-collocated piezoelectric patches bonded on a thin plate (having its two most important dimensions in the plane (x, y)) as shown in Figure 3. 6.

Similar to the case of beam, a uniform distribution in the z-direction is assumed for the electric field and the electric displacement. Also piezoelectric patches are polarized in the z direction.

In this case and as we considered the variation along y-axis, two active moments appeared due to stresses induced in x-direction and y-direction.

3.2.2.1 Mechanical constitutive equation

We are in the case of thin components, so state of plane stress is applied. σ_1, σ_2 and σ_6 are considered while σ_3, σ_4 and σ_5 are neglected. Using equation (2.7), we obtain:

$$\begin{pmatrix}\varepsilon_1\\ \varepsilon_2\\ \varepsilon_6\end{pmatrix} = \frac{1}{Y}\begin{bmatrix}1 & -\upsilon & 0\\ -\upsilon & 1 & 0\\ 0 & 0 & 2(1+\upsilon)\end{bmatrix}\begin{pmatrix}\sigma_1\\ \sigma_2\\ \sigma_6\end{pmatrix} \quad (3.7)$$

The inverse relation may be written as

$$\begin{pmatrix}\sigma_1^m\\ \sigma_2^m\\ \sigma_6^m\end{pmatrix} = \frac{Y}{1-\nu^2{}_m}\begin{bmatrix}1 & \nu_m & 0\\ \nu_m & 1 & 0\\ 0 & 0 & \frac{1-\nu_m}{2}\end{bmatrix}\begin{pmatrix}\varepsilon_1\\ \varepsilon_2\\ \varepsilon_6\end{pmatrix} = \begin{bmatrix}c_{11}^m & c_{12}^m & 0\\ c_{12}^m & c_{11}^m & 0\\ 0 & 0 & c_6^m\end{bmatrix}\begin{pmatrix}\varepsilon_1\\ \varepsilon_2\\ \varepsilon_6\end{pmatrix} \quad (3.8)$$

$$\{\sigma^m\}_{3\times1} = [c^m]\{\varepsilon\}_{3\times1} \quad (3.9)$$

Where $\{\sigma^m\}$ is the in plane stresses for the elastic layer and $[c^m]$ is the compliance tensor for the elastic layer case of plane stress assumption.

3.2.2.2 Piezoelectric constitutive equation

The same as the case of beam, the formulation used is that of (ε, E) coupling represented by equation (3. 3).

By using equation (2.11) and taking into account the assumption of equation (3. 1), we get:

$$\begin{pmatrix} \varepsilon_1 \\ \varepsilon_2 \\ \varepsilon_6 \\ D_3 \end{pmatrix} = \begin{bmatrix} s_{11}^E & s_{12}^E & 0 & d_{31} \\ s_{12}^E & s_{11}^E & 0 & d_{31} \\ 0 & 0 & 2 \times 2(s_{11}^E - s_{12}^E) & 0 \\ d_{31} & d_{31} & 0 & \epsilon_{33}^\sigma \end{bmatrix} \begin{pmatrix} \sigma_1 \\ \sigma_2 \\ \sigma_6 \\ E_3 \end{pmatrix}$$

3. 10

Then, equation 3. 10 is transformed to (ε, E) coupling and we obtain:

$$\begin{pmatrix} \sigma_1^p \\ \sigma_2^p \\ \sigma_6^p \\ D_3 \end{pmatrix} = \begin{bmatrix} \frac{s_{11}^E}{s_{11}^{2\,E} - s_{12}^{2\,E}} & \frac{-s_{12}^E}{s_{11}^{2\,E} - s_{12}^{2\,E}} & 0 & -\frac{d_{31}}{s_{11}^E + s_{12}^E} \\ \frac{-s_{12}^E}{s_{11}^{2\,E} - s_{12}^{2\,E}} & \frac{s_{11}^E}{s_{11}^{2\,E} - s_{12}^{2\,E}} & 0 & -\frac{d_{31}}{s_{11}^E + s_{12}^E} \\ 0 & 0 & \frac{1}{2 \times 2(s_{11}^E - s_{12}^E)} & 0 \\ \frac{d_{31}}{s_{11}^E + s_{12}^E} & \frac{d_{31}}{s_{11}^E + s_{12}^E} & 0 & \epsilon_{33}^\sigma - 2\frac{d_{31}^2}{s_{11}^E + s_{12}^E} \end{bmatrix} \begin{pmatrix} \varepsilon_1 \\ \varepsilon_2 \\ \varepsilon_6 \\ E_3 \end{pmatrix}$$

3. 11

Using the same notation as in equation 3. 3, we can write equation 3. 11 as the following:

$$\begin{pmatrix} \sigma_1^p \\ \sigma_2^p \\ \sigma_6^p \\ D_3 \end{pmatrix} = \begin{bmatrix} c_{11}^p & c_{12}^p & 0 & -e_{31}^p \\ c_{12}^p & c_{11}^p & 0 & -e_{32}^p \\ 0 & 0 & c_6^p & 0 \\ e_{31}^p & e_{32}^p & 0 & \epsilon_p^\varepsilon \end{bmatrix} \begin{pmatrix} \varepsilon_1 \\ \varepsilon_2 \\ \varepsilon_6 \\ E_3 \end{pmatrix}$$

3. 12

Or in its compact form like the following:

$$\{\sigma^p\}_{3\times1} = [c^p]\{\varepsilon\}_{3\times1} - [e^p]^t_{3\times1} E_3$$
$$D_3 = [e^p]_{1\times3}\{\varepsilon\}_{3\times1} + \epsilon_p^\varepsilon E_3$$

3. 13

3.3. Displacement field

When we determined the displacement field in chapter 2, section 2.4, it was determined according to the neutral axis in the case of beam or the neutral plane in the case of a plate. The neutral axis (plane) is the middle axis (plane) of a homogenous, symmetric and isotropic beam (plate) if this beam (plate) is not curved before bend occurs. It is the only axis (plane) where

there are no longitudinal stresses or strains, all the other axes (planes) on one side of it are in a state of tension, while those on the opposite side are in compression.

In our case of study where non-collocated piezoelectric patches bonded on thin structures, the system is asymmetric. Then, the neutral axis (plane) is not confused with the middle of the structure. We noted by z_n, the distance from the bottom of the system to the neutral axis (plane). Then equations (2.17) in the case of a beam and (2.20) in the case of a plate should be rewritten as the following:

$$\{u\} = \begin{cases} u_1(x,y,z,t) \approx -(z - z_n)\partial_x w(x,t) \\ u_2(x,y,z,t) = 0 \\ u_3(x,y,z,t) \approx w(x,t) \end{cases} \quad \text{3. 14}$$

$$\{u\} = \begin{cases} u_1(x,y,z,t) \approx -(z - z_n)\,\partial_x w(x,y,t) \\ u_2(x,y,z,t) \approx -(z - z_n)\,\partial_y w(x,y,t) \\ u_3(x,y,z,t) \approx w(x,y,t) \end{cases} \quad \text{3. 15}$$

Where w is the transverse displacement of the neutral axis (plane) of the system, and z is referred from the bottom of the system according to the coordinate system taken in Figure 3.7. Figure 3.7 gives the geometric parameters for the system studied (top figures) and schematic figures for the position of the neutral axis (plane) in the case of this asymmetric studied system (bottom figures). t_m, t_p represent respectively the thickness of the elastic material and the piezoelectric layer. b, b_p represent respectively the width of the elastic material and the piezoelectric layer. l, l_p represent respectively the length of the elastic material and the piezoelectric layer and (x_{pi},y_{pi}) represent the coordinate position of the ith piezoelectric patch. z_n can be determined by using the first Newton law.

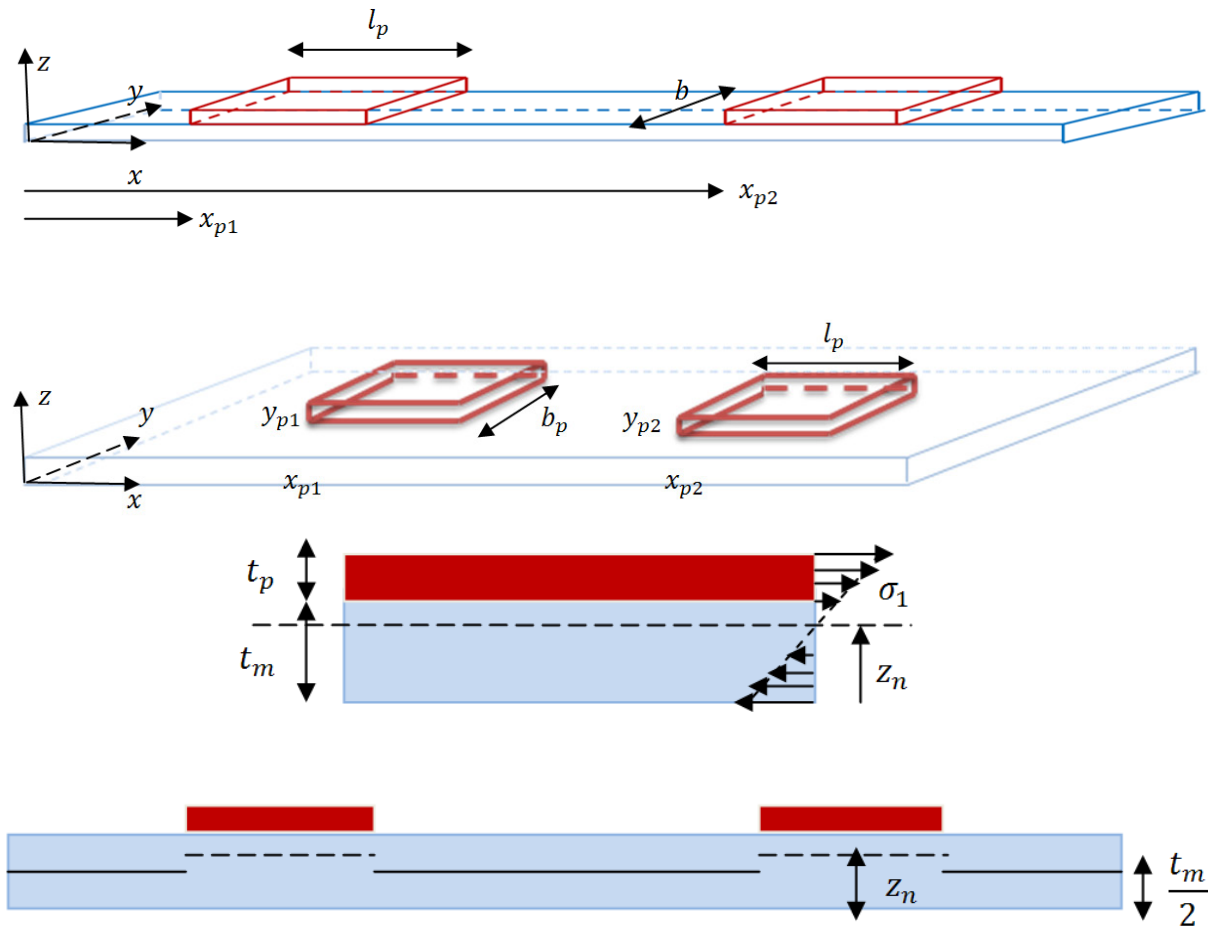

Figure 3.7: Geometric parameters for the system (top figures) and schematic figures for the position of the neutral axis (plane) in the case of this asymmetric studied system (bottom figures).

3.3.1 Neutral axis

Solving first Newton law gives:

$$\iint \sigma_1 dydz = 0 \qquad 3.16$$

Equation 3. 16 can be written as

$$b\int_0^{t_m} \sigma_1^m(z)dz + b\int_{t_m}^{t_m+t_p} \sigma_1^p(z)dz = 0 \qquad 3.17$$

The strain is calculated as a function of the flexion w using equation 2.2, them

$$\varepsilon_1 = \partial_x u_1 = -(z - z_n)\,\partial^2{}_x w(x,t) \qquad 3.18$$

Utilizing Hook's law (3. 2 & 3. 6) for each segment, while substituting strain relationship (3. 18), yields

$$\int_0^{t_m} c_{\ m}\,(z-z_n)dz \ + \int_{t_m}^{t_m+t_p} c_p(z-z_n)\,dz \ = 0$$

3. 19

And after simplification, the neutral plane z_n calculated from the bottom of the system according to the coordinate system adopted in

Figure 3.7 is equal to

$$z_n = \begin{cases} \frac{1}{2}\,\frac{c_m {t_m}^2 + c_p {t_p}^2 + 2c_p t_p t_m}{c_m t_m + c_p t_p} & if\ x \in to\ the\ piezoelectric\ pathes \\ \frac{t_m}{2} & if\ not \end{cases}$$

3. 20

We denote by x, the point that has an abscissa x

3.3.2 Neutral plane

Solving first Newton law gives:

$$\iint \sigma_1 dydz \ = 0$$
$$\iint \sigma_2 dxdz \ = 0$$

3. 21

Using equation 2.2, strains in x and y directions are determined in function of the transverse displacement w:

$$\varepsilon_1 = \ \partial_x u_1 = -\,(z-z_n)\,{\partial^2}_x w(x,y,t)$$
$$\varepsilon_2 = \ \partial_y u_2 = -\,(z-z_n)\,{\partial^2}_y w(x,y,t)$$

3. 22

Utilizing Hook's law (3. 8 & 3. 12), while substituting strain relationship (3. 22), yields

$$\int_{b_p} {\partial^2}_x w\ dy \left[\int_{t_p} c_{11}^p (z-z_n)dz + \int_{t_m} c_{11}^m (z-z_n)dz\right] +$$
$$\int_{b_p} {\partial^2}_y w\ dy \left[\int_{t_p} c_{12}^p (z-z_n)dz + \int_{t_m} c_{12}^m (z-z_n)dz\right] = 0$$

3. 23

$$\int_{l_p} {\partial^2}_x w\ dx \left[\int_{t_p} c_{12}^p (z-z_n)dz + \int_{t_m} c_{12}^m (z-z_n)dz\right] +$$
$$\int_{l_p} {\partial^2}_y w\ dx \left[\int_{t_p} c_{11}^p (z-z_n)dz + \int_{t_m} c_{11}^m (z-z_n)dz\right] = 0$$

3. 24

Equations (3. 23) and (3. 24) give

$$\int_{t_p} c_{11}^{p}(z-z_n)dz + \int_{t_m} c_{11}^{m}(z-z_n)dz = \int_{t_p} c_{12}^{p}(z-z_n)dz + \int_{t_m} c_{12}^{m}(z-z_n)dz$$

3. 25

And after simplification, the neutral plane z_n calculated from the bottom of the system according to the coordinate system adopted in

Figure 3.7 is equal to

$$\begin{cases} = \frac{1}{2}\dfrac{(c_{11}^{m} - c_{12}^{m})t_m{}^2 + (c_{11}^{p} - c_{12}^{p})t_p{}^2 + 2(c_{11}^{p} - c_{12}^{p})t_p t_m}{(c_{11}^{m} - c_{12}^{m})t_m + (c_{11}^{p} - c_{12}^{p})t_p} & if\ (x,y)\ \in to\ the\ piezoelectric\ pathes \\ = \dfrac{t_m}{2} & if\ not \end{cases}$$

3. 26

Be denoted by (x, y), the point that has an abscissa x and coordinate y.

3.4. Variational formulation

The variational equation is the last step before the numerical calculation. It will be used to write the element matrices of each element in the finite element formulation.

To obtain this equation, we should transform equation 2.32 represented again below in function of the flexion w(x, t) or w(x, y, t).

$$\int_V (-\rho\{\delta u\}^t\{\ddot{u}\} - \{\delta\varepsilon\}^t[c]\{\varepsilon\} + \{\delta\varepsilon\}^t[e]^t\{E\} + \{\delta E\}^t[e]\{\varepsilon\} + \{\delta E\}^t[\epsilon^{\varepsilon}]\{E\} + \{\delta u\}^t\{F_v\})dV + t_p\{\delta E\}Q = 0$$

3. 27

3.4.1 Case of 1D formulation

In the 1D case, w depends only of x direction so the integration in the y direction gives b, the width of the beam can be simplified from the equation.

In this case, each vector in the equation 3. 27 should be written as a function of w(x, t) and matrices must be replaced by what has been obtained in paragraph 3.2.1, then:

The variation of displacements can be written by:

$$\{\delta u\} = \begin{Bmatrix} -(z-z_n)\partial_x \delta w(x,t) \\ 0 \\ \delta w(x,t) \end{Bmatrix}$$

3. 28

The second derivative displacement is given by:

$$\{\ddot{u}\} = \begin{Bmatrix} -(z - z_n)\,\partial^2{}_t(\partial_x w(x,t)) \\ 0 \\ \partial^2{}_t(w(x,t)) \end{Bmatrix}$$

3. 29

The same, the strain tensor and the variation of strain are given by equation 3. 18:

$$\{\varepsilon\} = \varepsilon_1 = -(z - z_n)\,\partial^2{}_x w(x,t)$$
$$\{\delta\varepsilon\} = \delta\varepsilon_1 = -(z - z_n)\,\partial^2{}_x \delta w(x,t)$$

3. 30

The electric field is supposed to be uniformly distributed across the piezoelectric thicknesses and aligned on the normal to the mid-plane (z-direction), therefore:

$$\{E\} = E_{3pj}$$
$$\{\delta E\} = \delta E_{3pj}$$

3. 31

Where E_{3pi} is the electric field for the jth piezoelectric patch.

Volume density, stiffness tensor, piezoelectric constant tensor and dielectric permittivity tensor can be written in the case of 1 D formulation according to equations 3. 2 and 3. 6 by the following:

$$\rho = \begin{cases} \rho_p & if\ x \in to\ the\ piezoelectric\ pathes \\ \rho_m & if\ not \end{cases}$$
$$[c] = \begin{cases} c_p & if\ x \in to\ the\ piezoelectric\ pathes \\ c_m & if\ not \end{cases}$$
$$[e] = \begin{cases} e_p & if\ x \in to\ the\ piezoelectric\ pathes \\ 0 & if\ not \end{cases}$$
$$[\epsilon^{\varepsilon}] = \begin{cases} \epsilon_p^{\varepsilon} & if\ x \in to\ the\ piezoelectric\ pathes \\ 0 & if\ not \end{cases}$$

3. 32

Replacing equations 3. 28 to 3. 32 into the variational equation 3. 27 and taking the case where there are n piezoelectric patches bonded on the beam we obtain an integral over the volume depending on w(x,t). In this case, this integral is actually an integral over the surface equivalent to multiplying the surface integral by b and then integrates over the length of the beam. Moreover, the terms in z can be integrated.

Equation 3. 27 becomes:

$$\int_{x \notin piezo} A(x,t)dx + \int_{x \in piezo}[B(x,t) + qe_pE_{3pj}(t)\partial^2{}_x\delta w + \delta E_{3pj}(t)qe_p\partial^2{}_x w\,]dx -$$
$$\sum_{j=1}^{j=n}\delta E_{3pj}(t)\, l_p \mathrm{bt_p} \in_p E_{3pj}(t) - \mathrm{t_p}\sum_{j=1}^{j=n}\delta E_{3pj}(t)Q_{pj} - \{\delta \mathrm{w}\}\{F_z\} = 0$$

3. 33

F_z is the external mechanical forces applied to the beam having a component along z because that one takes into account the bending (forces along x are tensile forces and they are neglected in this modeling).

$$A(x,t) = \rho_m I_m \partial_x\delta w.\ \partial^2{}_t(\partial_x w) + b\rho_m t_m\ \delta w.\ \partial^2{}_t \mathrm{w} + I_m \mathrm{c_m}\ \partial^2{}_x\delta w.\ \partial^2{}_x w$$
$$B(x,t) = (\rho_p I_p + \rho_m I_m)\partial_x\delta w.\partial^2{}_t(\partial_x w) + b(\rho_p t_p + \rho_m t_m)\ \delta w.\ \partial^2{}_t \mathrm{w}$$
$$+(I_p \mathrm{c_p} + I_m \mathrm{c_m})\ \partial^2{}_x\delta w.\ \partial^2{}_x w$$
$$I_m = \mathrm{b}\int_0^{t_m}(z - z_n)^2\ \mathrm{dz} = \mathrm{b}\frac{1}{3}[(t_m - z_n)^3 + {z_n}^3]$$
$$I_p = \mathrm{b}\int_{t_m}^{t_p+t_m}(z - z_n)^2\ \mathrm{dz} = \mathrm{b}\frac{1}{3}[(t_p + t_m - z_n)^3 - (t_m - z_n)^3]$$
$$\mathrm{q} = \mathrm{b}\int_{t_m}^{t_p+t_m}(z - z_n)\ \mathrm{dz} = \mathrm{b}\frac{1}{2}[(t_p + t_m - z_n)^2 - (t_m - z_n)^2]$$

3. 34

Where Q_{pj} is the electric charge for the jth piezoelectric patch.

3.4.2 Case of 2D formulation

In this case w depends on x and y, the volume integral of equation 3. 27 is transformed on surface integral by integrating the terms of z.

Doing the same as the 1D formulation case, the variation of displacements can be written by:

$$\{\delta u\} = \begin{Bmatrix} -(z - z_n)\ \partial_x\delta w(x,y,t) \\ -(z - z_n)\ \partial_y\delta w(x,y,t) \\ \delta w(x,y,t) \end{Bmatrix}$$

3. 35

The second derivative displacement is given by:

$$\{\ddot{u}\} = \begin{Bmatrix} -(z - z_n)\ \partial^2{}_t(\partial_x w(x,y,t)\ ) \\ -(z - z_n)\ \partial^2{}_t(\partial_{yx} w(x,y,t)\ ) \\ \partial^2{}_t(w(x,y,t)) \end{Bmatrix}$$

3. 36

The same, the strain tensor and the variation of strain are given by:

$$\{\varepsilon\} = \begin{Bmatrix} \varepsilon_1 \\ \varepsilon_2 \\ \varepsilon_6 \end{Bmatrix} = \begin{Bmatrix} \partial_x u_1 \\ \partial_y u_2 \\ \partial_x u_1 + \partial_y u_2 \end{Bmatrix} = \begin{Bmatrix} -(z - z_n)\, \partial^2{}_x w(x,y,t) \\ -(z - z_n)\, \partial^2{}_x w(x,y,t) \\ -2(z - z_n)\, \partial^2{}_{xy} w(x,y,t) \end{Bmatrix}$$

3. 37

The electric field is supposed to be uniformly distributed across the piezoelectric thicknesses and aligned on the normal to the mid-plane (z-direction), therefore:

$$\{E\} = E_{3pj}$$

$$\{\delta E\} = \delta E_{3pj}$$

3. 38

Where E_{3pi} is the electric field for the jth piezoelectric patch.

Volume density, stiffness tensor, piezoelectric constant tensor and dielectric permittivity tensor can be written in the case of 2D formulation according to equations 3. 9 and 3. 13 by the following:

$$\rho = \begin{cases} \rho_p & if\ (x,y) \in to\ the\ piezoelectric\ pathes \\ \rho_m & if\ not \end{cases}$$

$$[c] = \begin{cases} [c^p] & if\ (x,y) \in to\ the\ piezoelectric\ pathes \\ [c^m] & if\ not \end{cases}$$

$$[\mathrm{e}] = \begin{cases} [e^p]_{1\times 3} & if\ (x,y) \in to\ the\ piezoelectric\ pathes \\ 0 & if\ not \end{cases}$$

$$[\epsilon^{\varepsilon}] = \begin{cases} \epsilon_p^{\varepsilon} & if\ (x,y) \in to\ the\ piezoelectric\ pathes \\ 0 & if\ not \end{cases}$$

3. 39

Replacing equations 3. 35 to 3. 39 into the variational equation 3. 27 and taking the case where there are n piezoelectric patches bonded on the plate we obtain an integral over the volume depending on w(x, y, t). By integrating the terms of z, an integral over the surface x, y is obtained.

Equation 3. 27 becomes:

$$\iint_{(x,y)\notin \text{piezo}} A(x,y,t)dxdy + \iint_{(x,y)\in \text{piezo}} \left[B(x,y,t) + q \begin{bmatrix} \partial^2{}_x \delta w \\ \partial^2{}_y \delta w \\ 2\partial^2_{xy} \delta w \end{bmatrix} [e^p]^{\mathrm{t}}\, E_{3pj}(t) + \right.$$

$$\left. \delta E_{3pj}(t) q [e^p] \begin{bmatrix} \partial^2{}_x \delta w \\ \partial^2{}_y \delta w \\ 2\partial^2_{xy} \delta w \end{bmatrix} \right] \mathrm{dxdy} - \sum_{j=1}^{j=n} \delta E_{3pj}(t)\, l_p b_p \mathrm{t_p}\, \epsilon_p^{\varepsilon} E_{3pj}(t) - \mathrm{t_p} \sum_{j=1}^{j=n} \delta E_{3pj}(t) Q_{pj} \quad -$$

$$\{\delta \mathrm{w}\}\{F_z\} = 0$$

3. 40

F_z is the external mechanical forces applied to the plate having a component along z because that one takes into account the bending (forces along x are tensile forces and they are neglected in this modeling).

$$A(x,y,t)= \rho_m I_m \begin{bmatrix}\partial_x \delta w \\ \partial_y \delta w\end{bmatrix}^t . \partial^2{}_t \begin{bmatrix}\partial_x w \\ \partial_y w\end{bmatrix} + \rho_m t_m\, \delta w . \partial^2{}_t \mathrm{w} + I_m \begin{bmatrix}\partial^2{}_x \delta w \\ \partial^2{}_y \delta w \\ 2\partial^2_{xy}\delta w\end{bmatrix}^t [c^m] \begin{bmatrix}\partial^2{}_x w \\ \partial^2{}_y w \\ 2\partial^2_{xy} w\end{bmatrix}$$

$$B(x,t) = (\rho_p I_p + \rho_m I_m)\begin{bmatrix}\partial_x \delta w \\ \partial_y \delta w\end{bmatrix}^t . \partial^2{}_t \begin{bmatrix}\partial_x w \\ \partial_y w\end{bmatrix} + (\rho_p t_p + \rho_m t_m)\, \delta w . \partial^2{}_t \mathrm{w} +$$

$$I_m \begin{bmatrix}\partial^2{}_x \delta w \\ \partial^2{}_y \delta w \\ 2\partial^2_{xy}\delta w\end{bmatrix}^t [c^m] \begin{bmatrix}\partial^2{}_x w \\ \partial^2{}_y w \\ 2\partial^2_{xy} w\end{bmatrix} + I_p \begin{bmatrix}\partial^2{}_x \delta w \\ \partial^2{}_y \delta w \\ 2\partial^2_{xy}\delta w\end{bmatrix}^t [c^p] \begin{bmatrix}\partial^2{}_x w \\ \partial^2{}_y w \\ 2\partial^2_{xy} w\end{bmatrix}$$

$$I_m = \int_0^{t_m} (z - z_n)^2 \, \mathrm{dz} = \frac{1}{3}\left[(t_m - z_n)^3 + {z_n}^3\right]$$

$$I_p = \int_{t_m}^{t_p + t_m} (z - z_n)^2 \, \mathrm{dz} = \frac{1}{3}\left[(t_p + t_m - z_n)^3 - (t_m - z_n)^3\right]$$

$$\mathrm{q} = \int_{t_m}^{t_p + t_m} (z - z_n) \, \mathrm{dz} = \frac{1}{2}\left[(t_p + t_m - z_n)^2 - (t_m - z_n)^2\right]$$

3. 41

Where Q_{pj} is the electric charge for the jth piezoelectric patch.

3.5. 1D finite element formulation

In a finite element formulation, the unknowns are the solution values at the nodes of the mesh and the displacement field {u} is related to the corresponding node values {u_i} by an interpolation functions. Lagrangian functions are not used in this problem because the solution w (x, t) must be C^1-continuous while Lagrange ensures C^0 continuity; the choice of Hermite elements satisfies this condition. Thus, with Hermite elements, the solution {u} that depends only on w (x, t) in this case, and it is written as follows on a segment Si:

$$\mathrm{w}(\mathrm{x}, \mathrm{t}) = [\lambda(x)]\{u_i\}$$

3. 42

Where $[\lambda(x)] = [\lambda_1(x) \quad \lambda_2(x) \quad \lambda_3(x) \quad \lambda_4(x)]$ are the interpolation functions [(Dhatt, et al., 2005)] and $\{u_i\} = \begin{bmatrix} w_i \\ \partial_x w_i \\ w_{i+1} \\ \partial_x w_{i+1}\end{bmatrix}$ are the unknowns in segment Si.

Therefore, to calculate the first spatial derivative, it suffices to derive the interpolation functions:

$$\partial_x w = [\partial_x \lambda(x)]\{u_i\}$$

3. 43

It is similarly for a second derivative or more.

Furthermore, with this formulation, we can express the variation in displacement δw:

$$\{\delta w\} = [\lambda(x)]\{\delta u_i\}$$

3. 44

Thus, the variational equation 3. 33 becomes a sum of integrals over each element:

$$\sum_{if\ \notin piezo} \Big[\{\delta u_i\}^t \int_{x_i}^{x_{i+1}} (b\rho_m t_m\ [\lambda]^t[\lambda] + \rho_m I_m[\partial_x\lambda]^t[\partial_x\lambda])dx\{\ddot{u_i}\} +$$

$$\{\delta u_i\}^t \int_{x_i}^{x_{i+1}} I_m c_m\, [\partial^2{}_x\lambda]^t[\partial^2{}_x\lambda]dx\{u_i\}\Big] +$$

$$\sum_{if\ \epsilon\ piezoj} \Big[\{\delta u_i\}^t \int_{x_i}^{x_{i+1}} b(\rho_p t_p + \rho_m t_m)\ \ [\lambda]^t[\lambda] + (\rho_p I_p + \rho_m I_m)[\partial_x\lambda]^t[\partial_x\lambda])dx\{\ddot{u_i}\} +$$

$$\{\delta u_i\}^t \int_{x_i}^{x_{i+1}} (I_p c_p + I_m c_m)[\partial^2{}_x\lambda]^t[\partial^2{}_x\lambda]dx\{u_i\} +$$

$$\{\delta u_i\}^t \int_{x_i}^{x_{i+1}} qe_p[\partial^2{}_x\lambda]^t dx\{E_{3pj}(t)\} + \{\delta E_{3pj}(t)\} \int_{x_i}^{x_{i+1}} qe_p[\partial^2{}_x\lambda]dx\,\{u_i\}\Big] -$$

$$\{\delta E_{3pj}(t)\}\, l_p bt_p \in_p \{E_{3pj}(t)\} - t_p\{\delta E_{3pj}(t)\}\{Q_{pj}\} - \{\delta u_i\}^t\{F_i\} = 0$$

3. 45

This equation will be used to determine the numerical equation in matrix form.

3.6. 2D finite element formulation

For the same reason as in the 1D case, Hermit elements are used as the interpolation functions in this problem because the solution w (x, y, t) must be C^1-continuous.

w (x, y, t) in this case reads as follows on a triangle Δi:

$$w(x, y, t) = [\lambda(x, y)]\{u_i\}$$

3. 46

Where $[\lambda(x, y)] = [\lambda_1, \lambda_2, \dots, \lambda_9]$ are the interpolation functions [(Dhatt, et al., 2005)], and

$\{u_i\} = \begin{bmatrix} w_i \\ \partial_x w_i \\ \partial_y w_i \\ w_{i+1} \\ \partial_x w_{i+1} \\ \partial_y w_{i+1} \\ w_{i+2} \\ \partial_x w_{i+2} \\ \partial_y w_{i+2} \end{bmatrix}$ are the unknowns of the triangle Δi.

Following the same procedure as in 1D formulation and integrating equation 3. 40 in the plane (x, y) of the system returns to integrate on each triangle and makes the sum:

$$\sum_{\Delta_i \notin \text{piezos}} \iint_{\Delta_i} \{\delta u_i\}^t \left[\left(\rho_m I_m \begin{bmatrix} \partial_x\lambda \\ \partial_y\lambda \end{bmatrix}^t \begin{bmatrix} \partial_x\lambda \\ \partial_y\lambda \end{bmatrix} + \rho_m t_m [\lambda]^t\,[\lambda] \right) \{\ddot{u}_i\} + I_m \begin{bmatrix} \frac{\partial^2\lambda}{\partial x^2} \\ \frac{\partial^2\lambda}{\partial y^2} \\ 2\frac{\partial^2\lambda}{\partial x \partial y} \end{bmatrix}^t [c^m] \begin{bmatrix} \frac{\partial^2\lambda}{\partial x^2} \\ \frac{\partial^2\lambda}{\partial y^2} \\ 2\frac{\partial^2\lambda}{\partial x \partial y} \end{bmatrix} \{u_i\} \right] dxdy +$$

$$\sum_{\Delta_i \in \text{piezoj}} \iint_{\Delta_i} \left[\{\delta u_i\}^t \left[\left((\rho_p I_p + \rho_m I_m) \begin{bmatrix} \partial_x\lambda \\ \partial_y\lambda \end{bmatrix}^t \begin{bmatrix} \partial_x\lambda \\ \partial_y\lambda \end{bmatrix} + (\rho_p t_p + \rho_m t_m)[\lambda]^t\,[\lambda] \right) \{\ddot{u}_i\} + \left(I_m \begin{bmatrix} \frac{\partial^2\lambda}{\partial x^2} \\ \frac{\partial^2\lambda}{\partial y^2} \\ 2\frac{\partial^2\lambda}{\partial x \partial y} \end{bmatrix}^t [C^m] \begin{bmatrix} \frac{\partial^2\lambda}{\partial x^2} \\ \frac{\partial^2\lambda}{\partial y^2} \\ 2\frac{\partial^2\lambda}{\partial x \partial y} \end{bmatrix} + I_p \begin{bmatrix} \frac{\partial^2\lambda}{\partial x^2} \\ \frac{\partial^2\lambda}{\partial y^2} \\ 2\frac{\partial^2\lambda}{\partial x \partial y} \end{bmatrix}^t [C^p] \begin{bmatrix} \frac{\partial^2\lambda}{\partial x^2} \\ \frac{\partial^2\lambda}{\partial y^2} \\ 2\frac{\partial^2\lambda}{\partial x \partial y} \end{bmatrix} \right) \{u_i\} + q \begin{bmatrix} \frac{\partial^2\lambda}{\partial x^2} \\ \frac{\partial^2\lambda}{\partial y^2} \\ 2\frac{\partial^2\lambda}{\partial x \partial y} \end{bmatrix}^t [e^p]^t \{E_{3pj}(t)\} + \{\delta E_{3pj}(t)\}\, q [e^p] \begin{bmatrix} \frac{\partial^2\lambda}{\partial x^2} \\ \frac{\partial^2\lambda}{\partial y^2} \\ 2\frac{\partial^2\lambda}{\partial x \partial y} \end{bmatrix} \{u_i\} \right] dxdy -$$

$$\{\delta E_{3pj}(t)\}\, l_p b_p t_p\, \epsilon_p^{\varepsilon} \{E_{3pj}(t)\} - t_p \{\delta E_{3pj}(t)\} \{Q_{pj}\} \quad - \{\delta u_i\}^t \{F_i\} = 0$$

3. 47

This equation will be used to determine the numerical equation in matrix form.

3.7. Numerical equation

Differentiating equations 3. 45 and 3. 47 with respect to $\{\delta u_i\}^t$, the mechanical equation is obtained. The same, differentiating with respect to $\{\delta E_{3pj}(t)\}$, the electrical equation is obtained.

With these equations, constructing elementary matrices for each element (segment and triangle) and assembling all thanks to the inter-element continuity property, the numerical equation is written, taken into account the boundary conditions in the assembly of matrices. Taking the case where there are N nodes of the mesh in the two cases.

3.7.1 Case of beam

Differentiating equations 3. 45 with respect to $\{\delta u_i\}^t$, the mechanical equation is obtained:

$$\sum_{if\ \notin\ piezo}\left[\int_{x_i}^{x_{i+1}}(b\rho_m t_m\ [\lambda]^t[\lambda]+\rho_m I_m[\partial_x\lambda]^t[\partial_x\lambda])dx\{\ddot{u_i}\}+\right.$$
$$\left.\int_{x_i}^{x_{i+1}} I_m c_m\,[\partial^2{}_x\lambda]^t[\partial^2{}_x\lambda]dx\{u_i\}\right]+$$
$$\sum_{if\ \epsilon\ piezoj}\left[\int_{x_i}^{x_{i+1}} b(\rho_p t_p+\rho_m t_m)\ [\lambda]^t[\lambda]+(\rho_p I_p+\rho_m I_m)[\partial_x\lambda]^t[\partial_x\lambda])dx\{\ddot{u_i}\}+\right.$$
$$\left.\int_{x_i}^{x_{i+1}}(I_p c_p+I_m c_m)[\partial^2{}_x\lambda]^t[\partial^2{}_x\lambda]dx\{u_i\}+\int_{x_i}^{x_{i+1}} qe_p[\partial^2{}_x\lambda]^t dx\{E_{3pj}(t)\}\right]-\{F_i\}=0$$

3. 48

Using equation 3. 48, elementary matrices for each segment are constructed as the following:

$$M_{mm\_elem}\begin{cases}\int_{x_i}^{x_{i+1}} b(\rho_p t_p+\rho_m t_m)\ [\lambda]^t[\lambda]+(\rho_p I_p+\rho_m I_m)[\partial_x\lambda]^t[\partial_x\lambda])dx \\ \qquad if\ x\in to\ \text{the}\ piezoelectric\ pathes \\ \int_{x_i}^{x_{i+1}} (b\rho_m t_m\,[\lambda]^t[\lambda]+\rho_m I_m[\partial_x\lambda]^t[\partial_x\lambda])dx \\ \qquad ifnot\end{cases}$$

M_{mm_elem} has dimension 4×4

$$K_{mm\_elem}\begin{cases}\int_{x_i}^{x_{i+1}} (I_p c_p+I_m c_m)\left[\partial^2{}_x\lambda\right]^t\left[\partial^2{}_x\lambda\right]dx & if\ x\in to\ \text{the}\ piezoelectric\ pathes \\ \int_{x_i}^{x_{i+1}} I_m c_m\left[\partial^2{}_x\lambda\right]^t\left[\partial^2{}_x\lambda\right]dx & ifnot\end{cases}$$

K_{mm_elem} has dimension 4×4

$$K_{mvpj\_elem}\begin{cases}\int_{x_i}^{x_{i+1}} qe_p\left[\partial^2{}_x\lambda\right]^t dx & at\ the\ jth\ piezoelectric\ patch\end{cases}$$

K_{mvpj_elem} has dimension 4×1

3. 49

Assembling all thanks to the inter-element continuity property, the numerical mechanical equation is written:

$$[M_{mm}]\{\ddot{U_i}\}+[K_{mm}]\{U_i\}+[K_{mvpj}]\{E_{3pj}\}=\{F_i\}$$

3. 50

$[M_{mm}]$: the structural mass matrix has dimension 2N×2N,

$[K_{mm}]$: the structural stiffness matrix has dimension 2N×2N,

$[K_{mvpj}]$: the piezoelectric stiffness matrices for the n piezoelectric patches (j=1 to n), where $[K_{mvpj}] = [K_{mvp1} \quad \cdots \quad K_{mvpj} \quad \ldots \quad K_{mvpn}]$, has dimension 2N× n.

$\{U_i\}$: the vector with nodal structural displacements has dimension 2N×1,

$\{E_{3pj}\}$: the vector with the electric fields for the n piezoelectric patches (j=1 to n) has dimension n× 1,

$\{F_i\}$: the vector with nodal forces has dimension 2N×1.

The same, differentiating 3. 45 with respect to $\{\delta E_{3pj}(t)\}$, the electrical equation is obtained:

$$\sum_{Si\,\epsilon\,piezoj}\left[\int_{x_i}^{x_{i+1}} qe_p[\partial^2{}_x\lambda]dx\,\{u_i\}\right] - l_p \mathrm{bt_p}\,\epsilon_p\,\{E_{3pj}(t)\} = \mathrm{t_p}\{Q_{pj}\}$$

3. 51

Using the above equation, elementary matrices for each segment are constructed as the following:

$$K_{vmpj\_elem}\left\{\int_{x_i}^{x_{i+1}} qe_p\left[\partial^2{}_x\lambda\right]dx \quad at\ the\ jth\ piezoelectric\ patch\right.$$

K_{vmpj_elem} has dimension 1×4

$$K_{vvpj_{elem}}\{-\,l_p \mathrm{bt_p}\,\epsilon_p \qquad at\ the\ jth\ piezoelectric\ patch$$

$K_{vvpj_{elem}}$ has dimension 1×1

3. 52

Assembling all thanks to the inter-element continuity property, the numerical mechanical equation is written:

$$[K_{vmpj}]\,\{U_i\} + [K_{vvpj}]\,\{E_{3pj}\} = t_p\{Q_{pj}\}$$

3. 53

$[K_{vmpj}] = [K_{mvpj}]^t$ has dimension n×2N

$[K_{vvpj}]$: the dielectric stiffness matrix for the n piezoelectric patches (j=1 to n), where

$$[K_{vvpj}] = \begin{bmatrix} K_{vvp1} & 0 & 0 & \cdots & 0 \\ 0 & \ddots & \cdots & 0 & \vdots \\ \vdots & 0 & K_{vvpj} & 0 & 0 \\ 0 & 0 & \cdots & \ddots & 0 \\ 0 & \cdots & 0 & 0 & K_{vvpn} \end{bmatrix}$$, has dimension n×n

$\{Q_{pj}\}$: the vector with the charges for the n piezoelectric patches (j=1 to n), has dimension n×1.

3.7.2 Case of plate

Differentiating equations 3. 47 with respect to $\{\delta u_i\}^t$, the mechanical equation is obtained:

$$\sum_{\Delta_i \notin \text{piezos}} \iint_{\Delta_i} \left[\left(\rho_m I_m \begin{bmatrix} \partial_x \lambda \\ \partial_y \lambda \end{bmatrix}^t \begin{bmatrix} \partial_x \lambda \\ \partial_y \lambda \end{bmatrix} + \rho_m t_m [\lambda]^t [\lambda] \right) \{\ddot{u_i}\} + I_m \begin{bmatrix} \frac{\partial^2 \lambda}{\partial x^2} \\ \frac{\partial^2 \lambda}{\partial y^2} \\ 2\frac{\partial^2 \lambda}{\partial x \partial y} \end{bmatrix}^t [c^m] \begin{bmatrix} \frac{\partial^2 \lambda}{\partial x^2} \\ \frac{\partial^2 \lambda}{\partial y^2} \\ 2\frac{\partial^2 \lambda}{\partial x \partial y} \end{bmatrix} \{u_i\} \right] dxdy + \sum_{\Delta_i \in \text{piezoj}} \iint_{\Delta_i} \left[\left((\rho_p I_p + \rho_m I_m) \begin{bmatrix} \partial_x \lambda \\ \partial_y \lambda \end{bmatrix}^t \begin{bmatrix} \partial_x \lambda \\ \partial_y \lambda \end{bmatrix} + (\rho_p t_p + \rho_m t_m)[\lambda]^t [\lambda] \right) \{\ddot{u_i}\} + \left(I_m \begin{bmatrix} \frac{\partial^2 \lambda}{\partial x^2} \\ \frac{\partial^2 \lambda}{\partial y^2} \\ 2\frac{\partial^2 \lambda}{\partial x \partial y} \end{bmatrix}^t [C^m] \begin{bmatrix} \frac{\partial^2 \lambda}{\partial x^2} \\ \frac{\partial^2 \lambda}{\partial y^2} \\ 2\frac{\partial^2 \lambda}{\partial x \partial y} \end{bmatrix} + I_p \begin{bmatrix} \frac{\partial^2 \lambda}{\partial x^2} \\ \frac{\partial^2 \lambda}{\partial y^2} \\ 2\frac{\partial^2 \lambda}{\partial x \partial y} \end{bmatrix}^t [C^p] \begin{bmatrix} \frac{\partial^2 \lambda}{\partial x^2} \\ \frac{\partial^2 \lambda}{\partial y^2} \\ 2\frac{\partial^2 \lambda}{\partial x \partial y} \end{bmatrix} \right) \{u_i\} + q \begin{bmatrix} \frac{\partial^2 \lambda}{\partial x^2} \\ \frac{\partial^2 \lambda}{\partial y^2} \\ 2\frac{\partial^2 \lambda}{\partial x \partial y} \end{bmatrix}^t [e^p]^t \{ E_{3pj}(t) \} \right] dxdy = \{F_i\}$$

3. 54

With this equation doing the same as the case of beam, constructing elementary matrices for each triangle and assembling all thanks to the inter-element continuity property, the numerical mechanical equation is written:

$$[M_{mm}] \{\ddot{U_i}\} + [K_{mm}] \{U_i\} + [K_{mvpj}] \{E_{3pj}\} = \{F_i\}$$

3. 55

$[M_{mm}]$, $[K_{mm}]$, $[K_{mvpj}]$, $\{U_i\}$ and $\{F_i\}$ have respectively 3N×3N, 3N×3N, 3N×n, 3N×1 and 3N×1 dimensions.

The same, differentiating 3. 47 with respect to $\{\delta E_{3pj}(t)\}$, the electrical equation is obtained:

$$\sum_{\Delta_i \in \text{piezoj}} \iint_{\Delta_i} q[e^p] \begin{bmatrix} \frac{\partial^2 \lambda}{\partial x^2} \\ \frac{\partial^2 \lambda}{\partial y^2} \\ 2\frac{\partial^2 \lambda}{\partial x \partial y} \end{bmatrix} \{u_i\} dxdy - l_p b_p t_p \epsilon_p^{\varepsilon} \{E_{3pj}(t)\} = t_p \{Q_{pj}\}$$

3. 56

Then, after constructing elementary matrices for each triangle and assembling all of them, the numerical electrical equation is given:

$$[K_{vmpj}]\{U_i\} + [K_{vvpj}]\{E_{3pj}\} = t_p\{Q_{pj}\} \quad (3.57)$$

3.7.3 Beam-plate numerical equation

By assembling mechanical and electrical equations in one matrix equation, we get:

$$\begin{bmatrix}[M_{mm}] & 0\\ 0 & 0\end{bmatrix}\begin{bmatrix}\{\ddot{U}_i\}\\ \{\ddot{E}_{3pj}\}\end{bmatrix} + \begin{bmatrix}[C_{mm}] & 0\\ 0 & 0\end{bmatrix}\begin{bmatrix}\{\dot{U}_i\}\\ \{\dot{E}_{3pj}\}\end{bmatrix} + \begin{bmatrix}[K_{mm}] & [K_{mvpj}]\\ [K_{vmpj}] & [K_{vvpj}]\end{bmatrix}\begin{bmatrix}\{U_i\}\\ \{E_{3pj}\}\end{bmatrix} = \begin{bmatrix}\{F_i\}\\ t_p\{Q_{pj}\}\end{bmatrix} \quad (3.58)$$

The structural damping matrix [C] is added to the system and it is determined experimentally to match the damping behavior of the real system (more detailed in chapter 4).

Particular cases for two and four piezoelectric patches are taken in appendix to better understanding. Sometimes it is better to use a formulation with the time derivatives of Q or a mix between Q and E as the cases of the two following subparagraphs.

3.7.4 Actuator – sensor

The first case treated is the case actuator-sensor where the patches actuators are deformed under the effect of an electric fields $E_{3pa}(t)$ and the patches sensors behave like an open circuit ($Q_{ps} = 0$), while no external loads applied. The letter 'a' is referred to actuators patches and the letter 's' to sensors patches. The equation 3.58 becomes:

$$\begin{bmatrix}[M_{mm}] & 0 & 0\\ 0 & 0 & 0\\ 0 & 0 & 0\end{bmatrix}\begin{bmatrix}\{\ddot{U}_i\}\\ t_p\{\ddot{Q}_{pa}\}\\ \{\ddot{E}_{3ps}\}\end{bmatrix} + \begin{bmatrix}[C_{mm}] & 0 & 0\\ 0 & 0 & 0\\ 0 & 0 & 0\end{bmatrix}\begin{bmatrix}\{\dot{U}_i\}\\ t_p\{\dot{Q}_{pa}\}\\ \{\dot{E}_{3ps}\}\end{bmatrix} +$$

$$\begin{bmatrix}[K_{mm} - \sum_{j\in a} K_{mvpj}K_{vvpj}^{-1}K_{vmpj}] & [K_{mvpa}K_{vvpa}^{-1}] & [K_{mvps}]\\ -[K_{vvpa}^{-1}K_{vmpa}] & [K_{vvpa}^{-1}] & 0\\ [K_{vmps}] & 0 & [K_{vvps}]\end{bmatrix}\begin{bmatrix}\{U_i\}\\ t_p\{Q_{pa}\}\\ \{E_{3ps}\}\end{bmatrix} = \begin{bmatrix}0\\ \{E_{3pa}\}\\ 0\end{bmatrix} \quad (3.59)$$

To clarify, a particular case of four piezoelectric patches where two patches are considered as actuators and the two others as sensors is taken in appendix.

3.7.5 Actuator – Actuator

In this case all patches are used as actuators while no external loads applied. The model system obtained from equation 3.58 is governed by the following matrix equation:

$$\begin{bmatrix}[M_{mm}] & 0 & 0\\ 0 & 0 & 0\\ 0 & 0 & 0\end{bmatrix}\begin{bmatrix}\{\ddot{U}_i\}\\ t_p\{\ddot{Q}_{pa}\}\end{bmatrix}+\begin{bmatrix}[C_{mm}] & 0 & 0\\ 0 & 0 & 0\\ 0 & 0 & 0\end{bmatrix}\begin{bmatrix}\{\dot{U}_i\}\\ t_p\{\dot{Q}_{pa}\}\end{bmatrix}+$$
$$\begin{bmatrix}[K_{mm}-\sum_{j\in a}K_{mvpj}K_{vvpj}^{-1}K_{vmpj}] & [K_{mvpa}K_{vvpa}^{-1}]\\ -[K_{vvpa}^{-1}K_{vmpa}] & [K_{vvpa}^{-1}]\end{bmatrix}\begin{bmatrix}\{U_i\}\\ t_p\{Q_{pa}\}\end{bmatrix}=\begin{bmatrix}0\\ \{E_{3pa}\}\end{bmatrix}$$

3. 60

A particular case of four piezoelectric patches is taken in appendix to clarify.

3.8 Conclusion of the chapter

Using this beam-plate numerical equation, we are able to analyze any asymmetric system consisted of non-collocated piezoelectric patches bonded on thin structures. In the following some examples are cited:

Using this numerical equation, we can calculate the resonance frequencies and determining the mode shapes. We can compute the transverse displacements of the system, stresses, and strains obtained by applying forces on the system or by applying electrical voltages on some piezoelectric patches; we can also determine the obtained voltages for others piezoelectric batches. Also we can compute the currents values and the electric charges of piezoelectric patches.

An experimental device will be built and tested in the next chapter to validate the model.

3.9 Appendix: Particular cases

1. Modeling of the system using FEM

In the case of two piezoelectric patches, the equation (3. 58) wrote as:

$$\begin{bmatrix} M_{mm} & 0 & 0 \\ 0 & 0 & 0 \\ 0 & 0 & 0 \end{bmatrix}\begin{bmatrix} \ddot{U}_\iota \\ \ddot{E}_{3p1} \\ \ddot{E}_{3p2} \end{bmatrix}+\begin{bmatrix} C_{mm} & 0 & 0 \\ 0 & 0 & 0 \\ 0 & 0 & 0 \end{bmatrix}\begin{bmatrix} \dot{U}_\iota \\ \dot{E}_{3p1} \\ \dot{E}_{3p2} \end{bmatrix}+\begin{bmatrix} K_{mm} & K_{mvp1} & K_{mvp2} \\ K_{vmp1} & K_{vvp1} & 0 \\ K_{vmp2} & 0 & K_{vvp2} \end{bmatrix}\begin{bmatrix} U_i \\ E_{3p1} \\ E_{3p2} \end{bmatrix}=\begin{bmatrix} F_i \\ t_p Q_{p1} \\ t_p Q_{p2} \end{bmatrix} \quad \text{(A.1.1)}$$

And if we have four piezoelectric patches for example, the equation (3. 58) should be written as:

$$\begin{bmatrix} M_{mm} & 0 & 0 & 0 & 0 \\ 0 & 0 & 0 & 0 & 0 \\ 0 & 0 & 0 & 0 & 0 \\ 0 & 0 & 0 & 0 & 0 \\ 0 & 0 & 0 & 0 & 0 \end{bmatrix}\begin{bmatrix} \ddot{U}_\iota \\ \ddot{E}_{3p1} \\ \ddot{E}_{3p2} \\ \ddot{E}_{3p3} \\ \ddot{E}_{3p4} \end{bmatrix}+\begin{bmatrix} C_{mm} & 0 & 0 & 0 & 0 \\ 0 & 0 & 0 & 0 & 0 \\ 0 & 0 & 0 & 0 & 0 \\ 0 & 0 & 0 & 0 & 0 \\ 0 & 0 & 0 & 0 & 0 \end{bmatrix}\begin{bmatrix} \dot{U}_\iota \\ \dot{E}_{3p1} \\ \dot{E}_{3p2} \\ \dot{E}_{3p3} \\ \dot{E}_{3p4} \end{bmatrix}+$$

$$\begin{bmatrix} K_{mm} & K_{mvp1} & K_{mvp2} & K_{mvp3} & K_{mvp4} \\ K_{vmp1} & K_{vvp1} & 0 & 0 & 0 \\ K_{vmp2} & 0 & K_{vvp2} & 0 & 0 \\ K_{vmp3} & 0 & 0 & K_{vvp3} & 0 \\ K_{vmp4} & 0 & 0 & 0 & K_{vvp4} \end{bmatrix}\begin{bmatrix} U_i \\ E_{3p1} \\ E_{3p2} \\ E_{3p3} \\ E_{3p4} \end{bmatrix}=\begin{bmatrix} F_i \\ t_p Q_{p1} \\ t_p Q_{p2} \\ t_p Q_{p3} \\ t_p Q_{p4} \end{bmatrix}$$

(A.1.2)

2. Actuator-sensor

Taking the case of four piezoelectric patches where the patch 1 and 3 are considered as actuators while the two others as sensors, the equation (3. 59) is written as:

$$\begin{bmatrix} M_{mm} & 0 & 0 & 0 & 0 \\ 0 & 0 & 0 & 0 & 0 \\ 0 & 0 & 0 & 0 & 0 \\ 0 & 0 & 0 & 0 & 0 \\ 0 & 0 & 0 & 0 & 0 \end{bmatrix}\begin{bmatrix} \ddot{U}_\iota \\ t_p \ddot{Q}_{p1} \\ t_p \ddot{Q}_{p3} \\ \ddot{E}_{3p2} \\ \ddot{E}_{3p4} \end{bmatrix}+\begin{bmatrix} C_{mm} & 0 & 0 & 0 & 0 \\ 0 & 0 & 0 & 0 & 0 \\ 0 & 0 & 0 & 0 & 0 \\ 0 & 0 & 0 & 0 & 0 \\ 0 & 0 & 0 & 0 & 0 \end{bmatrix}\begin{bmatrix} \dot{U}_\iota \\ t_p \dot{Q}_{p1} \\ t_p \dot{Q}_{p3} \\ \dot{E}_{3p2} \\ \dot{E}_{3p4} \end{bmatrix}+$$

$$\begin{bmatrix} K_{mm}-K_{mvp1}K_{vvp1}^{-1}K_{vmp1}-K_{mvp3}K_{vvp3}^{-1}K_{vmp3} & K_{mvp1}K_{vvp1}^{-1} & K_{mvp3}K_{vvp3}^{-1} & K_{mvp2} & K_{mvp4} \\ -K_{vvp1}^{-1}K_{vmp1} & K_{vvp1}^{-1} & 0 & 0 & 0 \\ -K_{vvp3}^{-1}K_{vmp3} & 0 & K_{vvp3}^{-1} & 0 & 0 \\ K_{vmp2} & 0 & 0 & K_{vvp2} & 0 \\ K_{vmp4} & 0 & 0 & 0 & K_{vvp4} \end{bmatrix}\begin{bmatrix} U_i \\ t_p Q_{p1} \\ t_p Q_{p3} \\ E_{3p2} \\ E_{3p4} \end{bmatrix}$$

$$=\begin{bmatrix} 0 \\ E_{3p1} \\ E_{3p3} \\ 0 \\ 0 \end{bmatrix}$$

(A.2.1)

3. Actuator-actuator

Consider the case where four piezoelectric patches are used as actuators, the equation (3. 60) should be written as:

$$\begin{bmatrix} M_{mm} & 0 & 0 & 0 & 0 \\ 0 & 0 & 0 & 0 & 0 \\ 0 & 0 & 0 & 0 & 0 \\ 0 & 0 & 0 & 0 & 0 \\ 0 & 0 & 0 & 0 & 0 \end{bmatrix} \begin{bmatrix} \ddot{U}_i \\ t_p\ddot{Q}_{p1} \\ t_p\ddot{Q}_{p2} \\ t_p\ddot{Q}_{p3} \\ t_p\ddot{Q}_{p4} \end{bmatrix} + \begin{bmatrix} C_{mm} & 0 & 0 & 0 & 0 \\ 0 & 0 & 0 & 0 & 0 \\ 0 & 0 & 0 & 0 & 0 \\ 0 & 0 & 0 & 0 & 0 \\ 0 & 0 & 0 & 0 & 0 \end{bmatrix} \begin{bmatrix} \dot{U}_i \\ t_p\dot{Q}_{p1} \\ t_p\dot{Q}_{p2} \\ t_p\dot{Q}_{p3} \\ t_p\dot{Q}_{p4} \end{bmatrix} +$$

$$\begin{bmatrix} K_{mm} - \sum_{a=1}^{4} K_{mvpa}K_{vvpa}^{-1}K_{vmpa} & K_{mvp1}K_{vvp1}^{-1} & K_{mvp2}K_{vvp2}^{-1} & K_{mvp3}K_{vvp3}^{-1} & K_{mvp4}K_{vvp4}^{-1} \\ -K_{vvp1}^{-1}K_{vmp1} & K_{vvp1}^{-1} & 0 & 0 & 0 \\ -K_{vvp2}^{-1}K_{vmp2} & 0 & K_{vvp2}^{-1} & 0 & 0 \\ -K_{vvp3}^{-1}K_{vmp3} & 0 & 0 & K_{vvp3}^{-1} & 0 \\ -K_{vvp4}^{-1}K_{vmp4} & 0 & 0 & 0 & K_{vvp4}^{-1} \end{bmatrix} \begin{bmatrix} U_i \\ E_{3p1} \\ E_{3p2} \\ E_{3p3} \\ E_{3p4} \end{bmatrix}$$

$$= \begin{bmatrix} 0 \\ E_{3p1} \\ E_{3p2} \\ E_{3p3} \\ E_{3p4} \end{bmatrix}$$

(A.3.1)

3.10 References

Bernard Y. et Razek A. Piezoelectric valve modeling and design [Revue] // AC2011. - 2011. - pp. pp.124-131..

Chen J.S., Chen S.H. et Wu K.C. Analysis of asymmetric piezoelectric composite beam, [Revue] // DTIP 2007. - 2007.

Corcolle R. [et al.] Modeling of a beam structure with piezoelectric materials: introduction to SSD techniques [Revue] // COMPEL: The International Journal for Computation and Mathematics in Electrical and Electronic Engineering. - 2008. - pp. pp. 205-214.

Corcolle R., Bouillault F. et Bernard , Y. Modeling of a plate with piezoelectric patches: Damping application [Revue] // IEEE Transactions on Magnetics. - 2008. - pp. vol. MAG 44, no.6, pp. 798-801.

de Abreu G.L.C.M., Ribeiro J.F. et Steffen V. Finite element modeling of a plate with localized piezoelectric sensors and actuators [Revue] // journal of the Braz. Soc. of Mech. Sci. & Eng.. - 2004. - pp. Vol. 26, No. 2.

Dhatt Gouri, Touzot Gilbert et Lefrancois Emmanuel Méthode des éléments finis [Livre]. - Paris : Lavoisier, 2005.

Hariri H., Bernard Y. et Razek A. Finite element model of a beam structure with piezoelectric, patches using RL shunt circuits [Revue] // AC2011, 14th International Conference on active systems for dynamics markets. - 2011. - pp. pp.124-13.

Hariri H., Bernard Y. et Razek A. Locomotion principles for piezoelectric miniature robots [Revue] // Proceedings on actuator 10. - 2010. - pp. pp. 1015-1020..

Hernandez C., Bernard Y. et Razek , A. A global assessment of piezoelectric actuated micro-pumps [Revue] // European. Physical Journal Applied Physics. - 2010. - pp. Vol. 51, Issue: 2,1-8..

Jalili N. Piezoelectric-Based Vibration Control, From Macro to Micro-Nano Scale Systems [Livre]. - [s.l.] : Springer, 2009.

Kayacik , O. [et al.] Integral equation approach for piezo patch vibration control of beams with various types of damping [Revue] // Journal of computers and structures 86. - 2008. - pp. pp. 357-366..

Lin C.C et Huang H.N. Vibration control of beam-plates with bonded piezoelectric sensors and actuators [Revue] // Journal of computers and structures 73. - 1999. - pp. pp. 239-248..
Liu G.R. Vibration control simulation of laminated composite plates with integrated piezoelectric [Revue] // Journal of sound and vibration. - 1999. - pp. Vol 220, Issue 5,827-846..
Nguyen C.H. et Pietrzko S.J. FE analysis of a PZT- actuated adaptive beam with vibration damping using a parallel R-L shunt circuit [Revue] // journal of finite elements in analysis and design 42. - 2006. - pp. pp. 1231-1239..
Park C.H. Dynamics modeling of beams with shunted piezoelectric elements [Revue] // journal of Sound and vibration 268. - 2003. - pp. pp. 115-129..
Qu G.M. [et al.] analysis of a piezoelectric composite plate with cracks [Revue] // Journal of composite structures. - 2006. - pp. vol. 72, no1,111-118..
Son K.J. [et al.] An ultrasonic standing-wave-actuated nano- positioning walking robot: Piezoelectric-metal composite beam modeling [Revue] // Journal of vibration and control,. - 2006. - pp. Vol. 12, no. 12, pp. 1293-1309..
Sunyoto S., Bernard Y. et Razek A. Design and realization of a linear piezoelectric actuator for orthopaedic applications [Revue] // Journal of Advanced Science. - 2006. - pp. Vol. 18, Issue: 0, pp. 162-165..
Tuttle M.E Review of the concepts of stress, strain and Hooke's law [Livre]. - Washington : [s.n.], 2009.
Varadan V.V. Closed loop finite element modeling of active/passive damping in structural vibration control [Revue] // journal of smart materials and structures 5 . - 1996. - pp. pp. 685-694.
Wang S. Y. Dynamic stability analysis of finite element modeling of piezoelectric composite plates [Revue] // International Journal of Solids and Structures. - 2003. - pp. Vol.41, Issue: 3-4,pp. 745-764..
Yan Y.J. et Yam L.H. Online detection of crack damage in composite plates using embedded piezoelectric actuators/sensors and wavelet analysis [Revue] // Journal of Composite Structures. - 2002. - pp. Vol 58, Issue 1,29-38..
Yasin M. Y., Ahmad N. et Alam M.N. Finite element analysis of actively controlled smart plate with patched actuators and sensors [Revue] // Latin American Journal of Solids and Structures. - 2010. - pp. Vol 7, No 3,227-247.

CHAPTER 4

EXPERIMENTAL VALIDATION OF MODELS

Chapter 4: Experimental validation of models

List of figures

List of tables

4.1 Introduction

An experimental device has been built and described in this chapter to validate our model obtained in chapter 3. First we present the experimental device, and then we begin the validation process by comparing the model results with experiment in the cases of beam and plates. The comparison will be done at resonance frequencies and concerned the deformation of the system for an applied voltage to actuator piezoelectric patches, as well as the obtained voltage for sensor piezoelectric patches.

4.2 Experimented device

To validate our Finite Element Model (FEM) experimentally, we took an aluminum thin beam/plate structure fixed at one end, the other being left free. Two ceramic PZT patches are bonded on one side of the beam/plate and they are polarized along the axis z. Properties and geometrical parameters for the piezoelectric ceramic PZT and the elastic structure (beam and plate) are presented in Table 4.1 and systems are shown in Figure 4.1 and Figure 4.2. A fixed-free boundary condition is taking into account during the assembly of matrices (appendix).

In the case of two piezoelectric patches, equation 3.58 becomes:

$$\begin{bmatrix} M_{mm} & 0 & 0 \\ 0 & 0 & 0 \\ 0 & 0 & 0 \end{bmatrix} \begin{bmatrix} \ddot{U}_i \\ \ddot{E}_{3p1} \\ \ddot{E}_{3p2} \end{bmatrix} + \begin{bmatrix} C_{mm} & 0 & 0 \\ 0 & 0 & 0 \\ 0 & 0 & 0 \end{bmatrix} \begin{bmatrix} \dot{U}_i \\ \dot{E}_{3p1} \\ \dot{E}_{3p2} \end{bmatrix} + \begin{bmatrix} K_{mm} & K_{mvp1} & K_{mvp2} \\ K_{vmp1} & K_{vvp1} & 0 \\ K_{vmp2} & 0 & K_{vvp2} \end{bmatrix} \begin{bmatrix} U_i \\ E_{3p1} \\ E_{3p2} \end{bmatrix} = \begin{bmatrix} F_i \\ t_p Q_{p1} \\ t_p Q_{p2} \end{bmatrix} \quad 4.1$$

As we said in the previous chapter, the damping matrix [C] is added to the system and it is determined experimentally via Rayleigh damping to match the damping behavior of the real system.

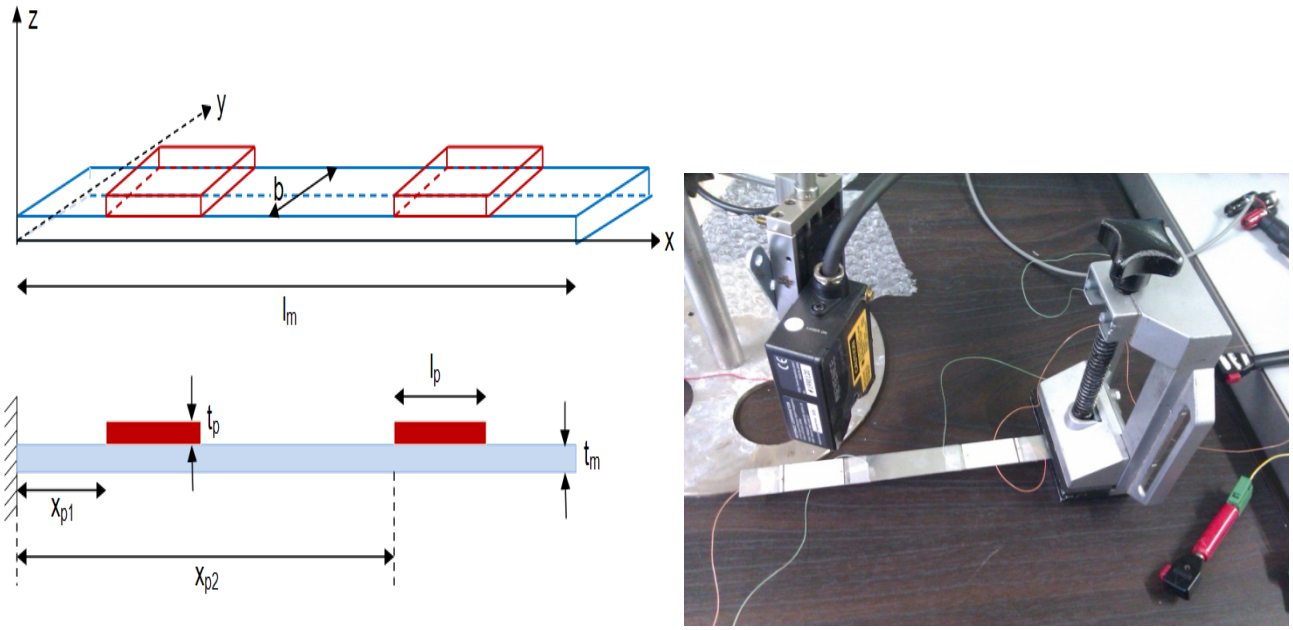

Figure 4. 1: beam experimented device

	PZT (p)	Elastic structure (m)
Young's modulus (Pa)	/	$c_m = 69 \times 10^9$
Poison's ratio	/	$\upsilon_m = 0.33$
Volume density (Kg.m^{-3})	$\rho_p = 7900$	$\rho_m = 2700$
Relative permittivity	$\varepsilon_{33r} = 1282$	/
Piezoelectric constant (m.V^{-1})	$d_{31} = -1.3 \times 10^{-10}$	/
Elastic compliances (Pa^{-1})	$S_{11} = 1.3 \times 10^{-11}$	/
	$S_{12} = -4.76 \times 10^{-12}$	/
Max peak to peak electric field(V.mm^{-1})	$E_{max} =$ 300	/
Max compressive strength (Pa)	$\sigma_{max} = 600 \times 10^6$	/
Plate dimensions		
Length × width × thickness (mm^3)	32×17×0.27	100 × 60 × 0.5
(l_p, l_m) × (b_p, b_m) × (t_p, t_m)		
Beam dimensions		
Length × width × thickness (mm^3)	32×17×0.27	180 × 17 × 0.5
(l_p, l_m) × (b_p, b_m) × (t_p, t_m)		
Piezo positions case of beam		
X_{p1}, X_{p2}(mm)	24,126	
Piezo positions case of plate		
X_{p1}, X_{p2},Y_p(mm)	10,58,21.5	

Table 4. 1: Properties and geometry of the system

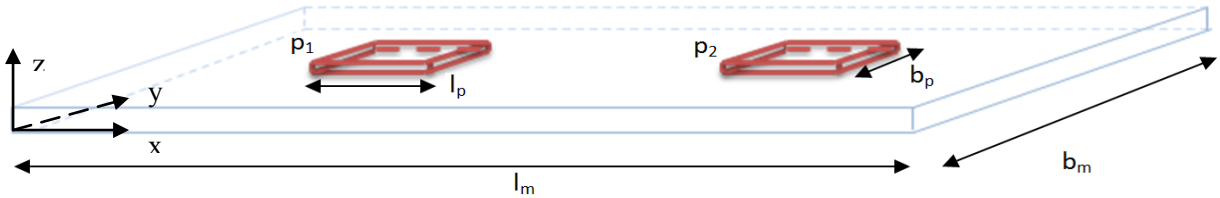

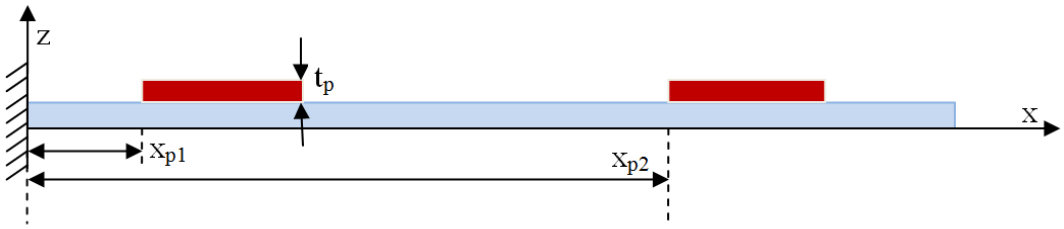

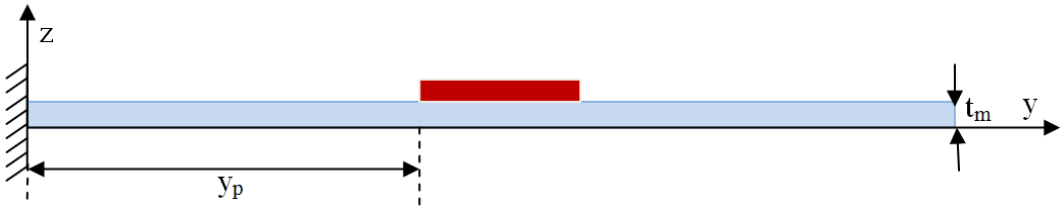

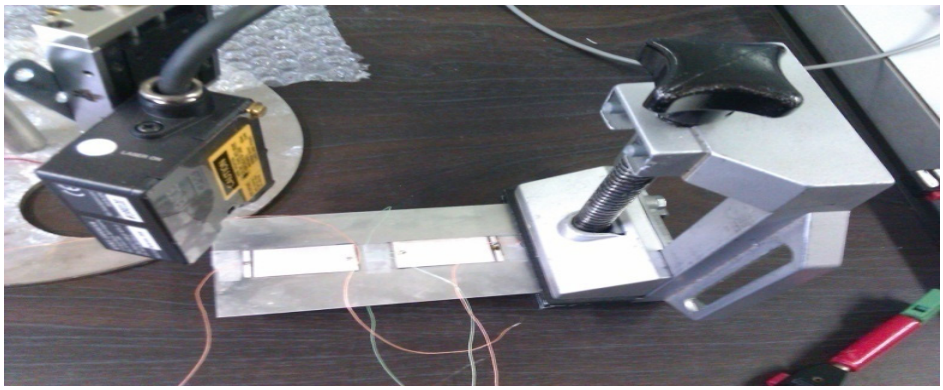

Figure 4. 2: Plate experimented device

4.3 Rayleigh damping

The Rayleigh damping is considered as a classical way to model the damping of the structure and is proved as effective way of considering damping for analysis of structures [(Clough, et al., 1995), (Craig, et al., 2006),(Liu, et al., 1994), (Pons, et al., 2004), (Giosan, 2006), (Chowdhury, et al., 2006)]. It uses the assumption that the damping matrix is proportional to a linear combination of the mass matrix and the stiffness.

$$[C_{mm}] = \alpha[M_{mm}] + \beta[K_{mm}] \quad (4.2)$$

α and β are the Rayleigh coefficients or the damping ratio, they are also called as mass proportional and stiffness proportional respectively. α and β have units of sec^{-1} and sec, respectively.

In the formulation of equation 4. 2 orthogonal transformation [(Pons, et al., 2004), (Chowdhury, et al., 2006)] form the following equation:

$$2\xi_i(2\pi f_i)\alpha + \beta(2\pi f_i)^2 \quad (4.3)$$

ξ_i is the damping ratio and f_i is the resonance frequency at the ith mode.

The relationship between damping ratio and frequency expressed by equation 4. 3 is shown graphically in Figure 4.3.

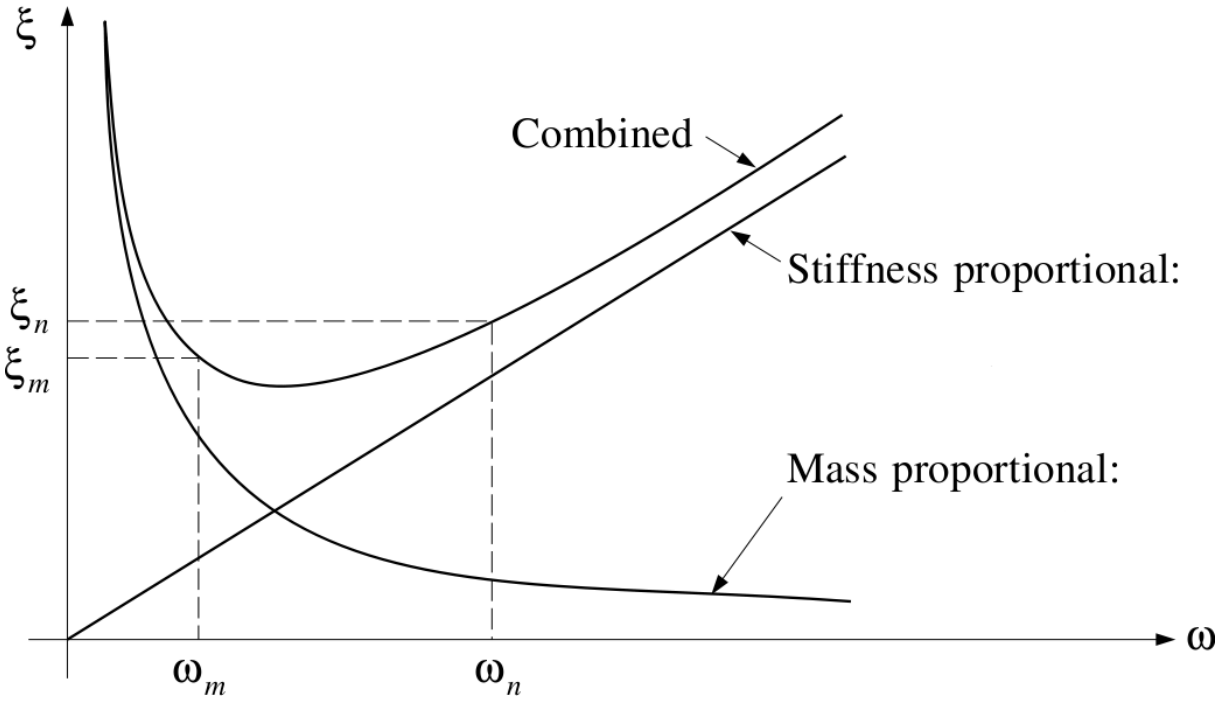

Figure 4.3: Relationship between damping ratio and frequency (for Rayleigh damping)

From this we can say that low fundamental frequency structure will show nonlinear damping properties in beginning with respect to frequency and will converge to linear proportionality with frequency as Eigen values increases with each subsequent mode.

Now it is apparent that the two Rayleigh damping factors, α and β, can be evaluated by the solution of a pair of simultaneous equations if the damping ratios ε_m and ε_n associated with two specific frequencies (modes) f_m, f_n are known. Writing equation 4. 3 for each of these two cases and expressing the two equations in matrix form leads to:

$$\begin{Bmatrix}\xi_m\\ \xi_n\end{Bmatrix} = \begin{bmatrix} {}^{1}/_{4\pi f_m} & \pi f_m \\ {}^{1}/_{4\pi f_n} & \pi f_m \end{bmatrix} \begin{Bmatrix}\alpha\\ \beta\end{Bmatrix} \quad 4.4$$

And the factors resulting from the simultaneous solution are:

$$\begin{Bmatrix}\alpha\\ \beta\end{Bmatrix} = \begin{bmatrix} {}^{1}/_{4\pi f_m} & \pi f_m \\ {}^{1}/_{4\pi f_n} & \pi f_m \end{bmatrix}^{-1} \begin{Bmatrix}\xi_m\\ \xi_n\end{Bmatrix} \quad 4.5$$

Rayleigh coefficients can be determined, by obtaining damping ratio ξ_i at two different frequencies w_i , as we can remark in equation 4. 5. Damping ratios were obtained experimentally from the frequency response curve shown in Figure 4.4 corresponding to the two chosen frequencies according to

$$\xi_i = \frac{w_{ui} - w_{li}}{2w_i}$$

4. 6

Where w_i is the resonance frequency for the ith vibration mode, w_{ui} and w_{li} are the upper and lower frequency for which the amplitude is 3dB below the amplitude at w_i [(Pons, et al., 2004),(Inman, 2001), (Brandt, 2011)].

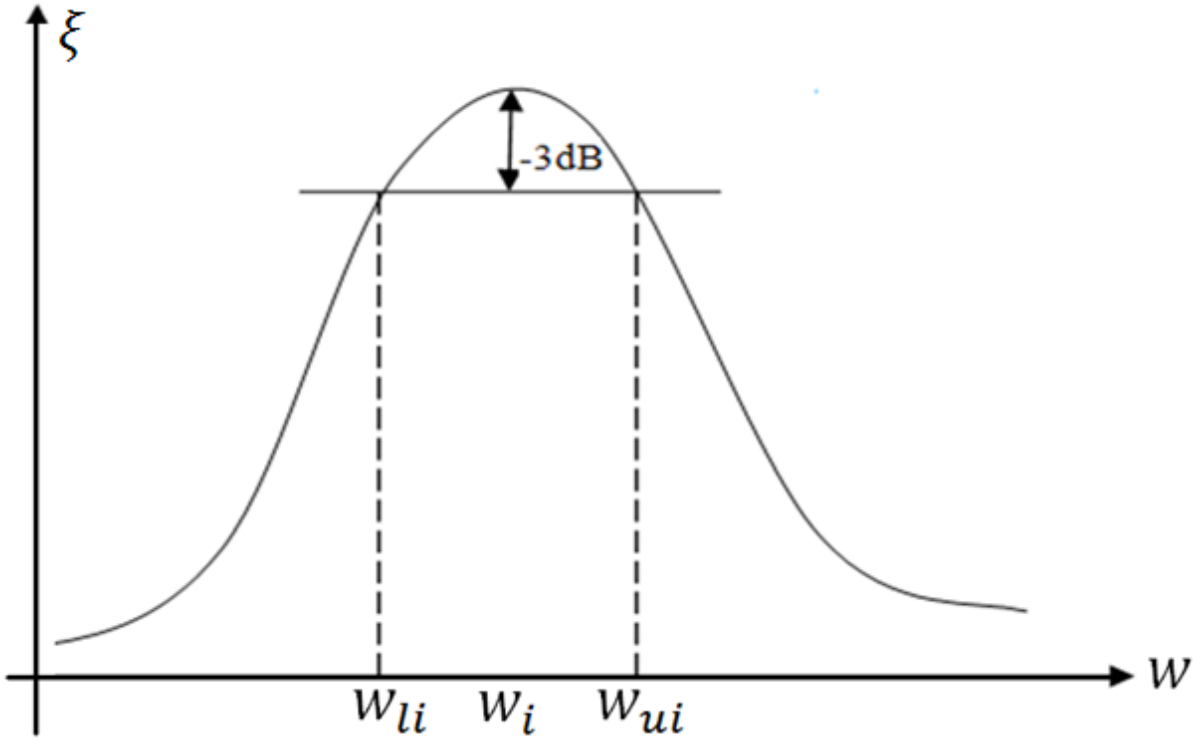

Figure 4.4: Resonance frequency curve

In most of the analysis problems, analyst assumes constant damping ratio for each mode of the structure. This assumption is totally based on previous experiences or on standard literature [(Giosan, 2006)], it is recommended in this case that w_m generally be taken as the fundamental frequency of the system and that w_n set among the higher frequencies of the mode that contribute significantly to the dynamic response ($\xi_1 = \xi_n = \xi$) [(Clough, et al., 1995)]. This method is still practical because it is quiet hard to measure damping ratio for each mode. But it is quiet unrealistic to assume constant damping ratio for all modes. Damping for structure varies mode to mode. Modal mass participation decreases with increasing in modes [(Kandge, 2007)]. In our case we will measure individual α and β for the first ten resonance frequencies and an equivalent value of α and β for all frequencies higher than the 10^{th} resonance frequency by curve fit method.

The experimental damping ratios and resulting Rayleigh coefficients corresponding of the first ten vibration modes were obtained from the system resonance curve and are shown in

Table 4.2 and Table 4.3 in case of beam and plate respectively (frequency are taken from paragraph 4.4.1). The curves fitting damping ratio versus frequency are also shown in Figure 4.5 and Figure 4.6 for the case of beam and plate respectively.

Frequency	Damp. Ratio (ζ)	α	β
f_1, f_2	0.0096 , 0.00743	1.2915	2.5420e-05
f_2, f_3	0.00743 , 0.00367	6.6939	1.8112e-06
f_3, f_4	0.00367 , 0.00321	7.7226	1.2758e-06
f_4, f_5	0.00321 , 0.00352	10.0257	1.0271e-06
f_5, f_6	0.00352 , 0.00327	23.4379	4.5358e-07
f_6, f_7	0.00327 , 0.00341	23.4221	4.5393e-07

Table 4.2: Experimental determination of damping parameters in the case of beam structure

Frequency	Damp. Ratio (ζ)	α	β
f_1, f_2	0.0167, 0.002	-20.1870	3.2992e-04
f_2, f_3	0.002, 0.00734	3.5262e+03	-9.8203e-04
f_3, f_4	0.00734, 0.00781	-356.2392	1.1308e-04
f_4, f_5	0.00781, 0.00868	8.3599e+03	-2.9620e-04

Table 4.3: Experimental determination of damping parameters in the case of plate structure

By using these curves (Figure 4.5 and Figure 4.6), we can obtain damping ratios for two given frequencies. Then by using equation 4. 5, the corresponding α and β values are shown in table 4.4.

	Beam structure	Plate structure
α	3.8661	1.7706
β	8.1030e-07	4.1158e-06

Table 4.4: Curve fitted parameters

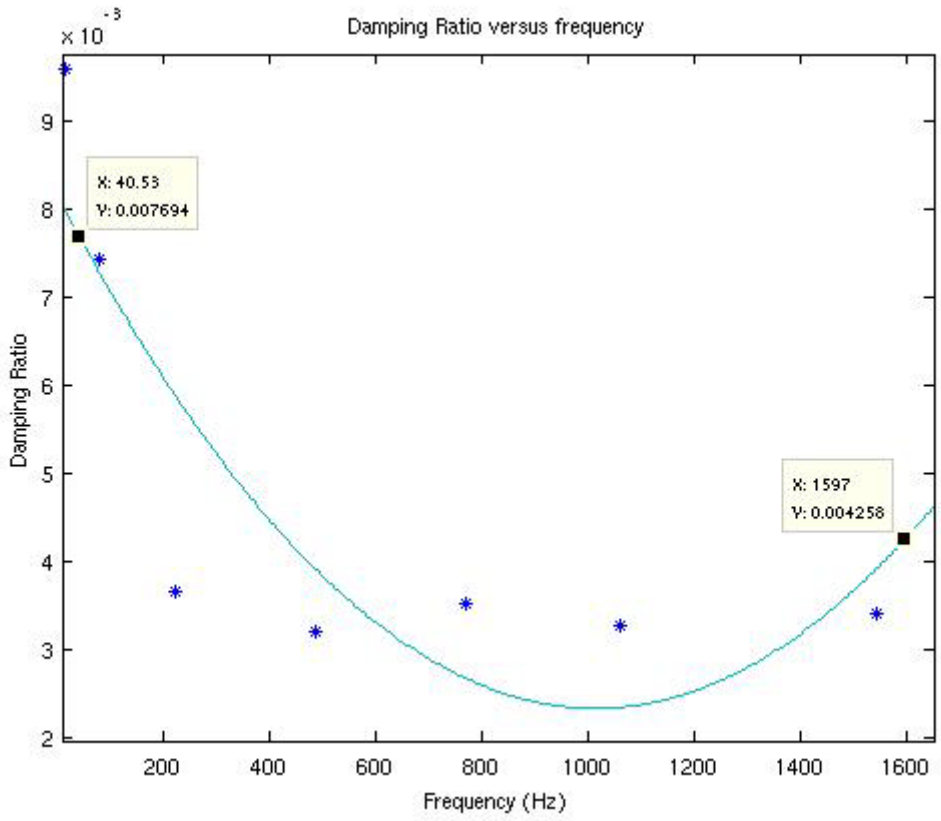

Figure 4.5: Curve fitted damping ratio versus frequency to beam structure

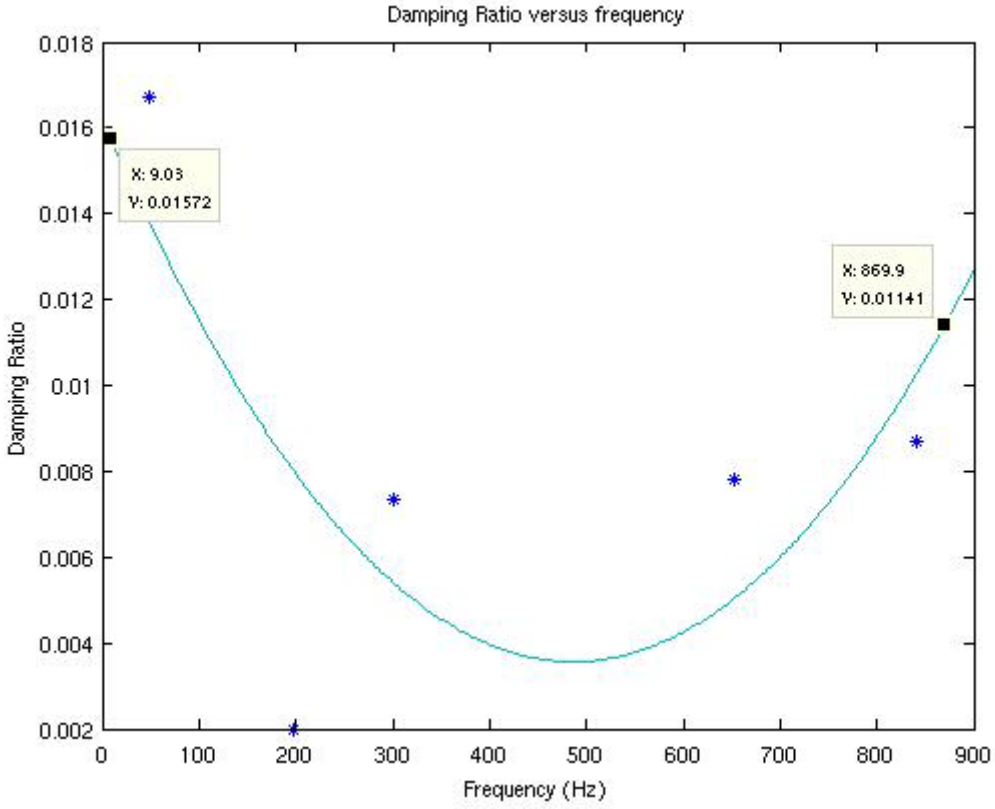

Figure 4.6: Curve fitted damping ratio versus frequency to plate structure

4.4 Validation process

We begin the process of model validation by comparing the resonant frequencies of the model (1D and 2D) with the experimental ones, then we apply a sinusoidal electrical voltage to one patch, we measure the transverse displacement of the beam/plate and the obtained electrical voltage for the other patch in the case of open circuit and resistance shunt circuit and we compare it with the model. All measures are done using a high resolution laser interferometer LK-G3001PV Keyence France.

4.4.1 Resonance frequencies validation

In short-circuit, the voltage E_{3p} is zero. In the case of an open circuit, the electric charge Q_p is constant. In this case, it is nil. The resonance frequencies and modes shapes of the system when the two electrodes of the piezoelectric patches are short circuited ($E_{3p} = 0$) are given by (referring to equation 4. 1):

$$([K_{mm}] - (2\pi f_n)^2 [M_{mm}])\{U\} = 0 \quad (4.7)$$

In the case where one patch is open circuited ($Q_{p1} = 0$) and the other is short circuited ($E_{3p2} = 0$), resonance frequencies and modes shapes of the system are given by (referring to equation 4. 1):

$$([K_{mm} - K_{mvp1}K_{vvp1}^{-1}K_{vmp1}] - (2\pi f_n)^2 [M_{mm}])\{U\} = 0 \quad (4.8)$$

By reversing the roles of the two patches, we obtain:

$$([K_{mm} - K_{mvp2}K_{vvp2}^{-1}K_{vmp2}] - (2\pi f_n)^2 [M_{mm}])\{U\} = 0 \quad (4.9)$$

In the case where the two patches are open circuited ($Q_p = 0$), resonance frequencies and modes shapes of the system are given by (referring to equation 4. 1):

$$([K_{mm} - K_{mvp1}K_{vvp1}^{-1}K_{vmp1} - K_{mvp2}K_{vvp2}^{-1}K_{vmp2}] - (2\pi f_n)^2 [M])\{U\} = 0 \quad (4.10)$$

These equations (4. 7, 4. 8, 4. 9 & 4. 10) give the resonance frequencies f_n and the modes shapes {U} at each resonance frequency.

This shows that the stiffness matrix depends on the electrical boundary conditions. The overall stiffness of the system increases if the electrodes are left open (the term K_{vvp}being negative), the resonant frequencies are slightly higher in the case of open circuit piezoelectric patches rather than short circuit.

Table 4. 5, Figure 4. 7 and Table 4. 6, Figure 4. 8 show the first resonance frequencies determined experimentally and by FEM in case of beam and plate respectively, where the first patch (p1) is short circuited and the second (p2) is open circuited (using equation 4. 9). Tables and figures show good agreement between model and measurements. The first eight modes shapes in the case of plate are given in Figure 4.9 (using equation 4. 9 for the 2D model). In the case of beam, modes shapes are validated but they aren't presented here.

After modes shapes and frequency validation in the case of beam and plate, the mass and stiffness matrices for models are partially validated. To complete models validation, a dynamic validation is doing in the next two paragraphs.

Mode order	*1*	*2*	*3*	*4*	*5*	*6*	*7*	*8*	*9*	*10*
FEM (1D)	11.92	76.13	221.21	486.85	772.04	1060.4	1546.6	2173	2746.4	3421.6
Experimental	12	77	225	515	837	1117	1645	2338	2843	3526

Table 4. 5: Eigen frequency for the beam structure in Hz

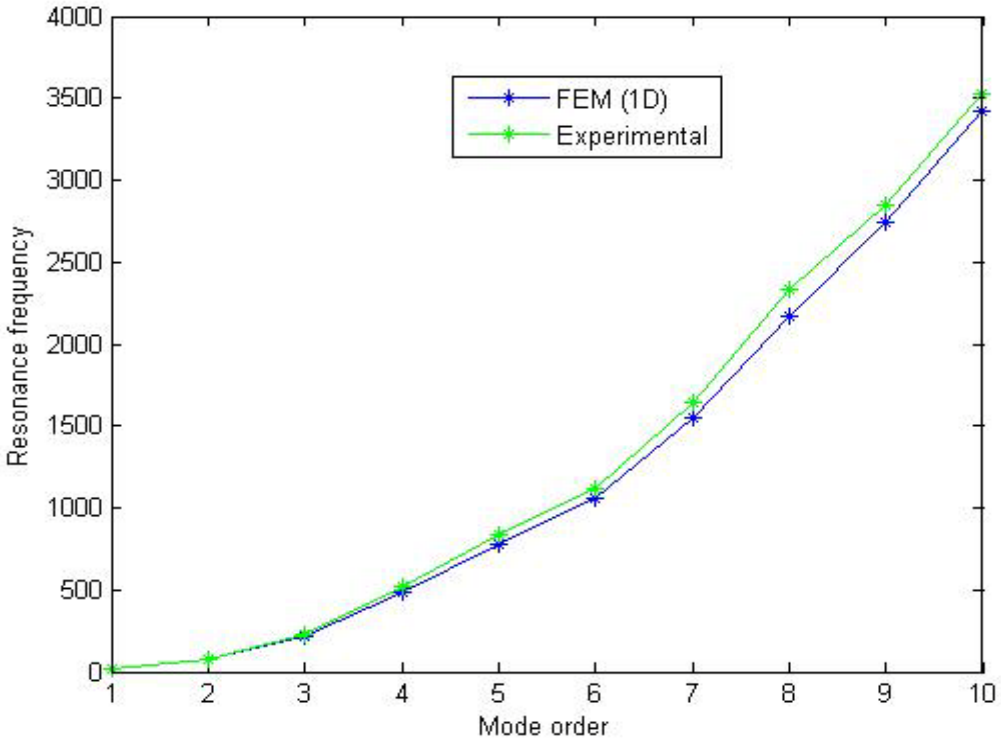

Figure 4. 7: Frequency comparison for beam structure

Mode	*FEM (2D)*	*Experimental*
1	48.22	43.5
2	197.84	190
3	300.28	271
4	653.27	629
5	841.02	905
6	1072.7	951
7	1240.8	1132
8	1337.9	1332
9	1814.6	1676
10	1906.8	1855
11	2029.6	1952
12	2470.2	2122
13	2604.8	2602
14	2778.6	2750
15	2958.2	2817

Table 4. 6: Eigen frequency for the plate structure in Hz

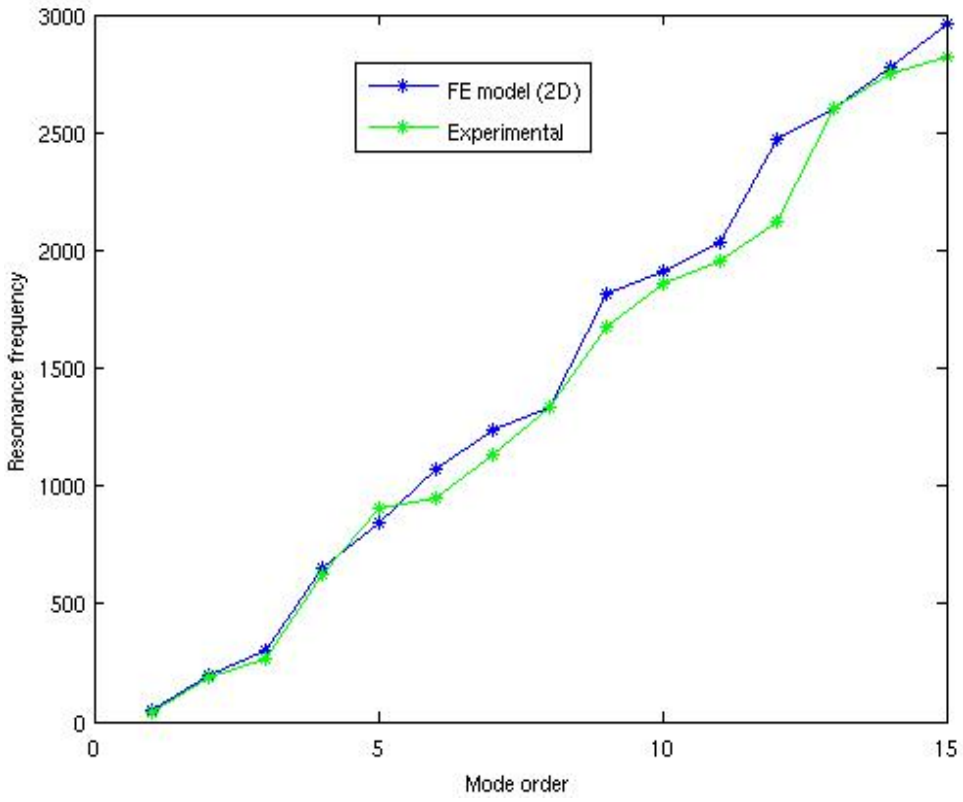

Figure 4. 8: Frequency comparison for plate structure

First bending mode : mode order (1)

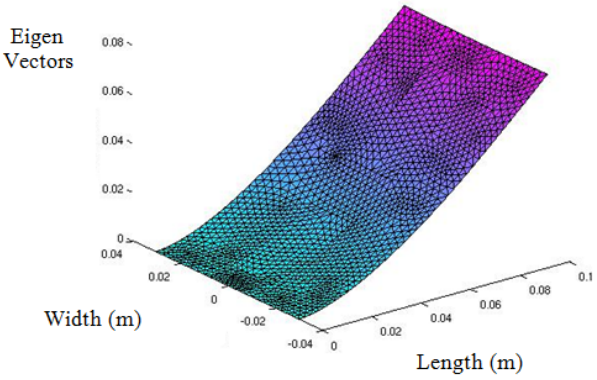

First twisting mode : mode order (2)

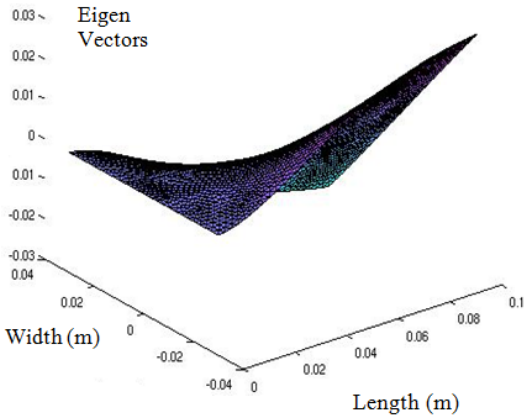

2nd bending mode : mode order (3)

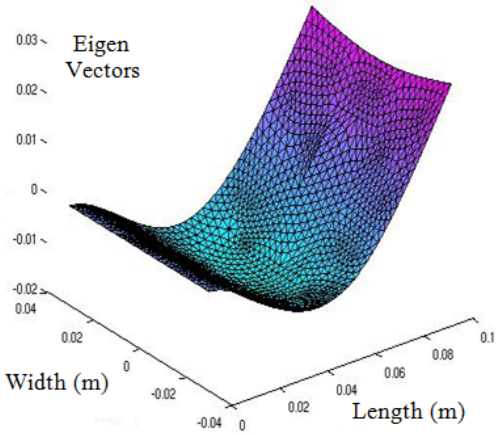

2nd twisting mode : mode order (4)

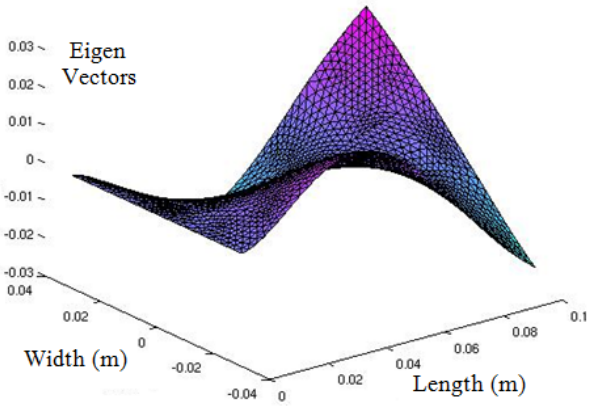

mode order 5

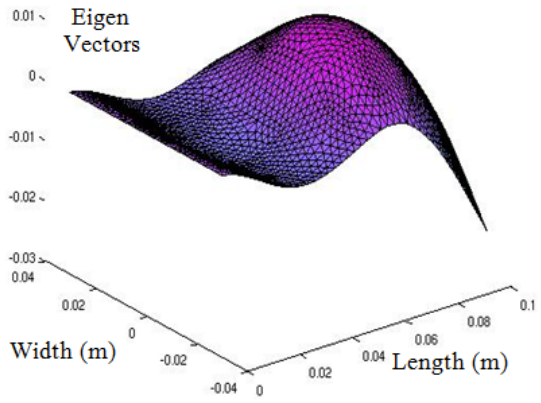

mode order 6

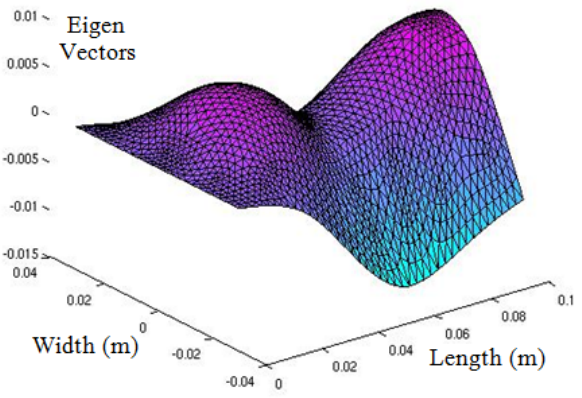

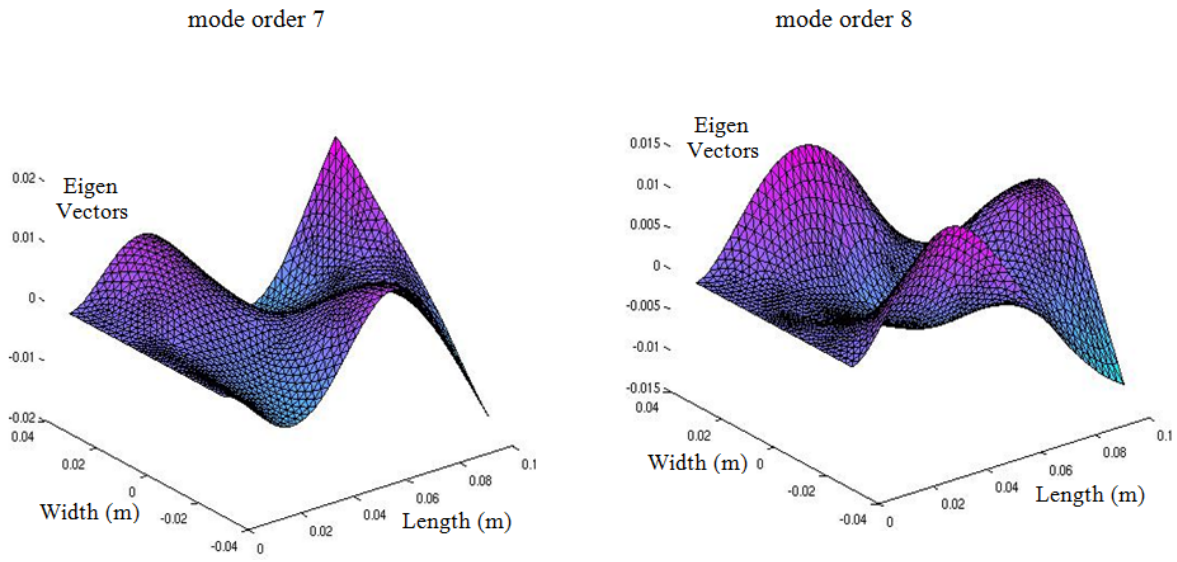

Figure 4. 9: Modes shapes for the plate structure

4.4.2 Transverse displacement validation

We treat here the case sensor-actuator where the first piezoelectric patch near from the fixed end is left as open circuited (sensor) while the second piezoelectric patch near from the free end is powered by a sinusoidal voltage (actuator). According to this and referring to equation 4. 1 and equation 3.59, transverse displacements (flexion) are given by:

$$\left[-(2\pi f_n)^2\begin{bmatrix} M_{mm} & 0 & 0 \\ 0 & 0 & 0 \\ 0 & 0 & 0 \end{bmatrix} + \mathrm{j}(2\pi f_n)\begin{bmatrix} C_{mm} & 0 & 0 \\ 0 & 0 & 0 \\ 0 & 0 & 0 \end{bmatrix} + \right.$$

$$\left.\begin{bmatrix} K_{mm} - K_{mvp2}K_{vvp2}^{-1}K_{vmp2} & K_{mvp1} & K_{mvp2}K_{vvp2}^{-1} \\ K_{vmp1} & K_{vvp1} & 0 \\ -K_{vvp2}^{-1}K_{vmp2} & 0 & K_{vvp2}^{-1} \end{bmatrix}\right]\begin{bmatrix} U_i \\ E_{3p1} \\ t_p Q_{p2} \end{bmatrix} = \begin{bmatrix} 0 \\ 0 \\ E_{3p2} \end{bmatrix}$$

4. 11

After this validation, we will be able to say that the mass and stiffness matrices are completely validated. To be more sure, the voltage at the piezoelectric sensor patch can be measured and compared with the model obtained voltage for different resonance frequencies. This procedure is done in paragraph 4.4.2.3, in the case of 2D model only. Also the piezoelectric capacitance can be determined by models and compared with the calculated one and the given capacitance in the datasheet. This procedure is done in paragraph 4.4.2.4, in the case of 1D model.

4.4.2.1 Case of beam

As we said before, we treat here the case sensor-actuator. The actuator is powered by a sinusoidal voltage of 10V amplitude and frequency equal successively to the first, second and third resonant frequency of the system. Measurements of displacement along the z axis are performed on all the length of the device and they are compared with the model results given by equation 4.11 in the case of 1D model. Figure 4.10 shows comparison between experimental and the 1D FEM for the transverse displacement along the z-axis all the length of the beam at the first resonance frequency. Figure 4.11 shows comparison between experimental and model at the second resonance frequency and Figure 4.12 shows comparison at the third one. Figures show also a good agreement between model and experimental as in the case of resonance frequency validation.

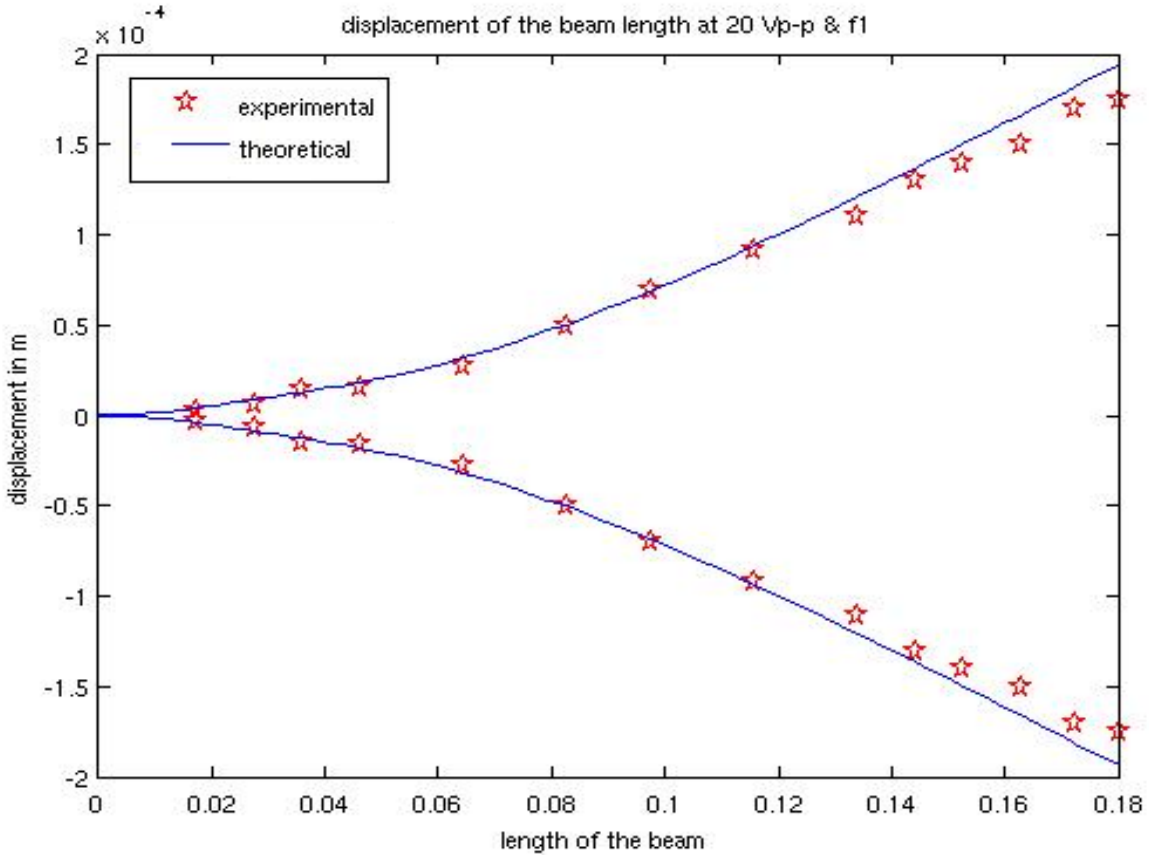

Figure 4. 10: Displacement at the first resonance frequency

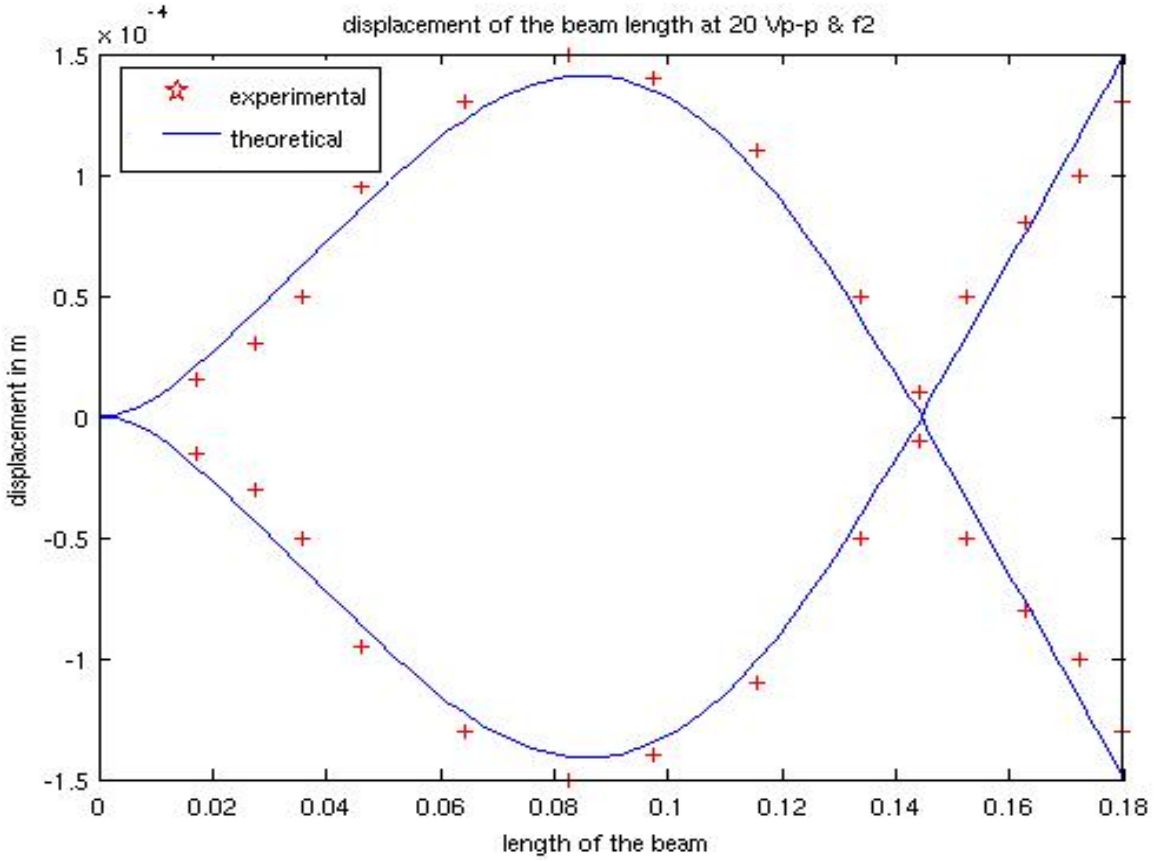

Figure 4. 11: Displacement at the second resonance frequency

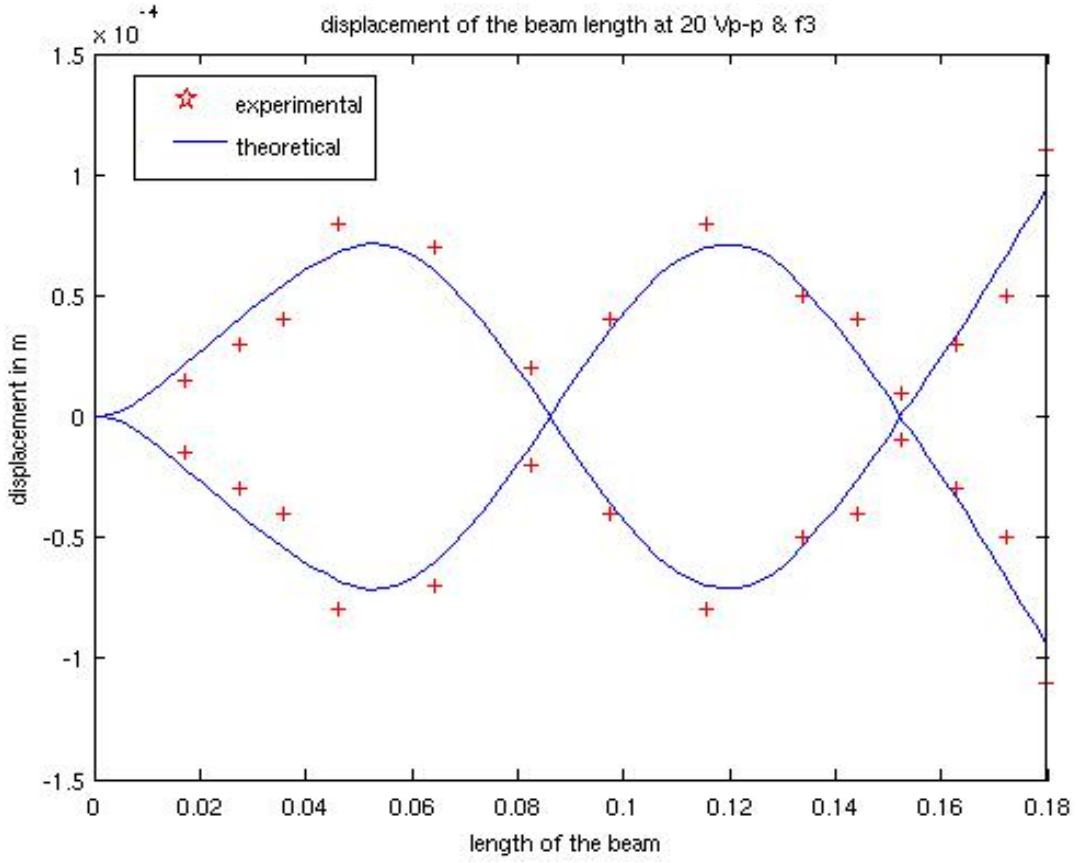

Figure 4. 12: Displacement at the third resonance frequency

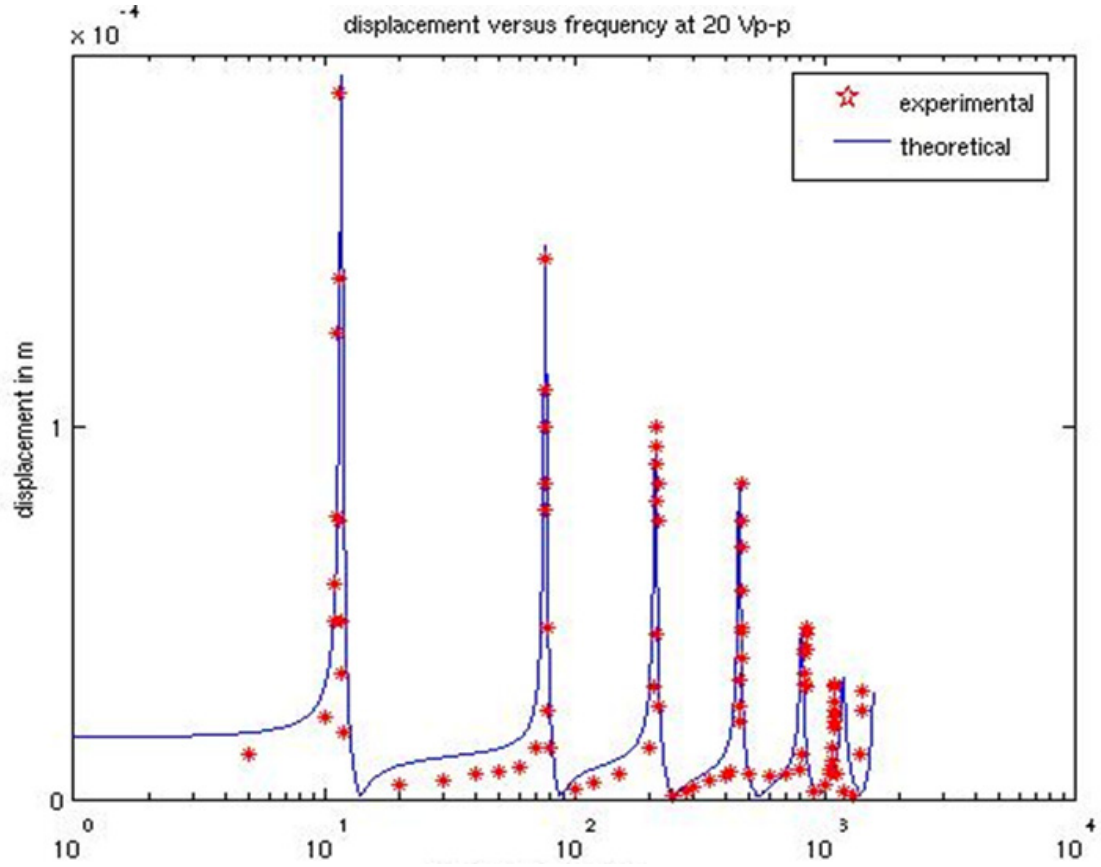

Figure 4.13: Tip displacement of the beam versus frequency

4.4.2.2 Case of plate

Same as beam case, we treat here the case sensor-actuator. But we are applying now a sinusoidal voltage of 20V amplitude and frequency equal successively to the first, second and fourth resonant at the actuator piezoelectric patch. Measurements of displacement along the z axis are performed on a portion of the device as shown Figure 4.14 and they are compared with the model results given by the equation 4.11 in the case of 2D model.

Figure 4.15 to Figure 4.20 show displacements comparison between experimental measurements and simulation results.

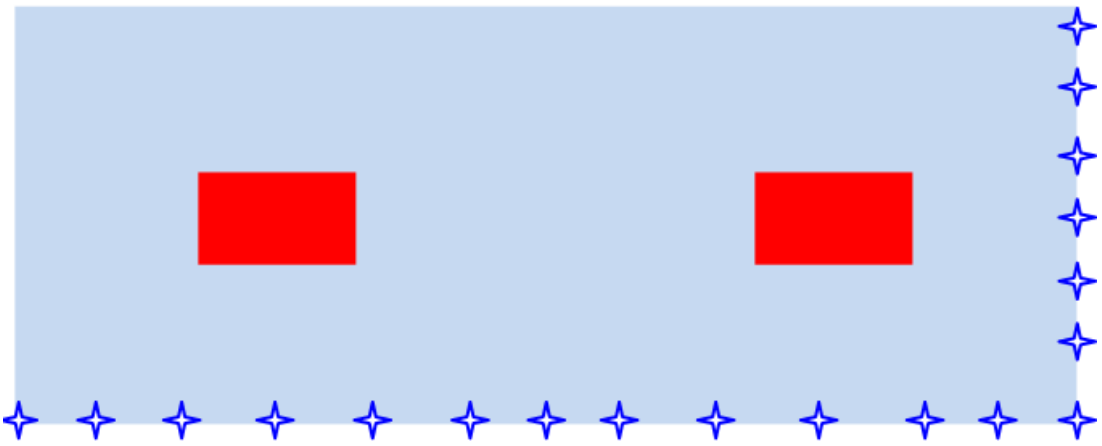

Figure 4.14: schematic top view of the experimental measurements points for the device

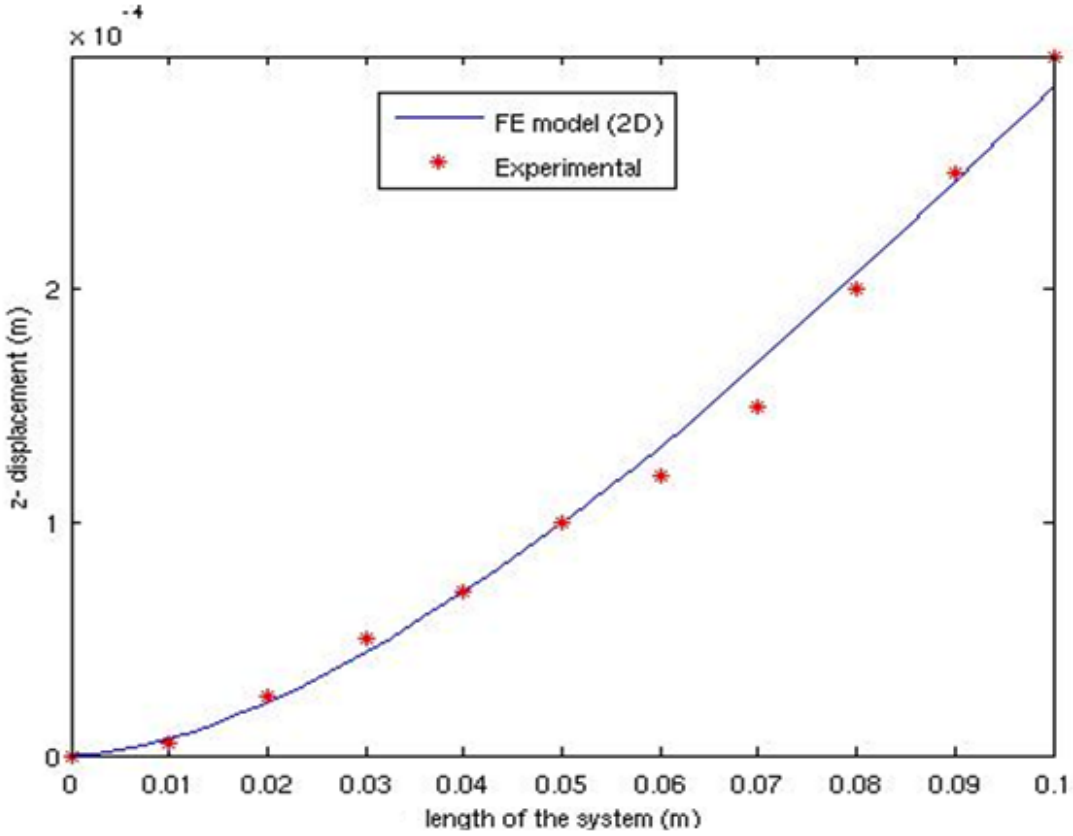

Figure 4.15: z-displacement along the length of the plate at the first resonance frequency

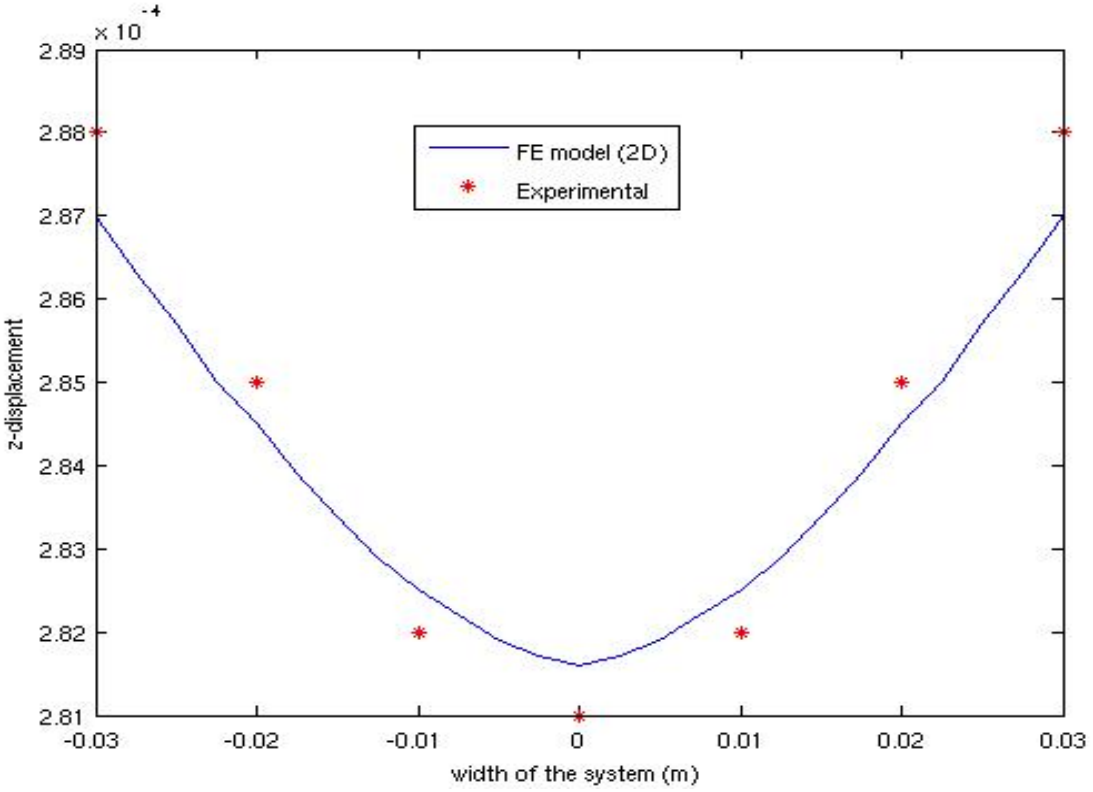

Figure 4.16: z-displacement along the width of the plate at the first resonance frequency

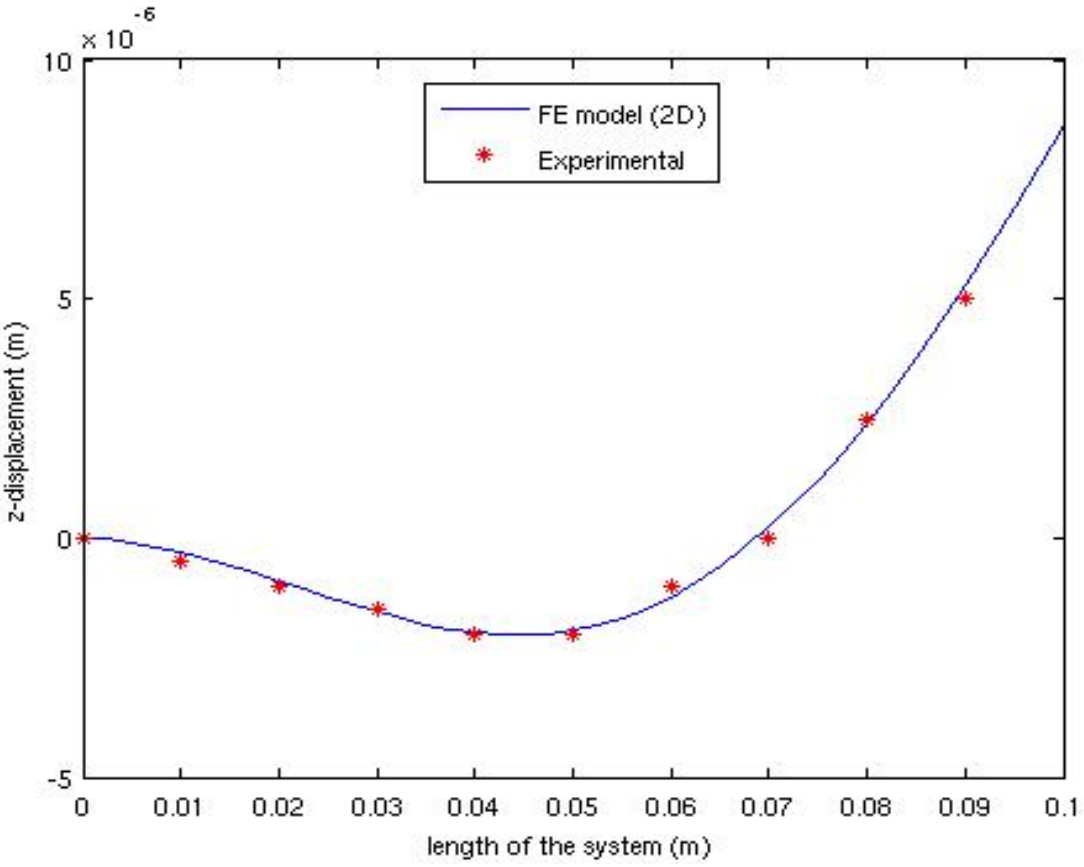

Figure 4.17: z-displacement along the length of the plate at the second resonance frequency

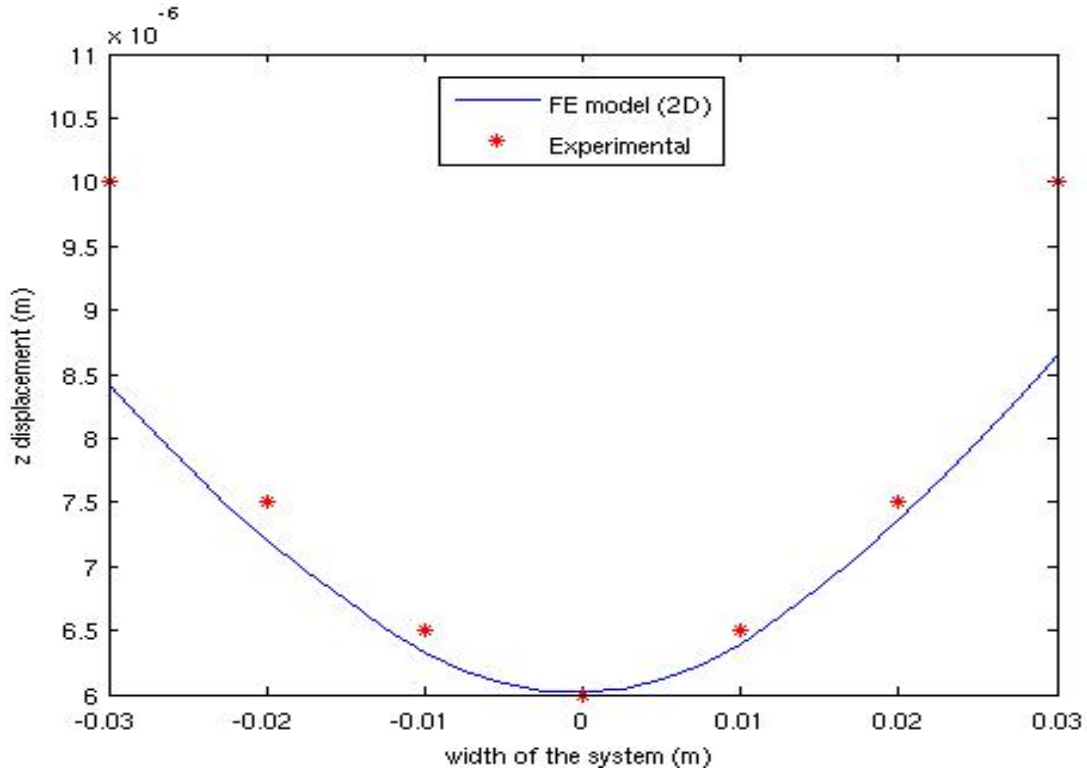

Figure 4.18: z-displacement along the width of the plate at the second resonance frequency

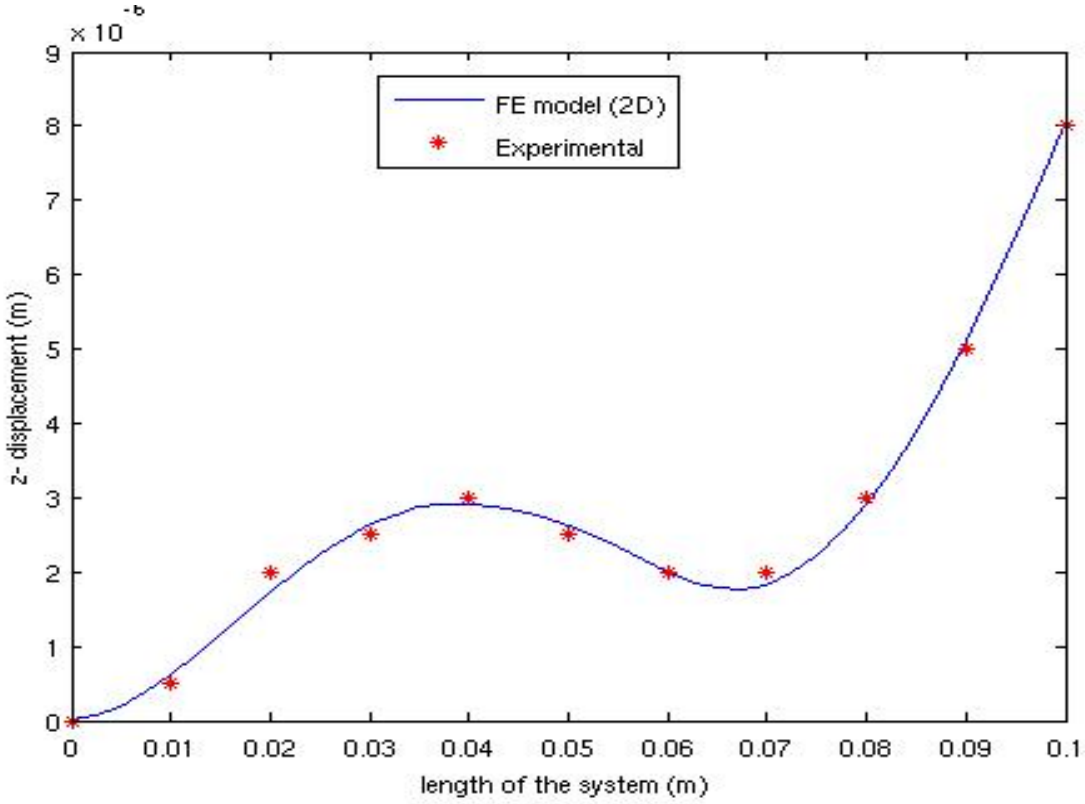

Figure 4.19: z-displacement along the length of the plate at the third resonance frequency

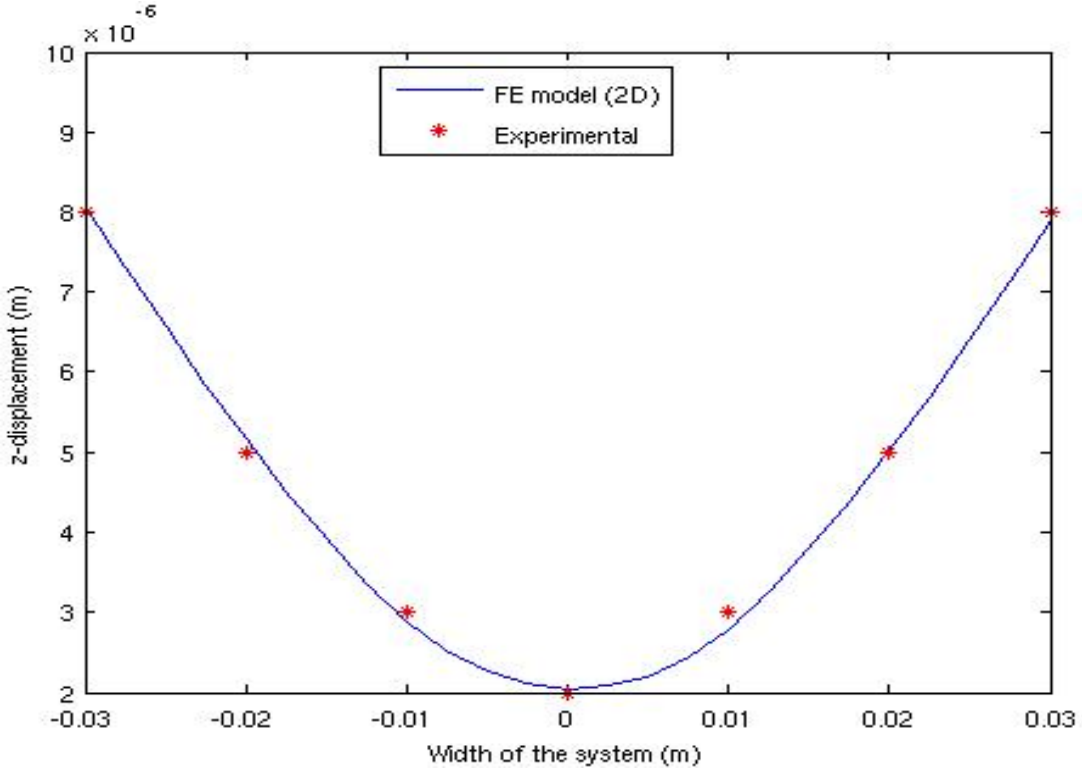

Figure 4.20: z-displacement along the width of the plate at the third resonance frequency

4.4.2.3 Piezoelectric sensors Validation

As we said before, the piezoelectric patch near from the free end is the actuator patch and it is powered by a sinusoidal voltage of 20V amplitude in the case of plate device. The other is the sensor piezoelectric patch. Figure 4.12 below shows this functionality.

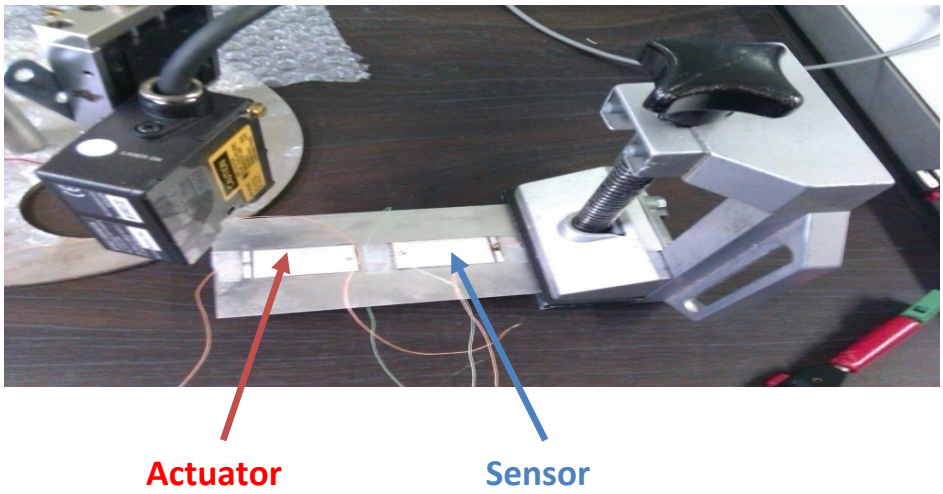

Figure 4.21: Piezoelectric actuator-sensor functionality

We are comparing the sensor functionality by measuring the obtained voltage for the piezoelectric sensor in the case of open circuit and shunt resistance circuit of 50 kΩ.

Equation 4.11 is used to determine voltage in case of open circuit piezoelectric sensor (E_{3p1}). This equation is repeated again below.

$$\left[-(2\pi f_n)^2\begin{bmatrix}M_{mm} & 0 & 0\\ 0 & 0 & 0\\ 0 & 0 & 0\end{bmatrix}+\mathrm{j}(2\pi f_n)\begin{bmatrix}C_{mm} & 0 & 0\\ 0 & 0 & 0\\ 0 & 0 & 0\end{bmatrix}+\right.$$

$$\left.\begin{bmatrix}K_{mm}-K_{mvp2}K_{vvp2}^{-1}K_{vmp2} & K_{mvp1} & K_{mvp2}K_{vvp2}^{-1}\\ K_{vmp1} & K_{vvp1} & 0\\ -K_{vvp2}^{-1}K_{vmp2} & 0 & K_{vvp2}^{-1}\end{bmatrix}\right]\begin{bmatrix}U_i\\ E_{3p1}\\ t_pQ_{p2}\end{bmatrix}=\begin{bmatrix}0\\ 0\\ E_{3p2}\end{bmatrix}$$

4. 12

Then, we considered that the sensor piezoelectric patch is connected to a resistance shunt circuit. So to introduce resistance in the model, the following equation will be used

$$E_{3p1}t_p = R\dot{Q}_{p1}$$

4. 13

To incorporate the resistance shunt circuit in the model, otherwise R, it is useful to appear $\dot{Q}_{p1}$ in the matrix equation, i.e to take it as an unknown. So referring to equation 3.58, mass matrix will be the same, damping and stiffness matrix will change. Obtained equation is similar to

equation 3.60 obtained in the case of actuator-actuator in paragraph 3.7.5 with the adding of equation 4. 13.

$$\begin{bmatrix} M_{mm} & 0 & 0 \\ 0 & 0 & 0 \\ 0 & 0 & 0 \end{bmatrix} \begin{bmatrix} \ddot{U}_i \\ t_p \ddot{Q}_{p1} \\ t_p \ddot{Q}_{p2} \end{bmatrix} + \begin{bmatrix} C_{mm} & 0 & 0 \\ 0 & -\frac{R}{t_p^2} & 0 \\ 0 & 0 & 0 \end{bmatrix} \begin{bmatrix} \dot{U}_i \\ t_p \dot{Q}_{p1} \\ t_p \dot{Q}_{p2} \end{bmatrix} +$$

$$\begin{bmatrix} K_{mm} - K_{mvp1}K_{vvp1}^{-1}K_{vmp1} - K_{mvp2}K_{vvp2}^{-1}K_{vmp2} & K_{mvp1}K_{vvp1}^{-1} & K_{mvp2}K_{vvp2}^{-1} \\ -K_{vvp1}^{-1}K_{vmp1} & K_{vvp1}^{-1} & 0 \\ -K_{vvp2}^{-1}K_{vmp2} & 0 & K_{vvp2}^{-1} \end{bmatrix} \begin{bmatrix} U_i \\ t_p Q_{p1} \\ t_p Q_{p2} \end{bmatrix} = \begin{bmatrix} 0 \\ 0 \\ E_{3p2} \end{bmatrix}$$

4. 14

Using the above equation, the influence of the shunt resistance circuit is taken. Equation 4. 14 can be rewritten as below; then the voltage for the piezoelectric sensor is calculated.

$$\left[-(2\pi f_n)^2 \begin{bmatrix} M_{mm} & 0 & 0 \\ 0 & 0 & 0 \\ 0 & 0 & 0 \end{bmatrix} + \mathrm{j}(2\pi f_n) \begin{bmatrix} C_{mm} & 0 & 0 \\ 0 & -\frac{R}{t_p^2} & 0 \\ 0 & 0 & 0 \end{bmatrix} + \right.$$

$$\left. \begin{bmatrix} K_{mm} - K_{mvp1}K_{vvp1}^{-1}K_{vmp1} - K_{mvp2}K_{vvp2}^{-1}K_{vmp2} & K_{mvp1}K_{vvp1}^{-1} & K_{mvp2}K_{vvp2}^{-1} \\ -K_{vvp1}^{-1}K_{vmp1} & K_{vvp1}^{-1} & 0 \\ -K_{vvp2}^{-1}K_{vmp2} & 0 & K_{vvp2}^{-1} \end{bmatrix} \right] \begin{bmatrix} U_i \\ t_p Q_{p1} \\ t_p Q_{p2} \end{bmatrix} = \begin{bmatrix} 0 \\ 0 \\ E_{3p2} \end{bmatrix}$$

4. 15

Experimental and model results for the two piezoelectric sensor cases (open circuit and shunt circuit) are illustrated in
Table 4.7. Also this table can affirm the validity of our model in the particular case of sensor functionality.

Frequency	***Open circuit***		***Resistance shunt circuit***	
	Experimental	***2D FE model***	***Experimental***	***2D FE model***
f1	2 V	2.1 V	0.5 V	0.53 V
f3	4 V	4.1 V	3.4 V	3.41 V
f5	14.5 V	14.2 V	12.5 V	12.9 V
f10	29 V	29.05 V	28.8 V	28.8 V
f14	12 V	12.09 V	11.8 V	11.8 V

Table 4.7: Obtained voltage for the piezoelectric sensor

4.4.2.4 Piezoelectric capacitance Validation

Let us now verify the capacitance value of the piezoelectric patch given in the datasheet of the appendix. Equation 3.58 in the case of no displacement of the device becomes:

$$[K_{vvpj}]\{E_{3pj}\} = t_p\{Q_{pj}\}$$

4. 16

In our particular case we have:

$$K_{vvp1}E_{3p1} = t_p Q_{p1}$$

4. 17

By using the above equation we can obtain the simulated capacitance C_p of the piezoelectric sensor. The value obtained by simulation is compared to the calculated one in the case of 1D FEM model and results are shown in Table 4. 8.

	Simulation	**Formula**
C_p	$\frac{K_{vvp2}}{t_p^2}$	$\frac{\varepsilon_{33r}^T \varepsilon_0 l_p b}{t_p}$
C_p(nF)	20	22

Table 4. 8: Comparison between simulation and analytic for the capacitance value

4.5 Conclusion and discussion

The model validation has been done. Now, it is useful to remind that our goal in this work is to create a traveling wave on thin structures using non-collocated piezoelectric patches in order to move the thin structures on a solid substrate. As we have seen in chapter 1, this traveling wave will be generated using the same operation principle as the linear traveling wave ultrasonic motors which were classified under the resonant drive locomotion. A short review about linear traveling wave ultrasonic motors is discussed in the next chapter.

Actually, in our literature review of chapter 1, there was no any traveling wave piezoelectric robots similar to the design that we proposed (non-collocated piezoelectric patches bonded on thin structures). But in the global point of view, linear traveling wave ultrasonic motors are similar to our design. That is why the same operation principle (resonant drive) will be used. Only one piezoelectric robot was reported in chapter 1 using the resonant drive locomotion and it is somewhat similar to our structure [(Son, et al., 2006)] but this robot uses a standing wave to create propulsion and not a traveling wave as we proposed. This robot will be presented briefly in the next chapter too.

The next two chapters (chapter 5 and 6) will be talking about the generation of a traveling wave on the beam while the generation of a traveling wave on the plate has been filed for a patent.

4.6 Appendix

1. Fixed-free boundary conditions

$$\begin{cases} w|_{x=0} = 0 \\ \partial_x w|_{x=0} = 0 \end{cases} \quad \text{(A.1.1)}$$

$$\begin{cases} \partial^2{}_x w|_{x=l} = 0 \\ \partial^3{}_x w|_{x=l} = 0 \end{cases} \quad \text{(A.1.2)}$$

4.7 References

Brandt Anders Noise and Vibration Analysis: Signal Analysis and Experimental Procedures [Livre]. - India : John Wiley & Sons , 2011.

Chowdhury Indrajit et Dasgupta Shambhu P. Computation of Rayleigh damping coeficients for large systems [Livre]. - U.A.E & India : [s.n.], 2006.

Clough Ray W. et Penzien Joseph Dynamics of structures [Livre]. - Berkeley : [s.n.], 1995.

Craig Roy R. et Kurdila Andrew J. Fundamentals of Structural Dynamics [Livre]. - U.S.A. : John Willey & Sons, 2006.

Giosan I. Dynamic analysis with damping for free standing structures using mechanical event simulation [Livre]. - Canada : [s.n.], 2006.

Inman Daniel J. Engineering vibration [Livre]. - U.S.A. : Prentice-Hall, 2001.

Kandge Ganesh Influence of mode dependent rayleigh damping on transient stress response [Rapport]. - Sweden : [s.n.], 2007.

Liu Man et Gorman D.G. Formulation of Rayleigh damping and its extensions [Revue] // Computers & structures. - 1994. - pp. 277-285.

Pons J.L. [et al.] Practical consideration of shear strain correction factor and Rayleigh damping in models of piezoelectric transducers [Revue] // Sensors and actuators. - 2004. - pp. 202-208.

Son K. J. [et al.] An ultrasonic standing-wave-actuated nano-positioning walking robot: Piezoelectric-metal composite beam modelling [Revue] // Journal of Vibration and Control, vol. 12, no. 12. - 2006. - pp. pp. 1293–1309.

CHAPTER 5

TRAVELING WAVE PIEZOELECTRIC BEAM ROBOT

Chapter 5: traveling wave piezoelectric beam robot

List of figures

List of tables

5.1 Introduction

This chapter is the base of our project, where we will apply the model developed in chapter 3 and validated in chapter 4 to demonstrate theoretically the generation of a traveling wave on a finite beam structure. Then an experimental prototype to validate the theoretical results will be presented in the next chapter.

As we now know, the operation principle of our robot is inspired from linear traveling wave ultrasonic motors. So, at the beginning of this chapter we will introduce the operation principal of our traveling wave piezoelectric beam robot by illustrating first a short review on linear traveling wave ultrasonic motors to be able to see the potential differences between our proposed robot and the others. For interested readers, an introduction to ultrasonic motors can be found in [(Sashida, et al., 1993)], a state of the art of piezoelectric linear motors is presented in [(Hemsel, et al., 2000)] and a comparative analysis and modeling of both standing and traveling wave ultrasonic linear motor is presented in [(Fernandez, et al., 2003)]. Note that, in our project we are interested only in the traveling wave linear motion.

After introducing the operation principal of our traveling wave piezoelectric beam robot, modeling of the piezoelectric robot will be presented by readapting the matrix equation obtained in chapter 3 to our case of application. Then the optimal design will be studied in details including dimensions of the robot, piezoelectric patches positions, optimal operating frequency and traveling wave performance of the robot. The next chapter will be dedicated to the manufacture and the experimental validation.

5.2 Operation principle

The idea is to generate a traveling wave in a beam structure to move this beam on a solid substrate using piezoelectric patches bonded on the beam surface. This idea is inspired from linear traveling wave ultrasonic motor [(Sashida, et al., 1993), (Ueha, et al., 1993)] and it is applied to robotic systems to move all the system instead of moving the slider as the case of linear traveling wave ultrasonic motors.

Several configurations were reported in literature to excite traveling waves in finite structures. Among them we can cite the one mode excitation presented first by Kuribayashi et al. [(Kuribayashi, et al., 1985)] and the two modes excitation presented first by B.G. Loh et al. [(Loh, et al., 2000)]. Both methods are presented for ultrasonic linear motor. Other methods used to generate traveling wave in finite beam structure, like feedback control method, active control method and adaptive control method are also exist in literature but they were not in

our field of interest in this project. Interested readers can refer to [(Gabai, et al., 2009)] where it presents an important review to excite traveling wave in finite beam structure.

The followings are some keys examples of traveling wave generated on a finite beam structure using two Langevin piezoelectric transducers; the principle of these following works is inspired from linear traveling wave ultrasonic motors theory:

C. Hernandez at LGEP laboratory, France [(Hernandez, 2010)] used two Langevin piezoelectric transducers to create a traveling wave on a finite beam, the traveling wave is created by actuating the two piezoelectric transducers (vibrator-vibrator: two modes excitation) and also by actuating one transducer while the other is used as absorber (vibrator-absorber: one mode excitation). He used the traveling wave to realize a linear pump system.

G.H. Kim and J.W. Park at the department of mechanical engineering, Chosun University, Korea [(Kim, et al., 2009)] used two piezoelectric Langevin transducers as vibrators to create the traveling wave on a finite beam. They studied theoretically the change in traveling wave direction according to frequency and verified it experimentally.

B.G. Loh and P.I. Ro at the department of mechanical aerospace engineering, North Carolina University, Raleigh, USA [(Loh, et al., 2000)] were demonstrate experimentally the possibility to generate a traveling wave on a finite length using two piezoelectric Langevin transducers as vibrator (two modes excitation). Some experimental tests are done in their works to characterize this linear traveling wave ultrasonic motor.

Figure 5.1 and Figure 5.2 show one mode excitation and two modes excitation linear traveling wave motors respectively. These two motors use two Langevin piezoelectric transducers to generate the traveling wave on a finite beam length.

Other type of traveling wave linear ultrasonic motors using piezoelectric patches bonded on an elastic structure as actuators and not Langevin actuators are presented also in literature. These types of motors use many piezoelectric patches bonded on one or both side of the elastic structure and also teeth on the structure to generate the traveling wave. As examples of such type of motors we can cite [(Bein, et al., 1997),(Roh, et al., 2001)]. These motors are presented in Figure 5.3 and Figure 5. 4.

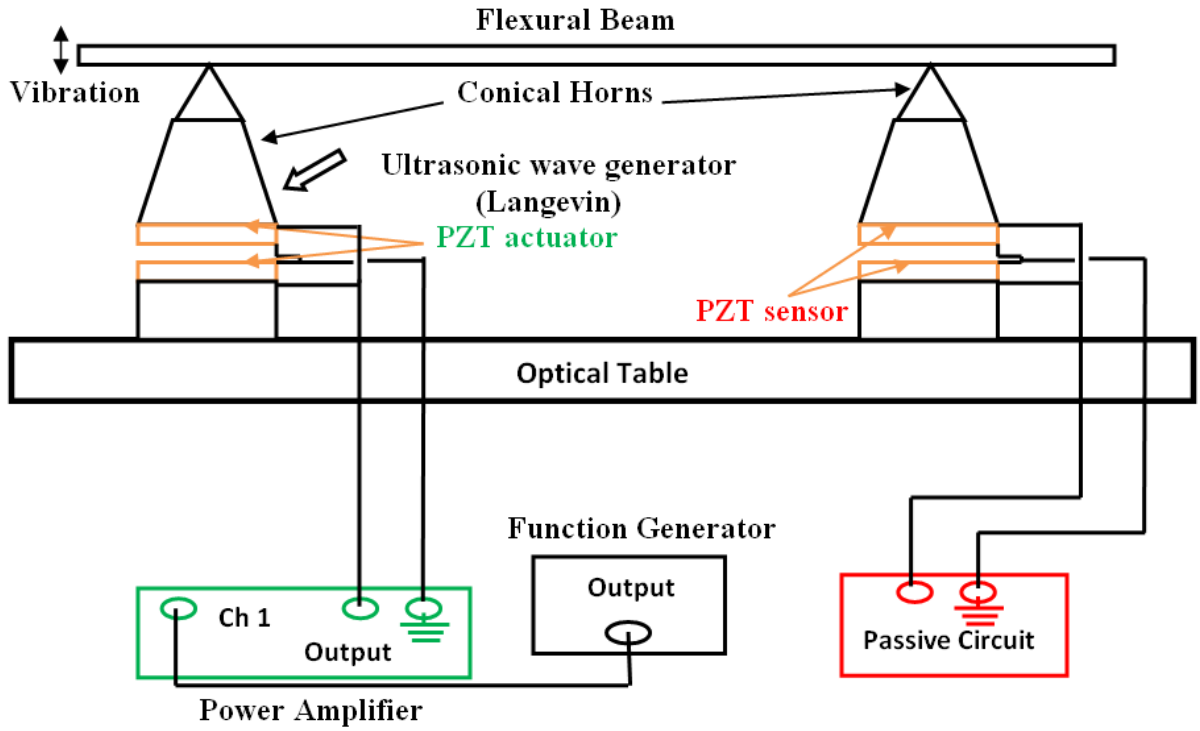

Figure 5.1: schematic figure for a one mode excitation linear traveling wave motor

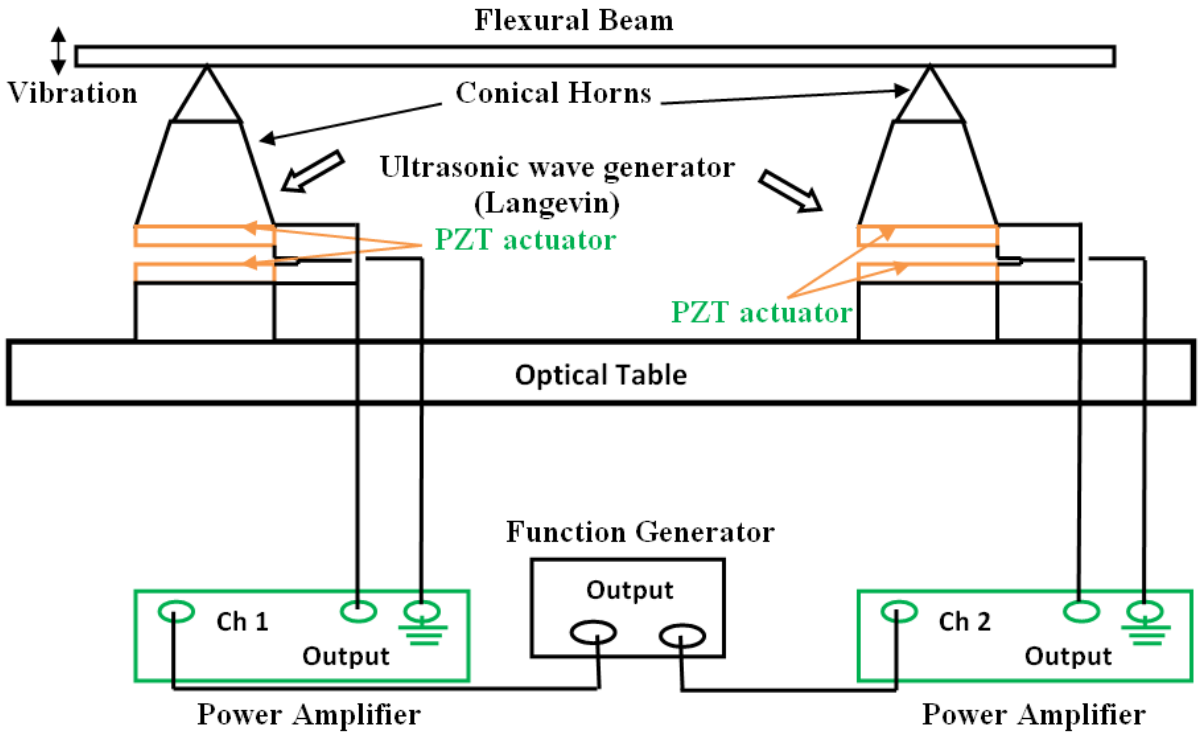

Figure 5.2: Schematic figure for a two modes excitation linear traveling wave motor

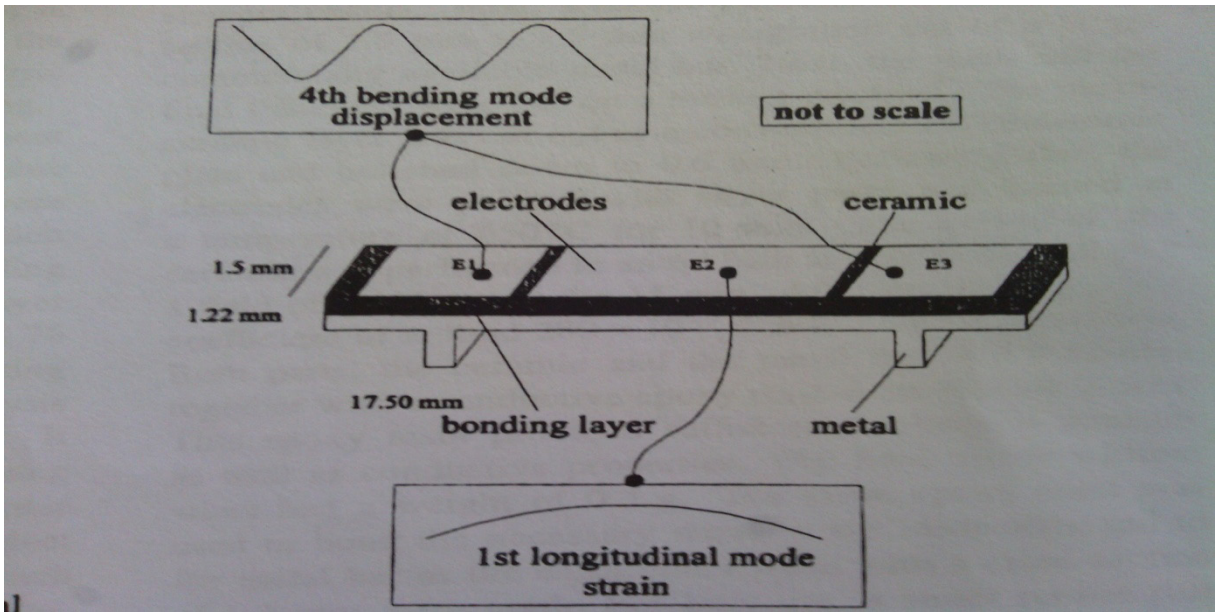

Figure 5.3: Linear ultrasonic motor uses the first longitudinal and the fourth bending mode [(Bein, et al., 1997)]

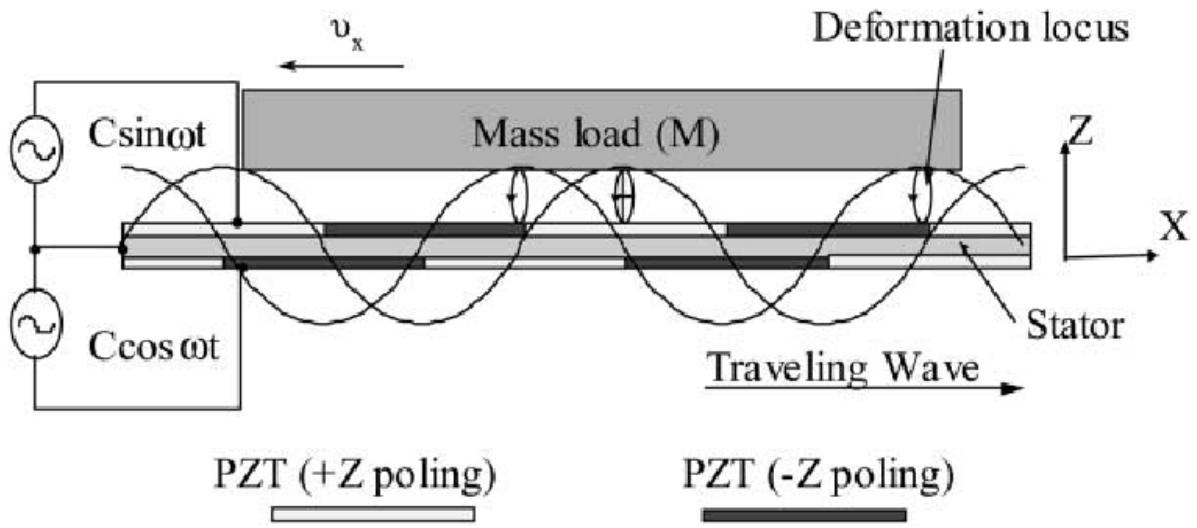

Figure 5. 4: Traveling wave ultrasonic linear motor presented by (Roh, et al., 2001)

Dual piezoelectric actuators for the traveling wave ultrasonic motor is presented in [(Suybangdum, et al., 2009)], this motor uses dual piezoelectric patches bonded on the beam structure but it uses teeth also to generate this traveling wave using the two modes excitation method (Figure 5. 5).

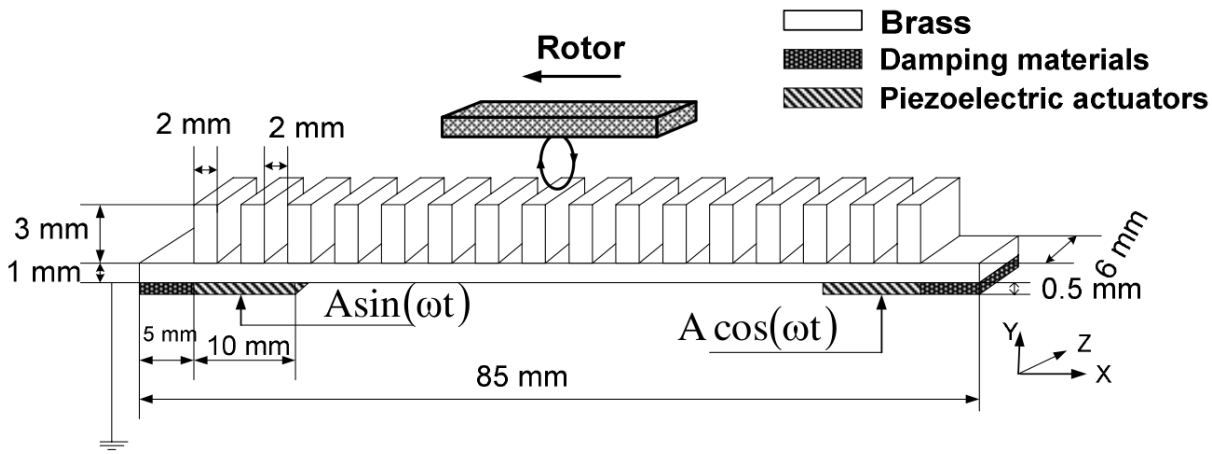

Figure 5. 5: The schematic diagram of the dual piezoelectric actuators ultrasonic linear motor presented by (Suybangdum, et al., 2009)

Initially, we started our project by a literature search on piezoelectric miniature robots that exist as it was presented in Chapter 1. We noticed that there is no robot based on this principle from which the originality of the work. The only robot that has been found and presented in Chapter 1, Section 1.4.5 uses the standing wave with legs to generate motion. Locomotion principle, schematic diagram and a prototype of this miniature walking robot are presented in [(Son, et al., 2006)] and shown here below in Figure 5.6.

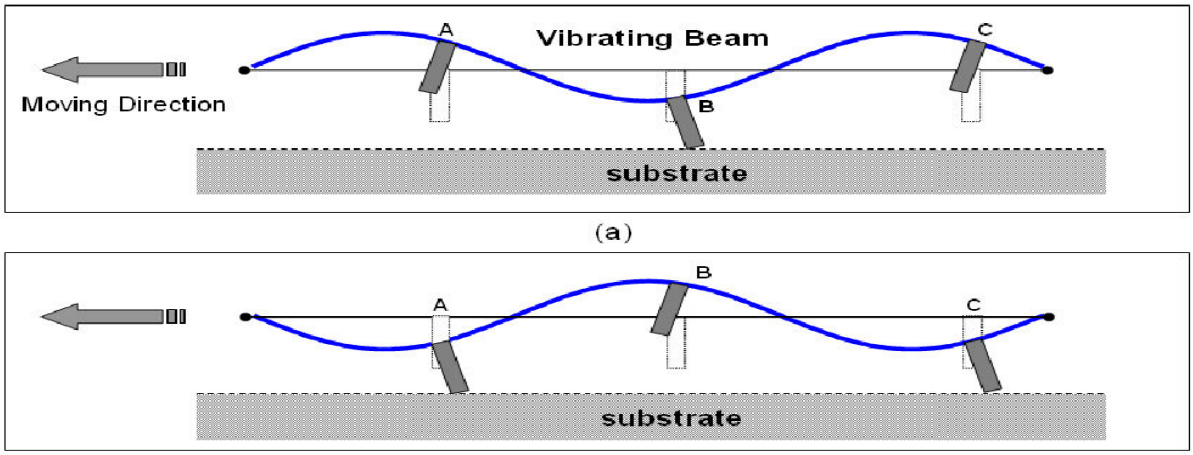

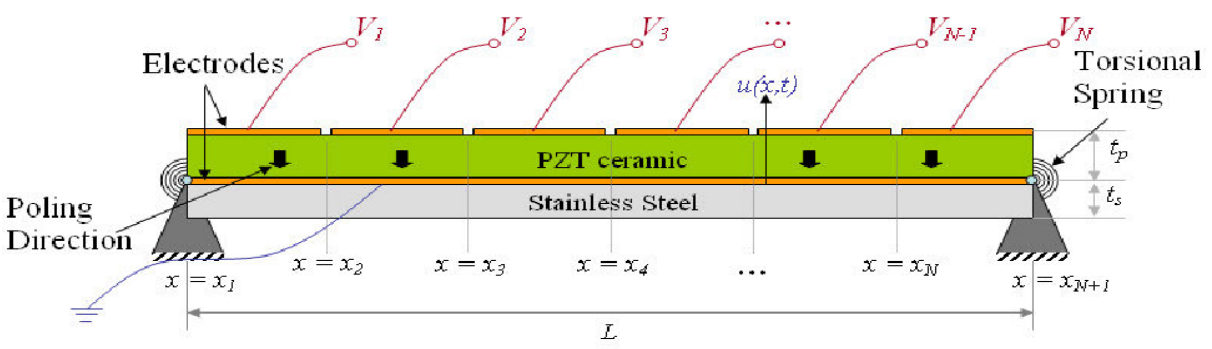

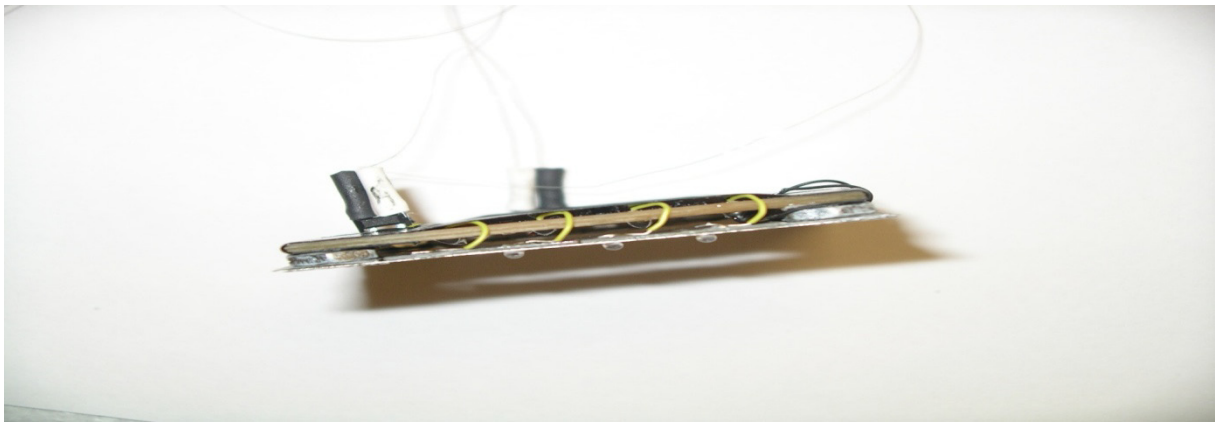

Figure 5. 6: Locomotion principle, schematic diagram and the fabricated prototype presented in [(Son, et al., 2006)]

This robot has the same structure as our robot. It consists of a piezoelectric layer bonded on a metal layer.

Our robot consists of only two piezoelectric patches bonded on a beam layer. The originality of our system compared to this robot and to all linear ultrasonic motors presented is that we use two piezoelectric patches without using teeth or legs - in robotic notation - to generate the traveling wave for robotic application as presented in Figure 5.7. What I meant by robotic application is that we are interested to move the entire system and not a slider (rotor) on the elastic beam (stator). The motion is generated using one mode or two modes excitation.

Before presenting the one mode and two modes excitation functionality of the traveling wave piezoelectric beam robot, it is necessary to remind about the definition of a standing and a traveling wave.

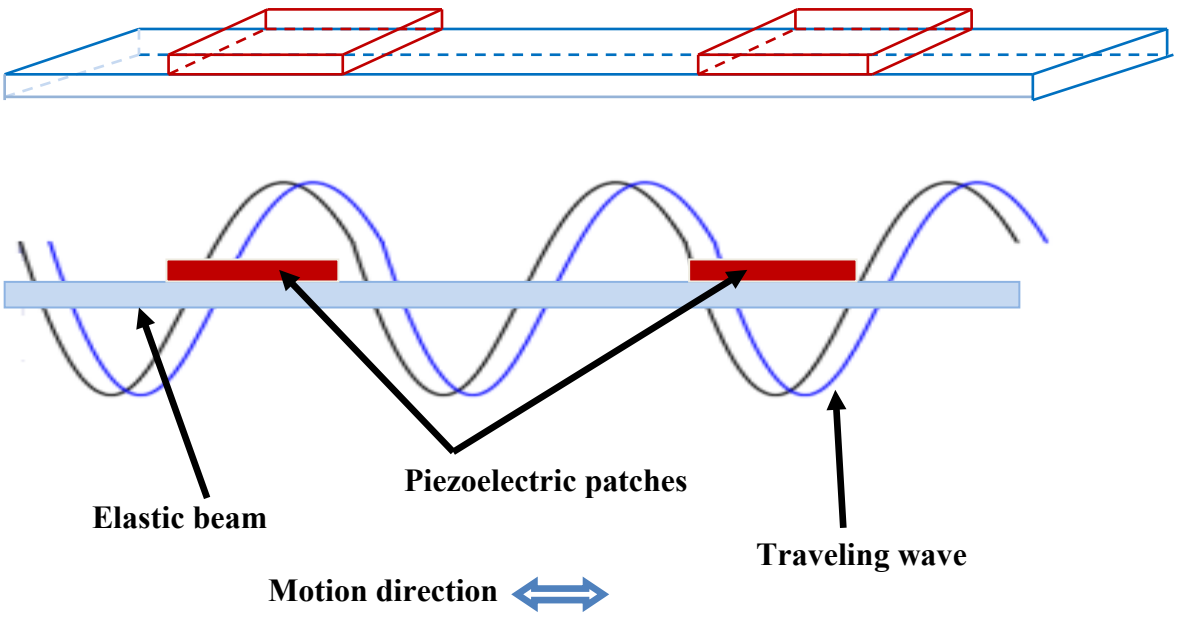

Figure 5.7: schematic diagram of the traveling wave piezoelectric beam robot. 3D view on the top and side view on the bottom

5.2.1 Standing wave and traveling wave

A standing wave is expressed by the formula: $u_s(x, t) = A\cos(kx)\sin(wt)$, and a travelling wave is expressed by: $u_p(x, t) = A\cos(kx-wt)$. Using the trigonometric relations, a standing wave can be expressed with two travelling waves and a travelling wave can be also expressed as two standing waves as shown below:

$$2A\cos(kx)\sin(wt) = A\sin(kx-wt) + A\sin(kx+wt) \quad (5.1)$$

$$A\cos(kx-wt) = A\cos(kx)\cos(wt) + A\cos(kx-\pi/2)\cos(wt-\pi/2) \quad (5.2)$$

Where k is the wave number and w is the angular frequency.

According to equation 5. 1, a standing wave is generated by superposition of two travelling waves with the same amplitude and frequency but moving in different directions. Also equation 5. 2 shows that, a travelling wave is generated by superposition of two standing waves with a phase difference of 90° from each other both in time and space.

Figure 5. 8 and Figure 5. 9 illustrate a pure standing wave and a pure travelling wave successively projected on a plane of length (x) and time (t) of a flexural beam. These figures will be used later to visualize the travelling wave performance in a beam structure.

After definition of standing wave and travelling wave, let us now introduce the one mode and two modes excitation functionality of this traveling wave piezoelectric beam robot schematized in Figure 5.7.

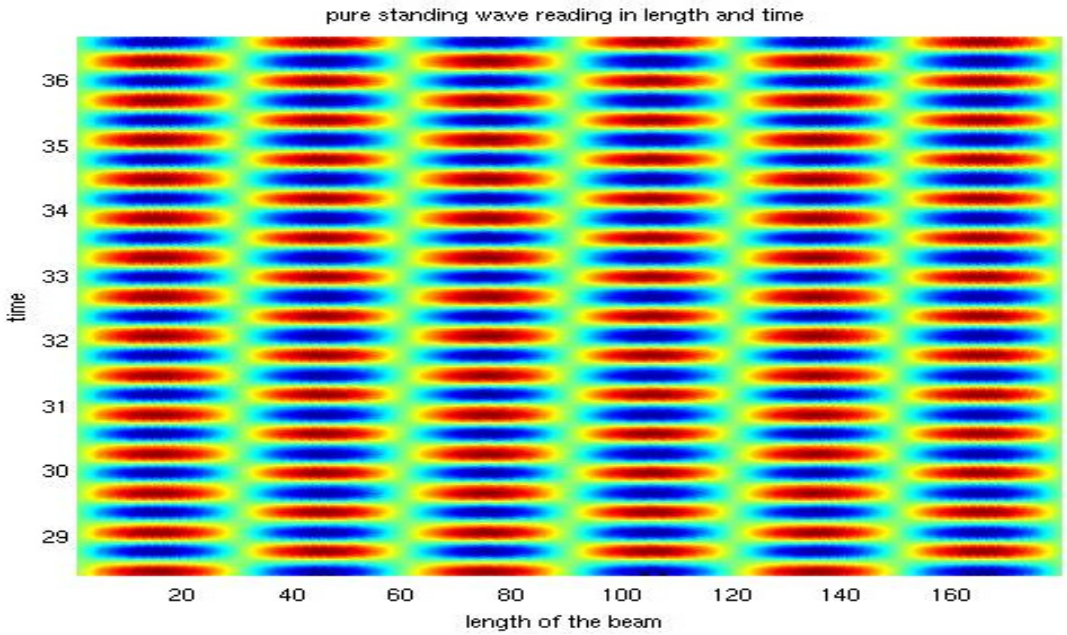

Figure 5. 8: Pure standing wave reading in length and time

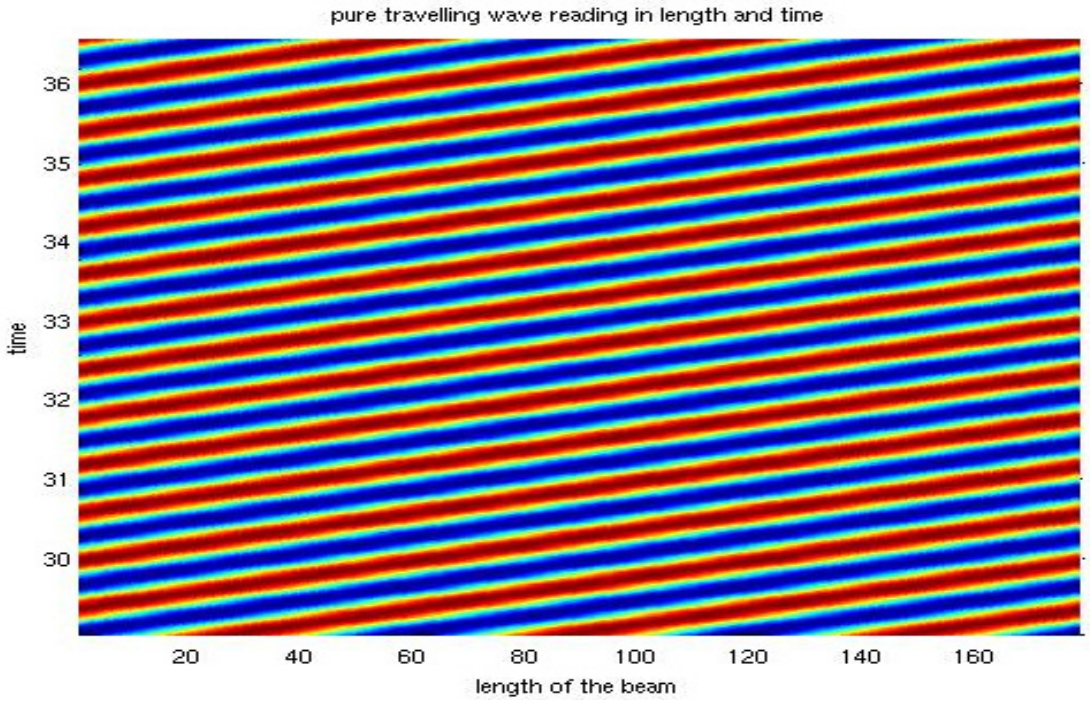

Figure 5. 9: Pure travelling wave reading in length and time

5.2.2 Operation principle case of one mode excitation

We repeat that our idea is to generate this traveling wave in a beam structure to move it on a solid substrate. The traveling wave is generated without using legs, with two non-collocated piezoelectric patches bonded on the beam surface (Figure 5.7).

As we know, pure linear traveling waves are usually observed on long structures and rarely on normal finite structures. In finite structures like beams, the excited vibration wave produced by one piezoelectric patch is partially reflected when it hits the boundaries, which create a mixture between standing and traveling waves; as a standing wave is generated by superposition of two traveling waves with the same amplitude and frequency but moving in opposite directions (equation 5. 1).

An additional piezoelectric patch can be used to avoid wave reflection. Our system consists of a beam structure, with two non-collocated piezoelectric patches attached to its surface. One patch produces the mechanical displacement of the beam by applying an electrical voltage, while the other converts this mechanical displacement into electrical energy which is then dissipated through passive RL electrical networks to avoid wave reflection. The device studied is presented in Figure 5.10.

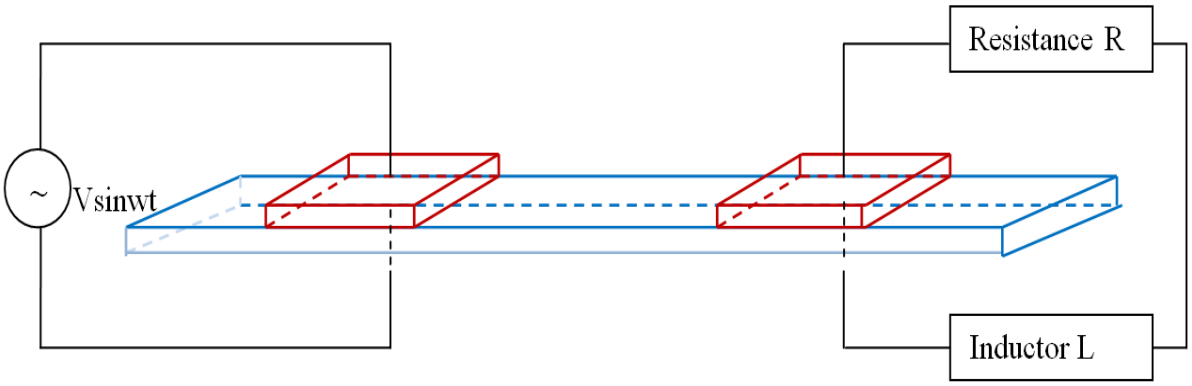

Figure 5.10: Schematic figure of the one mode excitation

It can be noted that, by switching the role of both piezoelectric patches, the motion direction will change. Series RL connection was chosen to study in this work as we can see in Figure 5.10, but this is not the only way to absorb wave. It was chosen due to the simplicity of its modeling and implementation. In order to obtain a great rate of travelling wave, in other term to avoid the maximum possible wave reflexion, R & L must be calculated to obtain the maximum ratio of power dissipated over power provided. The power dissipated is the power consumed by the electrical shunt circuit and the power provided is the power consumed by the patch actuator. Ratio of power dissipated over power provided must be calculated because not only the power dissipated depends on the charge (RL values), the power provided depends also on the charge, the applied frequency and piezoelectric patches positions.

As we said, many other passive methods exist in literature. For example Hariri et al. present in their paper [(Hariri, et al., 2011)] a comparison between open circuit, R shunt circuit, RL series connection and RL parallel connection for damping vibrations of the same asymmetric system (2 non-collocated piezoelectric patches bonded on thin beam). They demonstrated that RL series and Parallel give approximately the same result for this system. Also others passive techniques like SSDS (Synchronized Switch Damping on a Short circuit) and SSDI (Synchronized Switch Damping on an Inductor) are compared in [(Corcolle, et al., 2008)]. Semi passive techniques are given in [(Badel, 2006)] for damping applications. The advantage of RL series or parallel technique compared to other passive or semi passive techniques is the simplicity of its modeling and implementation but its major drawback is that it is not very effective at low frequencies. In our case we are not interested to work at low frequencies, in contrast we need a high frequency in order to get enough contact points between the robot and the ground to move the robot. Also we take into account that transverse displacement of the beam decreases with frequency.

Others types like feedback control method, active control method and adaptive control method are reviewed in [(Gabai, et al., 2009)] for damping application also. We should note that the active control method is somehow the two modes excitation method; it will be discussed in the next sub-section.

5.2.3 Operation principle case of two modes excitation

In one mode excitation, one patch is used as actuator to produce vibration on the beam while the other is used as sensor to convert this mechanical vibration into heating in the goal to produce a traveling wave on the beam. In two modes excitation, the two patches are used as actuators to produce the mechanical displacement of the beam in order to create the traveling wave. Due to this aim, the two piezoelectric patches producing the mechanical displacement of the beam by applying simultaneously two neighbored natural mode shapes of the beam at the same frequency but with a phase difference of 90°. The vibration can be approximated as the superposition of these two modes; this is called a two modes excitation.

It becomes clear now that, the principle of two modes excitation is based on the excitation of the two patches, at a frequency between two resonance frequencies. This principle is necessary to generate the traveling wave on the beam. At the resonance frequency, two progressive waves with the same amplitude propagating in opposite directions cancel each other, resulting in standing wave on the beam, so the beam robot will be stopped moving. Below or above the resonance frequency, one progressive wave is excited more than the other. The resulting waves propagate in the same direction as the waves with the greater amplitude propagate [(Loh, et al., 2000)]. This result was demonstrated theoretically and verified also experimentally in [(Kim, et al., 2009)] for linear traveling wave ultrasonic motors. They demonstrated that, the generated travelling wave changes direction according to the excitation frequency (left side of Figure 5.11).

Taking now the case where the two patches are actuated by Vsin(wt) and Vsin(wt+ φ) respectively. When φ equal to 90°, the traveling wave reaches its maximal speed. The motion direction can be reversed by changing phase difference from 90° to -90° without causing the motion speed to decrease. This result is demonstrated experimentally in [(Loh, et al., 2000)]. A plot representing the variation of speed versus phase difference is shown in the right side of Figure 5.11. Schematic figure for the two modes excitation at φ equal to 90° is represented in Figure 5.12.

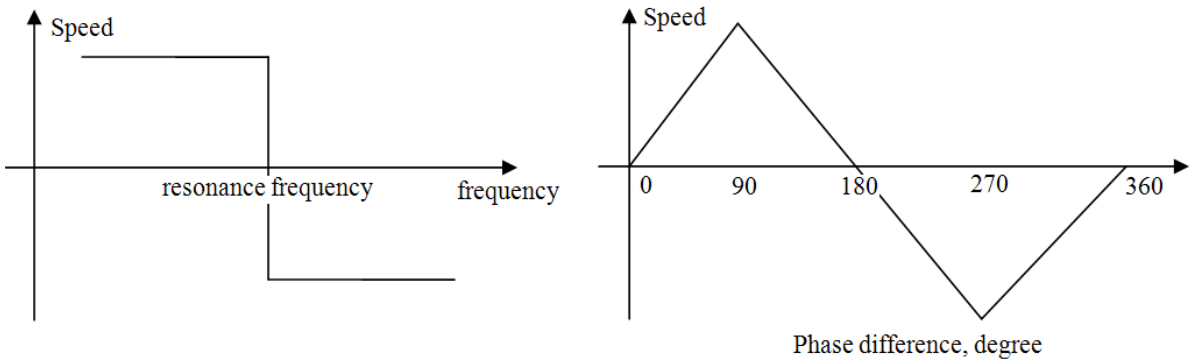

Figure 5.11: Variation of speed versus frequency (left) and variation of speed versus phase difference (left)

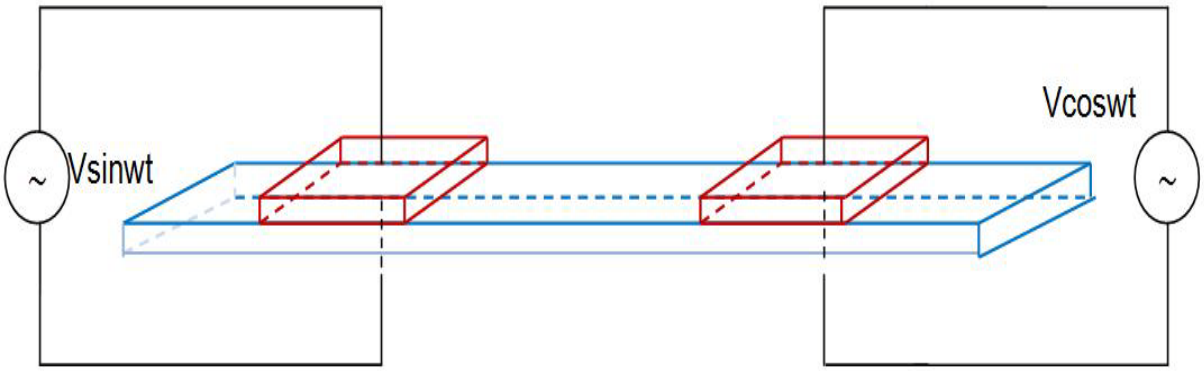

Figure 5.12: Schematic figure of the two modes excitation

5.3 Modeling of the piezoelectric beam robot

Take first the case of one mode excitation. In this case one patch (p2) is acting as actuator where a sinusoidal voltage is applied (Vsin(wt)) while the other (p1) is connected to series RL connection.

As the case of equation 4.15 when a resistance shunts circuit is added, the following equation will be used here to add series RL connection.

$$E_{3p1}t_p = R\dot{Q}_{p1} + \mathrm{L}\ddot{Q}_{p1} \qquad 5.3$$

The obtained equation is similar to equation 3.60 obtained in the case of actuator-actuator in section 3.7.5 with the addition of equation 5. 3.

$$\begin{bmatrix} M_{mm} & 0 & 0 \\ 0 & -\frac{L}{t_p^2} & 0 \\ 0 & 0 & 0 \end{bmatrix} \begin{bmatrix} \ddot{U}_l \\ t_p\ddot{Q}_{p1} \\ t_p\ddot{Q}_{p2} \end{bmatrix} + \begin{bmatrix} C_{mm} & 0 & 0 \\ 0 & -\frac{R}{t_p^2} & 0 \\ 0 & 0 & 0 \end{bmatrix} \begin{bmatrix} \dot{U}_l \\ t_p\dot{Q}_{p1} \\ t_p\dot{Q}_{p2} \end{bmatrix} +$$

$$\begin{bmatrix} K_{mm} - K_{mvp1}K_{vvp1}^{-1}K_{vmp1} - K_{mvp2}K_{vvp2}^{-1}K_{vmp2} & K_{mvp1}K_{vvp1}^{-1} & K_{mvp2}K_{vvp2}^{-1} \\ -K_{vvp1}^{-1}K_{vmp1} & K_{vvp1}^{-1} & 0 \\ -K_{vvp2}^{-1}K_{vmp2} & 0 & K_{vvp2}^{-1} \end{bmatrix} \begin{bmatrix} U_i \\ t_pQ_{p1} \\ t_pQ_{p2} \end{bmatrix} =$$

$$\begin{bmatrix} 0 \\ 0 \\ E_{3p2}(t) = \frac{V}{t_p}\sin(wt) \end{bmatrix}$$

5. 4

Equation 5. 4 is used to represent the piezoelectric beam robot in the case of one mode excitation. Where $\frac{V}{t_p}$ is the electric field amplitude, w = $2\pi f_n$, f_n is the resonance frequency. Otherwise, the last equation can be written as the following:

$$\begin{bmatrix} M & 0 & 0 \\ 0 & 0 & 0 \\ 0 & 0 & 0 \end{bmatrix} \begin{bmatrix} \ddot{U}_l \\ t_p\ddot{Q}_{p1} \\ t_p\ddot{Q}_{p2} \end{bmatrix} + \begin{bmatrix} C & 0 & 0 \\ 0 & -\frac{z_e}{t_p^2} & 0 \\ 0 & 0 & 0 \end{bmatrix} \begin{bmatrix} \dot{U}_l \\ t_p\dot{Q}_{p1} \\ t_p\dot{Q}_{p2} \end{bmatrix} +$$

$$\begin{bmatrix} K_{mm} - K_{mvp1}K_{vvp1}^{-1}K_{vmp1} - K_{mvp2}K_{vvp2}^{-1}K_{vmp2} & K_{mvp1}K_{vvp1}^{-1} & K_{mvp2}K_{vvp2}^{-1} \\ -K_{vvp1}^{-1}K_{vmp1} & K_{vvp1}^{-1} & 0 \\ -K_{vvp2}^{-1}K_{vmp2} & 0 & K_{vvp2}^{-1} \end{bmatrix} \begin{bmatrix} U_i \\ t_pQ_{p1} \\ t_pQ_{p2} \end{bmatrix} =$$

$$\begin{bmatrix} 0 \\ 0 \\ E_{3p2}(t) = \frac{V}{t_p}\sin(wt) \end{bmatrix}$$

5. 5

Where

$$E_{3p1}t_p = z_e\dot{Q}_{p1}$$

$$z_e = jwL + R$$

5. 6

In frequency domain this equation can be rewritten as below:

$$\left[-(2\pi f_n)^2\begin{bmatrix}M_{mm} & 0 & 0\\ 0 & -\frac{L}{t_p^2} & 0\\ 0 & 0 & 0\end{bmatrix}+\mathrm{j}(2\pi f_n)\begin{bmatrix}C_{mm} & 0 & 0\\ 0 & -\frac{R}{t_p^2} & 0\\ 0 & 0 & 0\end{bmatrix}+\right.$$

$$\left.\begin{bmatrix}K_{mm}-K_{mvp1}K_{vvp1}^{-1}K_{vmp1}-K_{mvp2}K_{vvp2}^{-1}K_{vmp2} & K_{mvp1}K_{vvp1}^{-1} & K_{mvp2}K_{vvp2}^{-1}\\ -K_{vvp1}^{-1}K_{vmp1} & K_{vvp1}^{-1} & 0\\ -K_{vvp2}^{-1}K_{vmp2} & 0 & K_{vvp2}^{-1}\end{bmatrix}\right]\begin{bmatrix}U_i\\ t_pQ_{p1}\\ t_pQ_{p2}\end{bmatrix}=\begin{bmatrix}0\\ 0\\ E_{3p2}\end{bmatrix}$$

5. 7

Take now the case of two modes excitation. In this case the two patches are acting as actuators where two sinusoidal voltages are applied with the same amplitude and a phase difference of 90° (Vsin(wt) & Vcos(wt)).

The obtained equation is similar to equation 3.60 obtained in the case of actuator-actuator in section 3.7.5 in the case where two patches are used. So, the equation that represents the piezoelectric beam robot case of two modes excitation is given below by

$$\begin{bmatrix}M_{mm} & 0 & 0\\ 0 & 0 & 0\\ 0 & 0 & 0\end{bmatrix}\begin{bmatrix}\ddot{U}_i\\ t_p\ddot{Q}_{p1}\\ t_p\ddot{Q}_{p2}\end{bmatrix}+\begin{bmatrix}C_{mm} & 0 & 0\\ 0 & 0 & 0\\ 0 & 0 & 0\end{bmatrix}\begin{bmatrix}\dot{U}_i\\ t_p\dot{Q}_{p1}\\ t_p\dot{Q}_{p2}\end{bmatrix}+$$

$$\begin{bmatrix}K_{mm}-K_{mvp1}K_{vvp1}^{-1}K_{vmp1}-K_{mvp2}K_{vvp2}^{-1}K_{vmp2} & K_{mvp1}K_{vvp1}^{-1} & K_{mvp2}K_{vvp2}^{-1}\\ -K_{vvp1}^{-1}K_{vmp1} & K_{vvp1}^{-1} & 0\\ -K_{vvp2}^{-1}K_{vmp2} & 0 & K_{vvp2}^{-1}\end{bmatrix}\begin{bmatrix}U_i\\ t_pQ_{p1}\\ t_pQ_{p2}\end{bmatrix}=$$

$$\begin{bmatrix}0\\ E_{3p1}(t)=\frac{V}{t_p}\cos(wt)\\ E_{3p2}(t)=\frac{V}{t_p}\sin(wt)\end{bmatrix}$$

5. 8

The equation can be rewritten in frequency domain as below:

$$\left[-(2\pi f_n)^2\begin{bmatrix}M_{mm} & 0 & 0\\ 0 & 0 & 0\\ 0 & 0 & 0\end{bmatrix}+\mathrm{j}(2\pi f_n)\begin{bmatrix}C_{mm} & 0 & 0\\ 0 & 0 & 0\\ 0 & 0 & 0\end{bmatrix}+\right.$$

$$\left.\begin{bmatrix}K_{mm}-K_{mvp1}K_{vvp1}^{-1}K_{vmp1}-K_{mvp2}K_{vvp2}^{-1}K_{vmp2} & K_{mvp1}K_{vvp1}^{-1} & K_{mvp2}K_{vvp2}^{-1}\\ -K_{vvp1}^{-1}K_{vmp1} & K_{vvp1}^{-1} & 0\\ -K_{vvp2}^{-1}K_{vmp2} & 0 & K_{vvp2}^{-1}\end{bmatrix}\right]\begin{bmatrix}U_i\\ t_pQ_{p1}\\ t_pQ_{p2}\end{bmatrix}=\begin{bmatrix}0\\ E_{3p1}\\ E_{3p2}\end{bmatrix}$$

5. 9

We should note that during assembly of matrices free-free boundary conditions are taking into account (Appendix).

5.4 Optimal design

Our goal is to demonstrate the generation of a traveling wave on a beam. For this purpose, matrices equations obtained in the last section will be used here in order to determine optimal geometric parameters of the system, type of material used for the beam, optimal operating frequency and optimal R & L values (case of one mode excitation) i.e. better travelling wave performance, being given dimensions of the beam.

The given dimensions of the beam are (l_m = 180 $\times$ b_m = 17 $\times$ t_m = 0.5 mm). Width of the piezoelectric patches was chosen to be the same as the beam width (b_p = 17 mm).

A study in [(Dehez, et al., 2010)] for ultrasonic motors using two Langevin piezoelectric transducers (punctual force applied on the beam) demonstrates that the location of the transducer has an influence on the vibration of the beam (transverse displacement). When the actuator is placed on a point corresponding to an anti-node of a given frequency, the transverse displacement will be maximized. At the opposite when it is placed at a node of this frequency, the transverse displacement will be completely absent. Actually here, in view of creating the better traveling wave, it is suggested to locate the transducers on the positions of the first antinodes observed from the ends of the beam. At first glance and taking that into account, the length of the piezoelectric patches should be equals to the half of the wave length ($\lambda/2$) being given the resonant mode of operation of the system and placed at the first antinodes observed from the ends of the beam as we can see in Figure 5.13.

Figure 5.13 shows the vibration of a beam at the 20^{th} and 7^{th} resonant modes and accordingly the piezoelectric patches length at each resonant mode. Actually, that cannot be working here because we need a high frequency in order to get enough friction points between the robot and the ground to move the robot forward. High resonance frequency means here small piezoelectric patches length and in this case the piezoelectric patches would not generate enough bending moment to create vibrations of the beam.

Also displacement cannot be more important if we place the patches at more anti-nodes than nodes because vibrations maybe canceled. Take for example the case of two punctual longitudinal forces (Langevin transducers) applied at two neighboring anti-nodes, vibrations can be canceled each other. The same in our case, piezoelectric patch is equivalent to two

bending moments at both ends of the patch [(Hariri, et al., 2011)]. The influence of piezoelectric positions on the traveling wave performance will be studied later in this chapter.

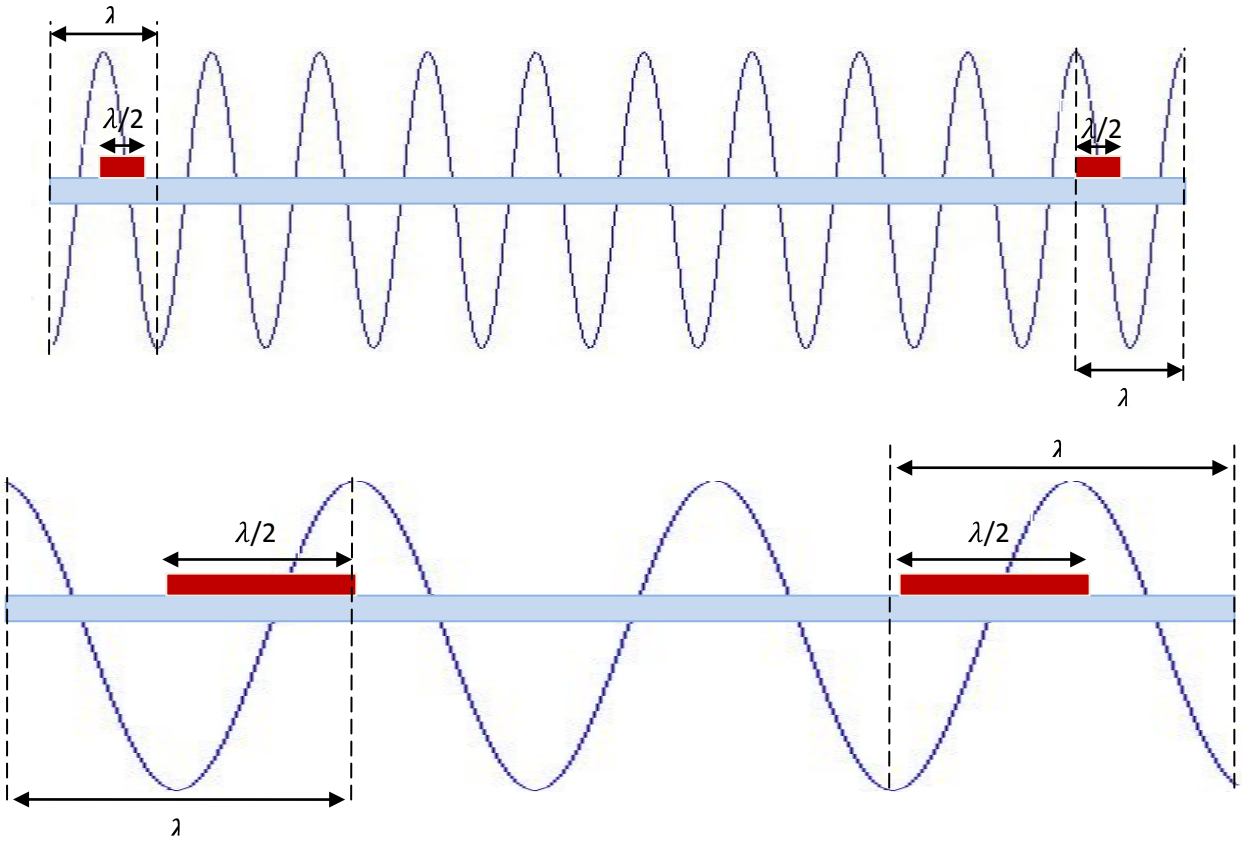

Figure 5.13: Length of the piezoelectric patches at the 20th (top figure) and 7th (bottom figure) resonant modes

Several conditions must be looking forward before talking about the length of patches. Firstly, polarization and applied electric field have the same directions, therefore transversal mode variation occurs in the piezoelectric patches; results in a variation along x-axis and y-axis. Cases of thin beam, only x-direction is considered (bending moment); therefore variation along y-axis is vanished (σ_1 is the only non zero stress). So for piezoelectric patches, it is

useful to have the length of patch more than its width. Secondly, it was demonstrated by simulations that the transverse displacement is smaller in the position where the piezoelectric patches are placed through the length of the beam. Figure 5. 14 shows transverse displacement through the length of the beam for several sampling time at the third (left figure) and fourth (right figure) resonant frequencies where two piezoelectric patches are placed near from both ends of the beam. It can be seen from figure that the transverse displacement is smaller in the position where the piezoelectric patches are placed. Also that affects the traveling wave performance at the position of patches because magnitude of waves decreases.

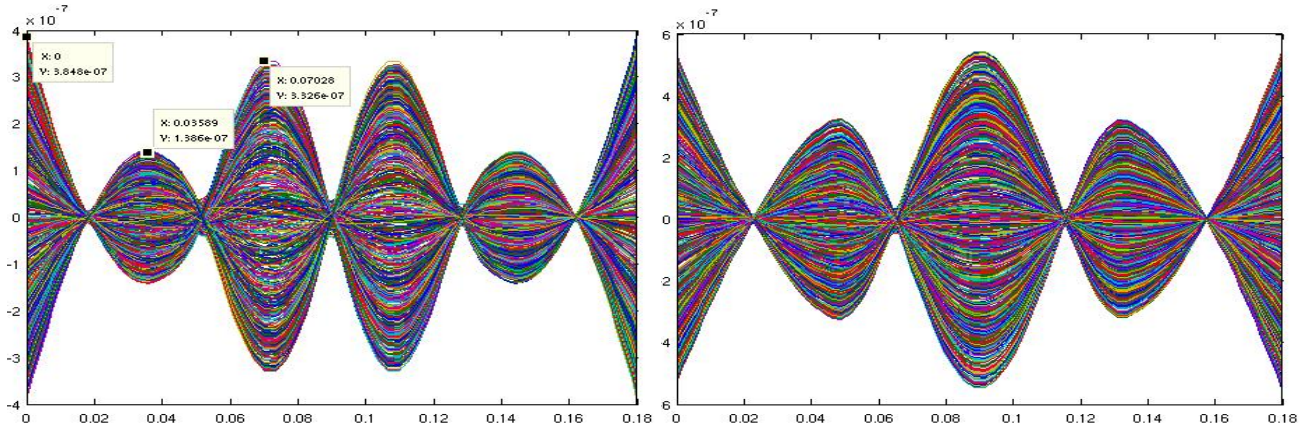

Figure 5. 14: Transverse displacement in time trough the length of a beam at the third (left) and fourth (right) resonant frequencies

As conclusion, for small piezoelectric patches length we cannot generate enough bending moment to create vibrations of the beam and big piezoelectric patches length decrease the transverse displacement in the position where the piezoelectric patches are placed and affects the traveling wave performance. But as we are in the case of thin beam where only x-direction is considered for modeling, it is good to have the length of patch more than its width. Practically, two times its width. Consequently the length of the piezoelectric patches was selected to be between 30 mm and 35 mm.

Being given dimensions of the beam and after determining the width and the length of the piezoelectric patches, thickness of piezoelectric patches and material used for the beam will be studied in the next sub-section.

5.4.1 Thickness of piezoelectric patches and material used for the beam

In this sub-section, we will study the influence of the thickness of the piezoelectric patches and the material rigidity of the structure on the amplitude of the transverse displacement and the resonance frequency of the system.

We are interested in the thickness which gives a maximum transverse displacement of the beam and this optimal thickness is the same for static and dynamic operation of the system (appendix of this chapter). So, a static study is done to determine this thickness at fixed-free boundary conditions because free-free boundary conditions cannot be solved in static operation [(Hariri, et al., 2011)].

The optimum thickness for the two patches is determined for a constant electric field applied to a patch, while the other is kept in open circuit. This particular case does not lose the generality of the study because the optimum thickness does not change if the voltage is applied to the first patch, the second or both patches at the same time.

By varying the thickness of the patches and calculating the transverse displacement at a given point for different rigidities of the beam (Table 5. 1), we obtain the curves of Figure 5.15. The decrease (in each curve) in of Figure 5.15 shows that when the thickness of the piezoelectric patches becomes large, the bending stiffness of the system becomes more important than the bending moment generated by piezoelectric patches [(Wang, et al., 1998)]. We can also see the influence of the stiffness of the structure on transverse displacement function of piezoelectric thickness.

Materials	***Young's modulus*** N/m^2	***Density*** Kg/m^3	***Poisson's ratio***
Aluminum	6.9×10^{10}	2700	0.33
Brass	11×10^{10}	8800	0.35
Steel	19.5×10^{10}	7700	0.3
Acrylic	0.31×10^{10}	1185	0.4

Table 5.1: Materials properties used for the elastic structure

Figure 5.15 shows that there is an optimal piezoelectric patches thickness for each material used. But which materials we should use? Is it the one that gives maximum transverse displacement (acrylic in this case)?

We are interested on the maximum transverse displacement but we are also interested on the maximum frequency to be nearest from the ultrasonic range. Figure 5.16 represents the first resonant frequency depending on the thickness of piezoelectric patches for different rigidities of the beam. The first resonant frequency is simulated when one patch is open circuited (p1) and the other is short circuited (p2) with free-free boundary conditions.

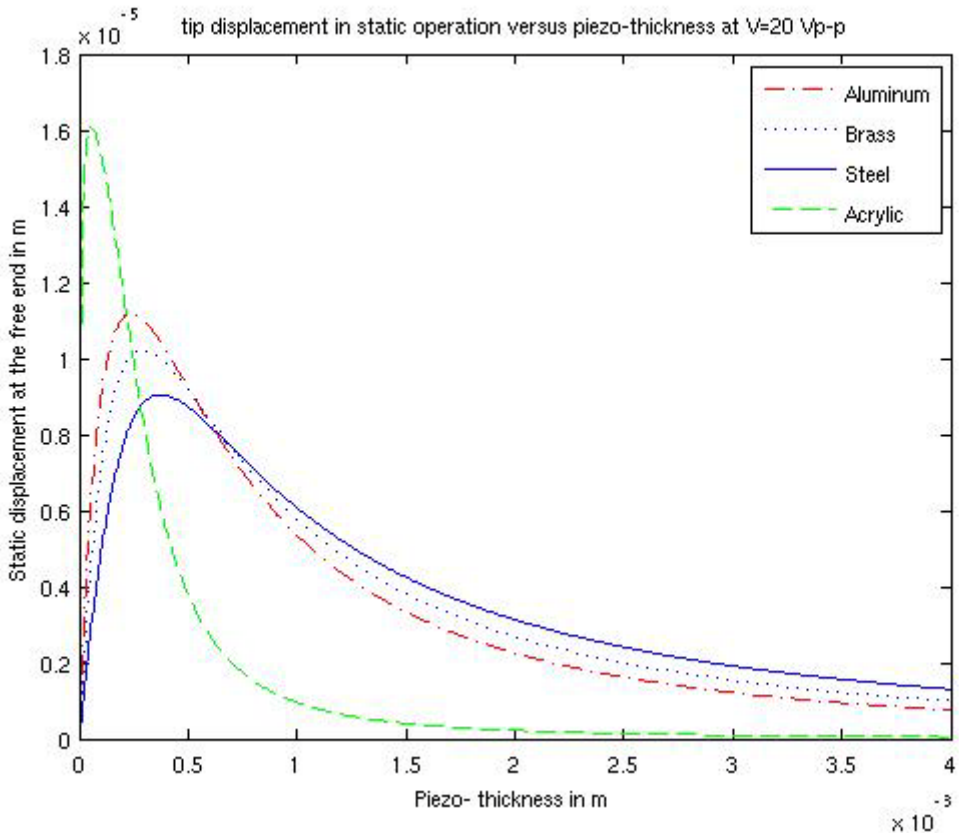

Figure 5.15: Displacements at the free end of the system depending on the thickness of piezoelectric patches

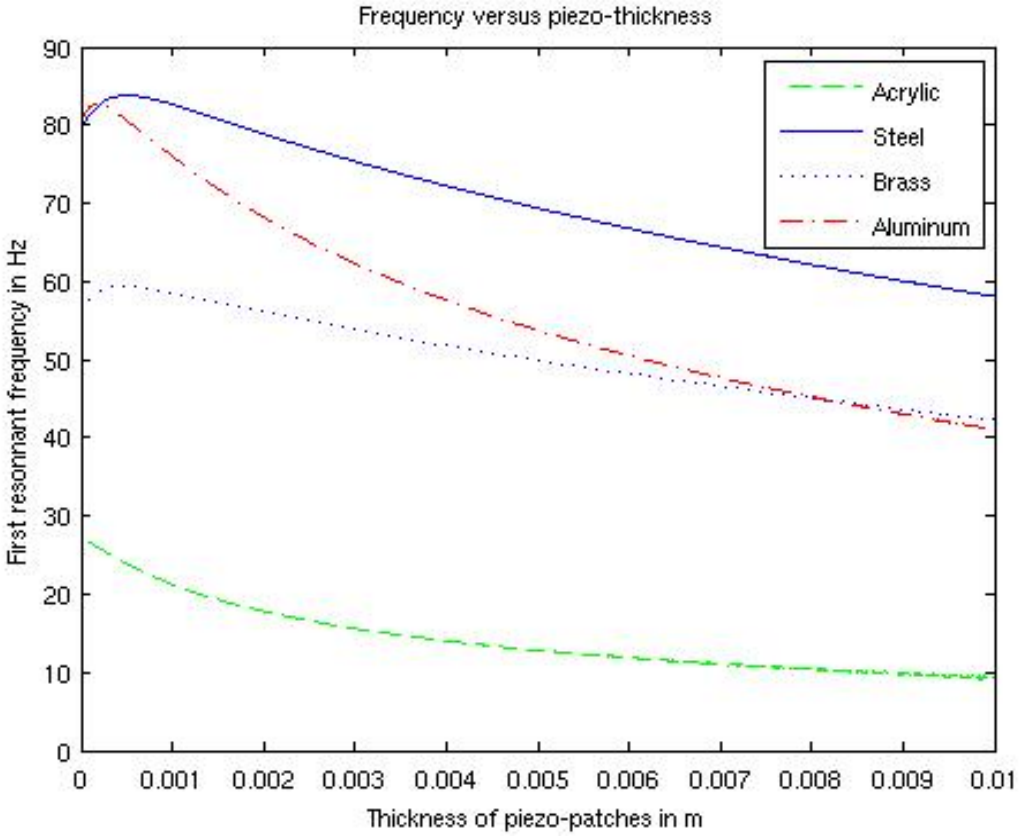

Figure 5.16: First resonant frequency depending on the thickness of piezoelectric patches

Assume for example that the 30th resonance frequency is the operation frequency of our system. In this case and basing on these above two figures, we can classify these materials used in our study in descending frequency order with respect to their optimum thicknesses by the following: Steel, aluminum, brass and acrylic. And in descending transverse displacement order relative to their optimum thicknesses by: Acrylic, aluminum, brass and steel.

As we are interested at the material that gives the best compromise between maximum transverse displacement and maximum frequency, aluminum was chosen at its optimal thickness to be the better elastic materials in our study. For this material and basing on Figure 5.15, the optimal piezoelectric patches thickness is equal to 0.27 mm compared to 0.5 mm thickness of the beam.

As the frequency depends in the boundary conditions used, we should calculate the resonance frequency of our piezoelectric robot with the free-free boundary conditions.

5.4.2 Resonance frequency

In this sub section we will study the influence of the operation mode (one or two modes excitation) and piezoelectric patches positions on the resonant frequencies of the robot.

As the frequency depends in the boundary conditions used, we should calculate the resonance frequency of our piezoelectric robot with the free-free boundary conditions (B.C). This B.C is taken during assembly of matrices.

For one mode excitation, equation 4.8 is used to calculate the resonance frequency. This equation is repeated again here below.

$$([K_{mm} - K_{mvp1}K_{vvp1}^{-1}K_{vmp1}] - (2\pi f_n)^2\,[M_{mm}])\{\mathrm{U}\} = 0 \qquad 5.10$$

For two modes excitation, equation 4.7 should be used. This equation is repeated again below.

$$([K_{mm}] - (2\pi f_n)^2[M_{mm}])\{\mathrm{U}\} = 0 \qquad 5.11$$

Figure 5.17 describes geometric parameters of our system. This geometric parameters and properties of the system (piezoelectric PZT ceramic and aluminum) are given in Table 5.2. At the moment, we are fixing the piezoelectric patches at a given position as shown in Table 5.2 and we will study the influence of modes of operation (one mode or two modes excitation) to the resonance frequencies.

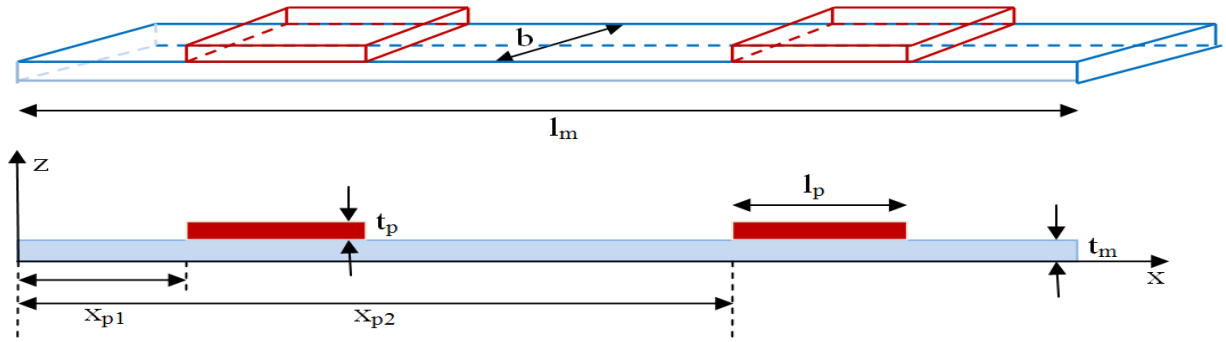

Figure 5.17: Geometric parameters of the system

	PZT (p)	Elastic structure (m)
Young's modulus (Pa)	/	$c_m = 69 \times 10^9$
Poison's ratio	/	$\upsilon_m = 0.33$
Volume density (Kg.m^{-3})	$\rho_p = 7900$	$\rho_m = 2700$
Relative permittivity	$\varepsilon_{33r} = 1282$	/
Piezoelectric constant (m.V^{-1})	$d_{31} = -1.3 \times 10^{-10}$	/
Elastic compliances (Pa^{-1})	$S_{11} = 1.3 \times 10^{-11}$	/
$S_{12} = -4.76 \times 10^{-12}$	/	
Max peak to peak electric field(V.mm^{-1})	$E_{max} = 300$	/
Max compressive strength (Pa)	$\sigma_{max} = 600 \times 10^6$	/
Length × width × thickness (mm^3)	32×17×0.27	180 × 17 × 0.5
(l_p, l_m) × (b_p, b_m) × (t_p, t_m)		
X_{p1}, X_{p2}(mm)	24,126	

Table 5.2: Geometric parameters and properties the PZT patches and aluminum beam

Table 5.3 shows simulation results for the 20 first resonant frequencies, cases of one mode and two modes excitation at fixed piezoelectric patches positions. From this table, we can consider that, practically there are no change in frequency between the one mode and the two modes excitation. So, operation modes do not affect the resonance frequencies of the system.

Mode order	One mode excitation (Hz)	Two modes excitation (Hz)
1	82.7	82.7
2	250.8	250
3	534.8	531.4
4	819.4	816.5
5	1094	1093.9
6	1567.7	1565.3
7	2184.5	2175.9
8	2741.7	2734.7
9	3425.3	3423.9
10	4295.5	4295.3
11	5023.7	5023
12	5780.4	5780.3
13	6860.9	6860.8
14	7957.9	7957.9
15	8996	8995.4

16	10358	10354
17	11811	11804
18	12985	12983
19	14294	14294
20	15903	15897

Table 5.3: 20 First resonant frequencies cases of one mode and two modes excitation at a fixed piezoelectric patches positions

Let us now study the influence of piezoelectric patches position on the resonance frequencies of the system. For this purpose, four positions are taken as we show in Table 5.4 and frequencies are calculated using equation 5. 11 (case of two modes excitation).

Piezoelectric patches positions (mm)	**PZT (p1 and p2)**
Position 1: X_{p1}, X_{p2}	24,124 (mm)
Position 2: X_{p1}, X_{p2}	14,134 (mm)
Position 3: X_{p1}, X_{p2}	5,143 (mm)
Position 4: X_{p1}, X_{p2}	48,100 (mm)

Table 5.4: Four different piezoelectric patches positions are taken to study

Piezoelectric patches positions are taken very closely to both ends of the beam (position 3), near from the middle (position 4) and also in two others positions near from both ends of the beam (position 1 & 2). By looking to Table 5.5 below, we can see that at each change in position, the resonance frequencies of the system also change.

Mode order	X_{p1}=**24**, Xp2=**124** **Position 1**	X_{p1}=**14**, Xp2=**134** **Position 2**	X_{p1}=**5**, Xp2=**143** **Position 3**	X_{p1}=**48**, Xp2=**100** **Position 4**
1	83.4	75.9	68.1	96.3
2	251.4	233.7	211.9	237.1
3	531.2	500.4	444.1	422.2
4	801.6	883.66	785.3	787.3
5	1080.4	1290.5	1238.4	1154.3
6	1579.3	1660.6	1760.2	1513.3
7	2184.6	2138	2289.4	2196.5
8	2733.6	2781.5	2847.7	2736.3
9	3448.4	3417.1	3539	3450.2
10	4293	4051.5	4397.4	4033.6
11	4952.8	4905	5337.8	5157.9
12	5753.8	5971.4	6241.2	5941.8
13	6905.4	6999.1	7121.1	6828.6
14	7958.1	7949.3	8146.8	7967.2
15	9028.9	9097.1	9389.3	9146.3
16	10471	10494	10717	10400
17	11790	11795	11947	11346
18	12827	12909	13113	13210
19	14259	14246	14468	14459
20	15895	15897	16090	15971

Table 5.5: Frequency in Hz for different piezoelectric patches positions

As conclusion resonance frequencies are calculated here in the case of free-free boundary conditions and it was found that changes in operation modes (one mode excitation or two modes excitation) do not change resonance frequencies but any change in piezoelectric patches position affect the resonance frequencies.

5.4.3 Optimal operating frequency

Optimal operating frequency is the one that gives the better traveling wave performance at fixed piezoelectric patches positions. Then changes in piezoelectric patches position affect the resonance frequencies of the system but, are that affect traveling wave performance (waveform and transverse displacement)?

In this sub-section two piezoelectric patches positions will be taken to answer this question.

Firstly, at each position taken we will study the optimal operating frequency means the better traveling wave performance (waveform and transverse displacement). Secondly, a comparison between the traveling wave performances for these two positions will lead to answer this question. The study will be done in the cases of one mode and two modes excitation. We will end up this sub-section by two optimal operating frequencies, one at each position. Then we will see the influence of piezoelectric patches position on the performance of the traveling wave and those in the case of one mode and two modes excitation. So, in the case of one mode excitation, two optimal operating frequencies at two different positions will be obtained. It is the same in the case of two modes excitation.

The first step is to study the optimal operating frequency at the first piezoelectric patches position and then to compare the performance of the traveling wave obtained at this position with the performance of the wave obtained by the optimal operating frequency for the second piezoelectric patches position. These two piezoelectric patches position are the position 1 (X_{p1}=**24** mm, Xp2=**124** mm) and position 2 (X_{p1}=**14** mm, Xp2=**134** mm) given above in Table 5.4 and they were chosen to be near from the both ends of the beam.

It is obvious that, when the waveform obtained at a given frequency is closer to the pure traveling waveform, the traveling wave ratio for this wave is higher. And when it is closer to the standing waveform, the traveling wave ratio for this wave is lower. The performance of the wave is defined in this thesis by the waveform and the transverse displacement because transverse displacement affects the speed of the robot. Better traveling wave means higher traveling wave ratio and higher transverse displacement. Figure 5.2 presented below will be used as references to compare the ratio of the traveling wave created. Figure 5.2 (a) represents a pure standing wave (at the left) and a pure traveling wave (at the right) reading in length and

time at its normalized colored magnitude. Figure 5.2 (b) is another representation for the pure standing (left) and pure traveling (right) wave and it represents normalized magnitude through the length of the beam for several times. In Figure 5.2 (c), the representation is for a quarter of a period.

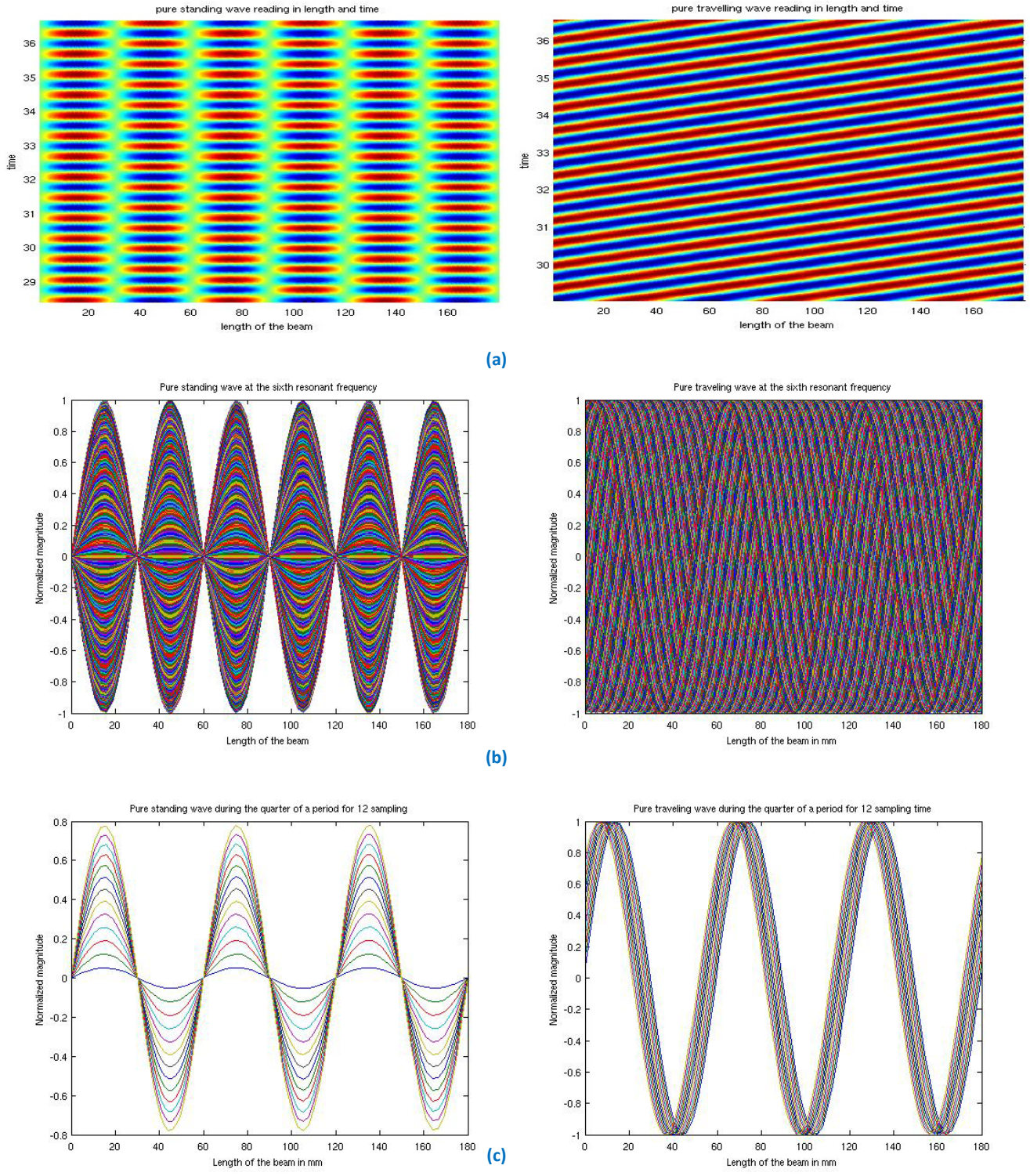

Figure 5.18: Pure standing wave (left) and pure traveling wave (right)

This figure will be used as references to compare the ratio of the traveling wave created. The optimal operating frequency is that gives the better traveling wave performance. In other words, it is the frequency that gives the closest form of a pure traveling wave with higher transverse displacement.

At fixed piezoelectric positions, the optimal operating frequency will be determined by testing the traveling wave performance at each frequency until to find the better performance by iterative simulations. Let us begin in the case of one mode excitation.

5.4.3.1 Case of one mode excitation

Operation principle of the one mode excitation is reminded here in the Figure 5. 19 below.

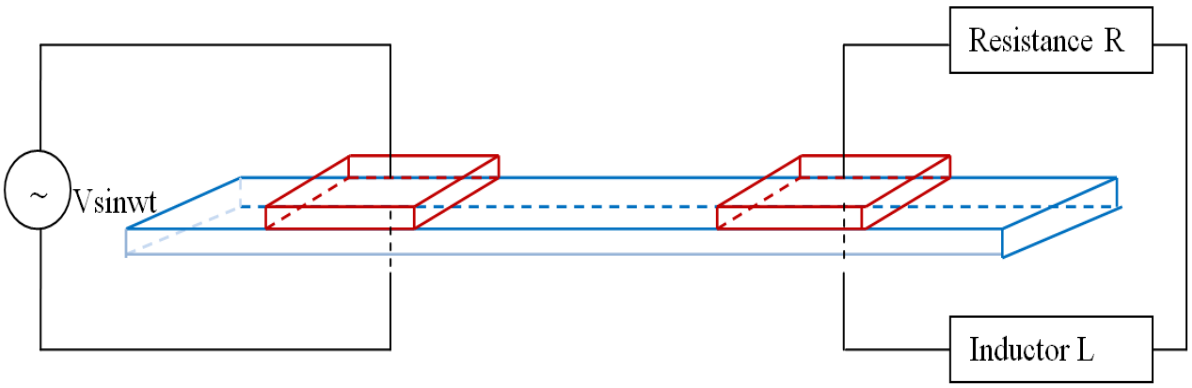

Figure 5. 19: Operation principle of the one mode excitation

In this case of one mode excitation, equations 5. 5 and 5. 7 will be used to determine the traveling wave on the beam. The first step is to determine R and L optimal values at each resonance frequency in order to have the better travelling wave performance. In order to obtain a great rate of travelling wave, in other words to avoid the maximum possible wave reflexion, R & L must be calculated to obtain the maximum ratio of power dissipated to power provided. Ratio of power dissipated P_d (power consumed by the electrical shunt circuit) over power provided P_p (power consumed by the patch actuator) is given below in equation 5.12

$$P_d = \frac{R}{2}(2\pi f_r)^2 \tilde{Q}_{p1}^2 \cos\left[\arg\left(Q_{p1}\right)\right]$$

$$P_p = \frac{1}{2} E_{3p2} t_p (2\pi f_r) \tilde{Q}_{p2} \cos\left[\arg\left(Q_{p2}\right) + \frac{\pi}{2}\right]$$

$$\rho = \frac{P_d}{P_p} = \frac{R}{E_{3p2} t_p} (2\pi f_r) \frac{\tilde{Q}_{p1}^2}{\tilde{Q}_{p2}} \frac{\cos[\arg(Q_{p1})]}{\cos\left[\arg(Q_{p2}) + \frac{\pi}{2}\right]}$$

5. 12

Where p1 is the sensor piezoelectric patch, p2 is the actuator piezoelectric patch, f_r is the resonance frequency and $\tilde{Q}_p$ is the modulus of the complex electric charge Q_p. This ratio represents the way to have the better traveling wave performance.

In RL series shunt circuit, the inductor is used to tune the shunt circuit to a resonant frequency of interest and the optimal L value is given in equation 5. 13 below. This leaves the shunt circuit with the resistive component only, which explains equation 5. 12. An impedance matching method is employed then to adjust the resistance in order to have the maximum ratio of power dissipated to power provided.

$$L_{opt} = \frac{1}{(2\pi f_r)^2 C_p}$$

5. 13

Where C_p is the electrical capacitance of the PZT sensor (p1) and it is equal to $\frac{K_{vvp1}}{t_p^2}$.

When the resistance is varied to get the maximum ratio of power dissipated over power provided after the inductor L is tuned, is the L has to be readjusted again? In other word is the frequency depends on R? It was demonstrated by Hariri et al in their paper [(Hariri, et al., 2011)] taken the particular case of a fixed-free beam with two non-collocated piezoelectric patches bonded on the beam for damping application, that the frequency depends on the value of R only in the case of small values of R compared to jwL and in this case L has to be readjusted again to tune the new resonant frequency. In all other cases, the variation of the frequency can be considered as negligible. We should note that equation 5. 13 is verified by simulation by Hariri et al in their paper [(Hariri, et al., 2011)].

At each resonance frequency an iterative simulations is done by varying R until to find its optimal value.

At position 1 (X_{p1}=**24** mm, X_{p2}=**124** mm), simulations show that the seventeenth resonant frequency (f_{17} = 11790 Hz according to Table 5.5) is the optimal operating frequency that gives the better traveling wave performance at this position (position 1). At position 2 (X_{p1}=**14** mm, X_{p2}=**134** mm**),** simulations show that the sixteenth resonant frequency (f_{16} = 10494 Hz according to Table 5.5) is the optimal operating one. By comparing these two positions at their optimal operating frequency, we noted that the traveling wave performance (waveform and transverse displacement) in position 1 is better than what we obtained in

position 2. Transverse displacement as the contact friction points between beam and the support affects the speed of the robot. These results will be verified experimentally in the next chapter.

Let us begin by demonstrating how we determined the optimal operating frequency at each position, and then by comparing these two optimal operating frequencies. Simulations are done by applying 40 V_{pp} sinusoidal waves at the actuator patch (p2).

5.4.3.1.1 Position 1

For position 1 at the 17th frequency, R & L optimal were determined, and then the traveling wave performance was simulated using equation 5. 5 (transient response simulation). Results show traveling wave performance are given in Figure 5.20 below. By comparing the figure to the pure traveling wave and pure standing wave, we get the traveling wave performance at the 17th frequency. Figure 5.20 on the top shows a mixture wave between traveling wave and a standing wave and it projected on a plane of length (x) in mm and time (t) in ms of a flexural beam at its transverse displacement. The figure on the bottom shows the same wave but in another representation. It represents transverse displacement in μm through the length of the beam in mm at each instant.

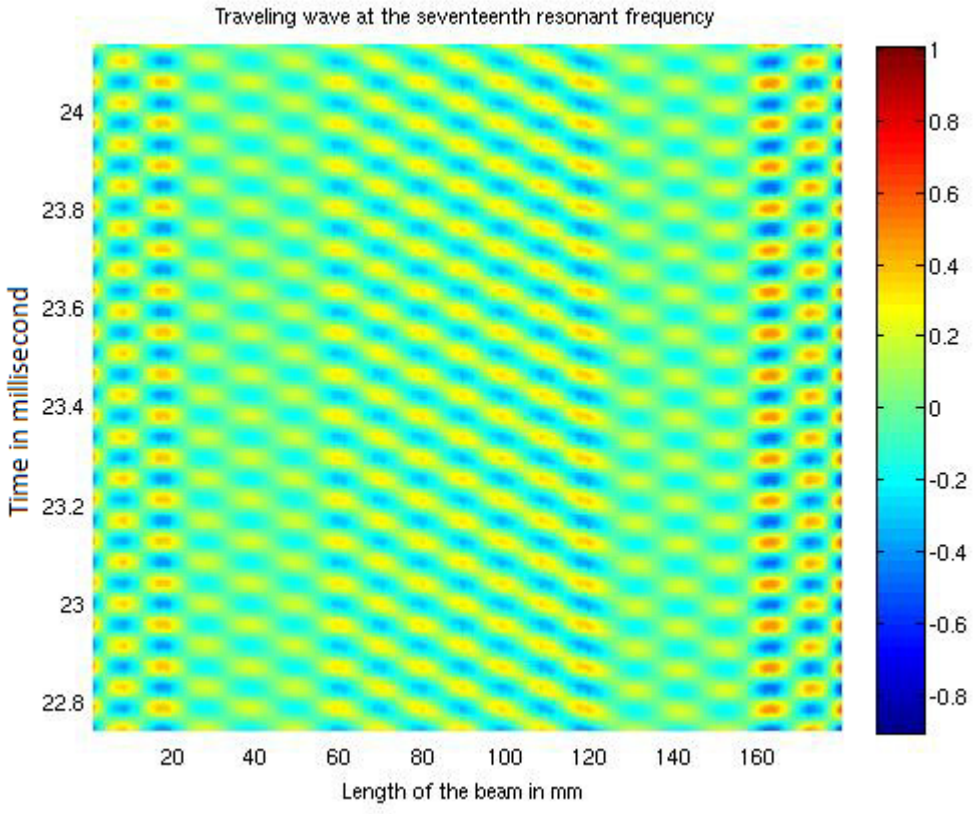

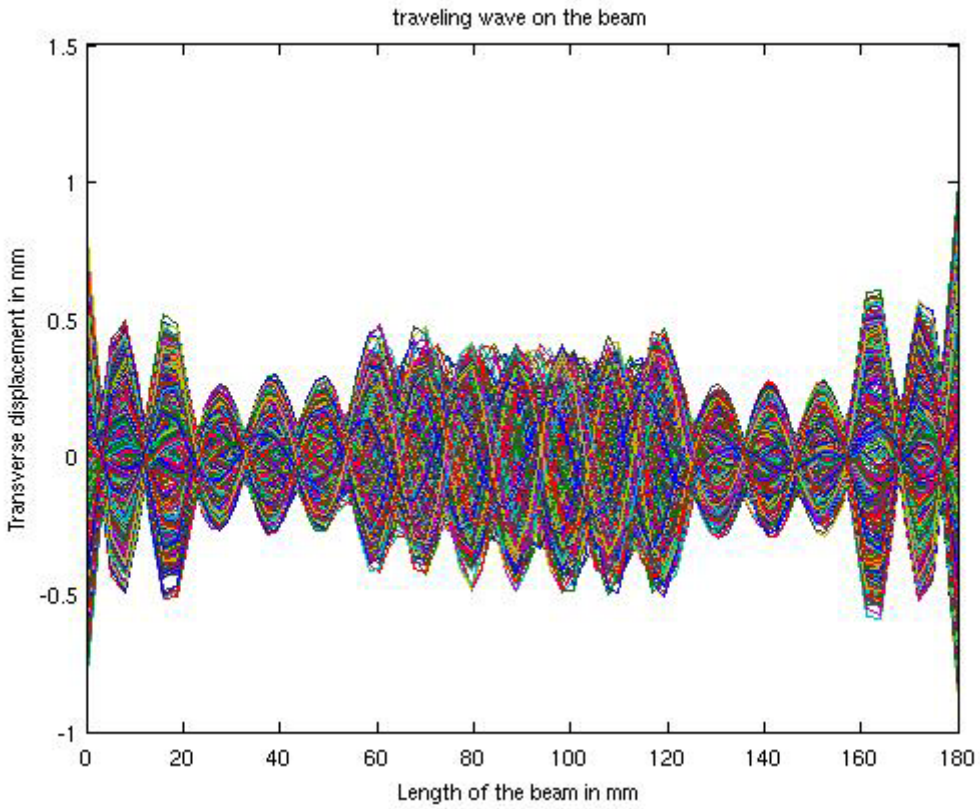

Figure 5.20: Traveling wave performance at the seventeenth resonant frequency

From Figure 5.20 as in the case of punctual forces (Langevin piezoelectric transducers), at the location of the contact surface between the beam and the patches (position 1), the vibration is less progressive than the place near the middle of the beam. Length of piezoelectric patches affects the transverse displacement and then affects the traveling wave performance. As we are far from piezoelectric patches positions (position 1) near from the middle of the beam, the traveling wave performance will be better. More we are near from piezoelectric patches positions (near from both ends of the beam), traveling wave performance will be worse.

The 6^{th}, 12^{th} and the 19^{th} resonant frequencies are taken here to compare them with the 17^{th} resonant frequency. That allows justifying the choice of the 17^{th} resonant frequency as the optimal one. Table 5.6 below shows R and L optimal values at each considered resonant mode. L was obtained by using equation 5. 13 and optimal R values was simulated using equation 5. 7 (frequency response simulation). Optimal R values obtained by simulation at 6^{th}, 12^{th}, 17^{th} and 19^{th} resonant frequencies are shown in Figure 5.21.

This figure shows the ratio of power dissipated (power consumed by the electrical shunt circuit) over power provided (power consumed by the patch actuator) versus resistance values at each considered resonant frequency. The values obtained depend on the resonant mode and piezoelectric patches positions. Comparing these ratios doesn't give any conclusion about

traveling wave performance at each frequency. To have the performance of the traveling waves at each frequency, a transient response simulation should be done.

FREQUENCY	R OPTIMAL	L OPTIMAL
f_6 = 1579.3 Hz	R_6 = 334 Ω	L_6 = 0.5022H
f_{12} = 5753.8 Hz	R_{12} = 8.75 Ω	L_{14}= 0.0198H
f_{17} = 11790 Hz	R_{17} = 9.75 Ω	L_{17} = 0.009H
f_{19} = 14259 Hz	R_{19}= 5.5 Ω	L_{19} = 0.0062H

Table 5.6: R & L optimal Value for series RL connection

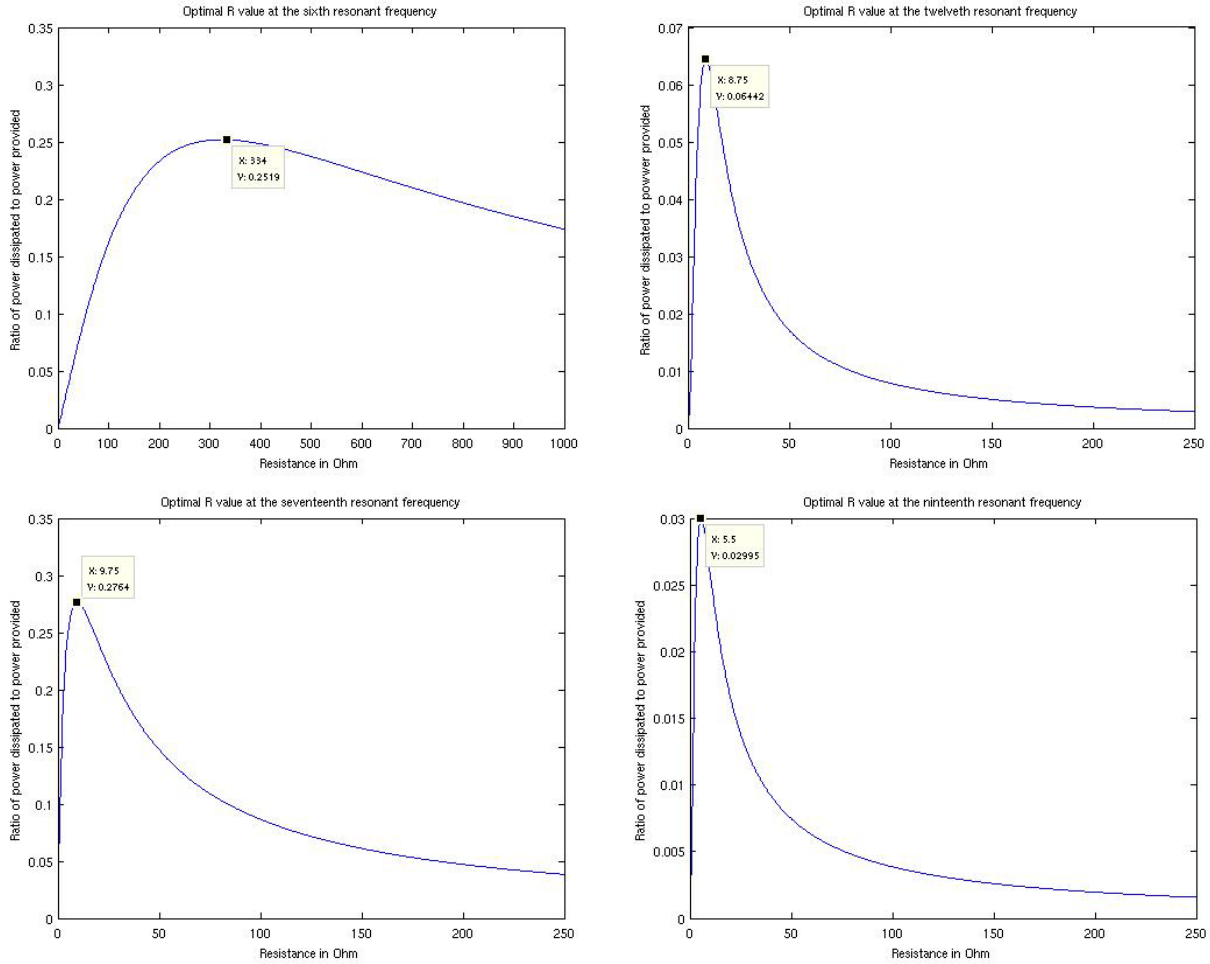

Figure 5.21: Optimal R values at 6th, 12th, 17th and 19th resonant frequencies

Figure 5.22 shows traveling wave performances for the 6th, 12th and 19th resonant frequencies. At small resonant frequencies, the waveform is closer to a standing wave than to a traveling wave, as the case of the 6th resonant frequency. That is explained by the fact that the RL shunt circuit is not very efficient to absorb the wave provided by the actuator patch (p2) due to the large displacements at small resonant frequencies. In general, transverse displacement decreases with frequency but that is not completely true because transverse displacement depends also on piezoelectric patches positions. Transverse displacement of the beam is

greater if the numbers of anti-nodes are more than the numbers of nodes at the contact surface between piezoelectric patches and the beam. We can see from Figure 5.22 that transverse displacement at the 17th resonant frequency is greater than at the 19th resonant one. From Figure 5.22 we can note that the 17th resonant frequency is the one that gives the better traveling wave performance and therefore it is the optimal one. Figure 5.23 is another representation of the traveling wave performance and it represents transverse displacement through the length of the beam at each instant at the 6th, 12th and 19th resonant frequencies. Same as we have seen in Figure 5.22, the waveform is closer to a standing wave at the 6th resonant frequency, traveling wave performance near from the middle of the beam is better than we have near from both ends of the beam and at piezoelectric patches positions. Transverse displacement at the 17th resonant frequency is greater than at the 19th resonant one. From Figure 5.23, the standing wave ratio (SWR) can be estimated.

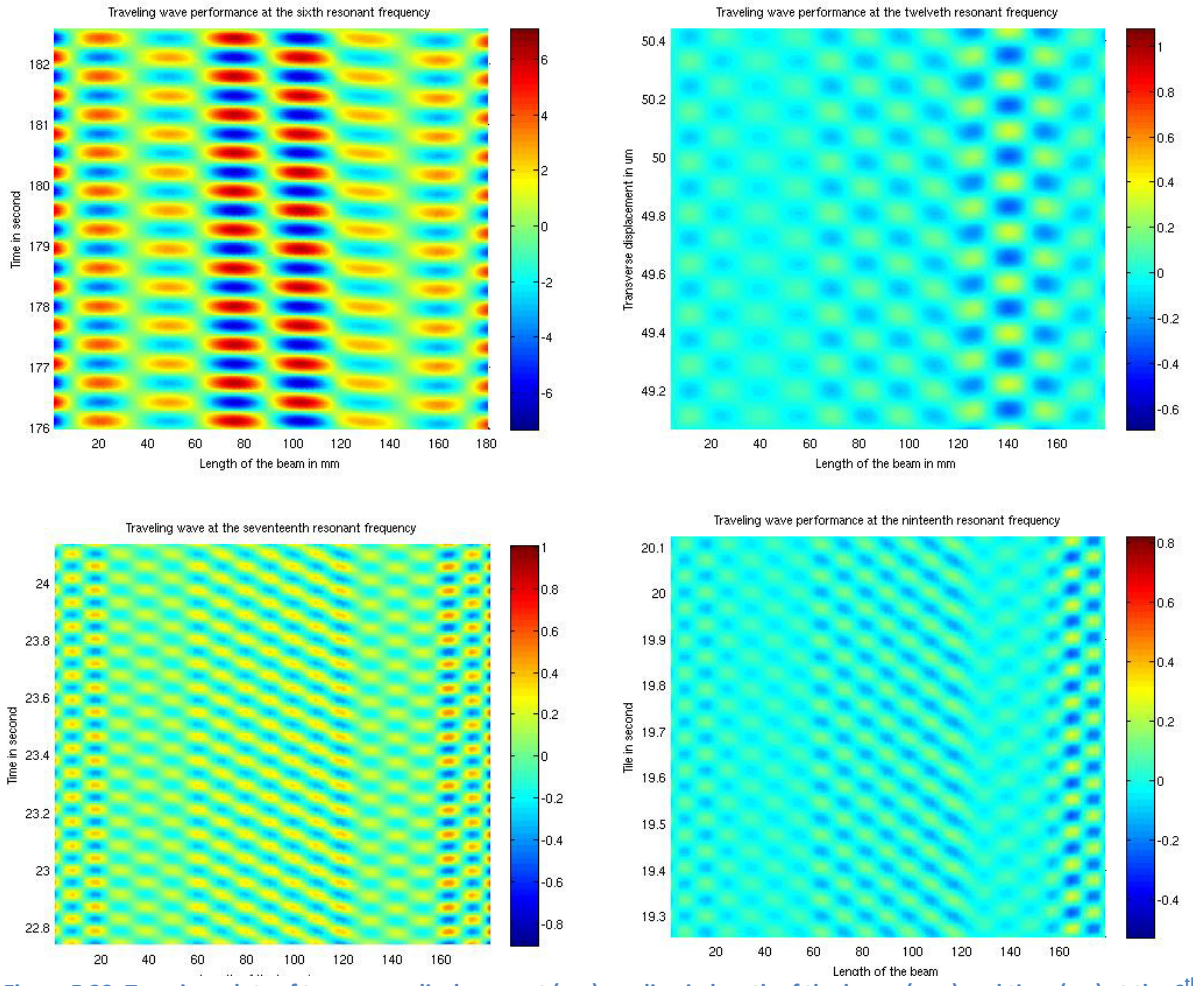

Figure 5.22: Top view plots of transverse displacement (um) reading in length of the beam (mm) and time (ms) at the 6th, 12th, 17th and 19th resonant frequencies

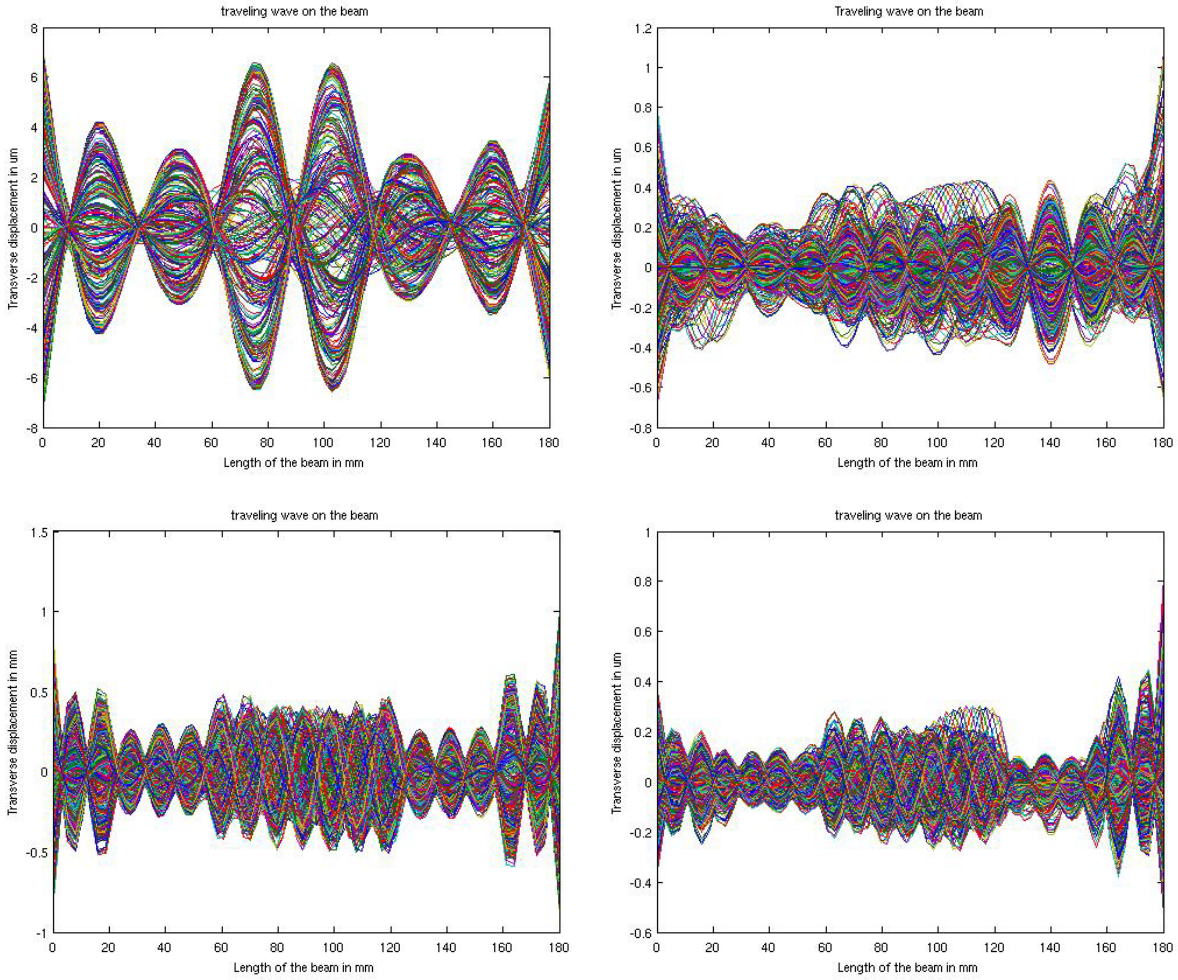

Figure 5.23: Transverse displacement (um) through the length of the beam (mm) at each instant at the 6th, 12th, 17th and 19th resonant frequencies

Frequency	f_6	f_{12}	f_{17}	f_{19}
SWR	6.577	3.6445	1.55	2.379

Table 5.7: Standing wave ratio at the 6th, 12th, 17th and 19th resonant frequencies

It is an indicator of the amount of wave reflection in a transmission line. It is defined as the ratio of the maximum and minimum amplitudes of the transverse displacement induced on the beam. The closer to one the less reflection exists, so the better traveling wave ratio.

$$\text{SWR}= \left\| \frac{A_{max}}{A_{min}} \right\| \quad (5.14)$$

Figures show that transverse displacement at 17th resonant frequency is higher than the one at 12th and 19th resonant frequencies. Transverse displacement as the contact friction points affects the speed of the robot. These results will be verified experimentally in the next

chapter. At position 1 and after testing all resonant frequencies, the 17th resonant one shows the better traveling wave performance comparing to others.

5.4.3.1.2 Position 2

For position 2, the 16th resonant frequency was the optimal one that gives the better traveling wave performance. Same procedure will be repeated in the following as at position 1. First, traveling wave performance at the optimal operating frequency is given separately. Then comparison between traveling wave performances are given for the 6th, 10th, 14th, 16th and 18th resonant frequencies. Same explanation as for position 1, Figure 5.24 represents traveling wave performance at the optimal operating frequency at this given position.

Table 5.8 shows R & L optimal values at the 6th, 10th, 14th, 16th and 18th resonant frequencies. The same like for position 1, the optimal L value was determined using equation 5. 13 and Figure 5.25 shows optimal R values obtained by simulation. Figure 5.26 represents travelling wave performances at each considered frequency reading in length (mm) and time (ms) at the vibration amplitude of the beam (transverse displacement in µm). Figure 5.27 shows travelling wave performance and it represents transverse displacement (µm) through the length of the beam (mm) at each instant. This figure helps to calculate the SWR. Table 5.9 shows standing wave ratio at each considered frequency.

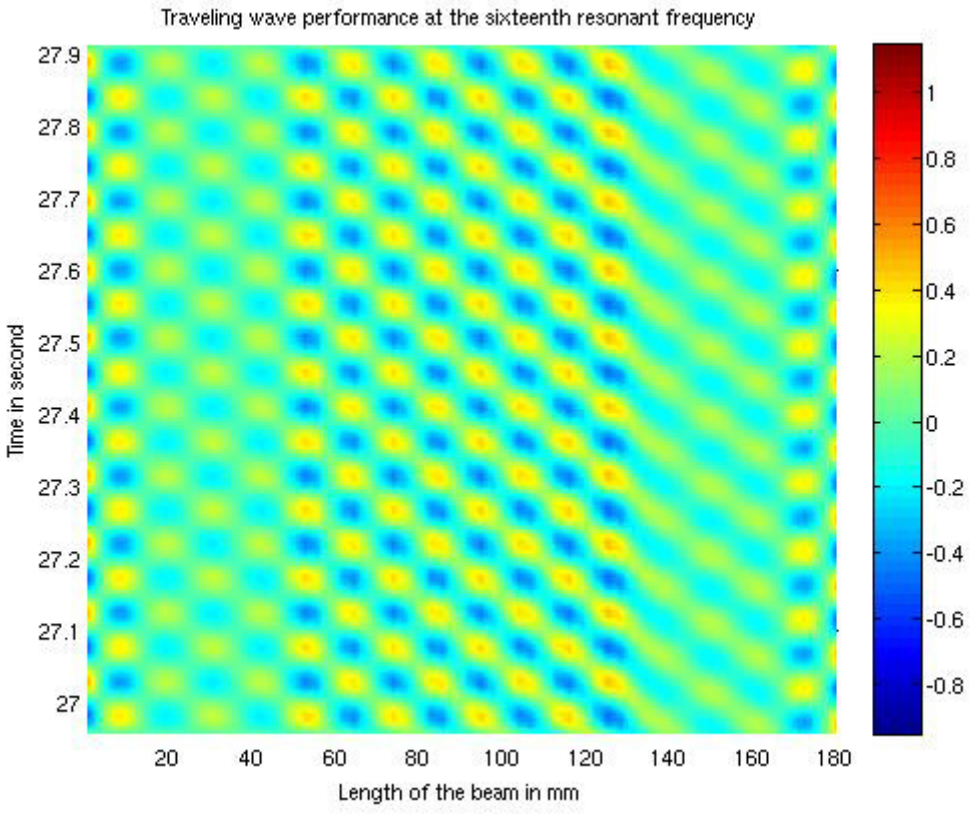

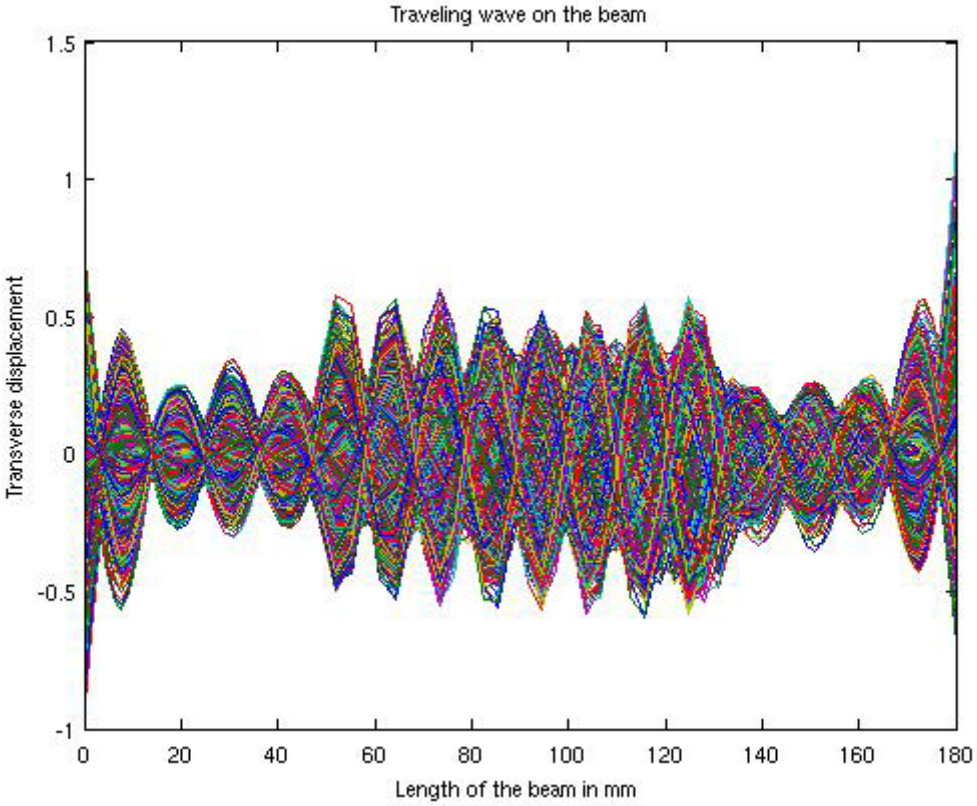

Figure 5.24: Traveling wave performance at the sixteenth resonant frequency

FREQUENCY	R OPTIMAL	L OPTIMAL
f_6 = 1660.6 Hz	R_6 = 194 Ω	L_6 = 0.4543H
f_{10} = 4051.5 Hz	R_{10} = 23.5Ω	L_{10} = 0.0763H
f_{14} = 7949.3 Hz	R_{14} = 9.25 Ω	L_{14}= 0.0198H
f_{16} = 10494 Hz	R_{16} = 23.75 Ω	L_{16} = 0.0114H
f_{18} = 12909 Hz	R_{18}= 7 Ω	L_{18} = 0.0075H

Table 5.8: R & L optimal values for series RL connection

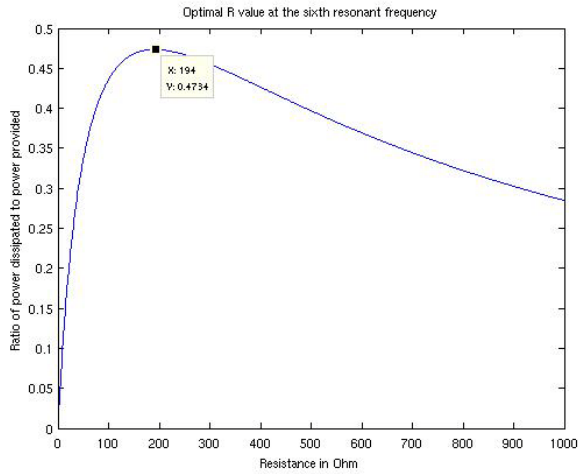

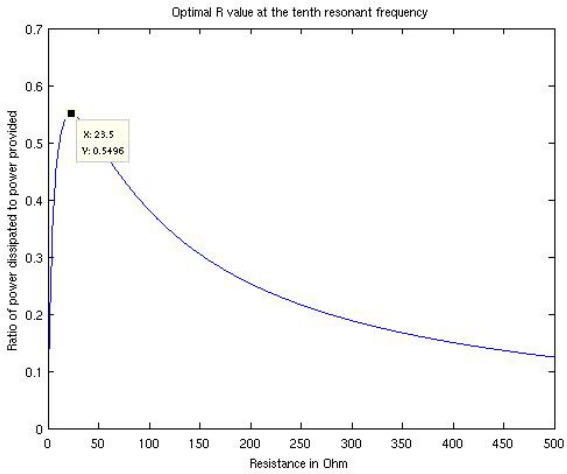

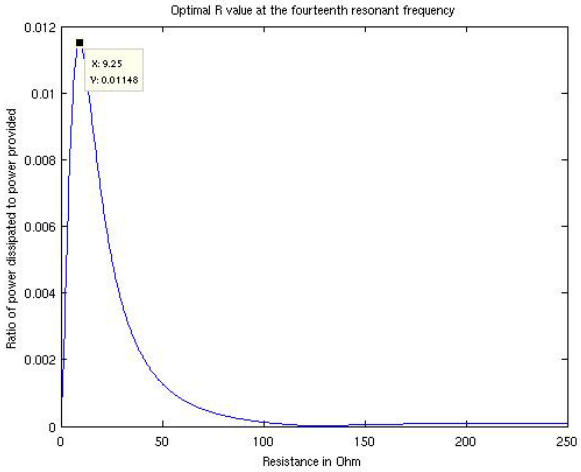

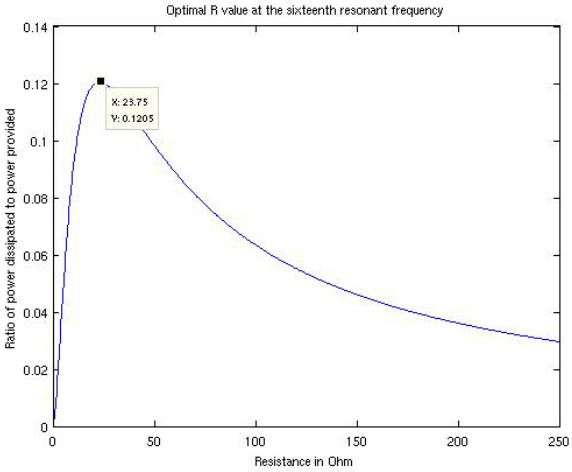

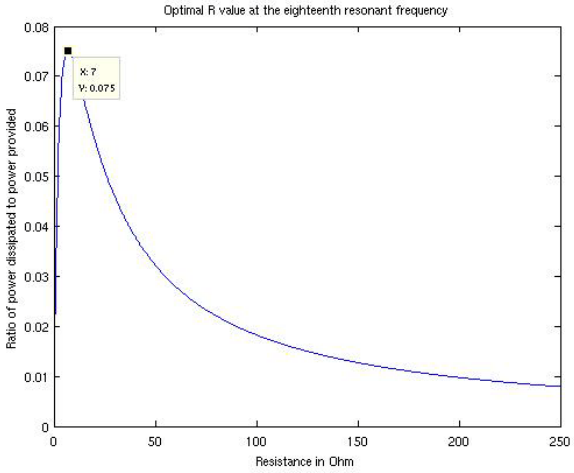

Figure 5.25: Optimal R values at 6th, 10th, 14th, 16th and 18th resonant frequencies

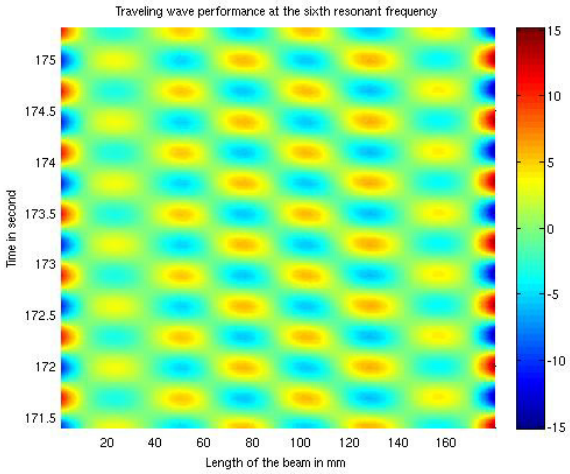

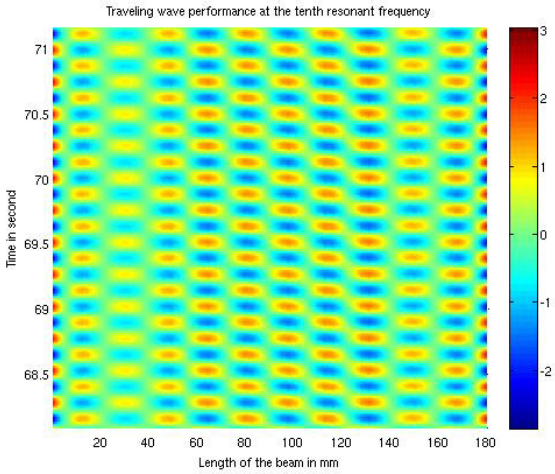

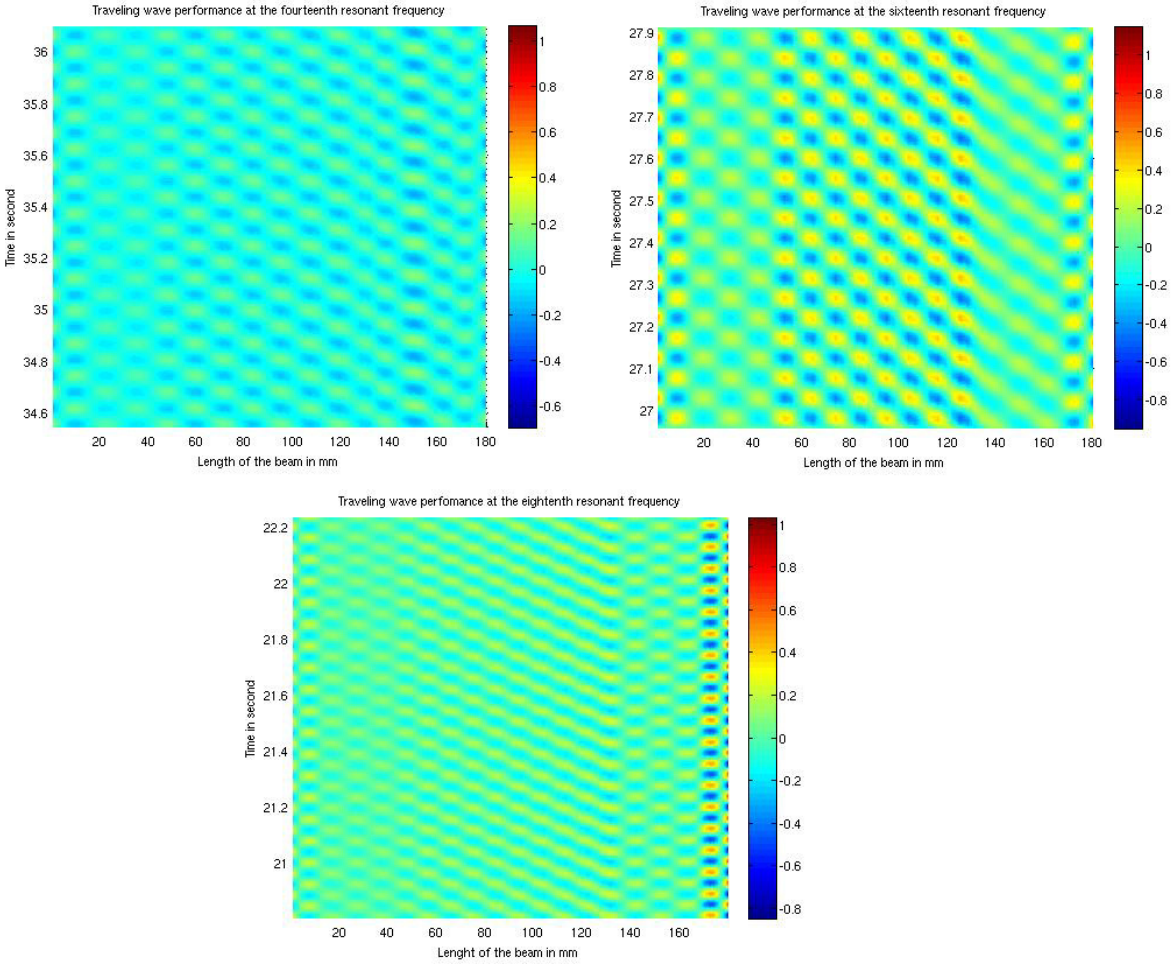

Figure 5.26: Top view plots of transverse displacement (um) reading in length of the beam (mm) and time (ms) at the 6th, 10th, 14th, 16th and 18th resonant frequencies

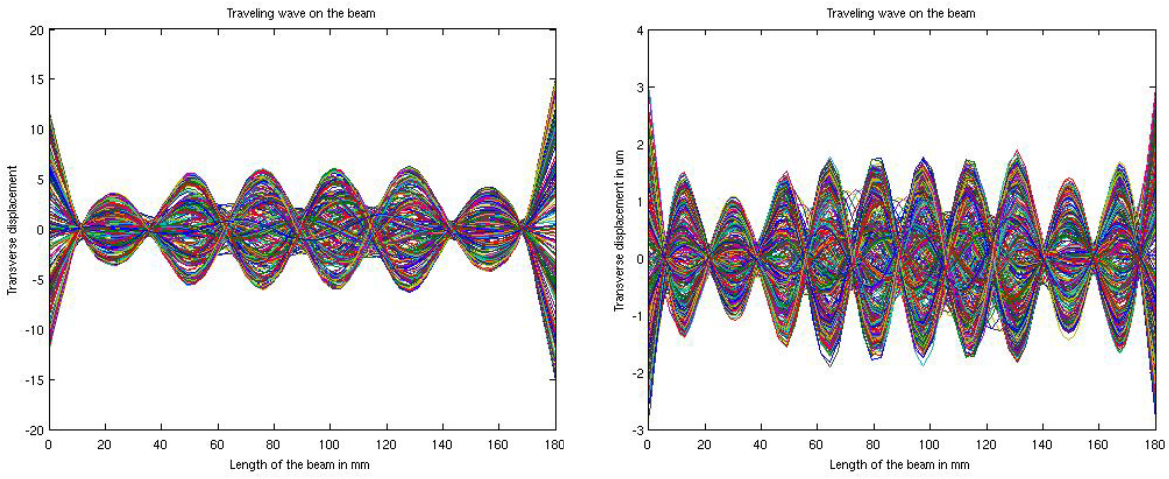

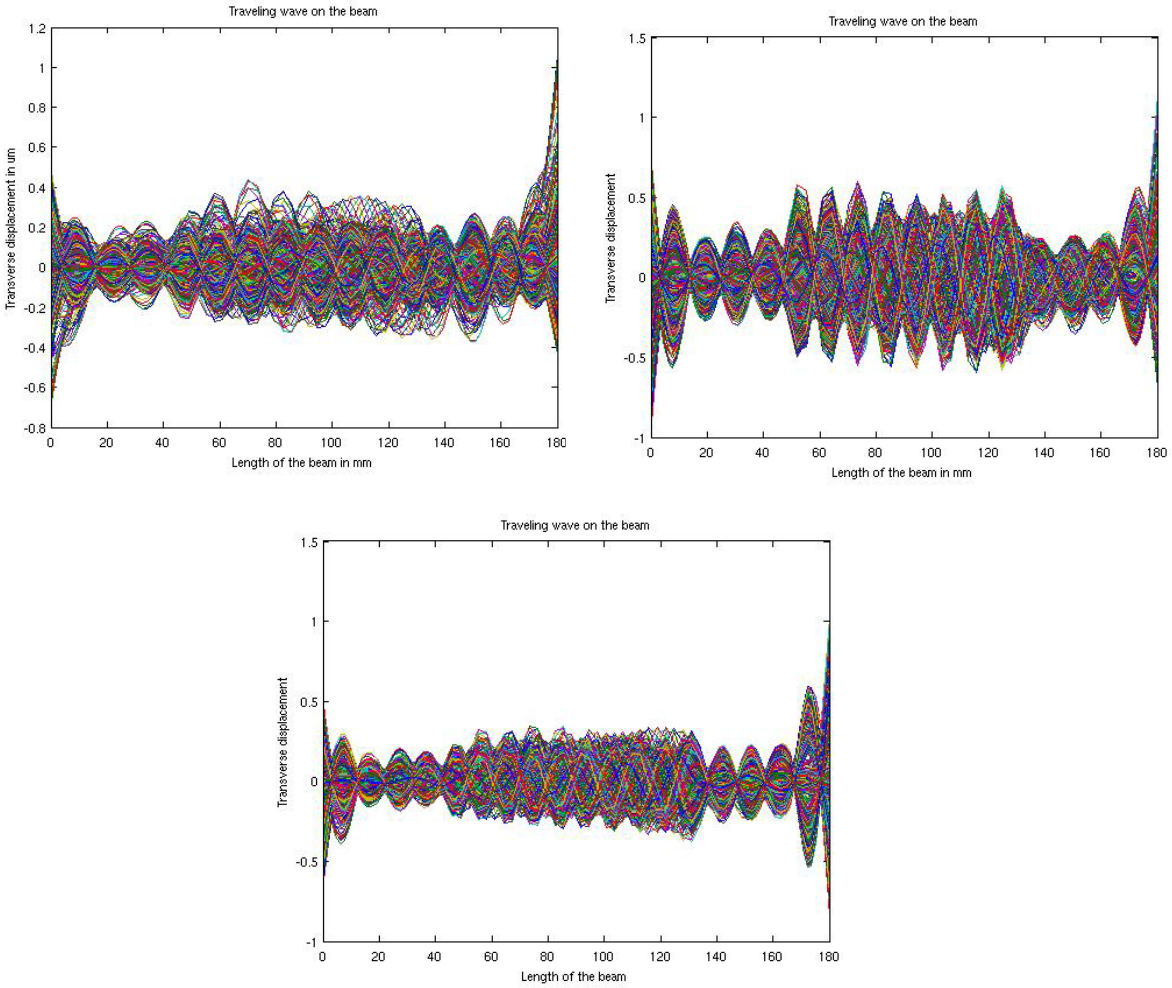

Figure 5.27: Transverse displacement (um) through the length of the beam (mm) at each instant at the 6th, 10th, 14th, 16th and 18th resonant frequencies

Frequency	f_6	f_{10}	f_{14}	f_{16}	f_{18}
SWR	6.056	3.991	2.594	1.843	2.7

Table 5.9: Standing wave ratio at the 6th, 10th, 14th, 16th and 18th resonant frequencies

Figures show that transverse displacement at 16th resonant frequency is higher than the one at 14th and 18th resonant frequencies. Transverse displacement as the contact friction points affects the speed of the robot. These results will be verified experimentally in the next chapter. At position 2 and after testing all resonant frequencies, the 16th resonant one shows the better traveling wave performance comparing to others.

5.4.3.1.3 Influence of positions on the performance of the traveling wave

Here is done a comparison between traveling wave performances at the optimal operating frequency for each position. The performance of the 17th resonant frequency at position 1 is

compared with the 16th resonant frequency at position 2. If we watch only the SWR (SWR_{16} = 1.843 & SWR_{17} = 1.55), it is closer to one at the 17th resonant frequency. Therefore traveling wave ratio is better at this frequency. We can see clearly from Figure 5.28 below the variation of amplitudes near from the middle of the beam for the 16th resonant frequency at position 2 while the amplitudes for the 17th resonant frequency at position 1 remain constant. It can be argued that the waveform is more progressive at the 17th resonant frequency.

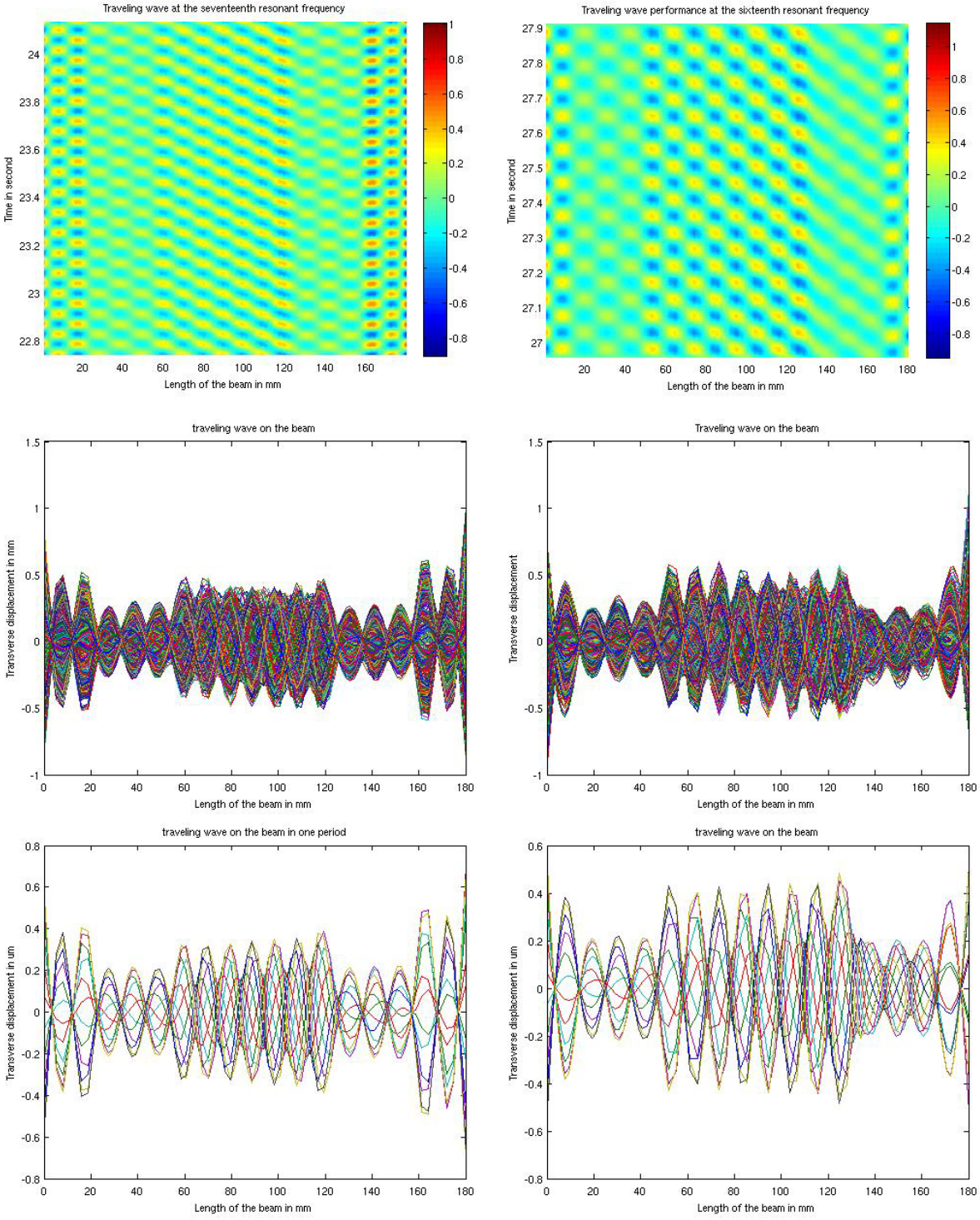

Figure 5.28: Traveling wave performance for the 17th resonant frequency at position 1 (left) and for the 16th resonant frequency at position 2 (right)

5.4.3.1.4 Actuator-absorber & Absorber-actuator

By switching the role of both piezoelectric patches, the motion direction will change. Let us verify that by taking equation 5. 5 and replacing the role of patches. Below the equation 5. 5 in the case where the patch p1 is the actuator patch and the patch p2 is the sensor patch.

$$\begin{bmatrix} M & 0 & 0 \\ 0 & 0 & 0 \\ 0 & 0 & 0 \end{bmatrix} \begin{bmatrix} \ddot{U}_i \\ t_p\ddot{Q}_{p1} \\ t_p\ddot{Q}_{p2} \end{bmatrix} + \begin{bmatrix} C & 0 & 0 \\ 0 & 0 & 0 \\ 0 & 0 & -\frac{z_e}{t_p^2} \end{bmatrix} \begin{bmatrix} \dot{U}_i \\ t_p\dot{Q}_{p1} \\ t_p\dot{Q}_{p2} \end{bmatrix} +$$

$$\begin{bmatrix} K_{mm} - K_{mvp1}K_{vvp1}^{-1}K_{vmp1} - K_{mvp2}K_{vvp2}^{-1}K_{vmp2} & K_{mvp1}K_{vvp1}^{-1} & K_{mvp2}K_{vvp2}^{-1} \\ -K_{vvp1}^{-1}K_{vmp1} & K_{vvp1}^{-1} & 0 \\ -K_{vvp2}^{-1}K_{vmp2} & 0 & K_{vvp2}^{-1} \end{bmatrix} \begin{bmatrix} U_i \\ t_pQ_{p1} \\ t_pQ_{p2} \end{bmatrix} =$$

$$\begin{bmatrix} 0 \\ E_{3p1}(t) = \frac{V}{t_p}\sin(wt) \\ 0 \end{bmatrix}$$

5. 15

Using equation 5. 5 and 5. 15, the direction of motion is represented in the black arrow below in the Figure 5.29.

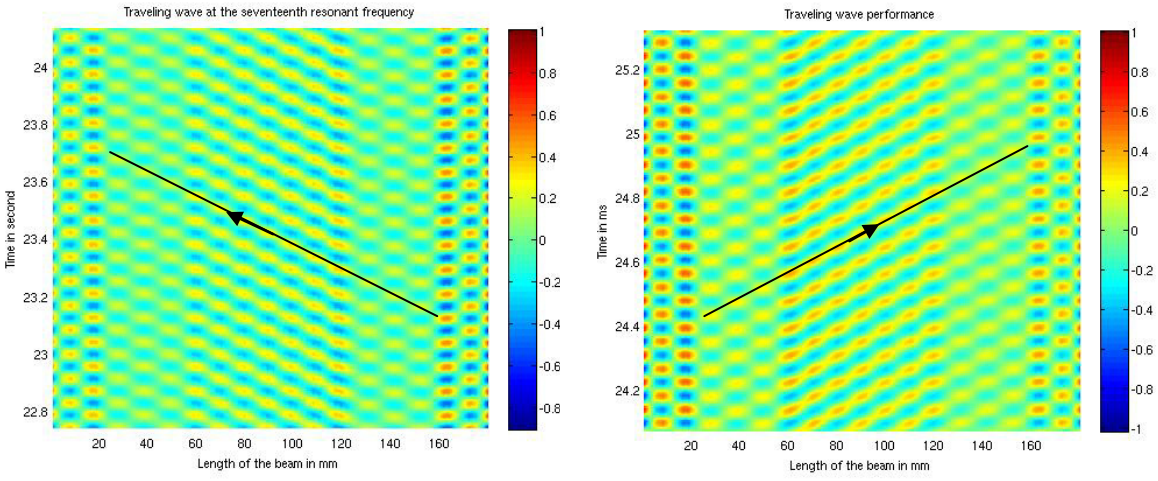

Figure 5.29: Actuator (p2)-absorber (p1) in the left and absorber (p2)-actuator (p1) in the right

Figure 5.30 represents the traveling wave performance when the patch p1 is taken as an actuator while the patch p2 is open circuited. Figure shows a standing wave on the beam which is completely logic when there is no absorption of the reflected wave.

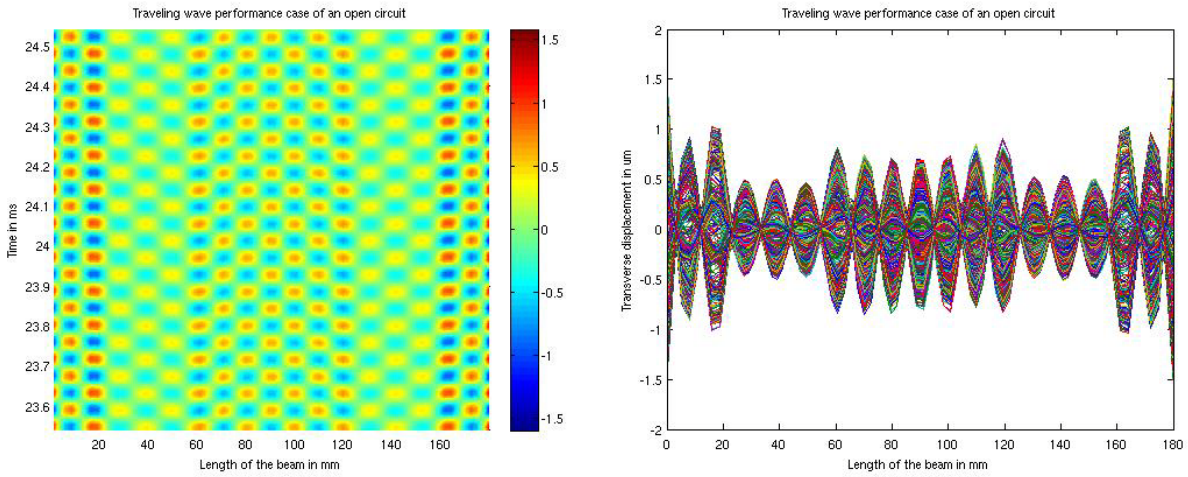

Figure 5.30: Wave performance case of an open circuit

5.4.3.2 Case of two modes excitation

Operation principle of the two modes excitation is reminded here in the Figure 5.31 below.

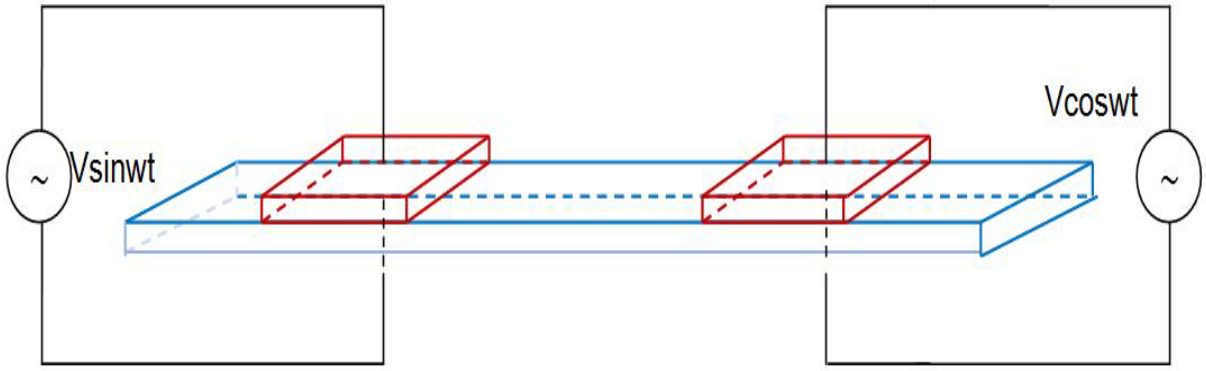

Figure 5.31: Schematic figure of the two modes excitation

The principle of two modes excitation is based on the excitation of the two patches, at a frequency between two resonance frequencies. Iterative simulations are done at each frequency between two successive resonance frequencies for the two piezoelectric patches positions. This frequency is taken as the middle of the two successive resonance frequencies.

Simulations show that the middle of the sixteenth and seventeenth resonance frequencies (f_{16*17} = 11.1 kHz) is the optimal operating frequency at position 1 (X_{p1}=**24** mm, X_{p2}=**124** mm) and position 2 (X_{p1}=**14** mm, X_{p2}=**134** mm**)**. Then by comparing the performances of the

travelling waves (waveform and transverse displacement) obtained, we noted that the performance in position 1 is better than what we obtained in position 2. Transverse displacement as the contact friction points affects the speed of the robot. These results will be verified experimentally later in the next chapter. Simulation here is easier because there is no resistance and inductance calculated, it is enough to calculate the mid frequency between two resonance frequencies successive and apply equation 5.8. Simulations are done by applying 40 V_{pp} sinusoidal waves at each piezoelectric patch.

5.4.3.2.1 Position 1

At position 1, the mid frequency between the 16th and 17th resonance frequencies (f_{16*17}) is the one that gives the better traveling wave performance. Results show traveling wave performance is given in Figure 5.32 below. By comparing the figure to the pure traveling wave and pure standing wave, we get the traveling wave performance at f_{16*17}. As always, at the location of the contact surface between the beam and the patches, the vibration is less progressive than the place near the middle of the beam. Also, length of piezoelectric patches affects the transverse displacement and then affects the traveling wave performance.

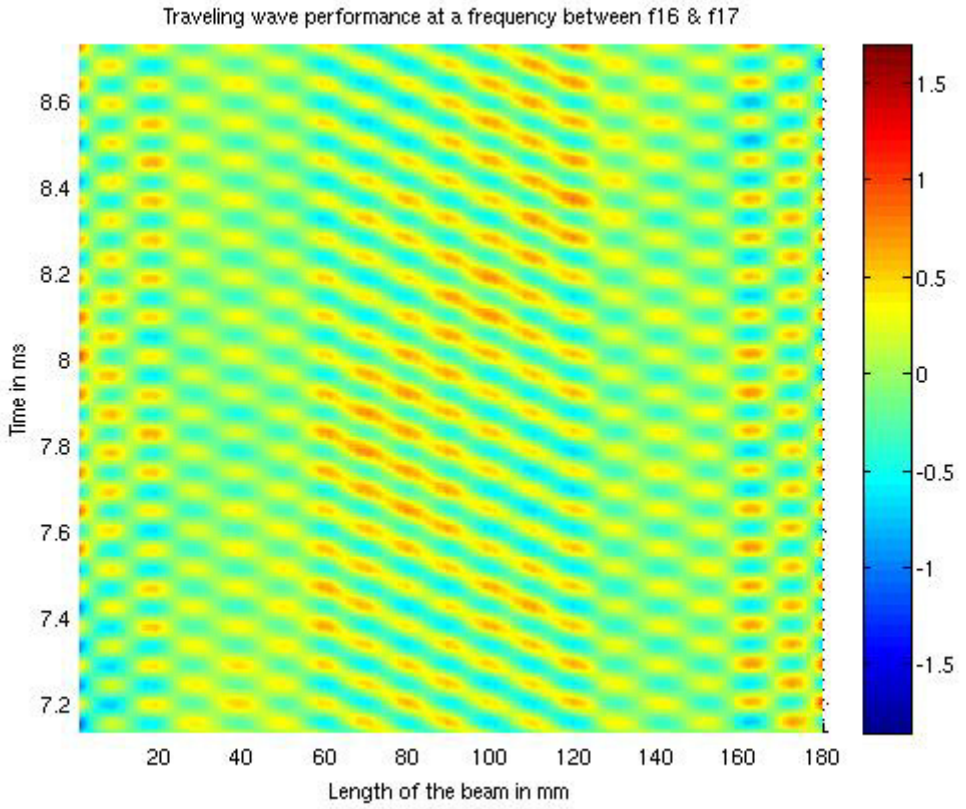

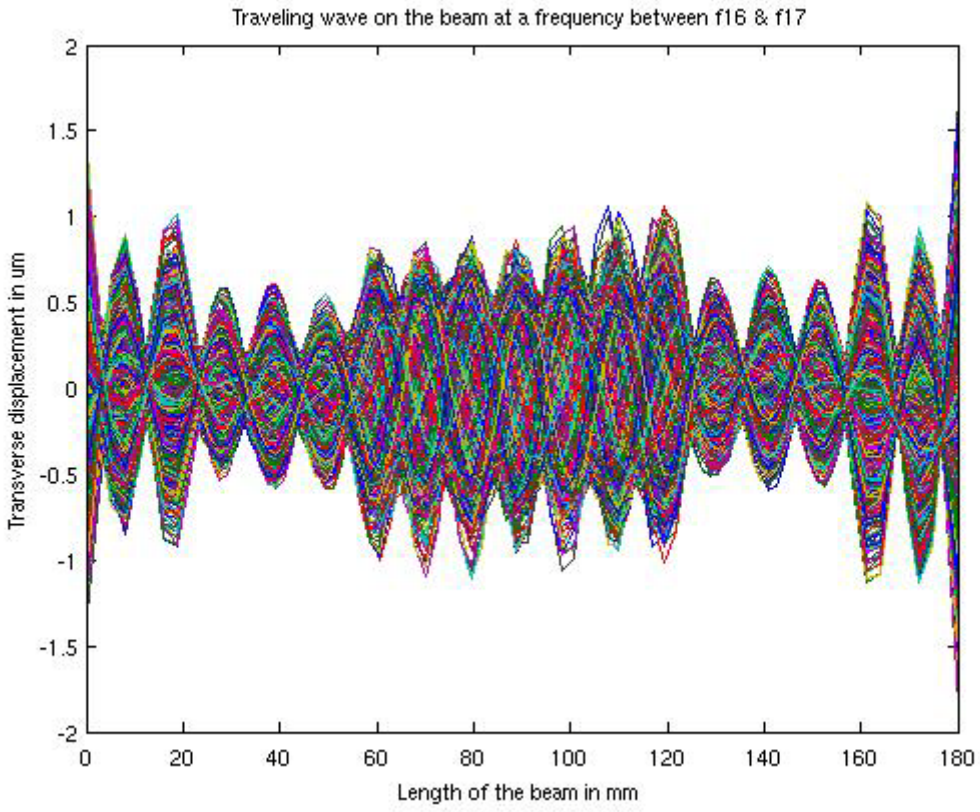

Figure 5.32: Traveling wave performance at a frequency between f_{16} & f_{17}

Here in the following three others frequencies are taken to compare them with f_{16*17}, they are given in Table 5.10.

n	f_n (Hz)	f_{n+1}(Hz)	$f_{n*(n+1)} = f_{excitation}$(Hz)
6	1579.3	2184.6	1882
14	7958.1	9028.9	8493,5
16	10471	11790	11130,5
17	11790	12827	12308,5

Table 5.10: Excitations frequencies

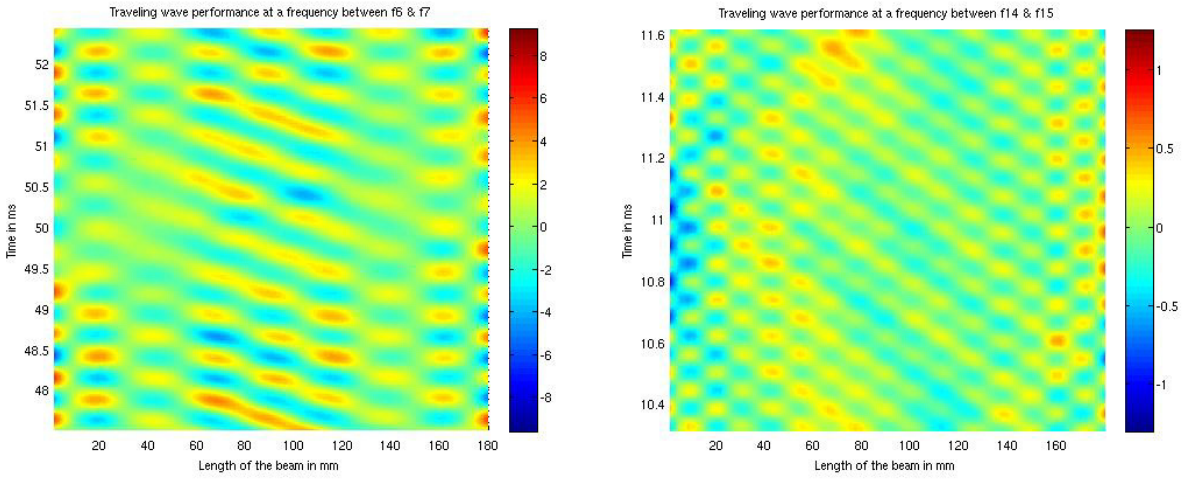

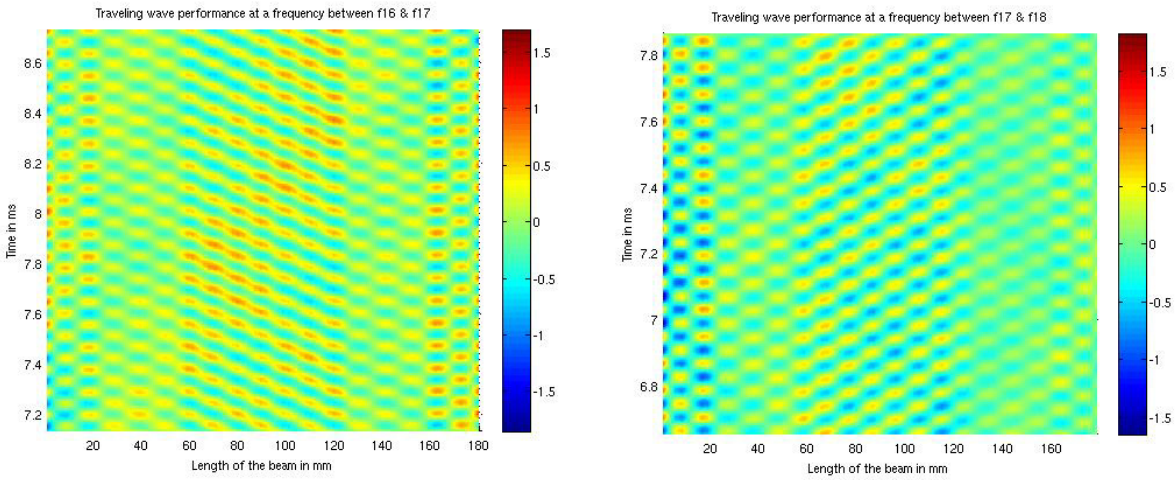

Figure 5.33: Traveling wave performances at different frequencies

Figure 5.33 shows traveling wave performances at these frequencies. It is clear from the figure that f_{16*17} has a good transverse displacement and the better traveling wave performance comparing to others. This figure shows also non homogeneity of the wave compared to the one mode excitation due to the excitation of two mode shapes at the same time. After testing all frequencies, f_{16*17} shows the better traveling wave performance at position 1.

5.4.3.2.2 Position 2

At position 2, also f_{16*17} shows the better traveling wave performance and it is represented in Figure 5.34 below. Let us take three others frequencies and compare them with f_{16*17}. Frequencies are given in Table 5.11. Frequencies are chosen arbitrarily, just to show how we obtain the optimum one. It is clear from Figure 5.35 that f_{16*17} gives the better traveling wave performance compared to other. Same as at position 1, the non homogeneity of waves is clear in this figures comparing to the one mode excitation. At position 2 and after testing all frequencies, f_{16*17} was the optimal one.

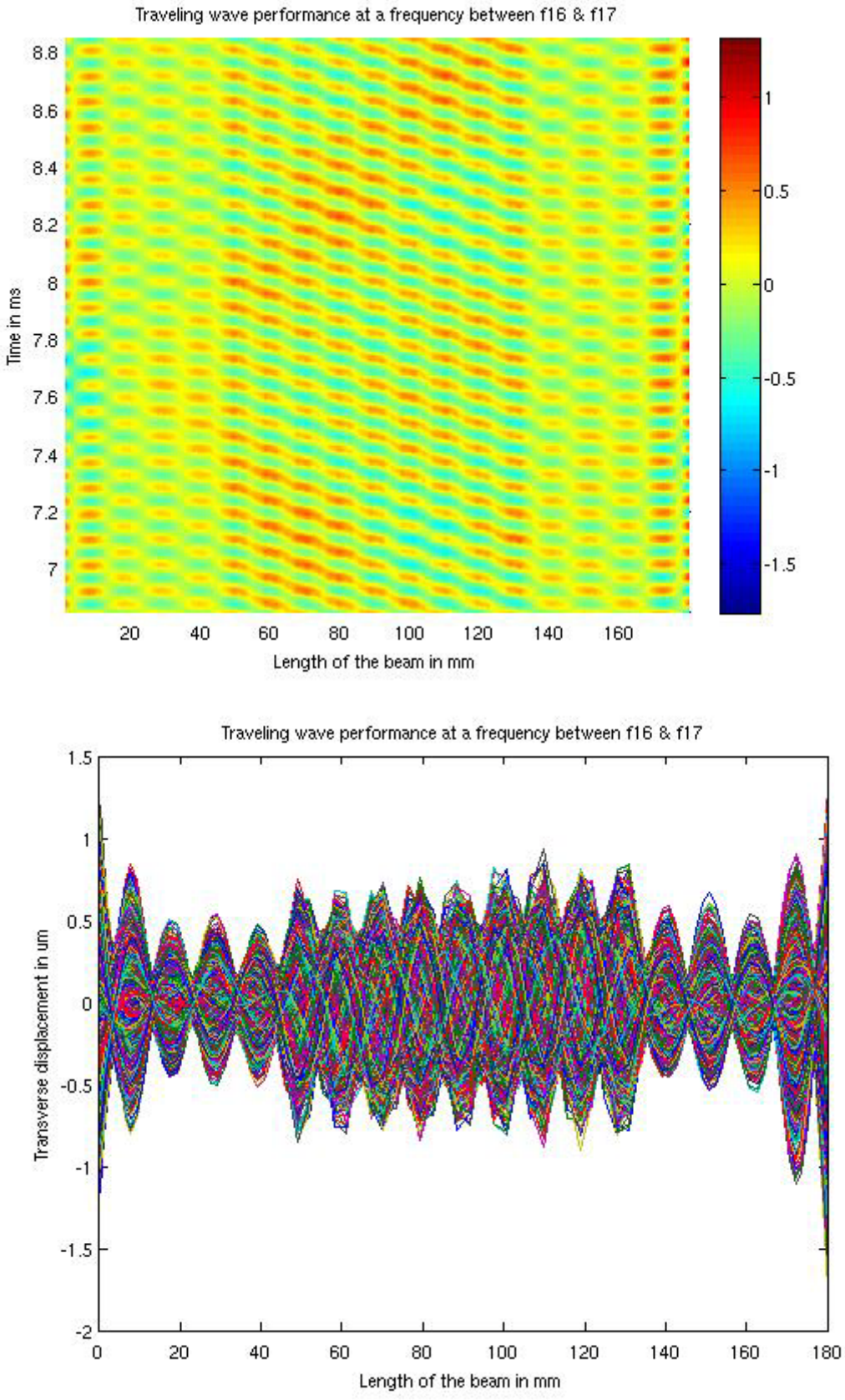

Figure 5.34: Traveling wave performance at a frequency between f_{16} & f_{17}

n	f_n (Hz)	f_{n+1}(Hz)	$f_{n*(n+1)} = f_{excitation}$(Hz)
11	5337.8	6241.2	5789,5
15	9097.1	10494	9795,5
16	10494	11795	11144,5
18	12909	14246	13577,5

Table 5.11: Excitations frequencies

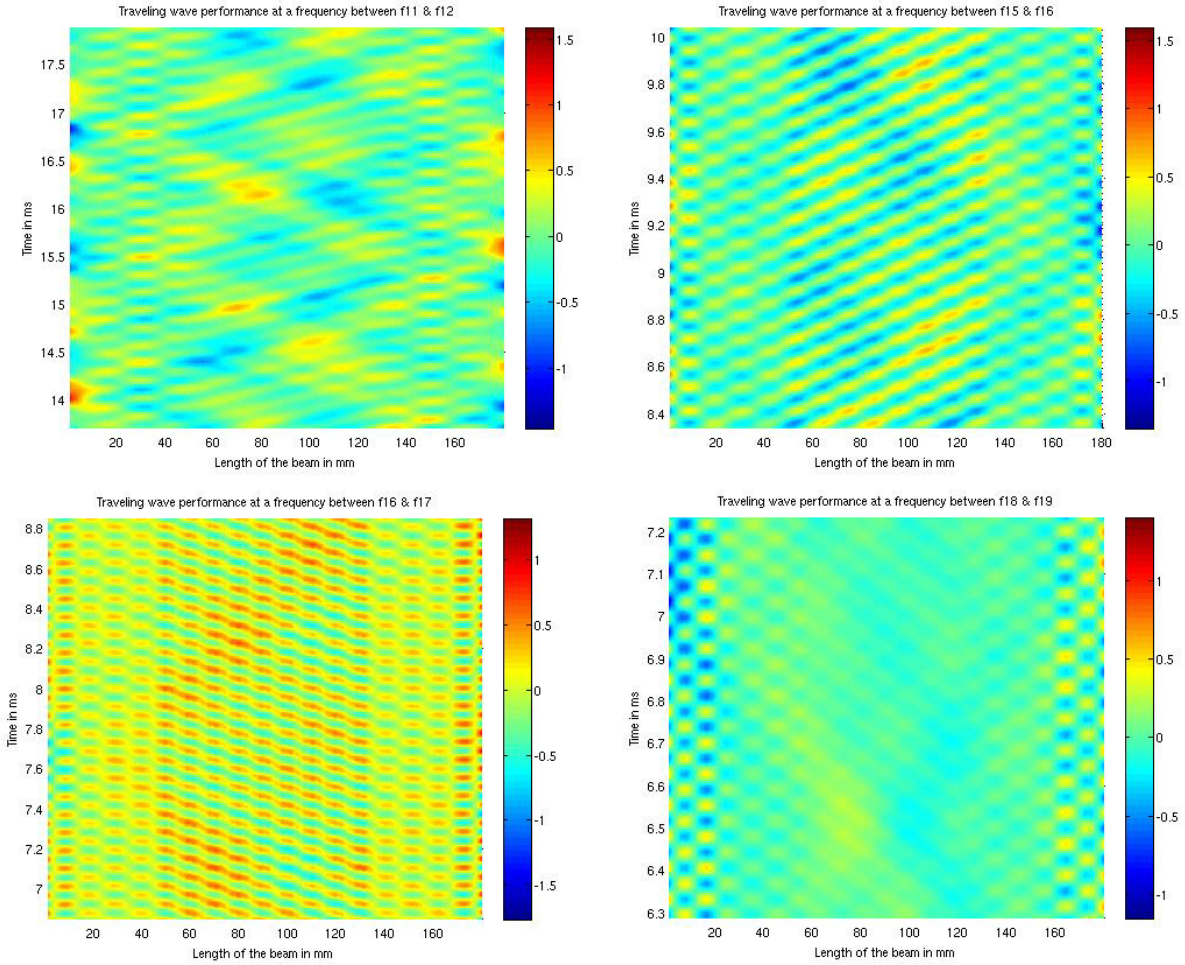

Figure 5.35: Traveling wave performances for different frequencies

5.4.3.2.3 Influence of positions on the performance of the traveling wave

To evaluate influence of patches position on the performance of the traveling wave, a comparison between traveling wave performances at the optimal operating frequency for each position is done. f_{16*17} was the optimal operating frequency for both positions. Here below in Figure 5.36, we can see again the representation of the traveling wave at each position to be able to compare the performance.

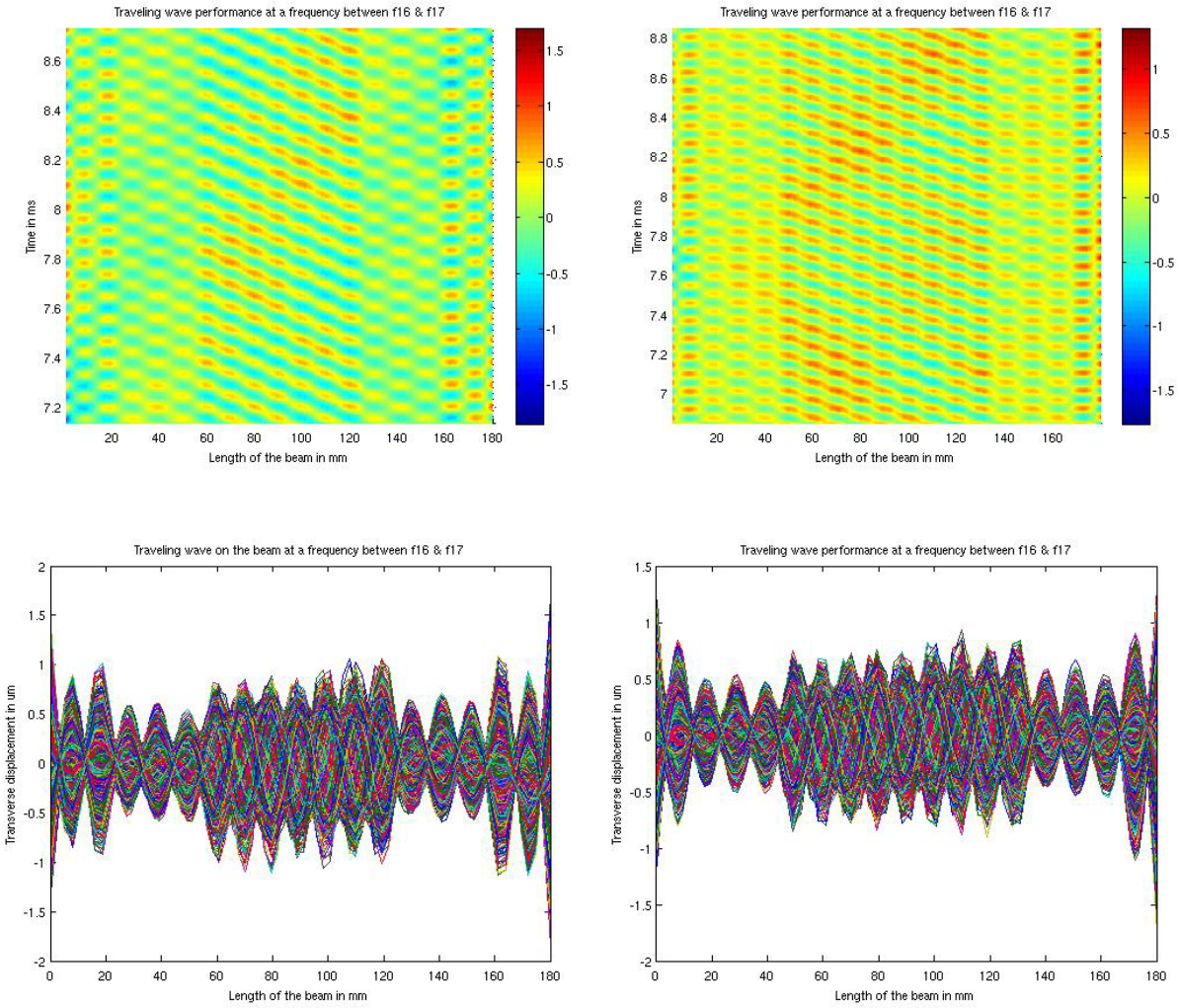

Figure 5.36: Traveling wave performances at position 1 (left) and position 2 (right)

Both waves show good traveling wave with larger displacements at position 1. It means that the position 1 leads to a higher robot speed. These results will be verified experimentally in the next chapter.

5.4.3.2.4 Two modes excitation functionality

As we said in the operation principle for this mode, this principle is based on the excitation of the two patches, at a frequency between two resonance frequencies. If we excite the two patches at the resonance frequency, two progressive waves with the same amplitude propagating in opposite directions cancel each other, resulting in standing wave on the beam. This result is shown in Figure 5.37 when we excited the two patches located at position 1 at the 17^{th} resonant frequency at $40V_{pp}$ sinusoidal voltage with 90° phase difference.

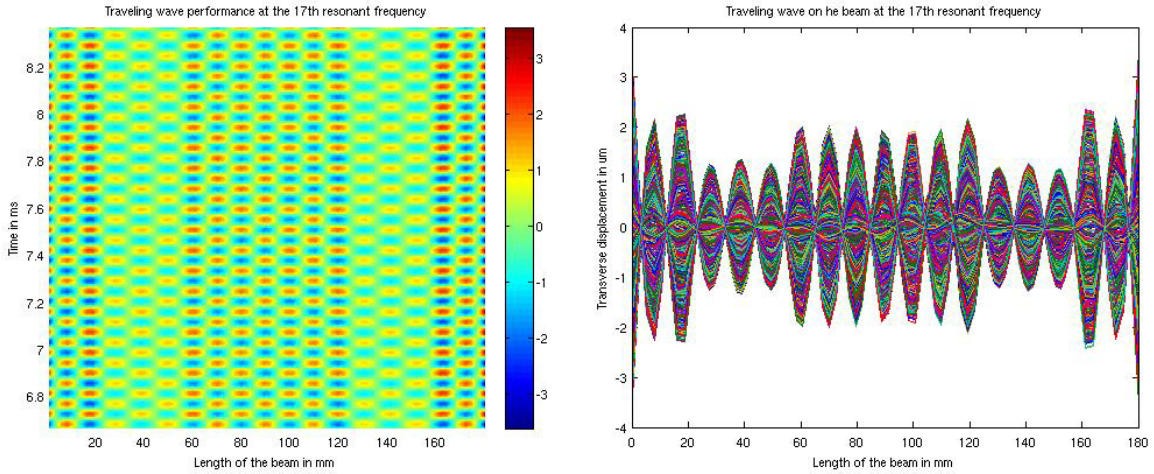

Figure 5.37: Traveling wave performance at the 17th resonant frequency

It was demonstrated in [(Kim, Park, & Jeong, 2009)] that traveling wave for linear travelling wave ultrasonic motors changes direction according to the excitation frequency. This result can be shown also in our case of application. Take the case of robot 1 corresponding to piezoelectric patches located at position 1 and apply $40V_{pp}$ sinusoidal voltage at frequencies given in Table 5.12 below. Results obtained are given in Figure 5.38. Direction of wave is represented by the black line. From figure we can deduce that wave change direction according to the excitation frequency.

n	f_n (Hz)	f_{n+1}(Hz)	$f_{n*(n+1)} = f_{excitation}$(Hz)	Wave propagation direction
14	7958.1	9028.9	8493,5	←
15	9028.9	10471	9750	→
16	10471	11790	11130,5	←
17	11790	12827	12308,5	→

Table 5.12: Wave propagation direction for different frequencies

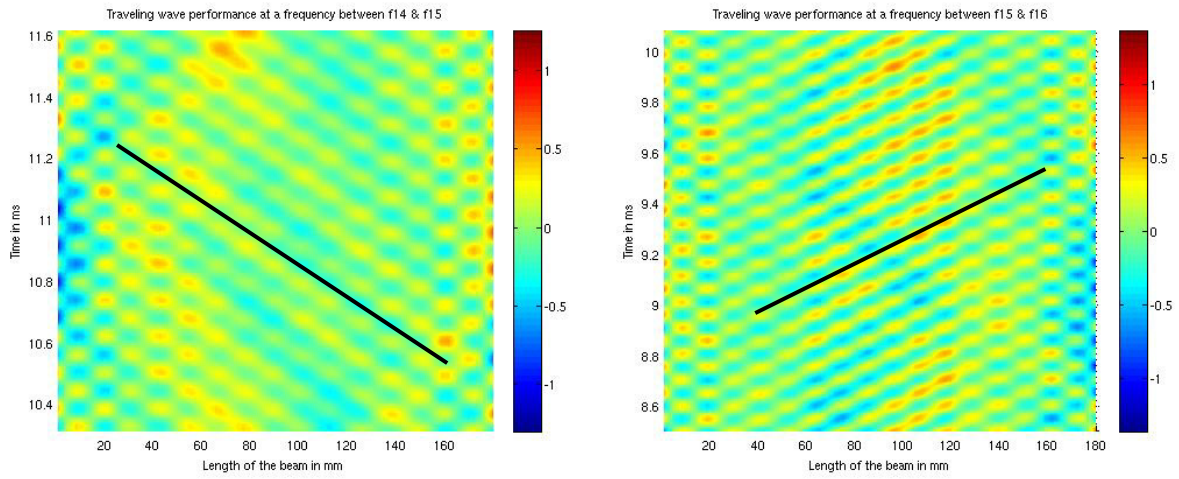

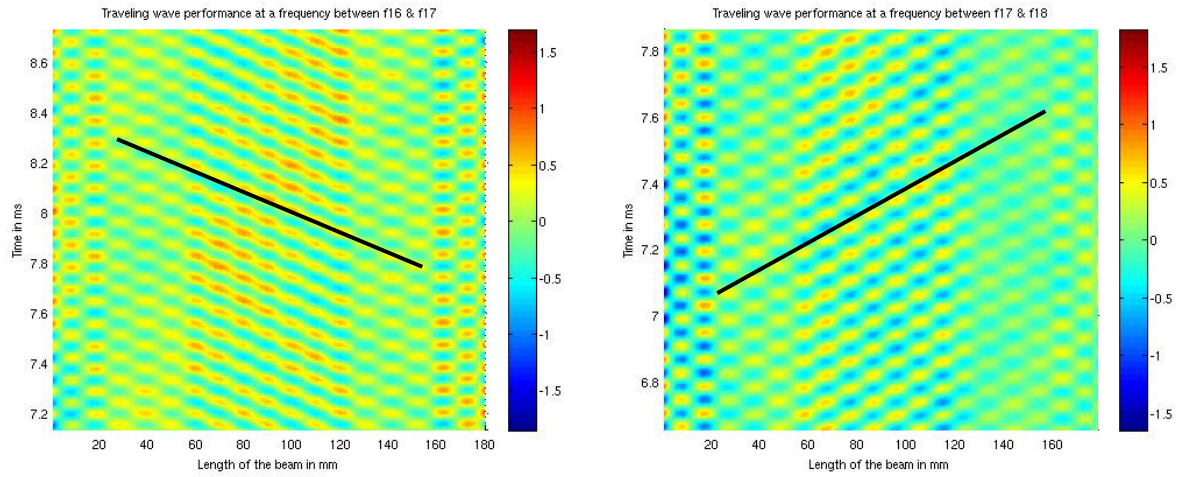

Figure 5.38: Traveling wave direction for different frequencies

Now, to verify the influence of phase let us apply two sin waves at the two patches without phase difference at f_{16*17}. The result is shown in Figure 5.39. Figure 5.39 shows a standing wave instead of a traveling wave and it confirms what we have shown in the operating principle of this mode. When φ equal to 0°, a standing wave is obtained and when φ equal to 90° (sin and cosine signals are applied), the traveling wave reaches its maximal speed.

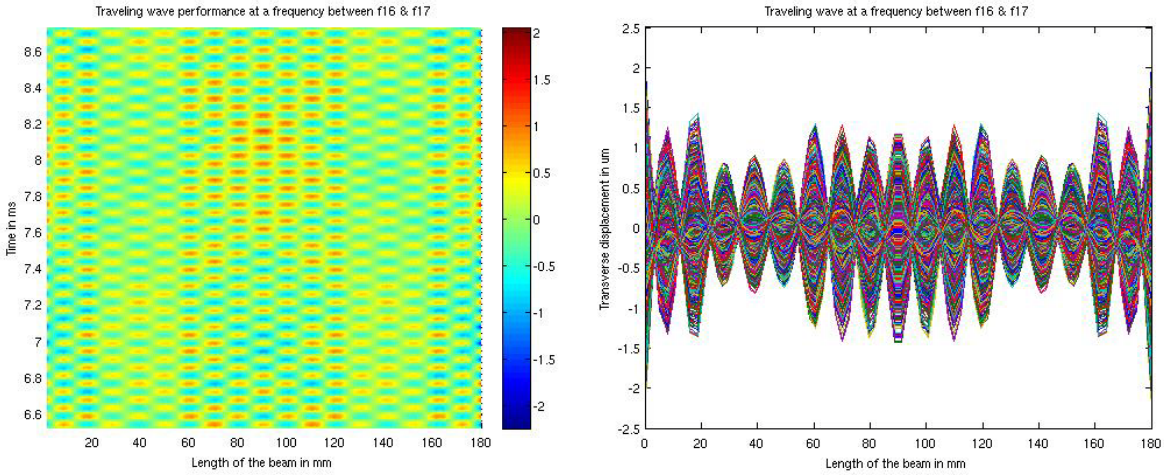

Figure 5.39: Traveling wave performance without phase difference at f_{16*17}

5.5 Conclusion and discussion

An aluminum beam was chosen with its given dimensions (180 mm × 17 mm × 0.5 mm). Piezoelectric patches dimensions were studied and they were chosen as the following (32 mm × 17 mm × 0.27 mm). Two piezoelectric patches positions near from the beam ends were studied for the one mode and the two modes excitation. Position 1 is given by the following (X_{p1}=24 mm, X_{p2}=124 mm) and position 2 is given by the following (X_{p1}=14 mm, X_{p2}=134 mm). Position 1 is shown the best performance in both one mode and two modes excitation. According to Table 5.13, performances of waves can be given in descending order as the

following: two modes excitation position 1, two modes excitation position 2, one mode excitation position 1 and one mode excitation position 2. In two modes excitation, we excite the two patches at a frequency between two resonances mode while in one mode excitation, one patch is excited at the resonance frequency and the other is used to absorb displacement in order to avoid wave reflection. That explains why the transverse displacements in two modes excitation are more important than in the case of one mode excitation even if in one mode excitation we excite at the resonance frequency. Wave propagation through the beam in two modes excitation is less homogeneous than in the case of one mode excitation. Figures show that amplitude has the same level near from the middle of the beam in case of one mode excitation while it is a little different with respect to time in the other case.

<table>
<tr><th colspan="2">One mode excitation</th></tr>
<tr><th>(1) Position 1 at f_{17}</th><th>(2) Position 2 at f_{16}</th></tr>
<tr><td> 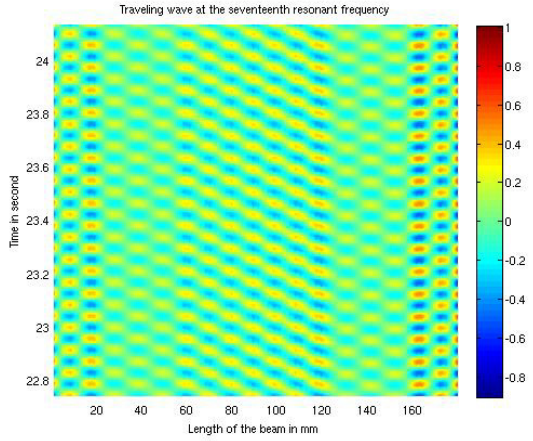
</td><td> 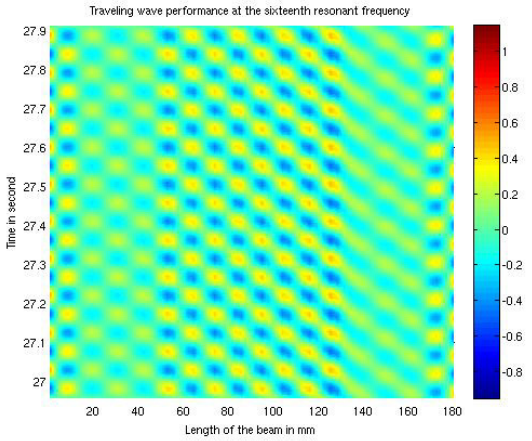
</td></tr>
<tr><th colspan="2">Two modes excitation</th></tr>
<tr><th>(3) Position 1 at f_{16*17}</th><th>(4) Position 2 at f_{16*17}</th></tr>
<tr><td> 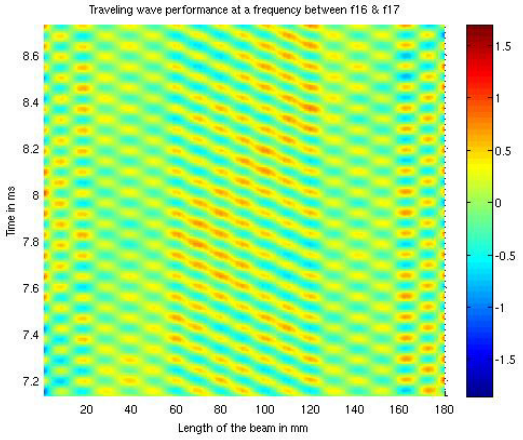
</td><td> 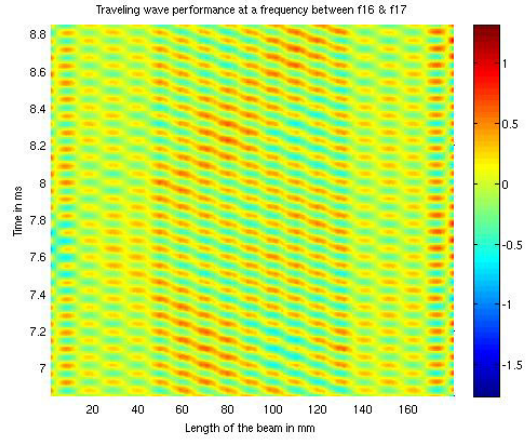
</td></tr>
</table>

Table 5.13: Optimal traveling wave performances for both modes at each position

The phase velocity for each case is extracted from figures in Table 5.13 and given by the following: υ_{ph1} = 238 m/s, υ_{ph2} = 218 m/s, υ_{ph3} = 234 m/s and υ_{ph4} = 232 m/s. The phase velocity can be determined analytically by $\upsilon = f\lambda$, where f is the applied frequency and λ is the wave length. That explains the values obtained for the phase velocity. We may note that, higher velocity doesn't mean better traveling wave performance because performance of wave depends on the waveform and transverse displacement.

Two robots should be manufactured later in the next chapter. Robot 1 corresponds to position 1 and robot 2 corresponds to position 2. An extra series RL shunt circuit must be connected to one of these two piezoelectric patches in the case of one mode excitation. For robot 1, the series RL circuit has been calculated and it is given by the following at the 17th resonant frequency (R_{17} = 9.75 Ω, L_{17} = 9 mH). For robot 2, the series RL circuit has been calculated and it is given by the following at the 16th resonant frequency (R_{16} = 23.75 Ω, L_{16} = 11.4 mH). Next chapter will be dedicated to robots manufacture processes, experimental validation of the beam robots, robots characterization and significance and benefits for this robot compared to other piezoelectric robots and traveling wave ultrasonic motors.

5.6 Appendix

1. *free-free boundary conditions*

$$\begin{cases} \partial^2{}_x w|_{x=0} = 0 \\ \partial^3{}_x w|_{x=0} = 0 \end{cases} \quad \text{(A.1.1)}$$

$$\begin{cases} \partial^2{}_x w|_{x=l} = 0 \\ \partial^3{}_x w|_{x=l} = 0 \end{cases} \quad \text{(A.1.2)}$$

2. *Static and dynamic optimal thickness*

2.1 unimorph piezoelectric actuator

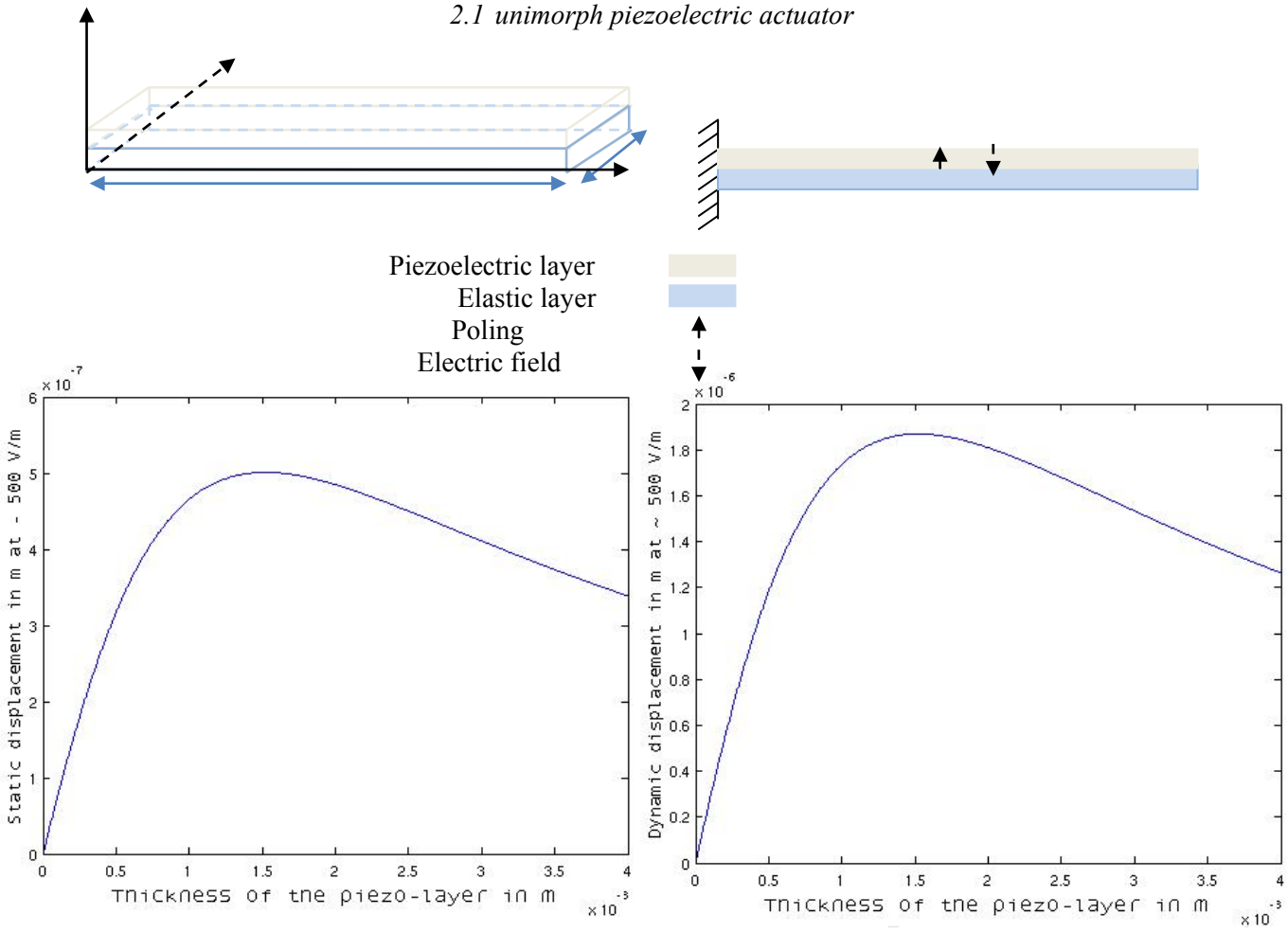

Static (left) and dynamic (right) transverse displacement at the free end of the unimorph piezoelectric actuator

The above curves show transverse displacement at the free end versus piezoelectric thickness in static (at the left) and dynamic (at the right) operations. In dynamic, transverse displacement is calculated at the first resonnant mode. Figure shows that the optimal piezoelectric thickness is the same in static and dynamic operations. Calculation is done for

this unimorph using the analytical code given by Hariri et al in [(Hariri, Bernard, & Razek, 2011)] for this unimorph.

2.2 *Two piezoelectric patches bonded on thin beam*

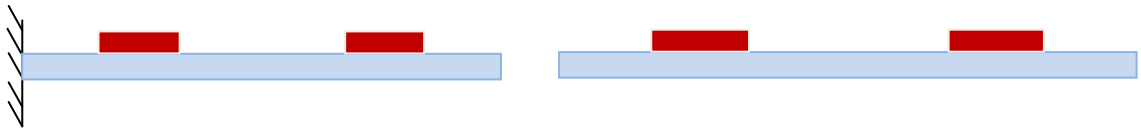

Fixed-free boundary conditions (B.C.) for static operation

Free-free B.C. for dynamic operation

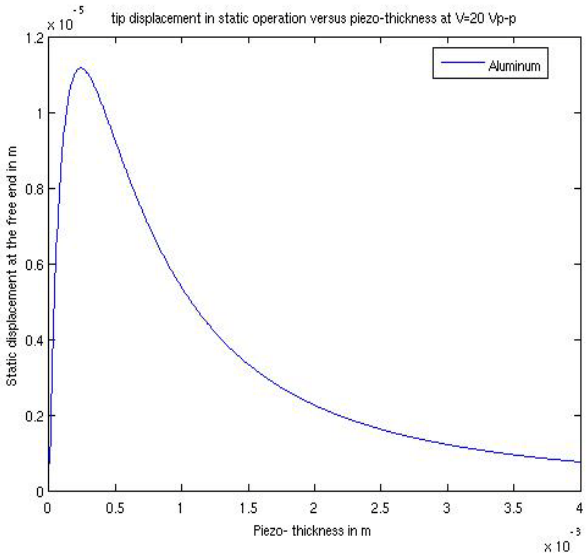

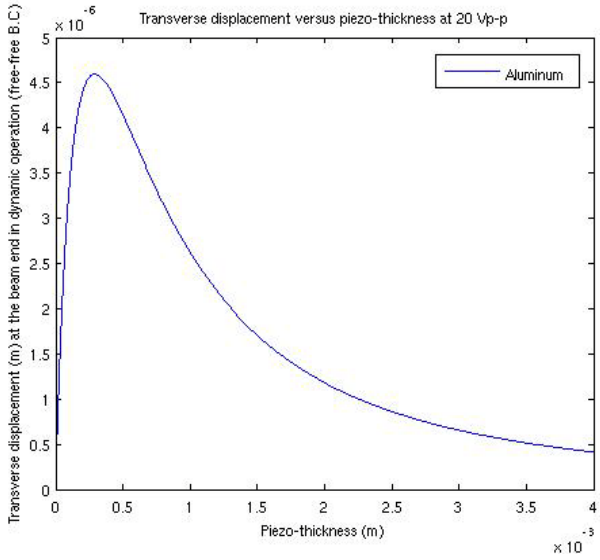

Static and dynamic transverse displacement at the free end versus piezoelectric thickness

Same as the unimorph case, in dynamic (right side figure) transverse displacement is calculated at the first resonant frequency. Figure shows that the optimal piezoelectric thickness is the same in static and dynamic operations.

2.3 *Conclusion and discussion*

We can draw from these two examples that the optimum thickness of the piezoelectric patch is the same in static and dynamic operation. So later in the case of a plate with piezoelectric

patches, we will start from this conclusion and work directly in static to determine the optimal thickness.

The purpose of these examples was to demonstrate that the optimal thickness is the same in static and dynamic, that is why the dimensions and properties of materials used are not given. Note that the unimorph piezoelectric actuator and the system with two piezoelectric patches presented here do not have the same size or same materials properties.

5.7 References

Badel A. Récupération d'énergie et contrôle vibratoire par éléments piezoélectriques suivant une approche non linéaire [Livre]. - Savoie : Thèse de Doctorat de l'Université de Savoie, 2006.

Bein T., Breitbach E.J. et Uchino K. A linear ultrasonic motor using the first longitudinal and the fourth bending mode [Revue] // Smart materials and structures. - 1997. - pp. 619-627.

Corcolle R. [et al.] Modeling of a beam structure with piezoelectric materials: introduction to SSD techniques [Revue] // COMPEL: The International Journal for Computation and Mathematics in Electrical and Electronic Engineering. - 2008. - pp. pp. 205-214..

Dehez B., Vloebergh C. et Labrique F. Study and optimization of traveling wave generation in finite-length beams [Revue] // journal of mathematics and computers in simulation 81. - 2010. - pp. pp. 290-301.

Fernandez, J.M. et Perriard Y. Comparative analysis and modeling of both standing and traveling wave ultrasonic linear motor [Revue] // Ultrasonic, IEEE Symposuim on volume 2. - 2003. - pp. 1770-1773.

Gabai R. et Bucher I. Excitation and sensing of multiple vibrating traveling waves in one-dimensional stuctures [Revue] // Journal of sound and vibration . - 2009. - pp. 406-425.

Hariri H., Bernard Y. et Razek A. Analytical and finite element model for unimorph piezoelectric actuator: Actuator design [Revue] // Proceedings of Piezo2011. - 2011. - pp. pp. 71-75.

Hariri H., Bernard Y. et Razek A. Finite element model of a beam structure with piezoelectric, patches using RL shunt circuits [Revue] // AC2011, 14th International Conference on active systems for dynamics markets. - 2011. - pp. pp.124-13.

Hemsel T. et Wallascheck J. Survey of the present state of the art of piezoelectric linear motor [Revue] // Ultrasonics 38. - 2000. - pp. 37-40.

Hernandez Camilio Realization of piezoelectric micropums, thesis at LGEP, Paris, France [Livre]. - Paris : University Paris-sud, 2010.

Kim G.H., Park J.W. et Jeong S.H. Analysis of dynamic characteristics for vibration of flexural beam in ultrasonic transport system [Revue] // Journal of mechanical science and technology. - 2009. - pp. 1428-1434.

Kuribayashi M., Ueha S. et Mori E. Excitaion conditions of a flexural traveling waves for a reversible ultrasonic linear motor [Revue] // Journal of the acoustical society od America 77. - 1985. - pp. 1431-1435.

Loh B.G. et Ro P.I. An object transport system using flexural ultrasonic progressive waves generated by two modes excitation [Revue] // IEEE transaction on ultrasonic, ferroelectrics, and frequency control. - 2000. - pp. 994-999.

Roh Y., Lee S. et Han W. Design and fabrication of a new traveling wave-type ultrasonic linear motor [Revue] // Sensors and actuators A 94. - 2001. - pp. 205-210.

Sashida T. et Kenjo T. An introduction to ultrasonic motors [Livre]. - Oxford : Clarendon Press, 1993.

Son K.J. [et al.] An ultrasonic standing-wave-actuated nano-positionning walking robot: piezoelectric-metal composite beam modeling [Revue] // Journal of vibration and control, vol.12. - 2006. - pp. 1293-1309.

Suybangdum P., Smithmaitrie P. et Laoratanakul P. Dual piezoelectric actuators for the traveling wave ultrasonic linear motor [Revue] // Fourth International Conference on Experimental Mechanics. - 18-20 November 2009.
Ueha S. et Tomikawa Y. Ultrasonic motors, theory and applications [Livre]. - Oxford : Oxford science publications, 1993.
Wang Q.M. et Cross L.E. Performance analysis of piezoelectric cantilever bending actuators [Revue] // Ferroelectrics. - 1998. - pp. vol. 215, pp. 187-213.
Wu S. Y. Piezoelectric shunts with parallel R-L circuit for smart structural damping and vibration control [Revue] // Proc. SPIE Symp. Smart Structures Materials Passive Damping Isolation. - 1996. - pp. pp. 259–269.

CHAPTER 6

ROBOT MANUFACTURING AND EXPERIMENTAL MEASUREMENTS

Chapter 6: Robot manufacturing and experimental measurements

List of figures

List of tables

6.1 Introduction

As we now know, the piezoelectric beam robot is composed of a 180 × 17 × 0.5 mm aluminum beam and two non-collocated piezoelectric 32 × 17 × 0.27 mm patches bonded on the beam. Two robots will be manufactured and tested in this chapter. Robot 1 corresponds to the case where the two piezoelectric patches are located at X_{p1}=24 mm and Xp2=124 mm from one beam end (position 1) and Robot 2 corresponds to the case where the two piezoelectric patches are located at X_{p1}=14 mm and Xp2=134 mm from one beam end (position 2). Then electronic circuits to supply piezoelectric actuators will be designed and RL shunt circuits for piezoelectric sensor will be realized. After fabrication processes, an experimental test will be done to verify theoretical results given in the last chapter. Robots speed versus applied voltage and versus embedded masses will be measured on a smooth glass flat surface; robots speed for different mechanical loads will be measured also. At the end a comparison between our robots and existing similar robots reviewed in the introduction of the last chapter and some linear traveling wave ultrasonic motors will be done.

6.2 Fabrication

The fabrication process is quite easy. All what we need is a glue to bond the piezoelectric patches on the beam at their specific positions. The glue used was Araldite 2013, it is a two component epoxy paste adhesive provided by Huntsman International LLC and it was chosen because it resists in water for water future applications.

The piezoelectric patches (NCE41) were purchased from Noliac, Inc, Denmark and they were chosen as wrap around electrode (WAE) shapes to be able to connect the two electrodes as shows Figure 6.1.

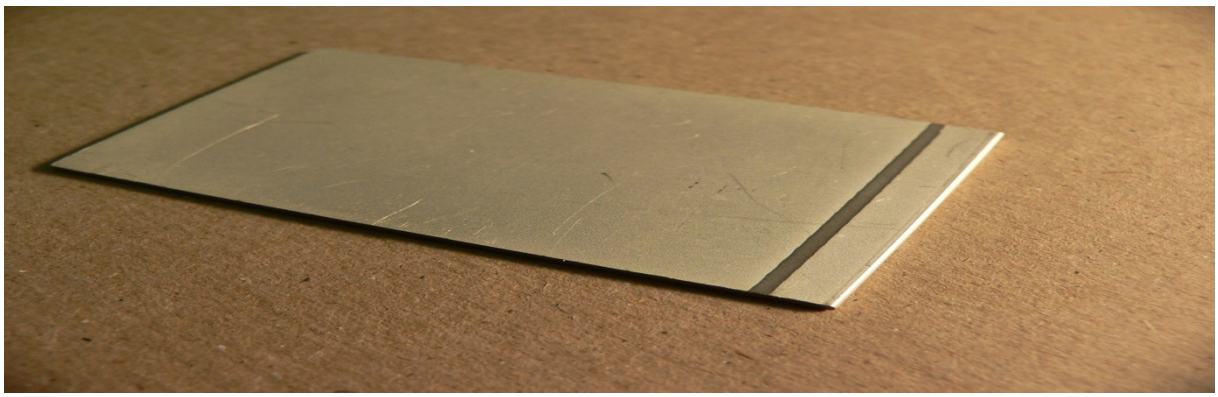

Figure 6.1 : Wrap around electrode (WAE) piezoelectric patch provided by Noliac, Inc

The last step to finish the manufacturing process is to bond each piezoelectric patch at its given position. Figure 6.2 presents the two prototypes robots.

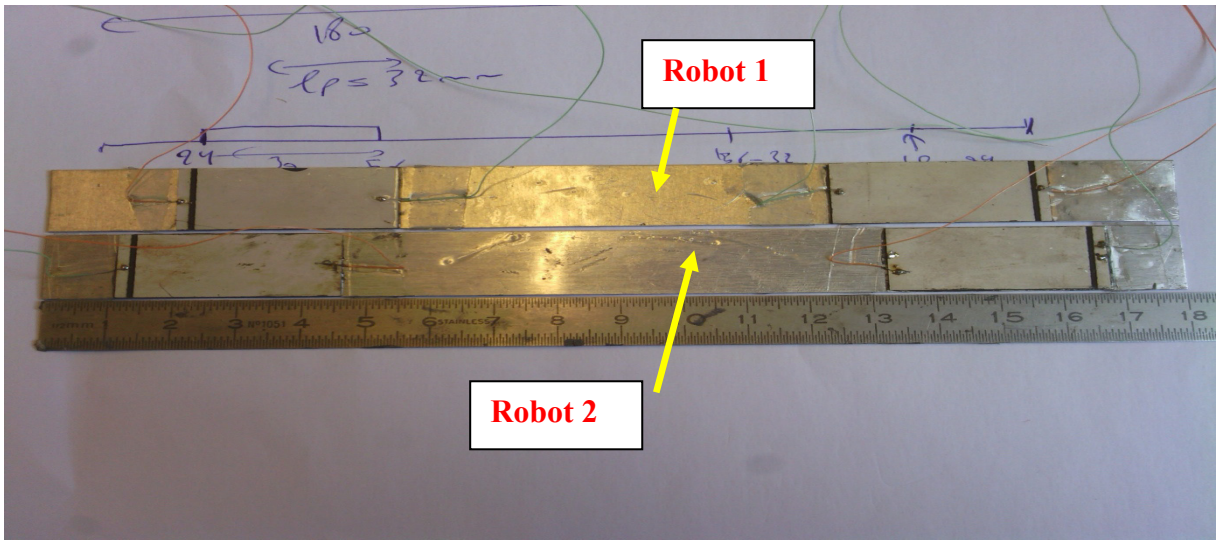

Figure 6.2 : Robot 1 where piezoelectric patches are located at position 1 & Robot 2 where piezoelectric patches are located at position 2

Two setups will be made for these robots. The first setup is the one mode excitation, when one patch is supplied by a sinusoidal signal coming from a function generator via a power amplifier used to amplify the signal provided by the function generator; the second patch is connected to a series RL circuit as shown Figure 6.3.

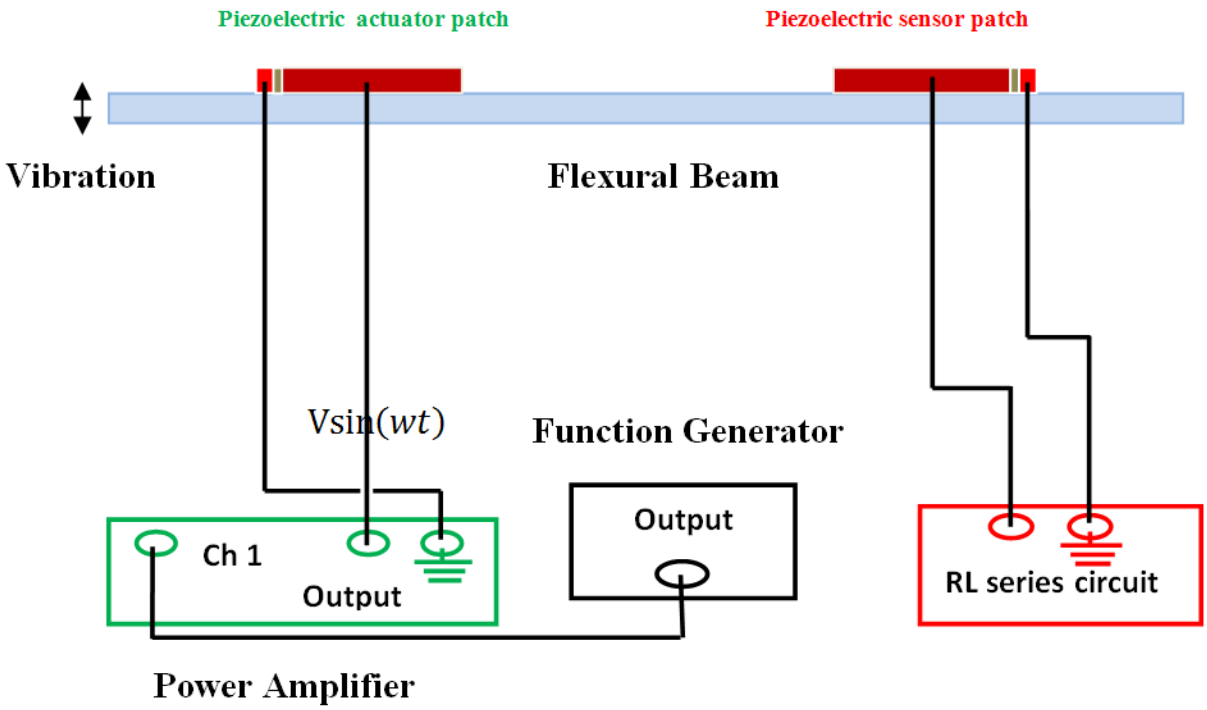

Figure 6.3 : Configuration of the one mode excitation

The second setup is the two modes excitation when the two piezoelectric patches are supplied by sinusoidal signals with phase difference of φ via two power amplifiers used to amplify the signal provided by the function generator and a phase shifter used to provide a phase shift between input and output signal as shown in Figure 6.4.

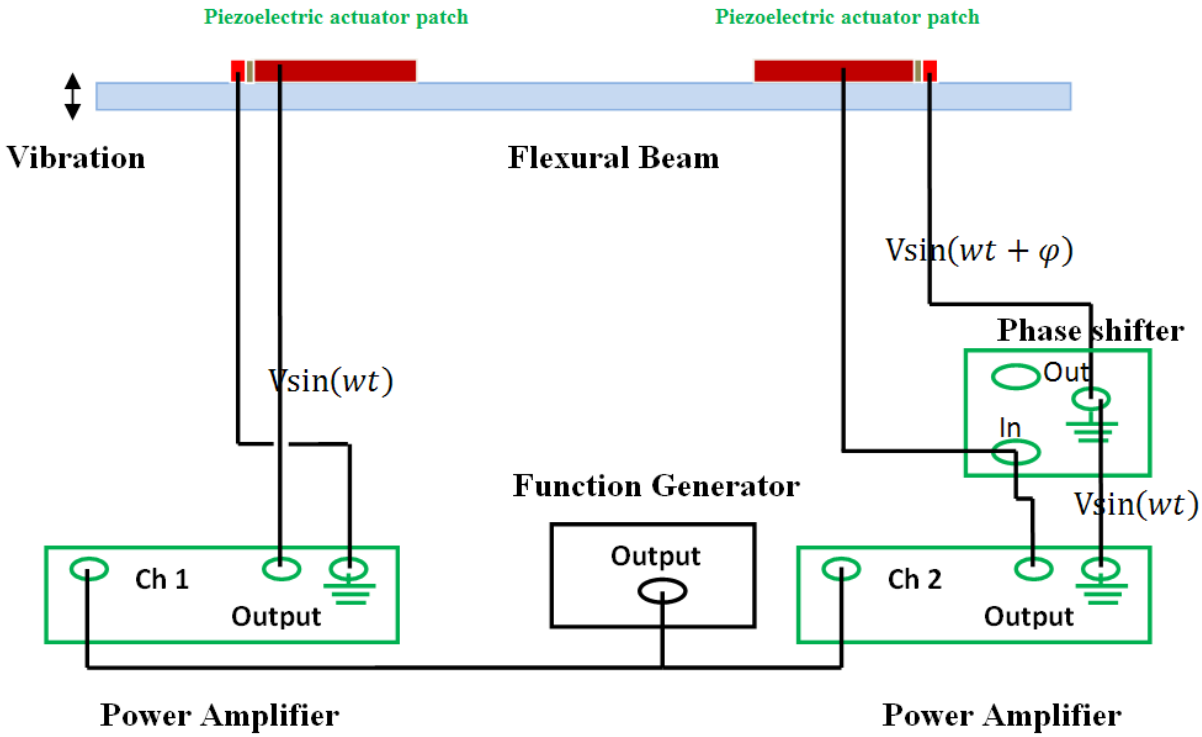

Figure 6.4 : configuration of the two modes excitation

The next step is the experimental realization of these two configurations, i.e. the choice of the power amplifier required, the realization of the phase shifter and the RL series connections. Note that at small frequencies, high inductance values is needed (equation 5.13: $L_{opt} = 1/(C_p w^2)$). Therefore a special synthetic variable inductance will be used.

6.3 Electronic and electric circuits design and realization

Let us begin by the choice of the power amplifier. Two essential criteria are needed to choose it, the maximum applied voltage to the piezoelectric patches and the maximum consumed current. $300 Vmm^{-1}$ is the maximum peak to peak electric field beyond which the piezoelectric material (NCE41) depolarizes. For a 0.27 mm of thickness patch, maximum peak to peak applied voltage is equal to 81 V_{pp}. Therefore, maximum applied voltage was chosen equal to 30 V, taking 10 V precaution to not depolarize the piezoelectric material and ensure that linear regime is remained. The maximum consumed current of the piezoelectric patch is approximated by taking the electrical equivalent circuit for the piezoelectric patch as a

capacitor (C_p). Therefore $I_{load} = (2\pi f_{max})C_p V_{max}$, where C_p is the capacitance of the piezoelectric patch, V_{max} is the maximum voltage applied and f_{max} is the maximum applied frequency. C_p is determined in chapter 4 and it is equal to 22 nF, V_{max} is equal to 30 V and f_{max} was chosen for experimental purpose equal to 35 kHz in order to be able to measure high frequencies. This gives I_{load} equal to 145 mA. In practice, the output current of the power amplifier should be taken at least 10 times the load current to avoid the destruction of the sinusoidal signal applied to the piezoelectric patch. The chosen power amplifier OPA549 is a Texas Instruments verifying these conditions.

A phase shifter is designed to work between 1 and 35 kHz. The circuit is formed by a capacitor, resistances and an operational amplifier (TL082). The phase is shifted by varying a resistance between two ends corresponding to the operating area (between 1 and 35 kHz). Power amplifiers schematic circuit and phase shifter schematic circuit with the printed circuit board (PCB) are given in the appendix for more details.

Synthetic inductor was preferred in the experimental realization to verify the existence of the traveling wave at low frequencies. Taking the example of the 6th resonance mode for robot 1 (f_6 = 1579.3 Hz), the optimal L value according to equation 5.13 ($L_{opt} = 1/(C_p w^2)$) is equal to 461 mH. This value can only be synthesized using active electronic circuit which is synthesized using resistances, a capacitance and two operational amplifiers. Schematic circuit for the synthetic inductor and its PCB (printed circuit board) are presented in the appendix. Voltages generated across piezoelectric patch experimentally are always less than a half of the applied voltage at the other piezoelectric patch (< 15 V) in our case of application (robots are free at both ends). Therefore the TL082 poses no problem in this case and it was chosen for the two operational amplifiers needed to realize the inductor. The synthetic inductor is designed to work between 1mH and 9500 H corresponding to an operating frequency area between 11 Hz and 35 kHz. The resulting circuit will act as an inductor L = k(R)C, where k is a mathematical function of R and C is a capacitance. k values must be varied between two limits corresponding to the desired inductors values. By varying resistances (k(R)), we should be careful to avoid saturation of internal nodes of the inductor. More details about the synthetic inductor and its PCB can be found in the appendix.

6.4 Experimental validation

After realizing the electronic circuits needed to move the robots, in this sub-section we will verify experimentally the performances of waves. Experimental implementation of the one mode and two modes excitation is shown in Figure 6.5 and Figure 6.6 respectively. In Figure 6.5, a power amplifier is used to amplify the signal supplied by the signal generator to the first piezoelectric patch, and then a series RL circuit with synthetic inductor is connected to the second piezoelectric patch. In Figure 6.6, power amplifiers are used to amplify signal provided by the signal generator to the piezoelectric patches.

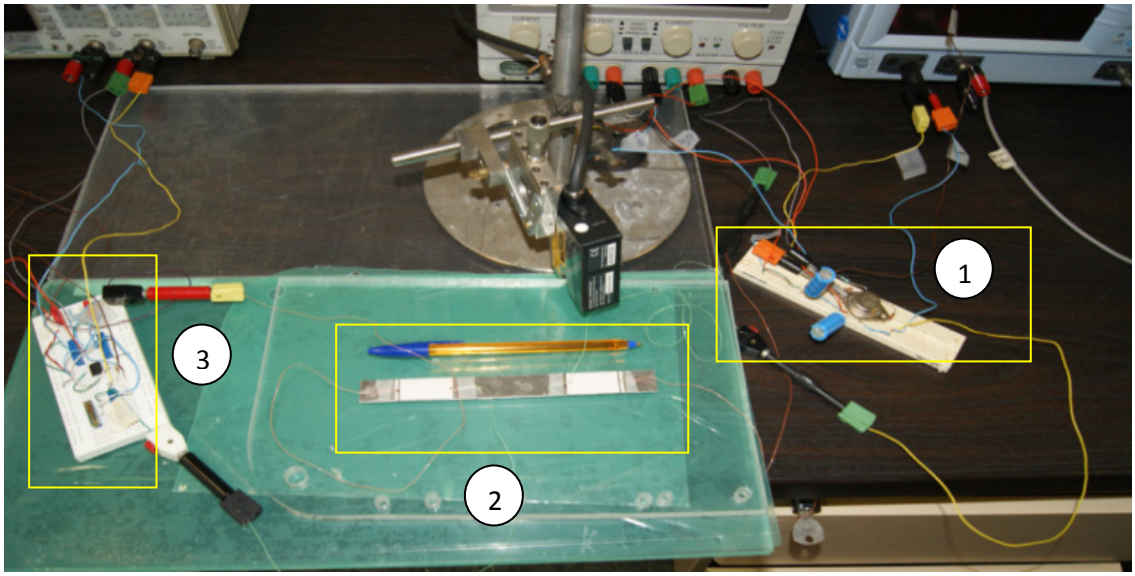

Figure 6.5: Robot structure for the one mode excitation operating principle (1: power amplifier, 2: robot body, 3: series RL synthetic inductor)

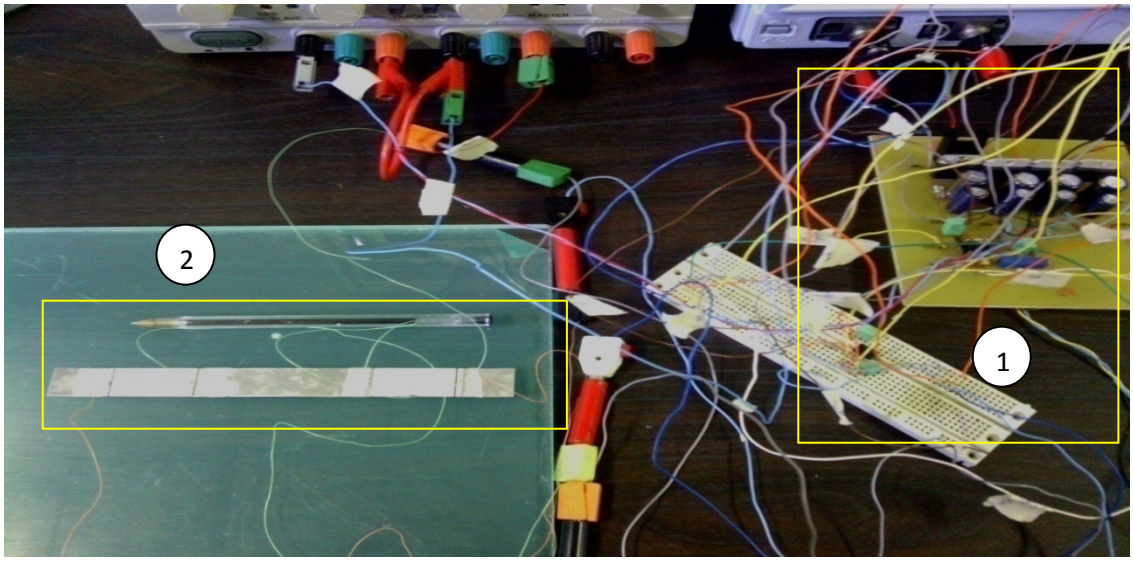

Figure 6.6: Robot structure for the two modes excitation operating principle (1: Power amplifiers, 2: robot body)

It was shown by simulation that the two modes excitation (2ME) gives better traveling waves performances than one mode excitation (1ME) but, it has the inconvenient of instability in the traveling wave. Also, simulations show that performance of traveling waves at position 1 seems better than that at position 2. Therefore, in a decreasing order of traveling wave performances (waveform and transverse displacement), we obtain: 2ME robot1, 2ME robot 2, 1ME robot 1 and 1ME robot 2. Experimentally velocity of robots should be classified in the same order.

Experimentally in one mode excitation, a large change in the optimal resistance with respect to the optimal inductive reactance and vice versa leads to stop the robot; a small change of optimal resistance with respect to the optimal inductive reactance and vice versa affects the speed of the robot. The robot was more sensitive to changes in the inductive reactance than in the resistance. Table 6.1 shows a comparison between simulation and experiment for resistance value, inductance value and optimal operating frequency for the one mode excitation. In the case of two mode excitation, simulations show that the optimal operating frequency is between 10.5 kHz (sixth resonant frequency) and 11.8 kHz (seventh resonant frequency) for both robots (robot 1 & robot 2). Experimentally, the optimal operating frequency is equal to 11.3 kHz for robot 1 and 10.7 kHz for robot 2.

	Robot 1		**Robot 2**	
	By simulation	**Experimentally**	**By simulation**	**Experimentally**
f_{opt}(kHz)	11.79	11.6	10.49	10.2
L_{opt}(mH)	9	8.2	11.4	9.7
R_{opt}(Ω)	9.75	Btw 5 & 15	23.75	Btw 10 & 30

Table 6.1: Simulation and experimental comparison for the one mode excitation

Speeds of robots are given at its optimal values with 20V amplitude in Table 6.2. Speeds are tested at least three times in each case and it was noted that no major changes in the speed values for each test. In the next sub-section; we will study experimentally robot speed for different applied voltages, influence of embedded mass on the robot speed and speed versus mechanical load for different applied voltages.

	Operating principle	Robot 1	Robot 2
Speed of robot (mm/s)	**2ME**	90.6	70.3
	1ME	48.76	35.37

Table 6.2 Robots speeds at 20 V amplitude

6.5 Robot characterization

Maximum applied voltage was chosen equal to 30V according to the maximum peak to peak electric field beyond which the piezoelectric material (NCE41) depolarize. All measurements here are taken for robot 1 for the one mode and two modes excitation at its optimal values obtained experimentally. Robot 1 is taken because it shows better performances in the two modes of operation (1ME & 2ME).

Speed as a function of voltage, speed as a function of embedded masses and speed as a function of dragged load are important in mobiles robotics applications. That is why; they have been measured to characterize our robot.

We measured first the robot speed on a smooth glass flat surface for different applied voltages. Figure 6.7 shows that robot speed varies linearly with the applied voltage. It also shows that speed of robot in the case of 2ME is higher than the 1ME. This result is in agreement with the simulation. At 30V amplitude robot 1 reaches 80.19 mm/s in the 1ME and 131.5 mm/s in the 2ME according to Figure 6.7.

After having shown the influence of the applied voltage on the velocity of the robot, we will see the influence of embedded masses on the velocity as shown in Figure 6.8 at 30V amplitude in the two modes operating principle. Figure 6.9 shows that the variation is linear between embedded masses and velocity. It also shows that the slope is greater in the case of two modes excitation. It means that when we increase the mass, velocity decreases much more in the case of 2ME than the case of 1ME. Actually that is due to the instability of wave in the case of two modes excitation as shown by simulation in chapter 5, Figure 5.33.

To determine the nominal operating point of the robot, we measured robot speed versus a mechanical load at a given applied voltage. For this aim, this mechanical load is considered to be the weight of the robot on an inclined plane (Figure 6.10) and it is given in the following equation:

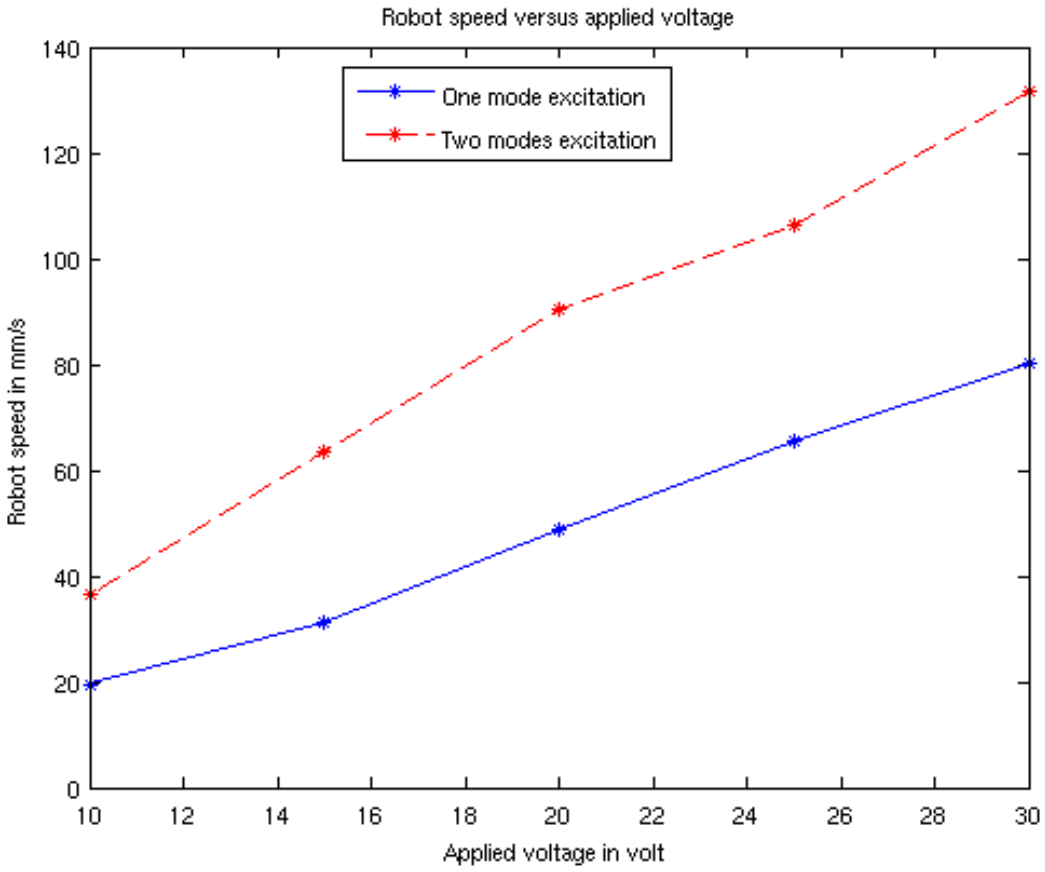

Figure 6.7: Robot speed versus applied voltage on a smooth glass flat surface for the one mode and two modes excitation

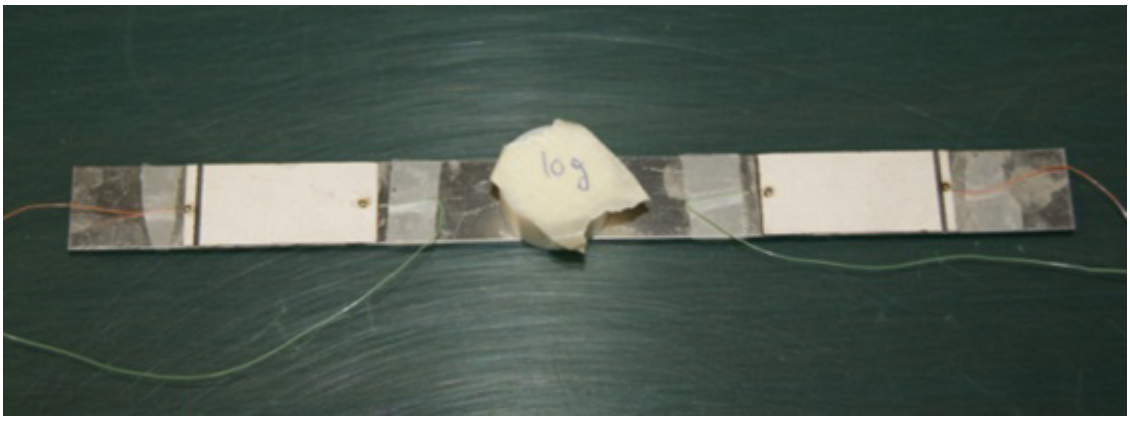

Figure 6.8: Embedded mass on the robot body

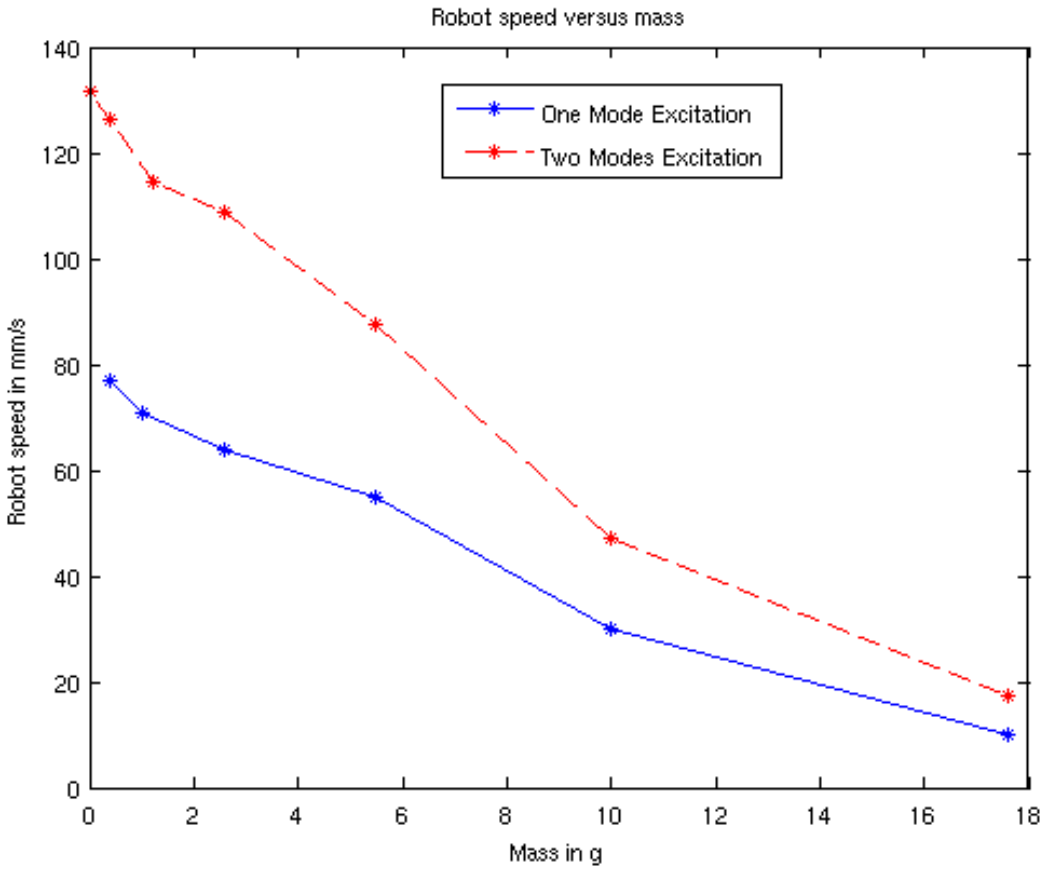

Figure 6.9: Robot speed versus embedded mass on a smooth glace flat surface for the one mode and two modes excitation

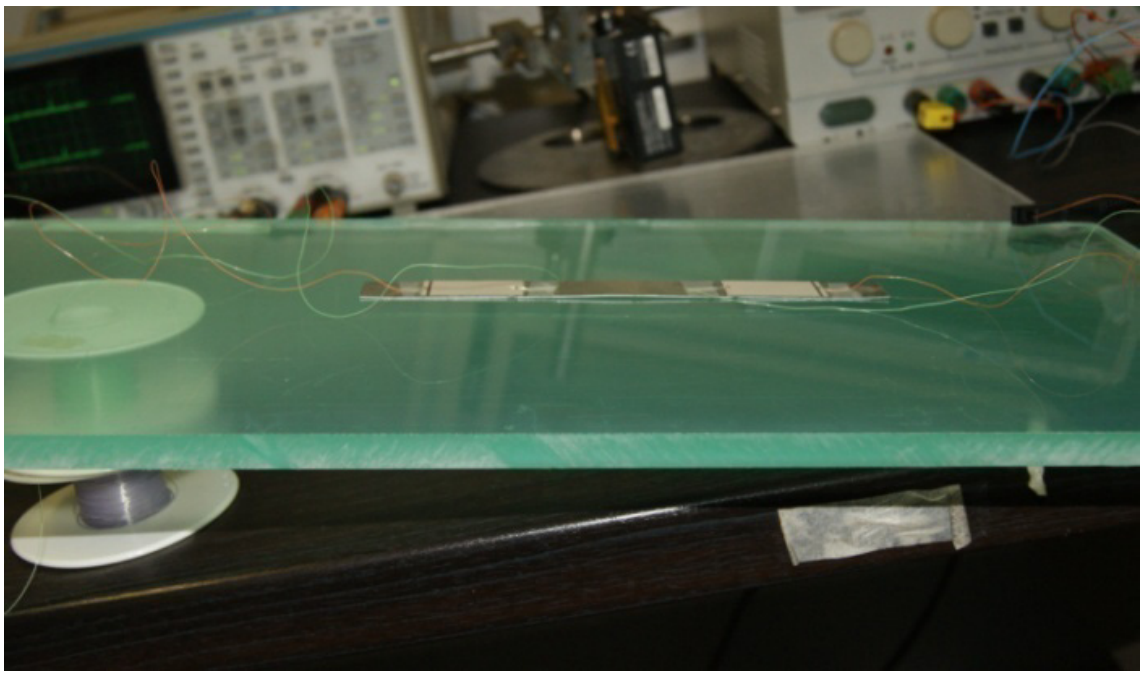

Figure 6.10: Robot speed measured on an inclined plane

F = M×g× sin(θ) at zero speed (friction force is equal to zero). Where M is the mass of the robot and it is equal to 5.2 g (beam, piezoelectric patches and adhesive masses), g is the gravitation force and θ is the inclination angle.

We have measured the robot speed for different positions of the inclined plane (different mechanical load). Figure 6.11 shows robot speed versus mechanical load for different applied voltages, where it becomes easy to determine the nominal operating point of the robot. At the same voltage, the maximum mass pulled is higher in the case of one mode excitation than the case of two modes excitation. In case of two modes excitation, this robot can provide 432 μW at its nominal operating point (7.2 mN, 60 mm/s) and it can provide 360 μW at its nominal operating point (9 mN, 40 mm/s) in the case of one mode excitation.

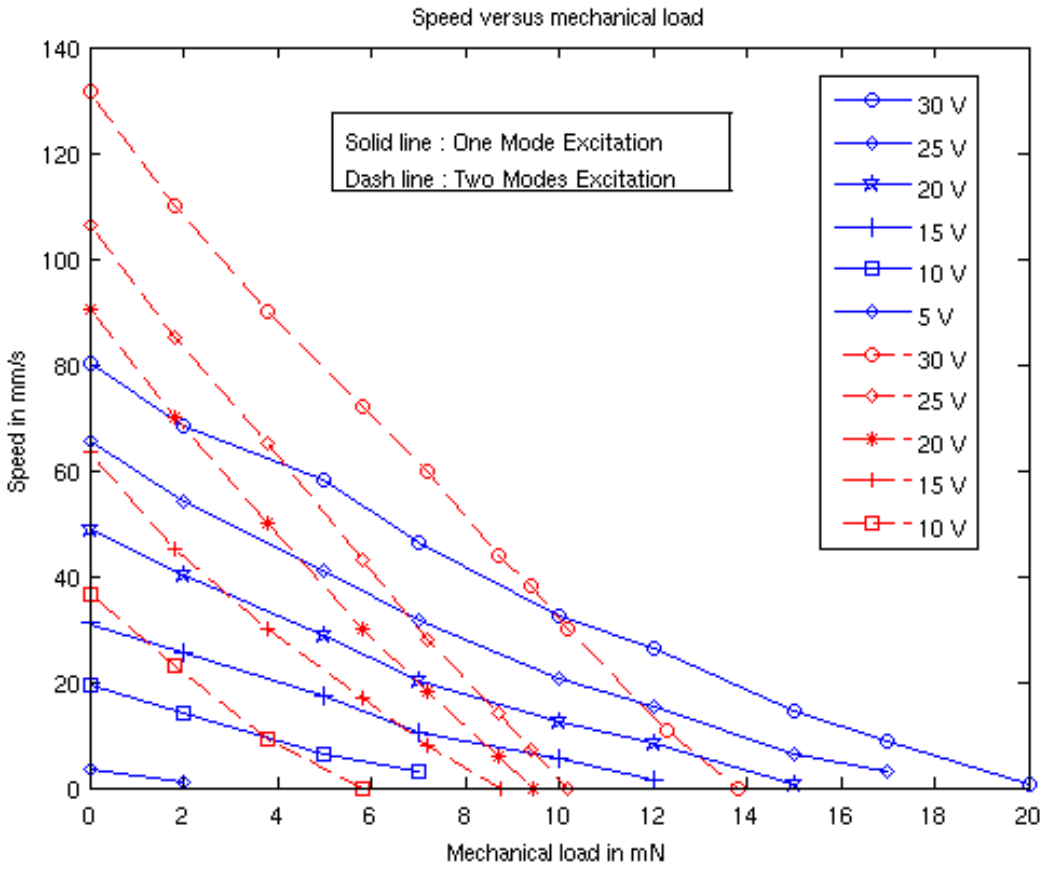

Figure 6.11: Speed versus dragged load for different voltage for the one mode and two modes excitation

6.6 Significance and benefits

In this sub-section we will compare the 1ME robot 1 and the 2ME robot 1 with others linear traveling wave piezoelectric motors having nearly the same structure [(Jeong, et al., 2007), (Loh, et al., 2000), (Roh, et al., 2001), (Suybangdum, et al., 2009)] and with the only one robot having almost the same structure but based on the ultrasonic standing wave principle, therefore it is using legs to create the motion of the robot [(Son, et al., 2006)]. Standing wave type linear piezoelectric motors using teeth to create slider motion have common points with the mentioned standing wave robot but are not presented here. This comparison is based mainly on the device structure and dimension, operating frequency, applied voltage and speed. The major drawbacks of piezoelectric actuators are high drive voltage and small deformations, so the applied voltage and speed are taken as criteria in this comparison. Table 6.3 shows a comparison between the 1ME robot 1, the 2ME robot 1, some linear traveling wave piezoelectric motors having nearly the same structure and the only one robot having almost the same structure.

Description	Research group	Year	Devise structure & dimensions	Operating frequency	Applied voltage	Speed
1ME traveling wave piezoelectric beam robot (1ME robot 1) [(Hariri, et al., 2012)]	France, Laboratoire de Génie Electrique de Paris (LGEP)	2012	An aluminum beam (180×17×0.5mm) with 2 non-collocated piezoelectric patches (32×17×0.27mm) bonded on it and Series RL shunt circuit (R= 10Ω & L= 8.2 mH)	11.6 kHz	30V	81.19 mm/s on a glass surface
2ME traveling wave piezoelectric beam robot (2ME robot 1) [(Hariri, et al., 2012)]	France, Laboratoire de Génie Electrique de Paris (LGEP)	2012	An aluminum beam (180×17×0.5mm) with 2 non-collocated piezoelectric patches (32×17×0.27mm) bonded on it	11.3 kHz	30V	131.5 mm/s on a glass surface

Description	Research group	Year	Devise structure & dimensions	Operating frequency	Applied voltage	Speed
An object transport system using flexural ultrasonic progressive waves generated by two mode excitation [(Loh, et al., 2000)]	USA, Department of mechanical aerospace engineering, North Carolina State University	2000	An aluminum beam (500×11×3.1mm) , two aluminum horns and two Langevin transducers	27 kHz	400V	96 mm/s with no additional mass on the slider (30g slider weight)
Design and fabrication of a new traveling wave-type ultrasonic linear motor [(Roh, et al., 2001)]	Korea, School of mechanical engineering, department of sensor engineering and school of computer and communicatio n	2001	A aluminum stator (75×8×1mm), two piezoelectric ceramic plates (75×8×0.5mm) bonded on the stator and silicon rubber layer (75×8×5mm)	23.5kHz	100V	400mm/s when operating with a load mass of 100g. The speed is improved to 1200 mm/s by equipping the motor with teeth that were 5mm long
An ultrasonic standing-wave-actuated nano-positionning walking robot [(Son, et al., 2006)]	USA, Department of mechanical engineering Carnegie Mellon University	2006	A stainless steel beam (30×5×0.3 mm) & piezoelectric beam with 5 insulation gaps (30×6×0.508 mm)	14.2 kHz (forward motion) & 24.7 kHz (backward motion)	10V	58.6 mm/s (forward motion) & 33.7 mm/s (backwar d motion) on a silicon wafer

Description	Research group	Year	Devise structure & dimensions	Operating frequency	Applied voltage	Speed
A study on an object transport system using ultrasonic wave excitation [(Jeong, et al., 2007)]	Korea, USA Department of mechanical engineering, Chosun University, and department of mechanical aerospace engineering, North Carolina State University	2007	An aluminum beam (350×14×3 mm) two aluminum horns and two Langevin transducers	25.5 kHz	500V	82.94 mm/s (transporting 20g object)
Dual piezoelectric actuators for the traveling wave ultrasonic linear motor [(Suybangdum, et al., 2009)]	Thailand, Department of mechanical engineering, faculty of engineering and the national metal and materials technology center	2009	Brass beam (85×6×1 mm) with rectangular teeth (2×6×3 mm), two piezoelectric actuators (10×6×0.5) bonded on the bottom surface near both ends of the stator and two damping materials.	28.2 Hz	45V	143.8 mm/s at a preload of 95g

Description	Research group	Year	Devise structure & dimensions	Operating frequency	Applied voltage	Speed
1 ME traveling wave piezoelectric pump [(Hernandez, 2010)]	France, Laboratoire de Génie Electrique de Paris (LGEP)	2010	An aluminum beam (160×30×2.6 mm),two aluminum horns, two Langevin transducers and a parallel RL shunt circuit (R=1502Ω & L=5.12 mH)	28 kHz	15V	80mm/s
2 ME traveling wave piezoelectric pump [(Hernandez, 2010)]	France, Laboratoire de Génie Electrique de Paris (LGEP)	2010	An aluminum beam (160×30×2.6 mm),two aluminum horns and two Langevin transducers	28 kHz	15V	80mm/s

Table 6.3 : Piezoelectric devices comparison

Devices in Table 6.3 can be seen in different ways. According to their structures, it can be classified into: beam, two Langevin transducers [(Hernandez, 2010), (Jeong, et al., 2007), (Loh, et al., 2000)]; unimorph and bimorph piezoelectric actuators with insulations gaps [(Roh, et al., 2001), (Son, et al., 2006)]; and beam with two non-collocated piezoelectric patches bonded on the beam [(Suybangdum, et al., 2009), (Hariri, et al., 2012),(Hariri, et al., 2012)]. According to their operation principles, these devices can be classified into: one mode excitation traveling wave [(Hernandez, 2010), (Hariri, et al., 2012)]; two modes excitation traveling wave [(Hernandez, 2010), (Hariri, et al., 2012), (Jeong, et al., 2007), (Loh, et al., 2000)]; two standing waves combined to generate a traveling wave [(Roh, et al., 2001)]; and two standing waves for bidirectional motion (each wave for one direction) [(Son, et al., 2006)]. And according to their applications into: an object transport system [(Jeong, et al., 2007), (Loh, et al., 2000), (Roh, et al., 2001), (Suybangdum, et al., 2009)]; pumping

[(Hernandez, 2010)] and robotics [(Son, et al., 2006), (Hariri, et al., 2012), (Hariri, et al., 2012)].

In one side everything is related, speed depends on the applied voltage; frequency depends on dimensions and materials used, also the speed depends on device weight (slider, with or without embedded electronics). In the other hand each design depends in the requested specification. Sometime the frequency can be the issue and we build our design based on this, as did Hernandez in his thesis [(Hernandez, 2010)]. Sometime dimensions can be the issue and we build our system based on that, as we did in this thesis (dimensions of the beam were given). It could be also the speed or the applied voltage.

We will not compare specifications and characteristics for each device relative to the others, because each device has been designed by responding to a given specification. But in general point of view, our robot shows an easy manufacturing process because of its simple structure. Two piezoelectric patches bonded on a beam and that is all. No legs, no teeth are needed, also no Langevin transducers, horns and screws. Also it is easier to miniaturize compared to the others.

The optimal working frequency is a consequence of a given system, even if it was given and the design was based on it. So we will not look at the frequencies of these devices but, a vision of the set of dimensions, applied voltage & speed is important. Basing on that, our robot shows good performance compared to the others, especially because it doesn't use any amplification like teeth or legs.

6.7 Conclusion of this chapter

Two prototypes were fabricated and described in this chapter, robot 1 and robot 2. They were tested experimentally in one mode and two modes excitation in order to validate our simulation results given in the last chapter. Robot 1 that shows better speed was chosen to characterize it. Speed versus applied voltage, speed versus embedded mass and speed versus mechanical force were measured. After characterization, robot 1 is compared with other devices having some common points. Robot 1 has an optimal operating frequency equal to 11.3 kHz, travelling at 131.5 mm/s at 30V amplitude without embedded mass in the case of two modes excitation. At the same voltage, this robot can provide 432 μW (7.2 mN, 60 mm/s). It has an optimal operating frequency equals to 11.6 kHz, travelling at 81.19 mm/s at

30V amplitude without embedded mass in the case of one mode excitation. At the same voltage, this robot can provide 360 μW at its nominal operating point (9 mN, 40 mm/s).

6.8 Appendix

1. Power amplifiers and phase shifter circuits

Schematic circuit for the power amplifier

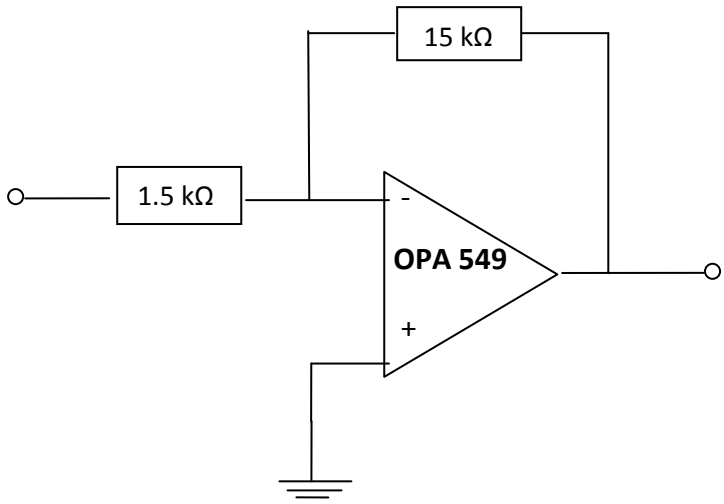

Schematic circuit for phase shifter

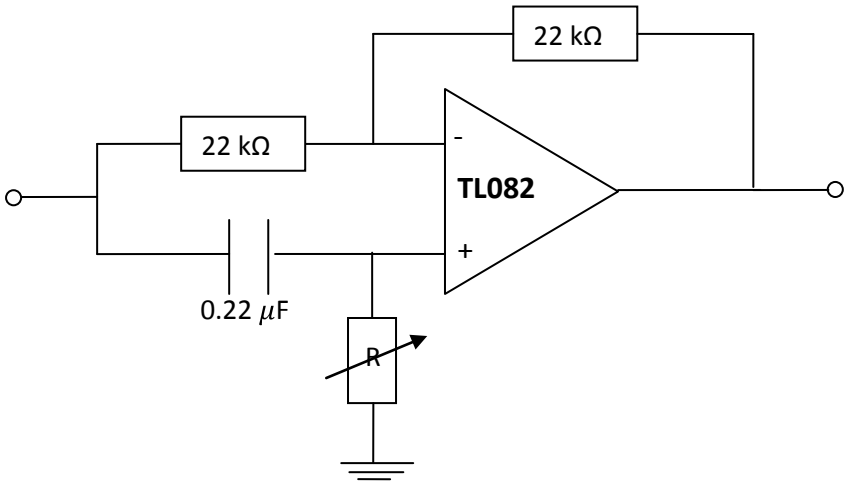

Phase shifter transfer function: $H(jw) = \frac{1-jw\tau}{1+jw\tau}$ where $\tau = 0.22\mu\text{F} \times R$

Gain of the phase shifter: $\|H(jw)\| = 1$

Phase of the phase shifter: $\arg(H(jw)) = \pi - 2\arctan(w\tau)$

Below are the schematic figure and the PCB for the phase shifter and power amplifiers used in our experimental test case of beam robots.

Schematic figure for the phase shifter and power amplifiers

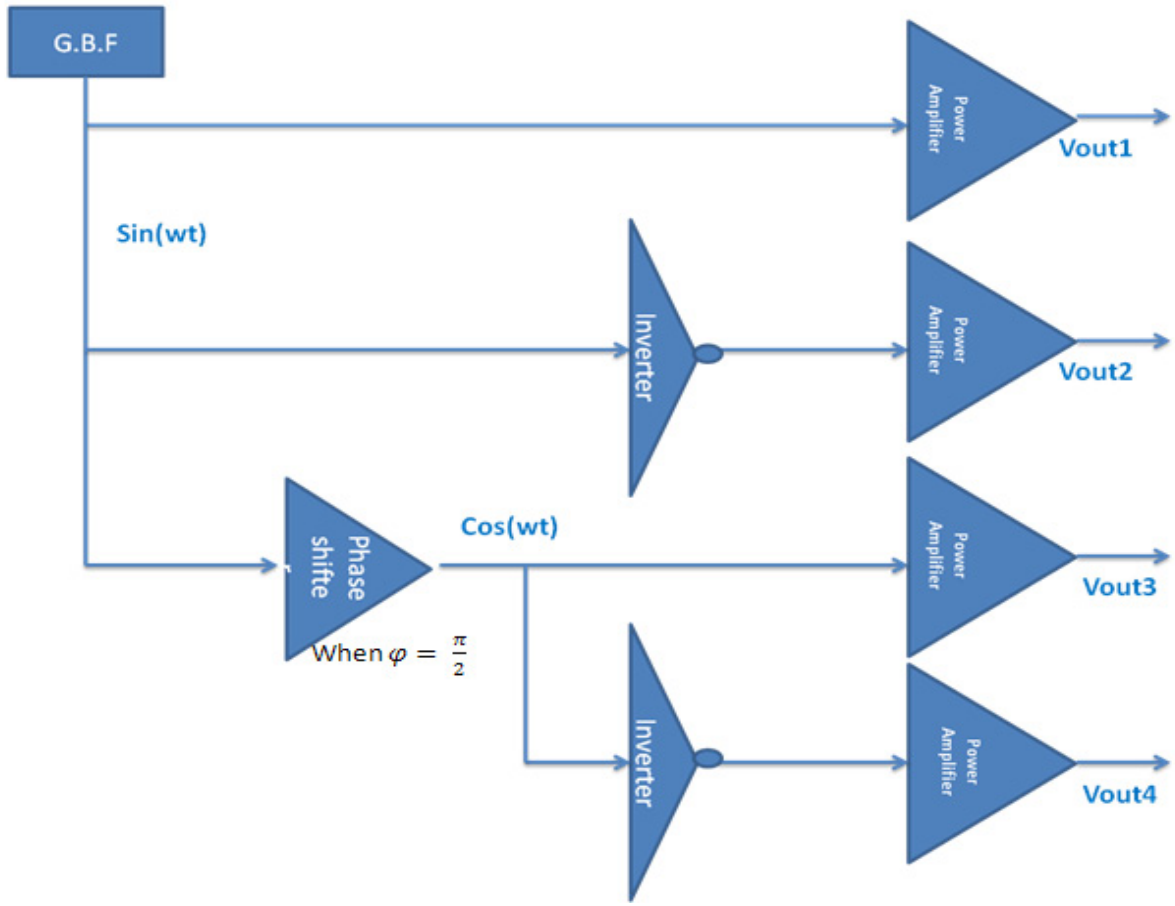

PCB (printed circuit board) for the phase shifter and power amplifiers

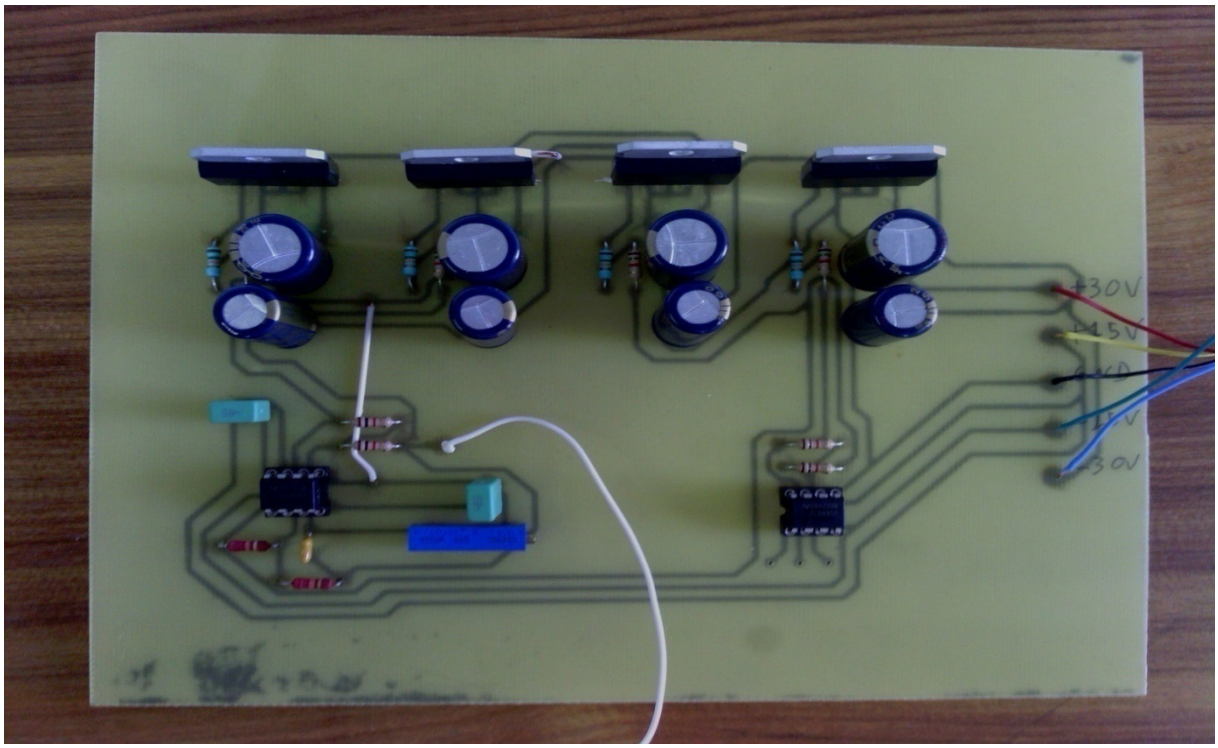

2. *Synthetic inductor circuit*

Grounded inductor given in [(Reza Moheimani, et al., 2006)**]**

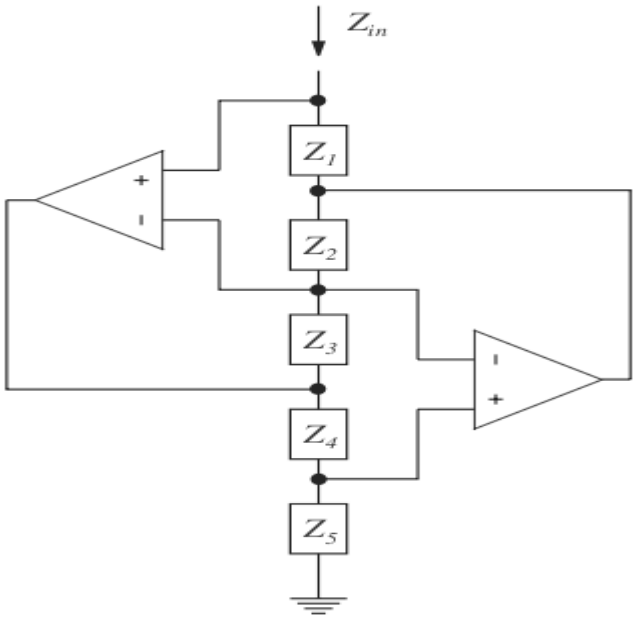

The equivalent impedance observed at the terminals of this synthetic inductor is:

$$Z_{in} = \frac{Z_1 Z_3 Z_5}{Z_2 Z_4}$$

Allowing Z_4 to be a capacitor, C, and replacing other impedances with resistors, the resulting circuit will act as an inductor L = kC, where $k = \frac{R_1 R_3 R_5}{R_2}$ .Below is the circuit test board used in our experimental tests.

Circuit test board for the synthetic inductor

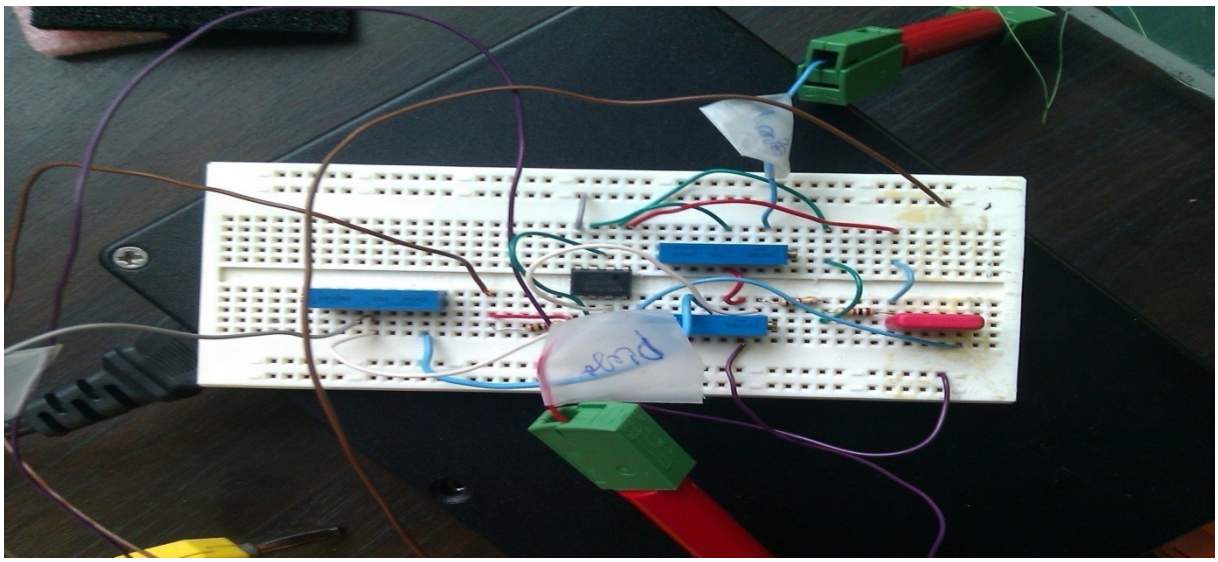

6.9 References

Hariri H., Bernard Y. et Razek A. Modeling and Experimental Study of a one Mode Excitation Travelling Wave Piezoelectric Miniature Robot [Revue] // Journal of vibration and control. - 2012. - p. submitted .

Hariri H., Bernard Y. et Razek A. Modeling and Experimental Study of a Two Modes Excitation Travelling Wave Piezoelectric Miniature Robot [Revue] // Actuator12. - 2012. - pp. pp. 346-349.

Hernandez C. réalisation d'une micropompe à actionnement piézoélectrique [Rapport]. - Gif sur Yvette : Laboratoire de Génie Electrique de Paris, 2010.

Jeong S.H. [et al.] A study on an object transport system using ultrasonic wave excitation [Revue] // Journal of mechanical science and technology. - 2007. - pp. pp. 941-945.

Loh B.G et Ro P.I An object transport systemusing flexural ultrasonic progressive waves generated by two mode excitation [Revue] // IEEE transaction on ultrasonics, ferroelectrics and frequency control. - 2000. - pp. pp. 994-998.

Reza Moheimani S.O. et Fleming Andrew J. Piezoelectric transducers for vibration control and damping [Livre]. - University of Newcastle, University Drive, Callaghan, NSW 2308,Australia : Springer, 2006.

Roh Y., Lee S. et Han W. Design and fabrication of a new traveling wave-type ultrasonic linear motor [Revue] // Sensors and actuators A 94. - 2001. - pp. 205-210.

Son K.J. [et al.] An ultrasonic standing-wave-actuated nano- positioning walking robot: Piezoelectric-metal composite beam modeling [Revue] // Journal of vibration and control,. - 2006. - pp. Vol. 12, no. 12, pp. 1293-1309..

Suybangdum P., Smithmaitrie P. et Laoratanakul P. Dual piezoelectric actuators for the traveling wave ultrasonic linear motor [Revue] // Fourth International Conference on Experimental Mechanics. - 18-20 November 2009.

CHAPTER 7

OVERVIEW

Chapter 7: Overview

List of figures

List of tables

7. 1 Introduction

As said in the forward of this thesis, the aim of this work is to create a traveling wave on a thin plate to move it with multi degrees of freedom using piezoelectric patches (Figure 7.1). Creation of a traveling wave on a thin beam was presented on chapter 5 and chapter 6 (Figure 7.2). Two operation principles are presented and used to move the thin beam using two piezoelectric patches, the one mode excitation and the two modes excitation. The optimal design and the fabrication process were also presented in these chapters.

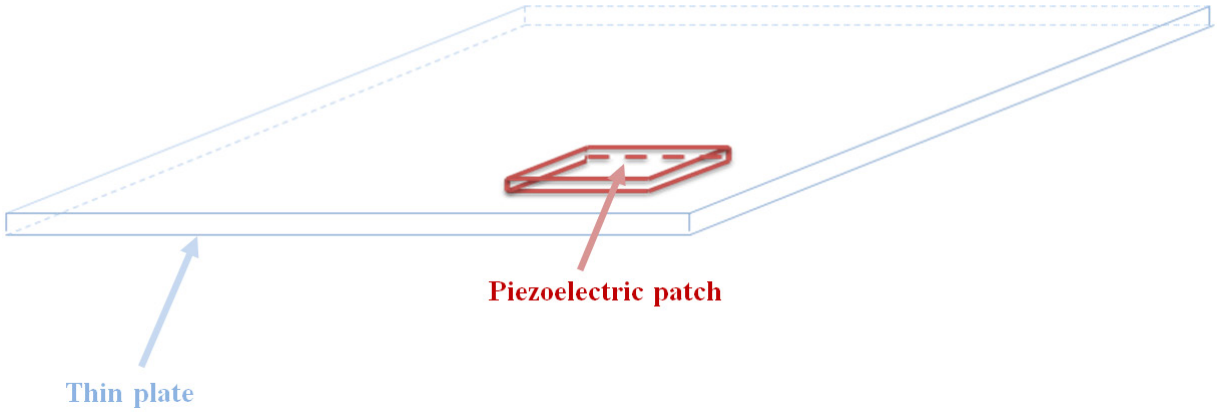

Figure 7.1: One piezoelectric patch bonded on thin plate

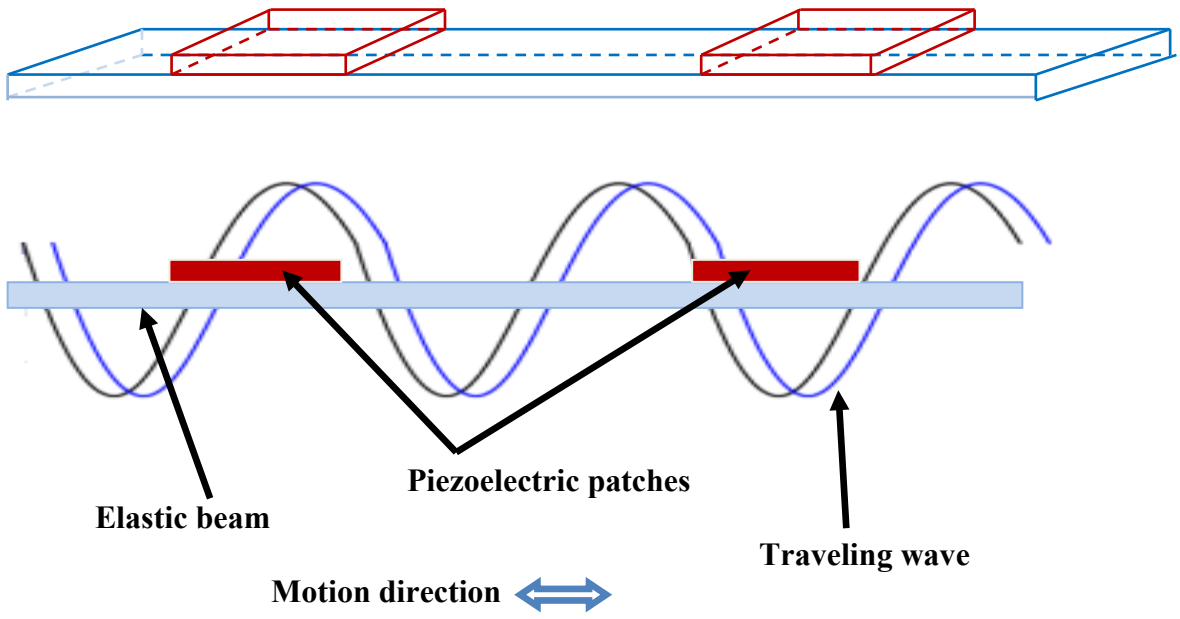

Figure 7.2: Schematic diagram of the traveling wave piezoelectric beam robot. 3D view on the top and side view on the bottom

The creation of a traveling wave on thin plate using piezoelectric patches (Figure 7.1) has not been presented yet. Actually the aim of our work, this traveling wave piezoelectric plate robot

will not be presented in this manuscript. The dimensions, design, fabrication processes, simulation and experimental results have been filed for a patent.

This chapter is entitled overview and I mean by that all other applications could be done using our developed finite element model. First, we will present the possibility to design piezoelectric transformers using our developed finite element model and a prototype will be presented for this purpose. Second, a damping vibration of thin beam and plate will be presented using our developed model and will be verified experimentally. Third active control of flexible structure will be reviewed shortly, then the active control principal using our finite element model is presented by transforming our finite element model into modal space, then into state space equation and at the end of this section transfer functions will be determined. Next, detecting damage in structure by the use of piezoelectric materials is presented and some papers will be cited. We will then talk about the necessity of an optimization topology such as stochastic algorithms in the case of complex structures, some papers will be taken as examples. Finally analytical models versus our finite element model will be presented by citing some analytical papers for thin structures with piezoelectric patches; also an electrical analogy will be given from our finite element model. So we will be able to represent any thin structure with piezoelectric patches actuators/sensors by an electrical equivalent circuit. . Electrical analogy is given in literature by using analytical models. This electrical analogy is also cited.

7. 2 Piezoelectric transformers

Two piezoelectric patches bonded on a plate when one piezoelectric patch is used as actuator while the other is used as sensor can be formed a piezoelectric transformer. A prototype is given in Figure 7.3 while the patch actuator is powered by a sinusoidal voltage of 20V amplitude and the patch sensor is left open circuited. Properties and geometric parameters for this prototype are given in Table 7.1.

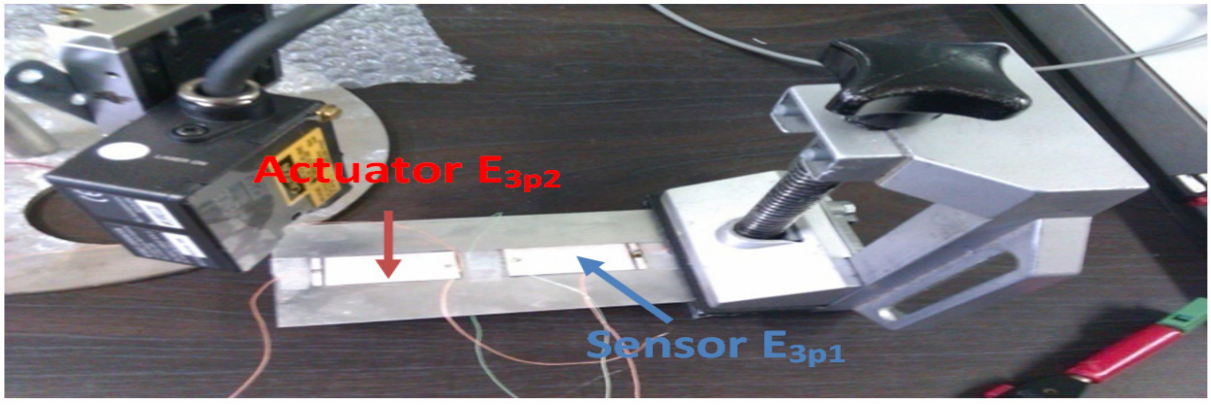

Figure 7.3: Piezoelectric transformers

	PZT (p)	Elastic structure (m)
Young's modulus (Pa)	/	E_m
Poison's ratio	/	υ_m
Volume density (Kg.m^{-3})	ρ_p = 7900	ρ_m
Relative permittivity	ε_{33r} = 1282	/
Piezoelectric constant (m.V^{-1})	d_{31} = - 1.3 × 10^{-10}	/
Elastic compliances (Pa^{-1})	S_{11} = 1.3 × 10^{-11}	/
	S_{12} = -4.76 × 10^{-12}	/
Max peak to peak electric field(V.mm^{-1})	E_{max} = 300	/
Max compressive strength (Pa)	σ_{max}= 600 × 10^6	/
Length × width × thickness (mm^3)	32×17×0.27	100 × 60 × 0.5
(l_p, l_m) × (b_p, b_m) × (t_p, t_m)		
X_{p1}, X_{p2}, y_p (mm)	10,58,21.5	

Table 7.1: Properties and geometry of the system

By using equation 4.12 of chapter 4, which is repeated below, the output voltage can be determined.

$$\left[-(2\pi f_n)^2\begin{bmatrix}M_{mm} & 0 & 0\\ 0 & 0 & 0\\ 0 & 0 & 0\end{bmatrix}+\mathrm{j}(2\pi f_n)\begin{bmatrix}C_{mm} & 0 & 0\\ 0 & 0 & 0\\ 0 & 0 & 0\end{bmatrix}+\right.$$

$$\left.\begin{bmatrix}K_{mm}-K_{mvp2}K_{vvp2}^{-1}K_{vmp2} & K_{mvp1} & K_{mvp2}K_{vvp2}^{-1}\\ K_{vmp1} & K_{vvp1} & 0\\ -K_{vvp2}^{-1}K_{vmp2} & 0 & K_{vvp2}^{-1}\end{bmatrix}\right]\begin{bmatrix}U_i\\ E_{3p1}\\ t_pQ_{p2}\end{bmatrix}=\begin{bmatrix}0\\ 0\\ E_{3p2}\end{bmatrix}$$

7. 1

Simulations and experimental results are shown in Table 7.2 at a sinusoidal voltage of 20V for different frequencies. Noting that the prototype is not optimized for a given application, however our model can be used for optimal design by responding to desired specifications. This work is presented in [(Hariri, et al., 2012)].

Frequency (Hz)		**V_{in} (volt)**	**V_{out} (volt)**	
Simulation	**Experimental**		**Simulation**	**Experimental**
f1 = 48.32	**f1** = 43.5	20	2.1	2
f3 = 300	**f3** = 271	20	4.1	4
f5 = 841	**f5** = 905	20	14.2	14.5
f10 = 1906	**f10** = 1855	20	29.05	29
f14 = 2778	**f14** = 2750	20	12.09	12

Table 7.2: Simulations and experimental results for the piezoelectric transformer

7. 3 Damping vibration of thin beams and plates

Two systems are used to study in this section. The first one is a fixed-free thin beam with two piezoelectric batches bonded on it, the patch 1 (p1) near from the fixed end plays the role of a source of vibration and it is actuated by a sinusoidal voltage at the fourth resonance frequency (f_4= 486.85 Hz) and the role of the patch 2 (p2) near from the free end is to damp this vibration at the tip of the beam where three impedances (R, series RL and parallel RL) are connected successively at p2 (Figure 7.4).

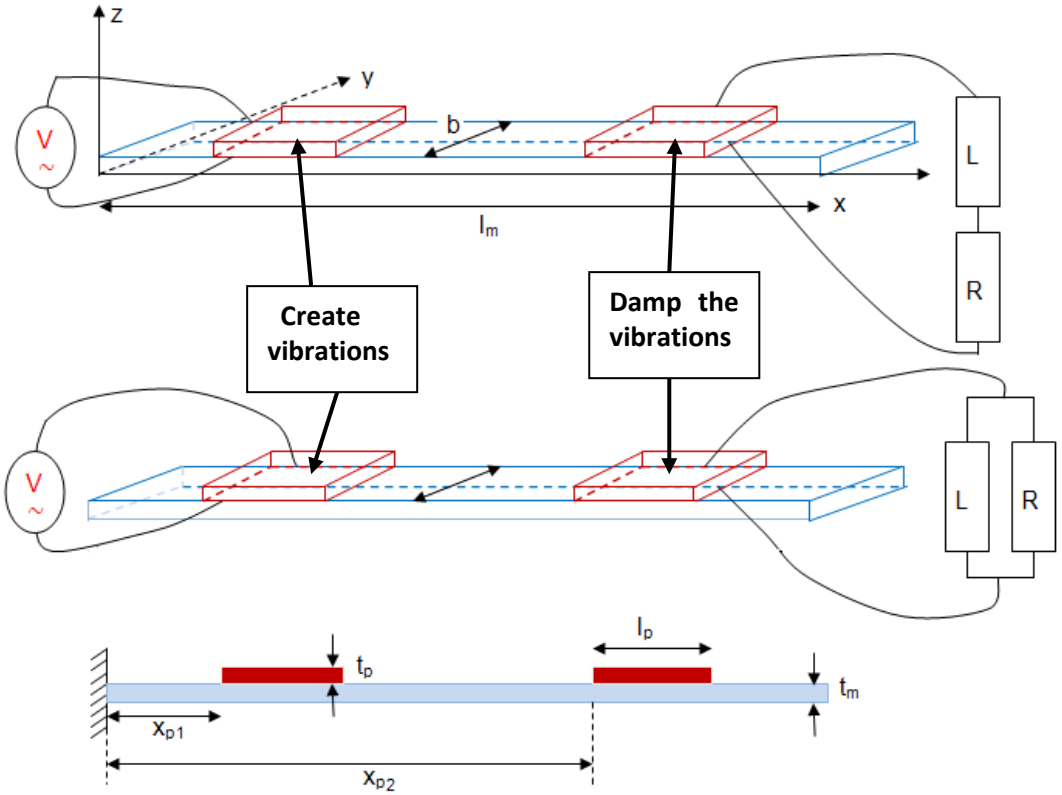

Figure 7.4: Geometric parameters of the beam with non-collocated PZT actuator/sensor and RL shunt circuits bonded to sensor face

These kinds of circuits (R, series RL and parallel RL) are known in the literature by the single mode damping [(Reza Moheimani, et al., 2006)] because they are able to suppress the vibration for one single frequency i.e. for each frequency there is an optimal electric circuit. We are taken, the fourth resonant mode of vibration at frequency f_4= 486.85 Hz to determine optimal values of the electrical circuits. The process stills the same for any other frequency.

The second system taken is a fixed-free thin plate with two piezoelectric patches bonded on it. In this system the patch 2 (p2) near from the free end is used as a source of vibration when a 20 volt sinusoidal voltage is applied and the patch 1 (p1) near from the fixed end is connected to a 50kΩ shunt resistance (Figure 7.5).

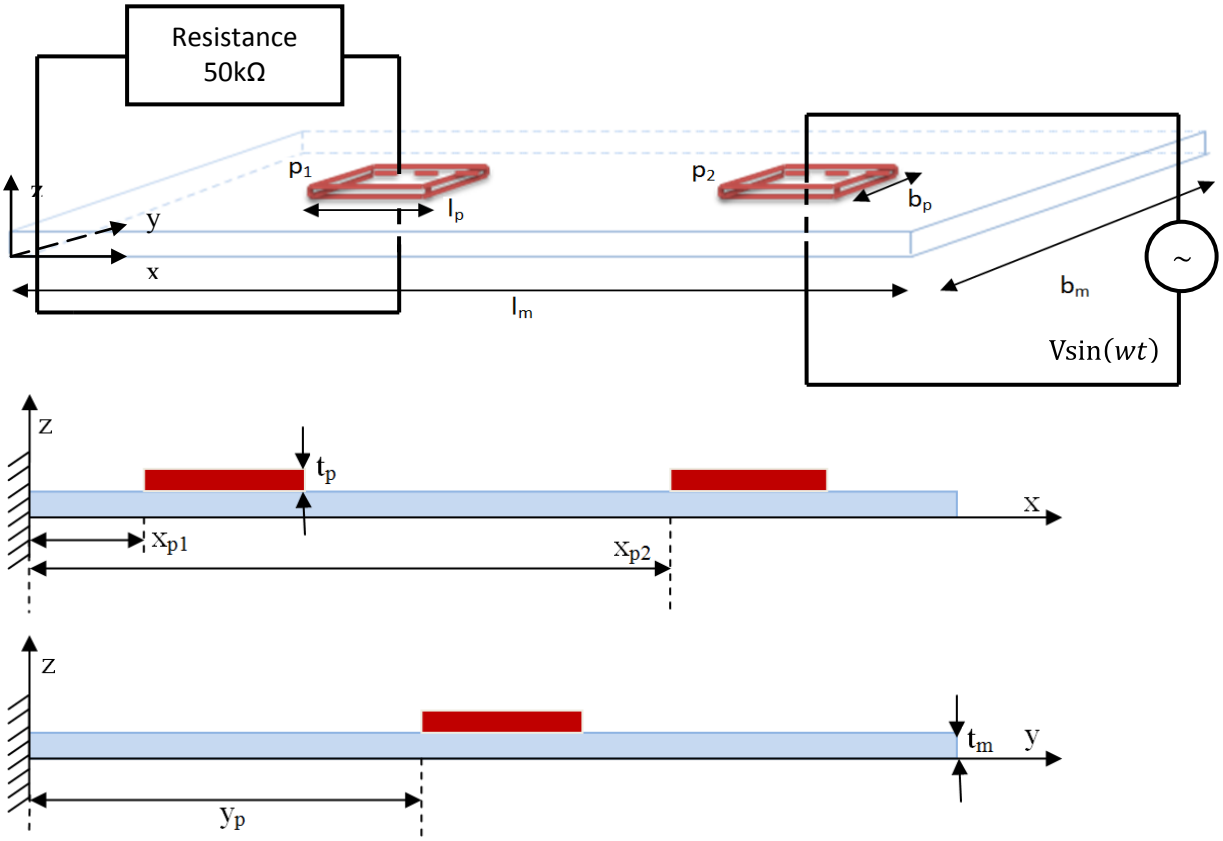

Figure 7.5: Geometric parameters of the plate with non-collocated PZT actuator/sensor and R shunt circuits bonded to sensor face

The idea behind this configuration was to see if damping near from the fixed end where there are large strains and small displacements can be more effective than near from the free end where there are large displacements and small strains. For this purpose, displacements at the tip of the plate are compared in the case of 50kΩ resistance shunt circuit and in the case of an open circuit. No optimal resistance is determined for this system. Optimal R, optimal series RL and optimal parallel RL values are determined below in the case of thin beam; in the case of plate we can flow the same process.

Properties and geometric parameters for these two systems presented in Figure 7.4 and Figure 7.5 are given in Table 7.3.

	PZT (p)	Elastic structure (m)
Young's modulus (Pa)	/	$c_m = 69 \times 10^9$
Poison's ratio	/	$\upsilon_m = 0.33$
Volume density (Kg.m^{-3})	$\rho_p = 7900$	$\rho_m = 2700$
Relative permittivity	$\varepsilon_{33r} = 1282$	/
Piezoelectric constant (m.V^{-1})	$d_{31} = -1.3 \times 10^{-10}$	/
Elastic compliances (Pa^{-1})	$S_{11} = 1.3 \times 10^{-11}$	/
	$S_{12} = -4.76 \times 10^{-12}$	/
Max peak to peak electric field(V.mm^{-1})	$E_{max} =$ 300	/
Max compressive strength (Pa)	$\sigma_{max} = 600 \times 10^6$	/
Plate dimensions		
Length × width × thickness (mm^3)	32×17×0.27	100 × 60 × 0.5
(l_p, l_m) × (b_p, b_m) × (t_p, t_m)		
Beam dimensions		
Length × width × thickness (mm^3)	32×17×0.27	180 × 17 × 0.5
(l_p, l_m) × (b_p, b_m) × (t_p, t_m)		
Piezo positions case of beam		
X_{p1}, X_{p2}(mm)	24,126	
Piezo positions case of plate		
X_{p1}, X_{p2},Y_p(mm)	10,58,21.5	

Table 7.3: Properties and geometry of the system

By using equation 7. 2, R, series RL and parallel RL optimal values are determined in the case of the beam where p1 is used as actuator and p2 is connected to the shunt circuit.

$$\left[-(2\pi f_n)^2\begin{bmatrix} M_{mm} & 0 & 0 \\ 0 & 0 & 0 \\ 0 & 0 & 0 \end{bmatrix} + \mathrm{j}(2\pi f_n)\begin{bmatrix} C_{mm} & 0 & 0 \\ 0 & 0 & 0 \\ 0 & 0 & -\frac{z_e}{t_p^2} \end{bmatrix} + \right.$$

$$\left.\begin{bmatrix} K_{mm} - K_{mvp1}K_{vvp1}^{-1}K_{vmp1} - K_{mvp2}K_{vvp2}^{-1}K_{vmp2} & K_{mvp1}K_{vvp1}^{-1} & K_{mvp2}K_{vvp2}^{-1} \\ -K_{vvp1}^{-1}K_{vmp1} & K_{vvp1}^{-1} & 0 \\ -K_{vvp2}^{-1}K_{vmp2} & 0 & K_{vvp2}^{-1} \end{bmatrix}\right]\begin{bmatrix} U_i \\ t_pQ_{p1} \\ t_pQ_{p2} \end{bmatrix} = \begin{bmatrix} 0 \\ E_{3p1} \\ 0 \end{bmatrix}$$

7. 2

Where z_e is the electrical impedance of the circuit and is written as

$$z_e = \begin{cases} R \\ jwL + R \ \ (series) \\ \frac{jwLR}{jwL+R} \ \ (parallel) \end{cases}$$

Where w is the frequency of the applied electric field E_{3p1}, L and R are the inductance and the resistance of the electrical circuit connected to the piezoelectric patch number two (p2).

Figure 7.6 shows displacement comparison between open circuit, optimal resistance shunt circuit, optimal RL shunt circuit in both series and parallel connections obtained by Hariri et al. in their paper [(Hariri, et al., 2011)]. The vibration suppression performance is evaluated

based on amplitude of the displacement. The best performance is obtained for minimal displacement. According to Figure 7.6, the optimal RL parallel shunt circuit shows a performance slightly better than the RL series shunt circuit.

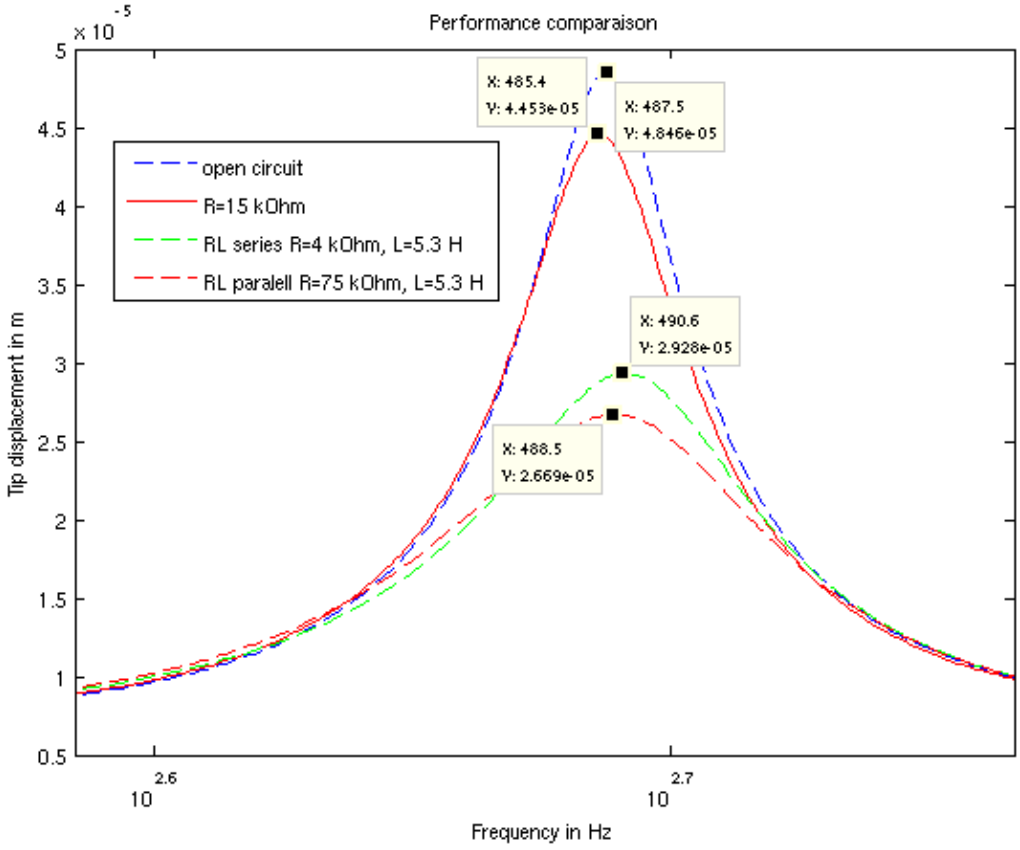

Figure 7.6: Performance comparison between shunt circuits

Figure 7.7 and Figure 7.8 show how the frequency depends on the value of R only in the case of small values of R compared to jwL in the case of series RL circuit and only in the case of large values of R compared to jwL in the case of parallel RL circuit. These results are given by Hariri et al in [(Hariri, et al., 2011)]. In this case L has to be readjusted again to tune the new resonant frequency. In all other cases, the variation of the frequency can be considered as negligible.

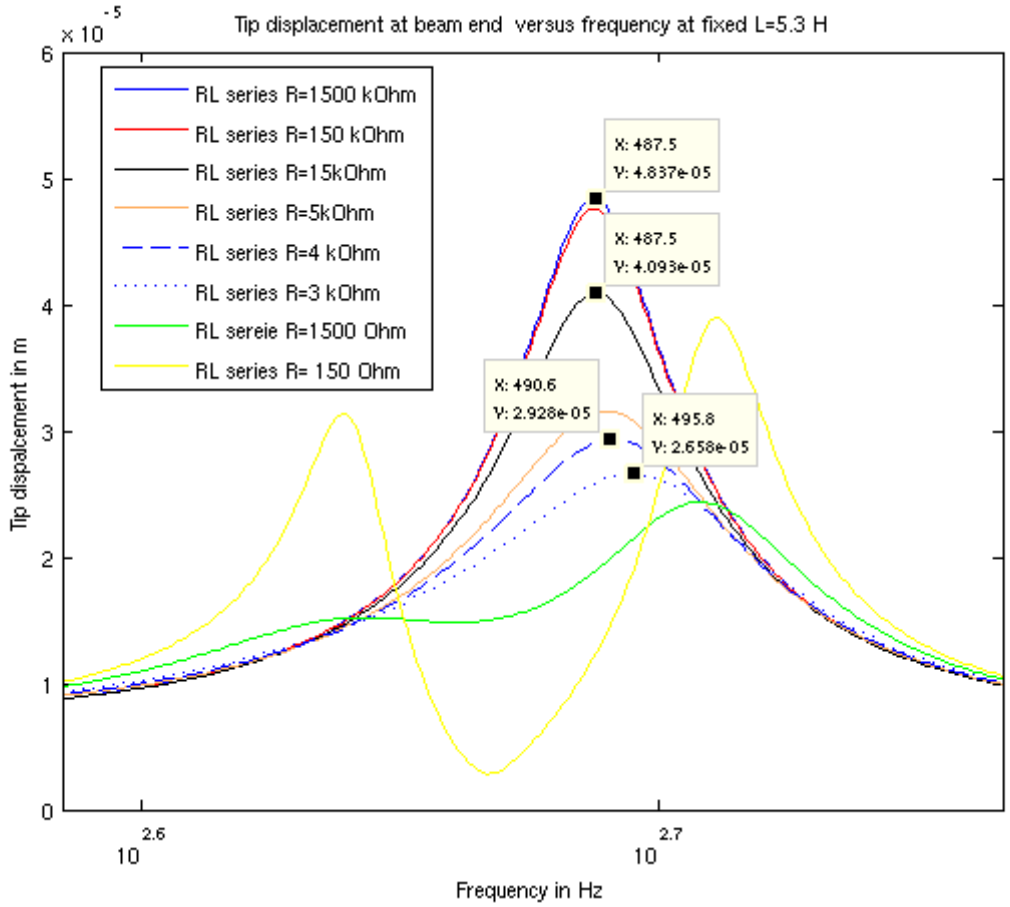

Figure 7.7: Optimal R value for series connection

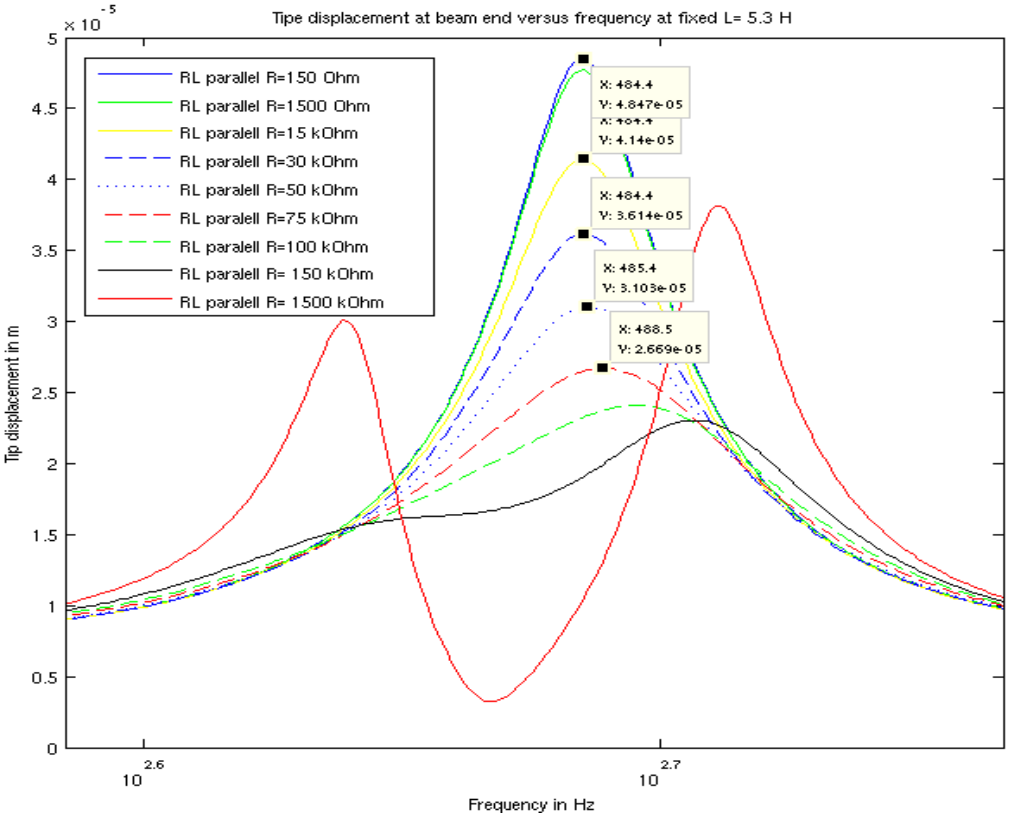

Figure 7.8: Optimal R value for parallel connection

Returning to the second system, the voltage obtained at the patch 1 (p1) with 50kΩ resistance shunt circuit (near from the fixed end) is compared with the case of an open circuit determined above in section "piezoelectric transformers'' Table 7.2. Simulation results are given in Table 7.4 and are obtained using equation 7. 3.

$$\left[-(2\pi f_n)^2\begin{bmatrix}M_{mm} & 0 & 0\\ 0 & 0 & 0\\ 0 & 0 & 0\end{bmatrix}+\mathrm{j}(2\pi f_n)\begin{bmatrix}C_{mm} & 0 & 0\\ 0 & 0 & -\frac{R}{t_p^2}\\ 0 & 0 & 0\end{bmatrix}+\right.$$

$$\left.\begin{bmatrix}K_{mm}-K_{mvp1}K_{vvp1}^{-1}K_{vmp1}-K_{mvp2}K_{vvp2}^{-1}K_{vmp2} & K_{mvp1}K_{vvp1}^{-1} & K_{mvp2}K_{vvp2}^{-1}\\ -K_{vvp1}^{-1}K_{vmp1} & K_{vvp1}^{-1} & 0\\ -K_{vvp2}^{-1}K_{vmp2} & 0 & K_{vvp2}^{-1}\end{bmatrix}\right]\begin{bmatrix}U_i\\ t_pQ_{p1}\\ t_pQ_{p2}\end{bmatrix}=\begin{bmatrix}0\\ 0\\ E_{3p2}\end{bmatrix}$$

7. 3

Frequency	*Open circuit (2D FE model)*	*Resistance circuit (2D FE model)*
f1	2.1 V	0.53 V
f3	4.1 V	3.41 V
f5	14.2 V	12.9 V
f10	29.05 V	28.8 V
f14	12.09 V	11.8 V

Table 7.4: Voltages obtained by simulation case of resistance shunt circuit

An experimental setup shown in Figure 7.9 is used to verify the simulation results obtained in Table 7.4.

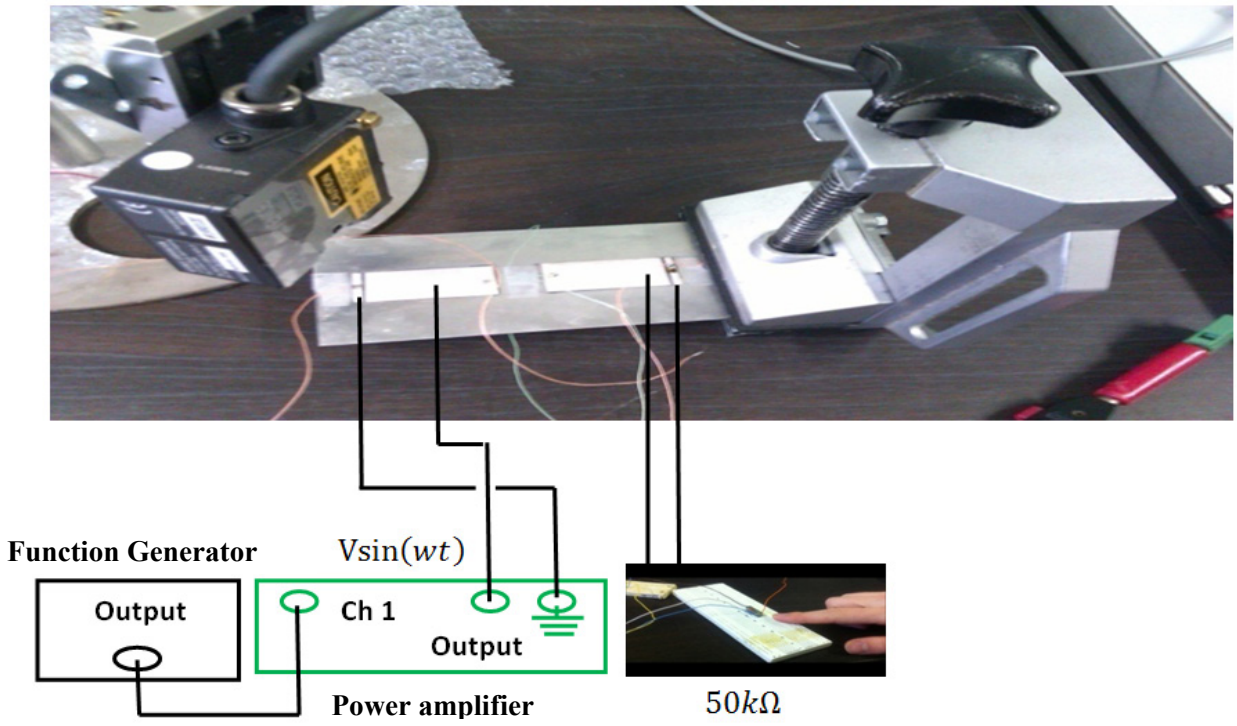

Figure 7.9: Experimental setup case of resistance shunt circuit

Experimental results are given in Table 7.5. These results are given by Hariri et al. in their paper [(Hariri, et al., 2012)].

Frequency	*Open circuit (experimentally)*	*Resistance circuit (experimentally)*
f1	2 V	0.5 V
f3	4 V	3.4 V
f5	14.5 V	12.5 V
f10	29 V	28.8 V
f14	12 V	11.8 V

Table 7.5: Voltages obtained experimentally case of resistance shunt circuit

Displacements at the tip of the plate were measured experimentally and shown a good ratio of damping. Actually, these results are not recorded during the experimental measurements. But by seeing Table 7.5, we can note decreases in voltage for different applied frequencies, which means decreases in strains near from the fixed end of the beam. Also Figure 7.6 gives an idea about the damping efficiency of a resistance compared to RL circuits and without forgetting that this resistance was chosen arbitrary and was not optimized. An optimization process can be done by following the same procedure as the case of beam.

It should be noted that the problem of piezoelectric shunt damping can be interpreted as a feedback control problem and vice versa [(Reza Moheimani, et al., 2006)].

7. 4 Active control of flexible structures

Our model can be used to control the structure by transforming the finite element model in nodal variables into modal model and then into state space. Therefore our system is represented by the state space equation. Then controller can be designed to reject external disturbances for example (no useful vibrations) or in order to maintain a desired shape [(Amitesh Punhani, 2008), (Yasin, et al., 2010)]. Particularly in our case, controller can be designed to control the vibration of the beam/plate in order to damp it or to generate a traveling wave instead of the passive circuits use. Kermani et al. in their paper [(Kermani, et al., 2003)] designed an LQR feedback controller on a simple cantilever beam using the state space equation in order to suppress the vibration at the end of the beam and they studied the influence of length and position of piezoelectric patch to the control efficiency. But that is not the only method, sometimes controller can be added directly to the finite element equation without transforming it into state space equation [(Liu, et al., 1999)]. Liu et al in their paper used a simple gain feedback control where the lower order modes which are predominant are considered in their vibration suppression problems, they incorporate the gain controller directly in the damping matrix of the finite element equation and they studied also the

influence of piezoelectric sensors/actuators position of on plate response using their gain controller. Actually, when we are interested in control, we can experimentally identify our system by using the black box system identification technique [(Reza Moheimani, et al., 2006)]. The books ‘’piezoelectric transducers for vibration control and damping’’ [(Reza Moheimani, et al., 2006)] and ‘’piezoelectric based vibration control from macro to micro-nano scale systems’’ [(Jalili, 2009)] include a big review for interested readers in vibration control of structure. Also a review on static and dynamic shape control of structures by piezoelectric actuation is given by Irschik in his paper [(Irschik, 2002)].

A schematic diagram for active control using two non-collocated piezoelectric patches for a flexible structure subjected to unnecessary disturbance is shown in Figure 7.10.

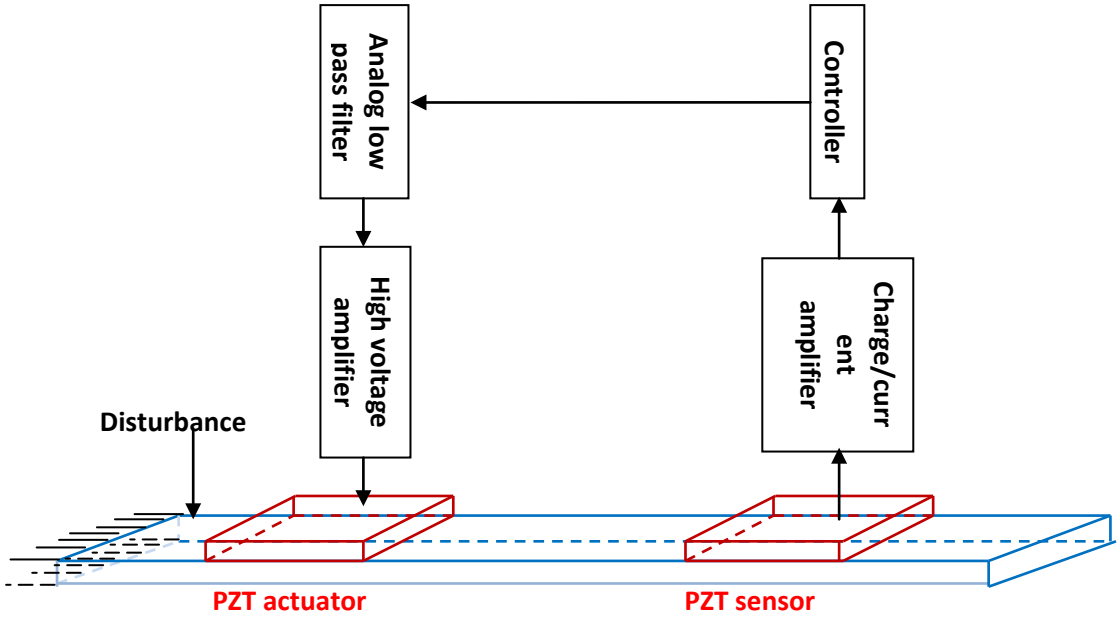

Figure 7.10: A schematic diagram for active control using two-non-collocated patches for a flexible structure subjected to unnecessary disturbance

This figure is taken in the case of a beam structure but nothing changes if it was taken in the case of a plate structure.

Our finite element model in nodal variables for piezoelectric patches bonded on thin structure (beam and plate) is given by equation 3.58. Equation 3.58 can be rewritten as below, where ‘’pa’’ for patches actuators, ‘’ps’’ for patches sensors and F_m is the body applied forces.

$$\begin{bmatrix} M_{mm} & 0 & 0 \\ 0 & 0 & 0 \\ 0 & 0 & 0 \end{bmatrix} \begin{bmatrix} \ddot{u}_m \\ \ddot{E}_{3pa} \\ \ddot{E}_{3ps} \end{bmatrix} + \begin{bmatrix} C_{mm} & 0 & 0 \\ 0 & 0 & 0 \\ 0 & 0 & 0 \end{bmatrix} \begin{bmatrix} \dot{u}_m \\ \dot{E}_{3pa} \\ \dot{E}_{3ps} \end{bmatrix} + \begin{bmatrix} K_{mm} & K_{mvpa} & K_{mvps} \\ K_{vmpa} & K_{vvpa} & 0 \\ K_{vmps} & 0 & K_{vvps} \end{bmatrix} \begin{bmatrix} u_m \\ E_{3pa} \\ E_{3ps} \end{bmatrix} = \begin{bmatrix} F_m \\ t_p Q_{pa} \\ 0 \end{bmatrix} \quad (7.4)$$

Then this equation can be rewritten as follows

$$K_{vmps}u_m + K_{vvps}E_{3ps} = 0$$

7.5

$$M_{mm}\ddot{u}_m + C_{mm}\dot{u}_m + K_{mod}u_m = F_m - K_{mvpa}E_{3pa}$$

7.6

Where $K_{mod} = [K_{mm} - K_{mvps}K_{vvps}^{-1}K_{vmps}]$ is the modified stiffness.

Where (7.5) is the sensor equation and (7.6) is the dynamic equation of motion

Equations (7.6) can be written into modal space as

$$\ddot{q} + \Lambda\dot{q} + \Omega^2 q = \Phi^{\mathrm{T}}[F_m - K_{mvpa}E_{3pa}]$$

7.7

And equation (7.5) as the following

$$K_{vmps}\,\Phi q + K_{vvps}E_{3ps} = 0$$

7.8

q is a new variable derived by the following model transformation: $u_m = \Phi q$, where Φ is a modal matrix consisting of n natural modes of the system and can be expressed as

$\Phi = [\phi_1\ \phi_2\ \ldots.\ \phi_n]$

Where each column of this matrix equation is the eigen vector corresponding to each of the eigen values, Φ^{T} is Φ transposed, Ω is the matrix of the natural frequency and it is defined as

$$\Omega = diag(\,w_1\ w_2\ \ldots.\ w_n\,)$$

Where w_i is the ith natural frequency of the system and Λ is the diagonal modal damping matrix with the generic term $(2\xi_i w_i)$, where ξ_i is the modal damping ratio.

Interested readers refer to [(Yasin, et al., 2010), (Alazard, et al., 2000)], for more details about how we obtained these equations (equations 7. 7 & 7. 8). Also, the calculation of the transfer functions based on the modal decomposition (equations 7. 7 & 7. 8) is a well known technique in dynamic analysis of structures; some examples are given in [(De boe, 2003)]. The transfer functions are widely used in control of structures.

The system equation (7.7 & 7.8) can be written in terms of the state space as follows

$$\dot{x} = Ax + Bu$$

7.9

$$x = \begin{bmatrix} q \\ \dot{q} \end{bmatrix},\ A = \begin{bmatrix} 0 & I \\ -\Omega^2 & -\Lambda \end{bmatrix},\ B = \begin{bmatrix} 0 & 0 \\ \Phi^{\mathrm{T}} & -\Phi^{\mathrm{T}}K_{mvpa} \end{bmatrix},\ u = \begin{bmatrix} F_m \\ E_{3pa} \end{bmatrix}$$

And the output equation that relates the sensor voltage generated over piezoelectric patches to the state vector x is expressed as

$$y = Cx$$

7. 10

Where

$$y = \begin{bmatrix} E_{3ps} \\ \dot{E}_{3ps} \end{bmatrix},\ C = \begin{bmatrix} -k_{vvps}^{-1} K_{vmps} \Phi & 0 \\ 0 & -k_{vvps}^{-1} K_{vmps} \Phi \end{bmatrix}$$

As we said above, another very useful representation of the system to design controller is the transfer function representation and it is derived from the system equation in modal space (7.7 & 7.8). Two transfer functions are given by the following, G_{UEa} that represents the vector of applied actuator electric fields $E_{3pa}(s) = [E_{3pa1}(s), \ldots., E_{3pan}(s)]$ for n actuator to the beam deflection $u_m(s)$ (transverse displacement) and G_{EsEa} that relating the electric fields applied to the piezoelectric actuators $E_{3pa}(s) = [E_{3pa1}(s), \ldots., E_{3pan}(s)]$ to the electric fields measured at the piezoelectric sensors $E_{3ps}(s) = [E_{3ps1}(s), \ldots., E_{3psn}(s)]$ for n sensor (Figure 7.11). The following transfer functions are determined in the case of no applied forces ($F_m = 0$).

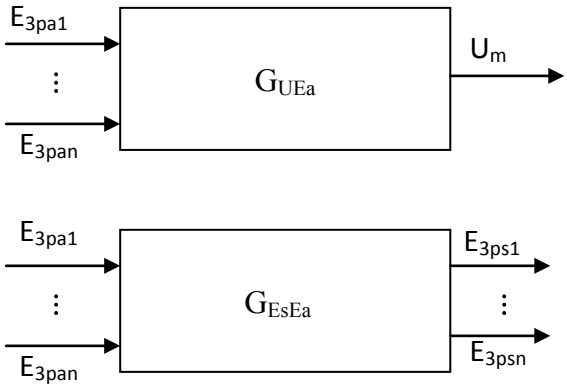

Figure 7.11: Schematic blocks of transfer functions

Applying the Laplace transform to (equations 7.7 & 7.8), assuming zero initial conditions, we obtain:

$$G_{UEa}(s) = \frac{U_m(s)}{E_{3pa}(s)} = \Phi \frac{1}{s^2 + s\Lambda + \Omega^2} \Phi^T [-K_{mvpa}]$$

7. 11

The transfer function at the specified position k is given by

$$G_{UEa}^{(k)}(s) = \Phi^{(k)} \frac{1}{s^2 + s\Lambda + \Omega^2} \Phi^{T(k)} [-K_{mvpa}]$$

7. 12

where $\Phi^{(k)} = [\phi_1^{(k)}\ \phi_2^{(k)}\ \ldots.\ \phi_n^{(k)}]$, $\phi_i^{(k)}$ is associated with the number of the coordinate of the position k.

$$G_{EsEa}(s) = \frac{E_{3ps}(s)}{E_{3pa}(s)} = [-k_{vvps}^{-1} K_{vmps}] \frac{1}{s^2 + s\Lambda + \Omega^2} \Phi\Phi^T [-K_{mvpa}]$$

7. 13

Taken the particular case of two piezoelectric patches where patch p1 functions as actuator and patch p2 functions as sensor then

$$G_{Es2Ea1}(s) = \frac{E_{3ps2}(s)}{E_{3pa1}(s)} = [-k_{vvps2}^{-1} K_{vmps2}] \frac{1}{s^2 + s\Lambda + \Omega^2} \Phi\Phi^T [-K_{mvpa1}]$$

7. 14

7. 5 Piezoelectric patches damage detection

Thanks to their electromechanical conversion ability, the piezoelectric transducers are used to detect damage in structures. Two approaches are used; in the first approach, piezoelectric patches are used as actuators and sensors while in the second approach all patches are used as sensors.

Highlighting a structural damage in the first approach is possible by measuring the Lamb waves [(Lemistre, et al., 2000)] or the electrical impedance spectrum [(Chaudhry, et al., 1994)] as shown in Figure 7.12. A variation of the propagation characteristics of the Lamb wave or a change in the electrical impedance spectrum comparing with a healthy structure indicates the presence of damage. The two piezoelectric patches are used to create lamb waves, measure its characteristic and the electrical impedance spectrum.

Note that, damage in the structure is introduced by reducing the stiffness associated on a mesh of the structure.

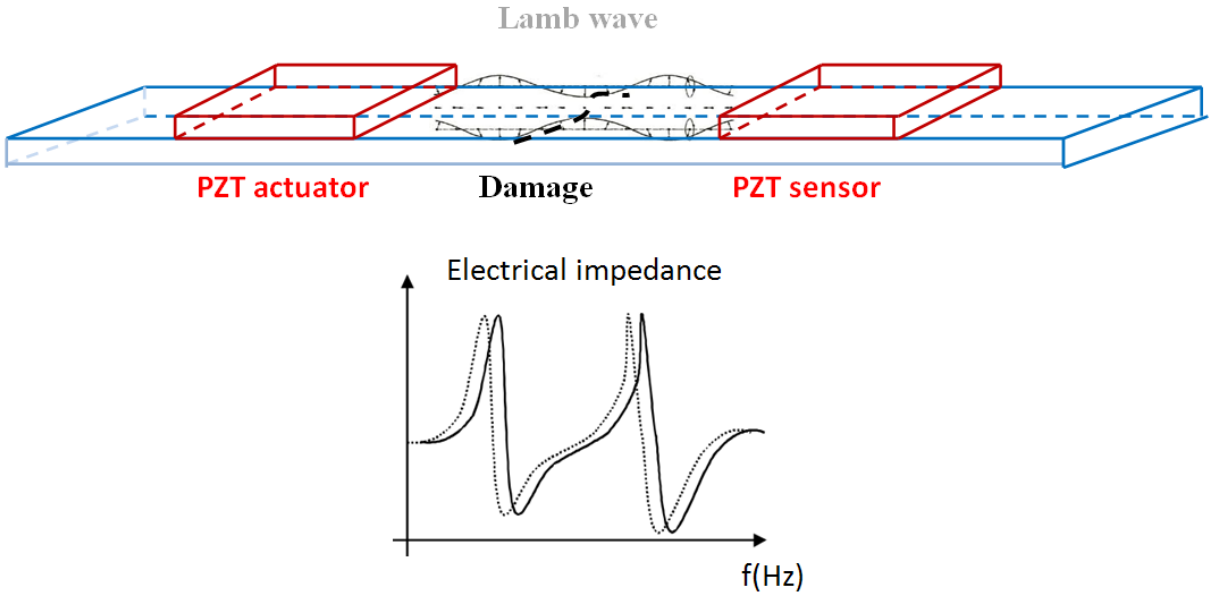

Figure 7.12: Damage detection using two piezoelectric transducers

In the second approach all piezoelectric patches are used as sensors to collocate data needed in this approach (Figure 7.13).

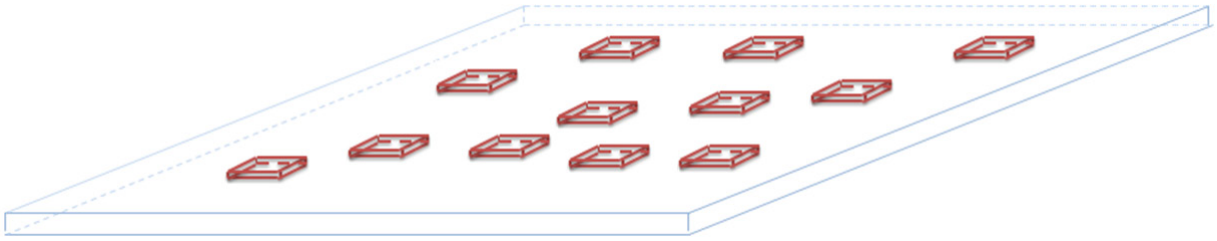

Figure 7.13: Plate with non-collocated piezoelectric sensors

The same as the first approach, the damage should be introduced in the model, and then a comparison with a healthy structure will be done. To detect damage using this approach (all patches are sensors) two techniques are used. The first is the minimization of errors in constitutive equations technique (MECE) and the second is a statistical approach by the principal component analysis (PCA). Examples about how to use these two techniques in structures by the use of piezoelectric materials can be found in thesis of Pascal de Boe (De boe, 2003). Detecting damage in structure by the use of piezoelectric materials is also presented in many papers in literature. The following three papers are taken as examples [(Li, et al., 2012), (Qu, et al., 2006), (Yan, et al., 2002)].

7. 6 Optimization topology

As we have seen in chapter 5, a deterministic optimization is done to obtain the optimal dimensions of piezoelectric patches, material used for the beam, optimal piezoelectric patches positions, and optimal operating frequency. Of course, not forgetting the load coupled on the patch piezoelectric sensor. The power consumed by the load depends on the load itself, on the piezoelectric patches actuators/sensors positions, on frequency, also piezoelectric patches dimensions.

Deterministic algorithm is not convenient when we are studying optimization for complex structures (case of plate for example with many piezoelectric patches actuators/sensors with different load coupled), computation time becomes longer when we scan all the space. Some stochastic algorithms based on finite element analysis are proposed in literatures. For example, Moita et al. [(Moita, et al., 2006)] proposed an algorithm to design laminated structures using piezoelectric materials; Nakasone et al. [(Nakasone, et al., 2008)] proposed an optimization topology to design piezoelectric sensors, actuators and energy harvesting devices. Hadjigeorgiou et al. [(Hadjigeorgiou, et al., 2006)] proposed a genetic optimization

for a beam with piezoelectric actuation to determine the optimal values for the location of the piezo-actuators, the optimal voltages for shape control and damage identification. Finite element method based design and optimization methodology for piezoelectric ultrasonic motors is given in [(Flueckiger, et al., 2010)]. Vibration control of smart hull structure with optimally placed piezoelectric actuators is studied in [(Sohn, et al., 2011)] using the finite element method. An optimization approach to optimal placement of collocated piezoelectric actuators and sensors on a thin plate is given in [(Halim, et al., 2001)].

7. 7 Analytical model versus finite element model

Two configurations are taken for our system in the case of beam structure, the one mode and the two modes excitation. Schematic figures for these two models are given again below

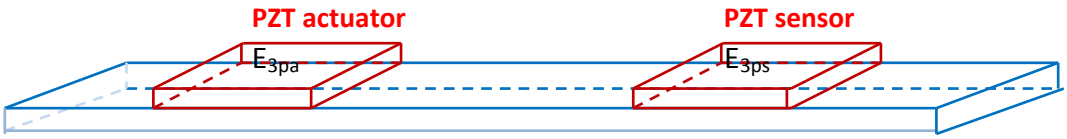

Figure 7.14: System 1: one mode excitation

Figure 7.15: System 2: two modes excitation

The transfer functions obtained in section 7.4 using our developed finite element model allow us to represent these two systems by the blocks below, where each block corresponds to a known transfer function.

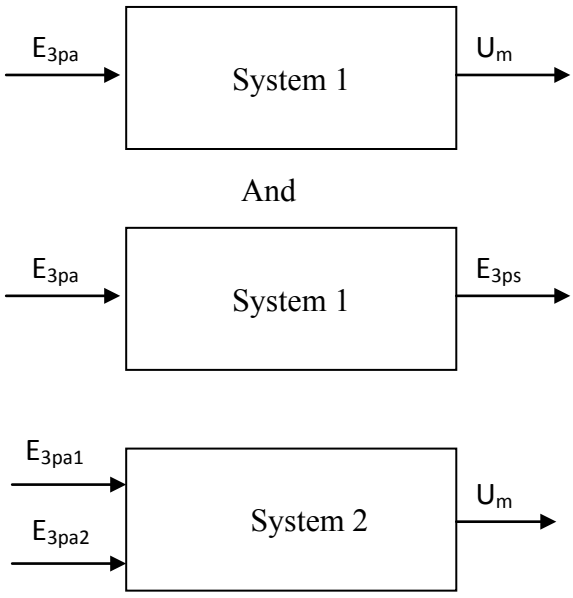

Figure 7.16: Blocks diagrams for system one and two

An electrical representation for the flexural vibration of a beam is proposed in [(Hernandez, 2010), (Sashida, et al., 1993)], their representation consists of considering the beam as an electrical transmission line. A transmission line is identified by its characteristic impedance which is the ratio of the voltage over the current for a signal anywhere along it. Similarly for the beam, it is possible to find a relationship between the forces and velocities at any point on it, giving in this manner the acoustic characteristic impedance for a flexural vibration of a beam. It was used by Hernandez [(Hernandez, 2010)] that $Z_{beam} = \frac{\gamma^3 YI}{w}$ where γ is the wave number of the beam, Y is the Young modulus, I is the moment of inertia and w is the applied frequency.

Applying this technique to the system 1, an electrical equivalent model for the system 1 can be constructed as shown in Figure 7.17.

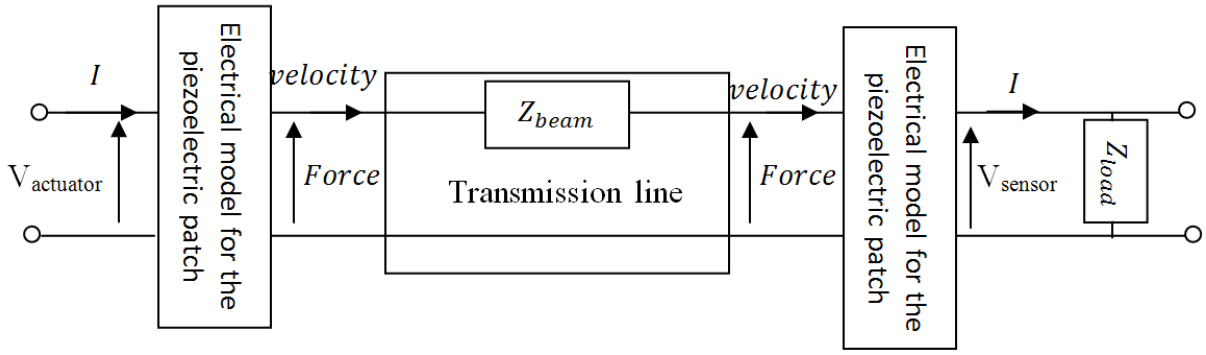

Figure 7.17: An electrical equivalent circuit for the system 1

The piezoelectric equivalent model shown in Figure 7.17 can be simplified to the static capacitor of the piezoelectric patch or it can be considered as Lumped or Mason model [(Hernandez, 2010)].

In order to obtain a traveling wave on the beam, Z_{load} should be designed to absorb the traveling wave generated by the PZT actuator. This can be ensured by making the equivalent impedance of the electrical model of the piezoelectric patch and the load impedance equal to the beam impedance. This is known in the theory of transmission lines by the impedance matching. So, this technique is helpful for determining Z_{load}. This method can be used also to determine analytically the transverse displacement on the beam. The equivalent electrical circuit case of a plate is more complicated.

The modal expansion method is used also in the literature to compute analytically the transverse displacement on the beam. This method is applied to linear traveling wave ultrasonic motors using two Langevin transducers [(Jeong, et al., 2007), (Loh, et al., 2000), (Hernandez, et al., 2010)]. We should note that all these papers report analytically the case of

two modes excitation, the case of one mode excitation when a passive electrical circuit is attached to one transducer is not reported analytically yet using the modal expansion method. When using this method, they assumed that the transducer actuator acts on the beam as a sinusoidal longitudinal force, which is not true in our systems because piezoelectric actuator patch acts on the beam as bending moments at the two ends of the patch [(Jalili, 2009), (Reza Moheimani, et al., 2006)].

Hariri et al. in their paper [(Hariri, et al., 2011)] developed an analytical model for a unimorph piezoelectric actuator given in Figure 7.18. This model can be extended to represent analytically the system 1 and 2 given above in Figure 7.14 & Figure 7.15.

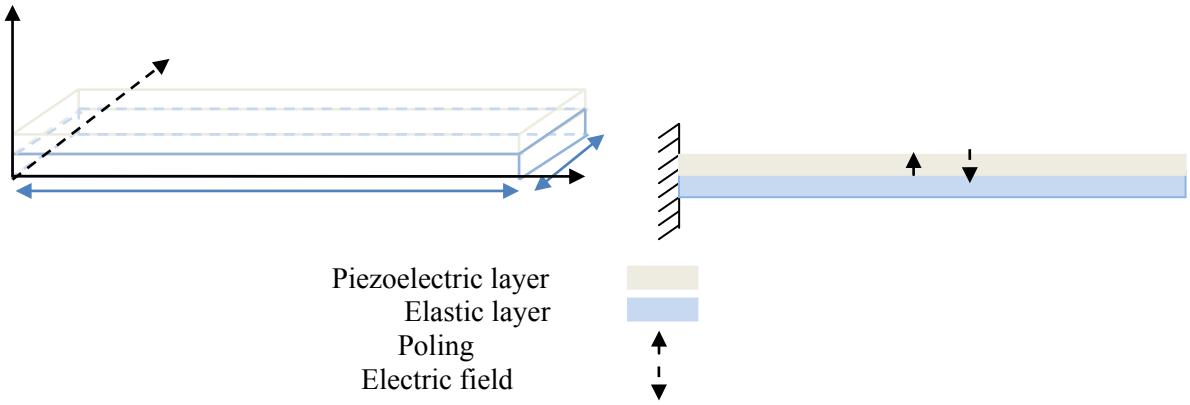

Figure 7.18: Unimorph piezoelectric actuator

The equation of motion found for this unimorph piezoelectric actuator was the following:

$$(EI)_{eq}\frac{\partial^4 w(x,t)}{\partial x^4} + (\rho A)_{eq}\frac{\partial^2 w(x,t)}{\partial t^2} = \mathrm{F_{eq}} \qquad 7.15$$

This equation is equivalent to the dynamic beam equation with $(EI)_{eq}$ is the equivalent flexural rigidity, $(\rho A)_{eq}$ is the equivalent mass per unit length and $\mathrm{F_{eq}}$ the equivalent applied force all along the actuator.

Damping factor is added into the equation of motion, and with free-free boundary conditions, the transverse displacement of the actuator is given by

$$\mathrm{w(x,t)} = \sum_{n=1}^{inf} \frac{-\mathrm{qe_p}E_3[\partial_x \emptyset_n(l) - \partial_x \emptyset_n(0)]}{(2\pi f_n)^2\sqrt{(1-\eta_n{}^2)^2+(2\zeta_n\eta_n)^2}}\ \emptyset_n(\mathrm{x})\ \sin(\Omega t - \psi_n) \qquad 7.16$$

More details can be found in [(Hariri, et al., 2011)].

The same unimorph system is taken in [(Chung, et al., 2009)] and it is extended for a piezoelectric fan for flapping wing application (Figure 7.19).

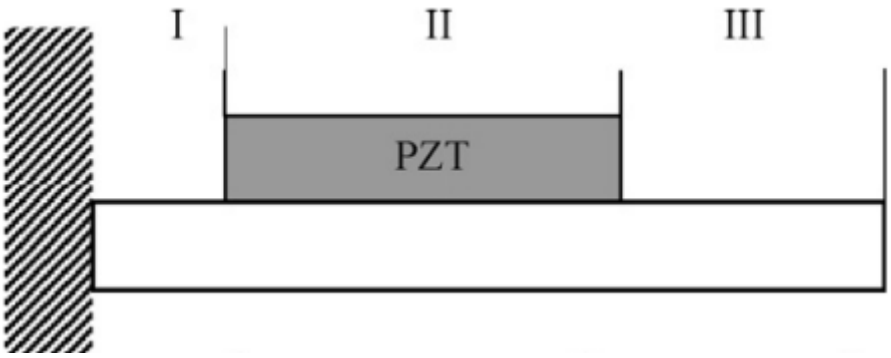

Figure 7.19: The scheme of a piezoelectric fan consisting of three sections. The piezoelectric material exists in the section II only [(Chung, et al., 2009)]

This system is solved by dividing it into sections; each section is solved individually and connected to the next section via boundaries conditions. At these points (where there are changes of sections), we must have the same transverse displacement, the same slope, the same bending moment and the same shear force. After solving each section and applying boundaries conditions, 12 constant unknowns and 12 equations are obtained. Details can be found in [(Chung, et al., 2009)].

Their study was limited to the computation of the resonance frequencies and not extended to dynamic equation. In fact, solving these equations is very heavy and not convenient; it takes a lot of calculation time.

As a result, extension this work to our case of study (two piezoelectric patches are used, then 20 equations should be solved) was not done. Finite element model shows the best way for our systems.

Actually instead of separating the solution into unimorph sections and beam section, Reza Moheimani et al. in their book [(Reza Moheimani, et al., 2006)] proposed to take the entire system and then to use unit step functions to take into account the spatial placement of piezoelectric patches. Reza Moheimani et al. are studied analytically the dynamic equation of a beam with a number of collocated piezoelectric actuator/sensor pairs. This work can be extended analytically to the case of non-collocated piezoelectric patches. Transfer functions obtained in their analytical model are similar to that presented in section 7.4 in this chapter using our finite element model with the difference that our model is for asymmetric structures when only piezoelectric patches are bonded in non-collocated way.

The advantage of our finite element model is that the transfer functions obtained in section 7.4 using our finite element model takes the same form in the case of thin plate structure as well as in the case of thin beam structure. The analytical work presented in the book of Moheimani

et al. [(Reza Moheimani, et al., 2006)] using unit step functions to take into account the spatial placement of piezoelectric patches in the case of a beam is extended by Li et al. in their paper [(Li, et al., 2005)] and Punhani in his PhD thesis [(Amitesh Punhani, 2008)] to the case of thin plate with two collocated piezoelectric actuator patches. Actually, their studies were limited in the case of two collocated piezoelectric actuator patches, no sensor patches are considered in their analytical models. Also, it is difficult to generalize the work for n collocated piezoelectric actuator/sensor pairs in the case of thin plate as did Moheimani et al. [(Reza Moheimani, et al., 2006)] in their book in the case of thin beam.

In our finite element model, n non-collocated piezoelectric actuator/sensor patches bonded on a thin bean and a thin plate are considered.

Using analytical equations for rectangular unimorph beam, Yang et al. in their paper [(Yang, et al., 2009)] presented an analogy between the mechanical and electrical domains of this piezoelectric coupling system and they presented this rectangular unimorph beam coupled with a load as two-port network as shown Figure 7.20.

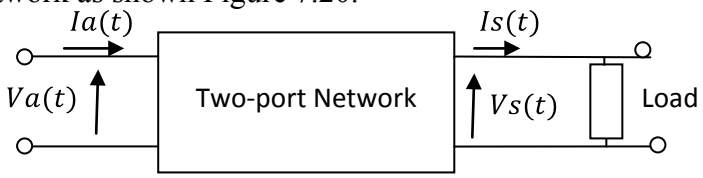

Figure 7.20 : Two-port network for rectangular unimorph beam

The same analogy is obtained basing in our finite element model by comparing equations 7.7 & 7.8 repeated again below. This analogy is shown in Table 7.6.

$$\ddot{q} + \Lambda\dot{q} + \Omega^2 q = \Phi^{\mathrm{T}}[F_m - K_{mvpa}E_{3pa}]$$

$$K_{vmps}\,\Phi\mathrm{q} + K_{vvps}E_{3ps} = 0$$

Equivalent circuit parameter for the ith mode	**Mechanical counterparts**
Electrical charge: $Q_i(t)$	Modal coordinate: $\frac{1}{t_p} q_i(t)$
Current: $i_i(t)$	Modal velocity: $\frac{1}{t_p}\dot{q}_i(t)$
Resistance: R_i	$t_p^2\ 2\xi_i w_i$
Capacitance: C_i	$1/(t_p^2\ w_i^2)$
Inductance: L_i	t_p^2
Voltage source: $V_i(t)$	$t_p\Phi_{\mathrm{i}}^{\mathrm{T}}[F_m(t) - K_{mvpa}E_{3pa}(t)]$
Ideal transformer ratio : N_i	Mechanoelectrical coupling: K_{vmps}

Table 7.6: Analogy between electrical and mechanical domains

Then an electrical representation of our system is obtained as shown Figure 7.21.

The (N+M)-port network represents electrical impedances network.

Figure 7.21: (N+M) port-network for thin plates with non-collocated piezoelectric patches actuators/senssors

Where $V_a(t) = [V_{a1}(t), \ldots, Va_N(t)]$, $I_a(t) = [I_{a1}(t), \ldots, Ia_N(t)]$, $V_s(t) = [V_{s1}(t), \ldots, Vs_M(t)]$ and $I_s(t) = [I_{s1}(t), \ldots, Is_M(t)]$.

The question now is: could we represent our system by (N+M+L+K)-port network mechanical and electrical impedances using our finite element model as shown in Figure 7.22?

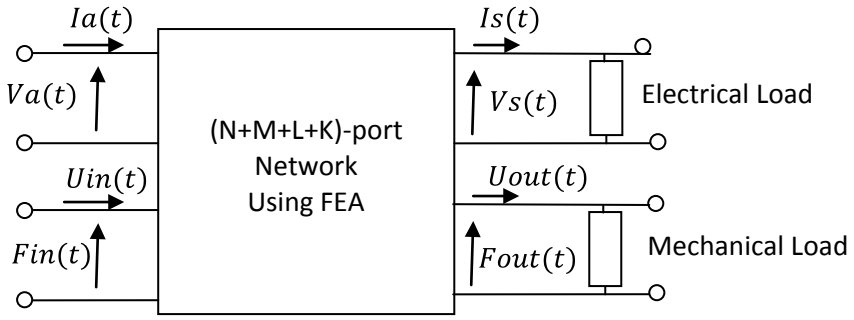

Figure 7.22: (N+M+L+K)-port network mechanical and electrical impedances

Where F is a mechanical effort vector and U is a mechanical flow vector.

$F_{in}(t) = [F_{in1}(t), \ldots, F_{inL}(t)]$, $U_{in}(t) = [U_{in1}(t), \ldots, U_{inL}(t)]$, $F_{out}(t) = [F_{out1}(t), \ldots, F_{outK}(t)]$ and $U_{out}(t) = [U_{out1}(t), \ldots, U_{outK}(t)]$.

This question still without answer in this manuscript is forwarded for perspective and future work. Two particular cases for 5-port network are taken in [(Li, et al., 2005), (Cho, et al., 2000)] using analytical models.

The system studied by Cho et al. is given in the Figure 7.23 and Figure 7.24. This system can be represented by 5-port network.

The system studied by Li et al. is given in Figure 7.25.

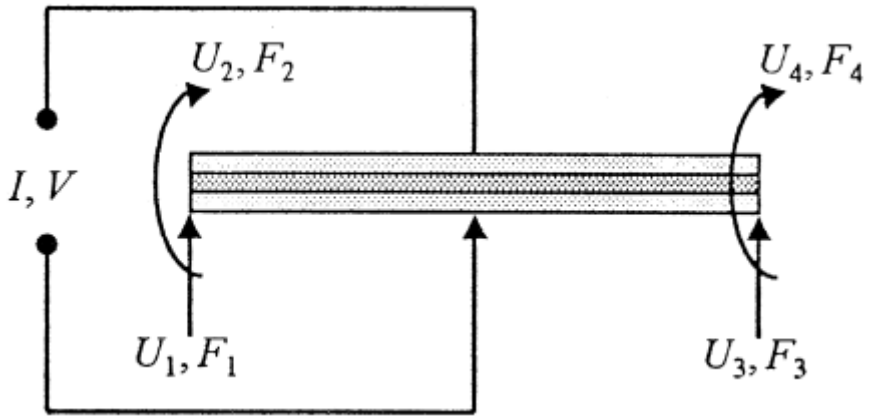

Figure 7.23: Flows and efforts of the piezoelectric bimorph beam [(Cho, et al., 2000)]

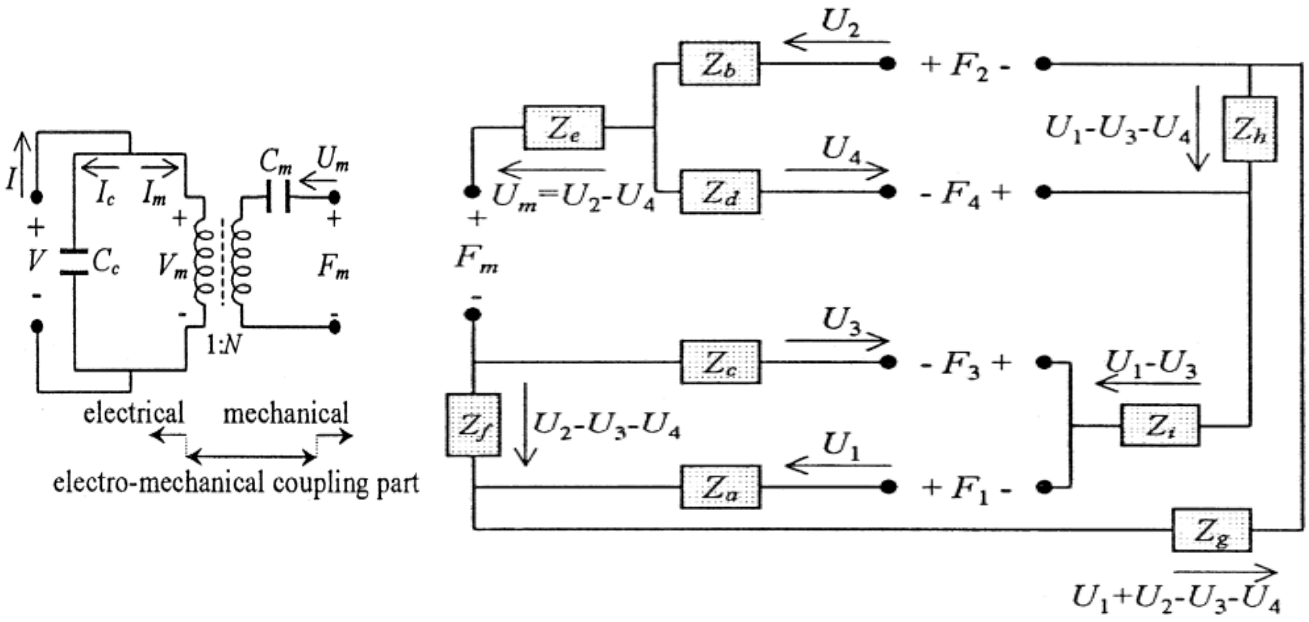

Figure 7.24: Equivalent electric circuit of the piezoelectric bimorph [(Cho, et al., 2000)]

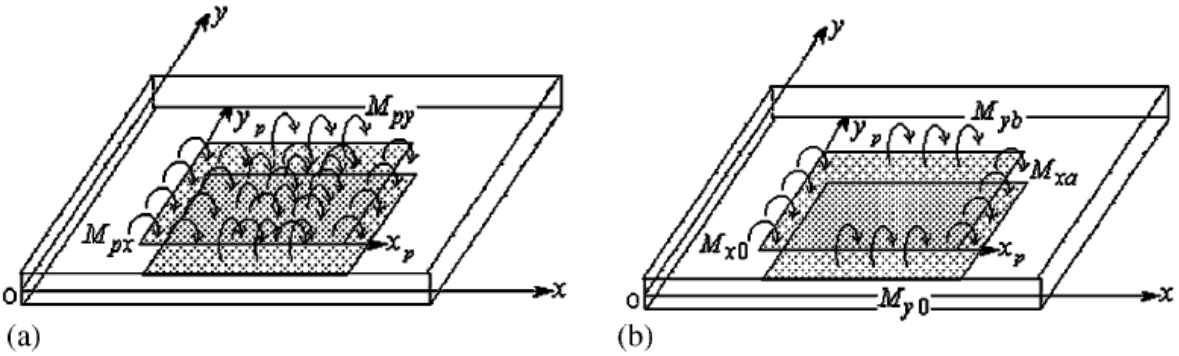

Figure 7.25: Models for the bending activation of dual 2D piezoelectric actuators: (a) dual piezoelectric 2D actuators producing line bending moments; (b) dual piezoelectric 2D actuators producing area bending moments [(Li, et al., 2005)]

Their electrical equivalent network can be represented by the block diagram shown in Figure 7.26 where 5-port network composed of one electrical impedance and mechanical impedances.

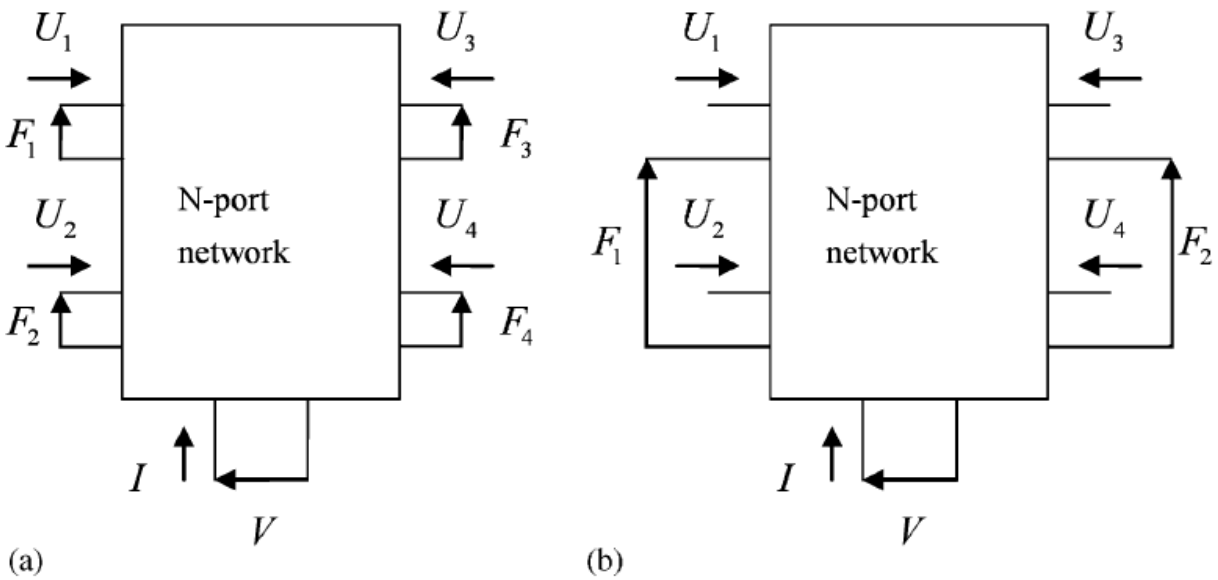

Figure 7.26: Electric network for 2D force actuator; (b) five-port equivalent electric network for 2D bending actuators[(Li, et al., 2005)]

Hence to resume, finite element simulation offers more generality in modeling especially in the case of complex structures, i.e. many patches on a thin plate instead of two patches for example, also a thin plate with non-collocated patches is more complicated to model analytically compared with thin plate with collocated ones. Also this finite element model can be used and implemented in many applications as integrating loads to piezoelectric sensors, generating control algorithm, in optimization topology, detecting damage in structures,…. Without forgetting, the finite element model is necessary in the case of complex thin structure such as presented in the figure.

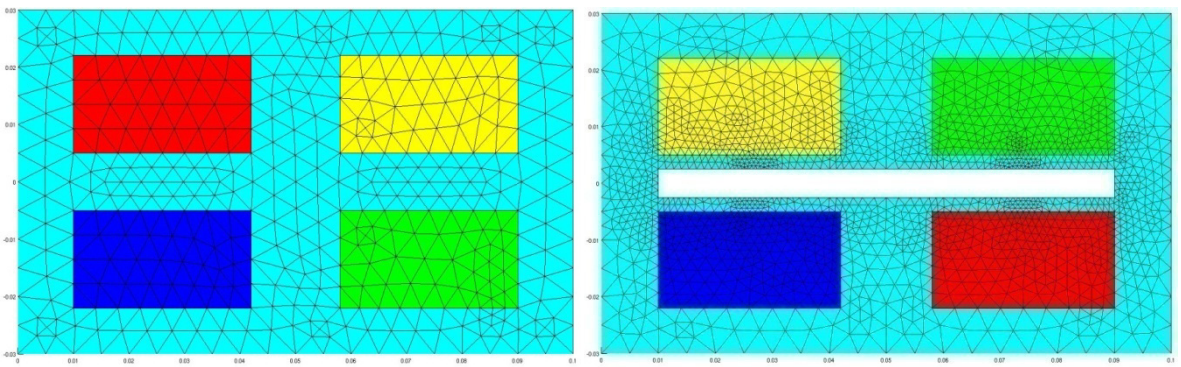

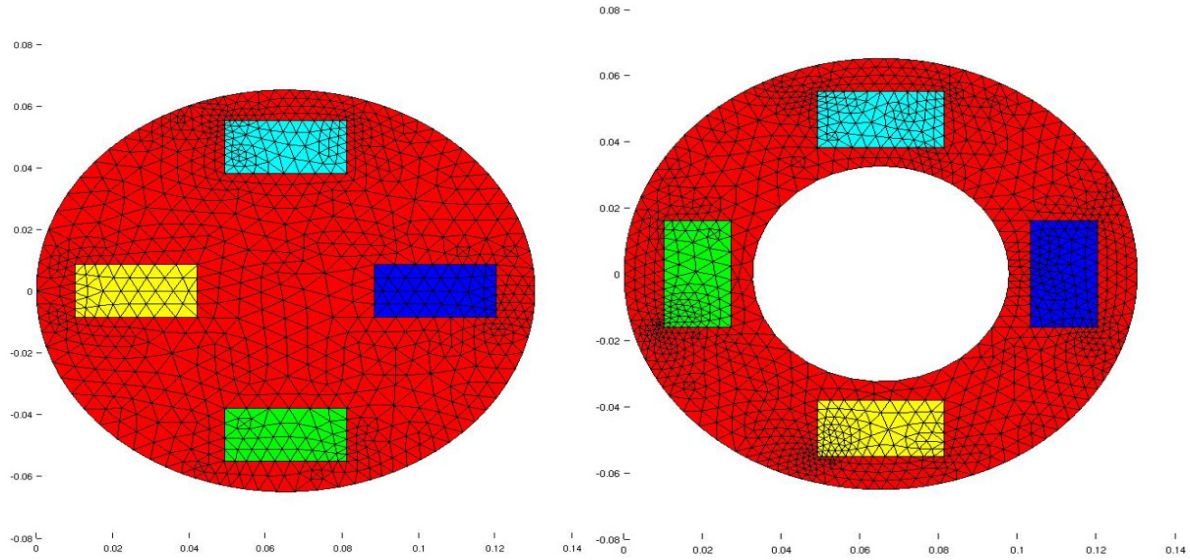

Figure 7.27: Non-collocated piezoelectric patches bonded on structures

7. 8 References

Alazard D. et Chrétien J.P. Commandes active des structures flexibles: applications spatiales et aéronotique s [Livre]. - Toulouse : Supaero , 2000.

Amitesh Punhani M.S. Shape and vibration control of laminated plates [Livre]. - Ohio, USA : Ohio state university, 2008.

Chaudhry Z., Sun F.P. et Rogers C.A. Health monitoring of space structures using impedance measurements [Revue]. - [s.l.] : Proceedings of the 5th International Conference on Adaptive Structures, 1994.

Cho Y.S. [et al.] Five-port electric circuit of piezoelectric bimorph beam [Revue]. - South Korea : Sensors and actuators, 2000. - 84.

Chung Hsien Chun [et al.] Developement of piezoelectric fans for flapping wing application [Revue]. - [s.l.] : Journal of sensors and actuators, 2009.

DE BOE Pascal Les éléments piézo-laminés appliqués à la dynamique des structures [Livre]. - Liège : Université de Liège, 2003.

Durou H. [et al.] 'power harvesting and management from vibrations: a multi-source strategy simulation for aircraft structure health monitoring [Revue]. - Toulouse : SPIE, 2008.

Flueckiger M., Fernandez J.M. et Perriard Y. Finite element method based design and optimization methodology for piezoelectric ultrasonic motors [Revue]. - Lausanne, Switzerland : Mathematics and computers in simulation , 2010. - 81.

Hadjigeorgiou E.P., Stavroulakis G.E. et Massalas C.V. Shape control and damage identification of beams using piezoelectric actuation and genetic optimization [Revue]. - Greece : International journal of engineering science , 2006. - 44.

Halim D. et Moheimani S.O.R. An optimization approach to optimal placement of collocated piezoelectric actuators and sensors on a thin plate [Revue]. - Australia : Mechatronics, 2001. - 13.

Hariri H., Bernard Y. et Razek A. A New Efficient Modeling Concept of Non-Collocated Piezoelectric Patches Bonded on thin Structure [Revue]. - [s.l.] : Submitted in Journal of mathematics and computers in simulations, 2012.

Hariri H., Bernard Y. et Razek A. Analytical and finite element model for unimorph piezoelectric actuator: Actuator design [Revue] // Proceedings of Piezo2011. - 2011. - pp. pp. 71-75.
Hariri H., Bernard Y. et Razek A. Finite element model of a beam structure with piezoelectric, patches using RL shunt circuits [Revue] // AC2011, 14th International Conference on active systems for dynamics markets. - 2011. - pp. pp.124-13.
Hernandez C. réalisation d'une micropompe à actionnement piézoélectrique [Rapport]. - Gif sur Yvette : Laboratoire de Génie Electrique de Paris, 2010.
Hernandez C., Bernard Y. et Razek A. Theoretical and experimental analysis of a two modes excitation linear motor using piezoelectric actuators [Revue]. - Bremen, Germany : Actuator10, 2010.
Irschik H. A review on static and dynamic shape control of structures by piezoelectric actuation [Revue]. - Austria : Engineering structures, 2002. - 24.
Jalili N. Piezoelectric-Based Vibration Control, From Macro to Micro-Nano Scale Systems [Livre]. - [s.l.] : Springer, 2009.
Jeong S.H. [et al.] A study on an object transport system using ultrasonic wave excitation [Revue] // Journal of mechanical science and technology. - 2007. - pp. pp. 941-945.
Kermani M.R., Moallem M. et Patel R.V. Parameter selection and control design for vibration suppression using piezoelectric transducers [Revue]. - [s.l.] : Control engineering practice , 2003.
Lemistre M. et Balageas D. Structural health monitoring based on diffracted Lamb waves analysis by discrete wavelet transform [Revue]. - Universitad Politecnica de Madrid, spain : Proceedings of the Conference on System Identification and Structural Health Monitoring, 2000.
Li G.Q., Yao C.C. et Tai H.Y. Equivalent electric circuits of thin plates with two-dimensional piezoelectric actuators [Revue]. - [s.l.] : Journal of sound and vibration, 2005. - 286.
Li J., Jang S. et Tang J. Modeling and analysis of a bimorph piezoelectric energy harverster for railway bridge health monitoring [Revue]. - [s.l.] : SPIE, 2012. - Vol. 8348.
Liu G.R. [et al.] Vibration control simulation of laminated composite plates with integrated piezoelectrics [Revue] // Journal of sound and vibration. - [s.l.] : Journal of sound and vibration, 1999. - pp. Vol 220, Issue 5,827-846..
Loh B.G et Ro P.I An object transport systemusing flexural ultrasonic progressive waves generated by two mode excitation [Revue] // IEEE transaction on ultrasonics, ferroelectrics and frequency control. - 2000. - pp. pp. 994-998.
Moita J.M.S. [et al.] Design of laminated structures using piezoelectric materials [Revue]. - Brazil : Porcceding of the 26th Iberian latin american congress on computational methods in engineering, 2006.
Nakasone P.H., Kiyono C.Y. et Silva E.C.N. Design of piezoelectric sensors, actuators, and energy harvesting devices using topology optimization [Revue]. - Brazil : SPIE, 2008. - Vol. 6932.
Qu G.M. [et al.] analysis of a piezoelectric composite plate with cracks [Revue] // Journal of composite structures. - 2006. - pp. vol. 72, no1,111-118..
Reza Moheimani S.O. et Fleming Andrew J. Piezoelectric transducers for vibration control and damping [Livre]. - University of Newcastle, University Drive, Callaghan, NSW 2308,Australia : Springer, 2006.
Sashida Toshllku et Kenjo Takashi An introduction to ultrasonic motors [Livre]. - Japan : Oxford scien publication, 1993.
Sohn J.W., Choi S.B. et Kim H.S. Vibration control of smart hull structure with optimally placed piezoelectric actuators [Revue]. - South korea : International jounral of mechanical sciences, 2011. - 53.
Yan Y.J. et Yam L.H. Online detection of crack damage in composite plates using embedded piezoelectric actuators/sensors and wavelet analysis [Revue] // Journal of Composite Structures. - 2002. - pp. Vol 58, Issue 1,29-38..
Yang Y. et Tang L. Equivalent circuit modeling of piezoelectric energy harvesters [Revue]. - Singapore : Journal of intelligent material systems and structures, 2009. - Vol. 20.

Yasin M. Y., Ahmad N. et Alam M.N. Finite element analysis of actively controlled smart plate with patched actuators and sensors [Revue] // Latin American Journal of Solids and Structures. - 2010. - pp. Vol 7, No 3,227-247.

CONCLUSION AND PERSPECTIVES

Conclusion and perspectives

At the beginning, in the forward of this thesis we told that the objective of this work was to answer the following two questions:

Is it possible using piezoelectric materials to move a mimetic Manta ray (Manta ray shape is considered as a thin plate) with multi degree of freedom on the earth by generating a traveling wave motion on a thin plate?

Is this robot can be extended based on the same prototype as in earth to create displacement on liquid (undulatory propulsion) and air environments like Manta ray fishes?

We are at the conclusion and no answers given for instant. All what we said is that: no information about the traveling wave piezoelectric plate robot because the concept has been filled for a patent. In other words that means, a traveling wave generated on a thin plate using distributed piezoelectric patches can move the plate in multi degree of freedom. For the second question, we should wait for the perspective in the next part of this chapter.

In the conclusion we will talk first about the beam traveling wave piezoelectric robot, then about the originality of this work and the last part of my conclusion is to present my work during these three years as a brief history. Then the perspectives of my work are proposed at the end.

1. Conclusion

In this manuscript, we presented the design procedure of a traveling wave beam piezoelectric robot and its realization. Being given dimensions of the beam (180 mm × 17 mm × 0.5 mm), we opted the following piezoelectric patches dimensions (32 mm × 17 mm × 0.27 mm) at these optimal positions (X_{p1}=24 mm, Xp2=124 mm). Two operating principles are studied and tested for this robot. The first one is called ‘’one mode excitation: 1ME’’, for this operation principle robot shows a velocity of 81.19 mm/s at 30V sinusoidal wave amplitude at 11.6 kHz without embedded mass and a nominal operating point of (9 mN, 40 mm/s) that corresponds to 360 μW power provided. The second one is called ’two modes excitation: 2ME’’, for this operation principle robot shows a velocity of 131.5 mm/s at 30V sinusoidal wave amplitude at 11.3 kHz without embedded mass and a nominal operating point of (7.2 mN, 60 mm/s) corresponds to 432 μW power provided. The two modes excitation shows higher velocity compared to the one mode, however the one mode is better in terms of homogeneity, which is because in the one mode excitation we excite at the resonance

frequency while we excite between two resonance frequencies in the two modes excitation. Let us talk now about the originality of this work.

What is it the originality of this work? Is that to demonstrate the generating of a traveling wave using the 1ME or the 2ME principle? Actually, the theory for the 1ME was demonstrated in 1993 by Sashida et al. [(Sashida, et al., 1993)] even before in 1985 by Kuribayashi et al [(Kuribayashi, et al., 1985)] and for the two modes excitation, Loh et al. [(Loh, et al., 2000)], they were introduced it in 2000. Also the generation of a traveling wave on a beam using these two operation principles is validated experimentally by Hernandez [(Hernandez, 2010)] in his PhD thesis at our laboratory. He used these two principles to generate the traveling wave on the beam for micro pumping application and his work has been patented. The concept of our system is different. In our case the generated traveling wave should move the entire system (robot application) and not just a slider lied on it. The originality was in the concept design proposed for this system. Our robot as we know is the first one in the literature that moves using two piezoelectric patches bonded on the same face of a beam structure. So the originality was in this original concept design. Behind this easy manufacture, a complicated optimal design hides. The aim of my work was to find this optimal design in order to create a traveling wave able to move the entire system (2 patches bonded on the beam), then to validate and prove it experimentally. What is more in the case of plate, it is that not only the concept design is new but also the operation principle ideas are new too. We still talking about the originality in this work, 2D finite element modeling for thin structures with collocated piezoelectric patches (symmetric structures) was done in the literature but, for asymmetric structures (thin structures with non-collocated piezoelectric patches actuator/sensor), we are the first that proposed a 2D finite element modeling for such structures thanks to the determination of the neutral plane for this asymmetric structure. Solving this kind of structure in 2D can saves time, especially if an optimal design is required. In the next paragraph I would like to introduce my work in these three years PhD as a brief history.

First I began by a bibliographic research on animal locomotion [(Biewener, 2003)] in the three medium displacements (earth, water & air) and on piezoelectric miniature robots existing in literature [(Hariri, et al., 2010), refers to chapter 1]. After seeing that there are no robots having the same structure as that we have proposed, we began working on our idea. The original idea was to artfully paste piezoelectric patches on a thin plate whose oscillations (induced by the piezoelectric actuation) recreate movement for the terrestrial environment. The proposed system forced me to do another bibliography search on all similar structures

(intelligent systems using piezoelectric material) as unimorph beams, bimorph beams, piezoelectric integrated beams, beams with piezoelectric patches (collocated or non-collocated), plates systems with piezoelectric patches, circular plates, etc. We found that there are many intelligent systems using piezoelectric materials in literature for applications such as damping vibrations, energy harvesting, detecting damage in structures [refers to chapter 7] and a few traveling wave ultrasonic motors [(Suybangdum, et al., 2009)]. Different ways are used to describe these systems, such as analytical models, equivalent circuit models (beam, plate) [refers to chapter 7] and finite element models [refers to chapter 3]. To have an optimal design for a given application, models were combined with optimization techniques (deterministic or stochastic technique) [refers to chapter 7]. We discussed in chapter 7 why the finite element model was our choice to describe our system. Also this decision was taken because a 1D finite element model for a beam with collocated piezoelectric patches for damping application was made by Romain CORCOLLE during his internship on MASTER 2 at the laboratory, so we did not begin from zero. Then the decision was taken to divide our work into two parts, traveling wave piezoelectric beam robot and traveling wave piezoelectric plate robot. Starting with modeling the two cases of study (beam and plate models), and comparing models with commercial finite element software (COMSOL 3.5a). After validation process, an optimal design was done using the modeling strategy developed in this thesis, then experimental prototypes were fabricated, and models were compared again with experimental results, as we have seen in chapter 4. I did not mention it before but, it is good to know that our developed finite element models have the advantage to have one dimension less than existing commercial finite element software; e.g. a beam with piezoelectric patches (collocated or non-collocated) is modeled in 2D using commercial finite element software but it can be modeled in 1D using our developed finite element model, idem in the case of plate with piezoelectric patches (collocated or non collocated) is modeled in 3D using commercial finite element software but it can be modeled in 2D using our developed finite element model. After an optimal design study in order to generate the traveling wave on the beam [refers to chapter 5], beam prototypes were tested and results are given in chapter 6. Plate prototype, simulations and experimental results were filled to a patent.

2. Perspectives

In the perspectives, we will propose a future state of the art for intelligent systems using piezoelectric materials; we will talk about how we can improve our finite element model to describe in a better way our robot, about how we can increase the degrees of freedom of our robot, also about how we can improve the efficiency of the robot by using other passive circuits, and a feedback control is proposed as perspectives to increase the autonomy of the robot. At the end a prototype is proposed for aquatic and terrestrial displacement. Then we will try to answer the question of miniaturization.

Actually, it is necessary to mention the fact that in the literature no historical research about intelligent systems using piezoelectric materials has been developed. Literature lacks in state of the art for smart structures incorporating piezoelectric materials and how they are classified in chronological order. It is a good idea to make a classification that studies the evolution of these systems integrating piezoelectric materials depending on the year.

As we have seen in chapter 6, robot characterization (speed as a function of voltage, speed as a function of embedded masses and speed as a function of mechanical load) is given only experimentally; as a matter of fact in our developed model there is no interaction between the robot and its environment (solid substrate in our case). The contact friction between the robot and the solid substrate can be modeled, and then the speed of the robot can be simulated and compared to the obtained experimental value. Here below are some papers studying systems with friction interaction using analytical or finite element models [(Meziane, et al., 2010), (Stavroulakis, et al., 1999), (Hurmuzlua, et al., 2004), (Khoei, et al., 2006), (Wriggers, 1969), (Pop, et al., 2011), (Juang, et al., 2009), (Duan, et al., 2007), (Denkowski, et al., 2011), (Mazeika, et al., 2012)]. Masses can also be integrated in our finite element model; an example is given in [(Rofooei, et al., 2009)]. Modeling the contact between the robot and its environment allows studying the affect of the environment to the resonance frequencies and displacements of the system.

A multi degrees of freedom (MDOF) system can be made from our presented traveling wave piezoelectric beam robot as shown in figure below. Cross combination can be made also. Other types of thin structures with or without holes can be used. A rotational and elliptical motion can be made for example by using cylindrical thin structures with piezoelectric patches.

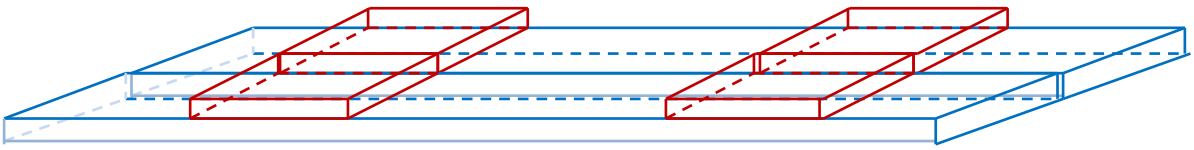

A two parallel traveling wave piezoelectric beam robots for MDOF application

The efficiency of the robot can be improved when we get better traveling wave ratio on the beam, it means when we have more wave absorption. RL shunt circuit was chosen due to the simplicity of its modeling and physical implementation, but other passive and semi active techniques show better absorption [(Badel, 2006)] and therefore allow to work at lower frequency.

An idea to increase autonomy of the robot i.e. to have low power consumption is to inject power provided by the PZT sensor patch to the PZT actuator patch by using a feedback control instead of using a passive shunt circuit. It was demonstrated by Eielsen et al [(Eielsen, et al., 2010)] that an RL series shunt circuit can act as an output feedback controller. This method is high cost, low stability and more complex compared to RL shunt circuit.

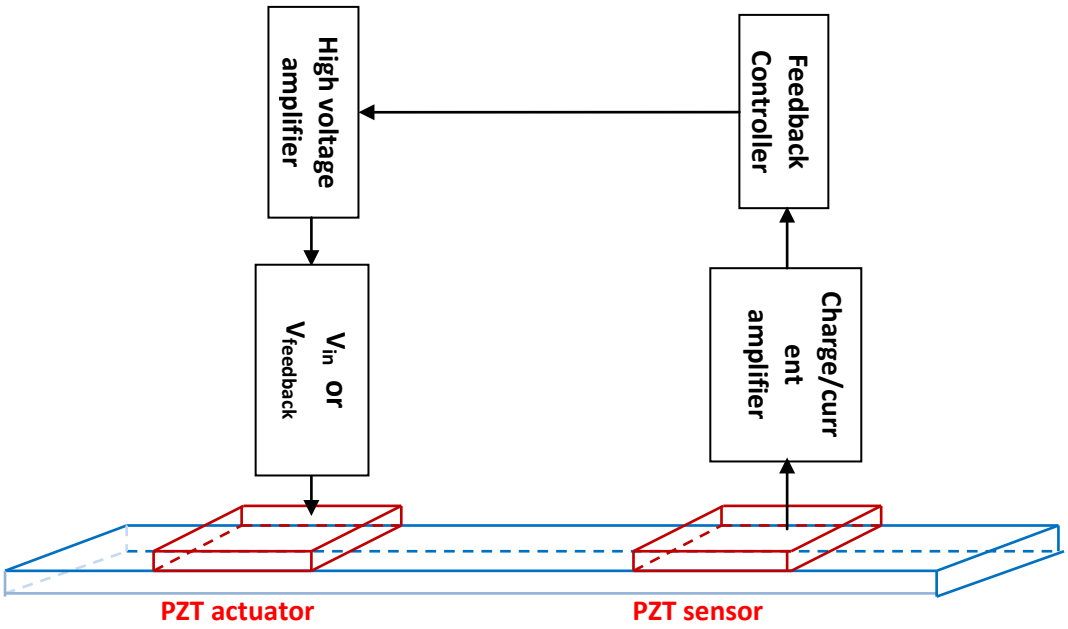

A schematic diagram using feedback controller to increase autonomy of the robot

The figure below is a combination between the beam piezoelectric robot studied in this thesis and the plate piezoelectric robot which was submitted for a patent. This design is proposed for aquatic and terrestrial locomotion.

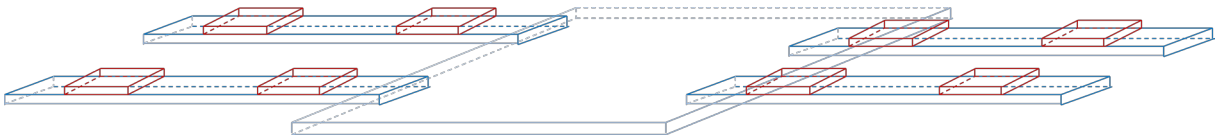

A schematic design for an aquatic and terrestrial robot

High displacement is needed in aquatic medium to move the robot; this displacement can be achieved using the first resonance frequency of these four fixed-free beams robots by applying it at the piezoelectric patches near from the fixed end. These for beams should act as legs to achieve the walking locomotion technique (phase difference applied at each patch near from the fixed end [refers to chapter 1]), and therefore a displacement in the aquatic medium. The plate structure is the robot body in the aquatic medium and it should be designed to carry the weight of the beams. Material for the plate has not to be the same as beams. Materials should be chosen according to frequency and displacement as in the case of terrestrial locomotion (graphs below [refers to chapter 5]) but, also the mass density should be chosen taking into account the mass density of water if the robot is designed for water use for example. Resonance frequencies of the system in water are affected by the water around, therefore the fluid dynamic equations must be added to our finite element model. That was not the case in terrestrial locomotion; the contact between robot and the solid support in terrestrial medium do not affect the resonance frequencies of the system.

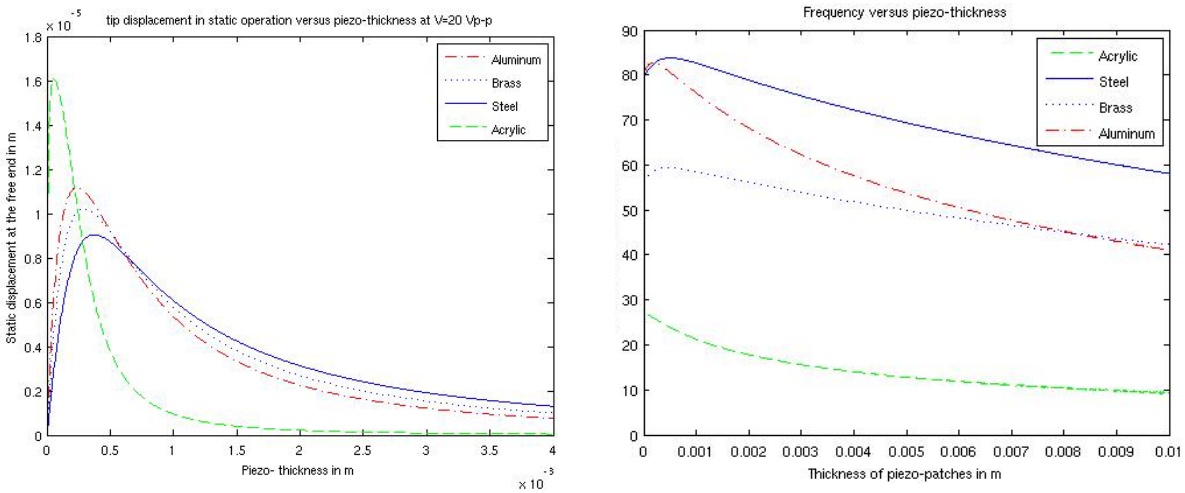

Figure 5.15 and 5.16 taken from chapter 5

Hence to conclude this paragraph, beam robots are responsible for motion in the aquatic medium and that is without using the second patches near from free ends. These patches come to help the robot body in terrestrial locomotion in the case where more speed is needed.

Optimal dimensions should be studied again in the case of aquatic medium and a compromise must be made if they are different from the terrestrial case. Also better material for terrestrial locomotion (aluminum [2700 kg/m^3]) among the three others presented in graphs above is not the best one for aquatic locomotion (referring to graphs below, acrylic [1400 kg/m^3] is better). We may note that these graphs do not take into account the effect of the water into displacements and frequencies; therefore these graphs did not reflect the optimal material and piezoelectric thickness in the water case. Other materials like glass, tungsten, diamond, titanium and magnesium can be also studied. Fiber material has usually lower mass density than the material itself and it is recommended to be used in aquatic and air mediums.

The same structure can be used to fly also. Other idea to amplify much more the displacement is to use the MFC, NASA piezocomposite actuator shown in figures below.

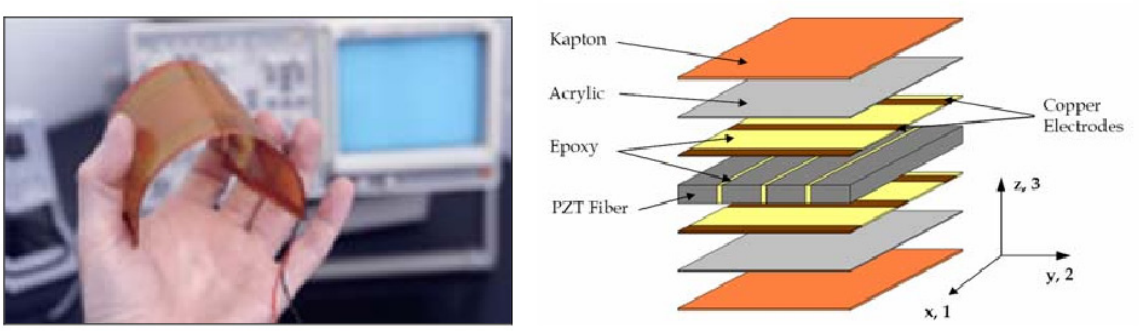

The Macro Fiber Composite (MFC) actuator. Left: A demonstration of the flexibility of the actuator. Right: Layers of the actuator. [(Bilgen, 2007)]

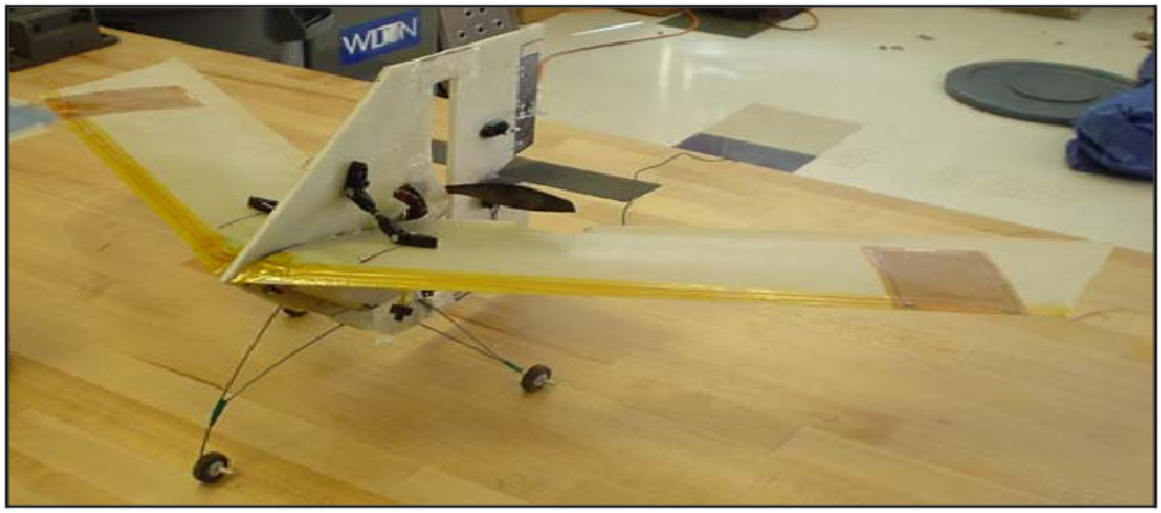

Fabricated micro air vehicle using MFC actuator [(Bilgen, 2007)]

Our designed and fabricated system is a prototype to validate the motion but this robot can be easily miniaturized and the developed equations remain applicable if we are over micrometer dimensions. Examples of miniaturized systems having same structures can be found in [(Jalili, 2009), (Senturia, 2002)].

References

Badel A. Récupération d'énergie et contrôle vibratoire par éléments piezoélectriques suivant une approche non linéaire [Livre]. - Savoie : Thèse de Doctorat de l'Université de Savoie, 2006.

BIEWENER A. Animal locomotion [Livre]. - [s.l.] : Oxford university press, 2003.

Bilgen O. Macro Fiber Composite Actuated Unmanned Air Vehicles: Design, Development, and Testing [Livre]. - [s.l.] : Virginia Polytechnic Institute and State University, 2007.

Denkowski Z., Migórski S. et Ochal A. A class of optimal control problems for piezoelectric frictional contact models [Revue]. - [s.l.] : Nonlinear Analysis: Real World Applications, 2011. - 12.

Duan W.H., Quek S.T. et Lim S.P. Finite element solution for intermittent-contact problem with piezoelectric actuation in ring type USM [Revue]. - [s.l.] : Finite Elements in Analysis and Design, 2007. - 43.

Eielsen A.A. et Fleming A.J. Pasive shunt damping of a piezoelectric stack nanopositioner [Revue]. - USA : American control conference, 2010.

Hariri H., Bernard Y. et Razek A. Locomotion principles for piezoelectric miniature robots [Revue] // Proceedings on actuator 10. - 2010. - pp. pp. 1015-1020..

Hernandez Camilio Realization of piezoelectric micropums, thesis at LGEP, Paris, France [Livre]. - Paris : University Paris-sud, 2010.

Hurmuzlua Y., Génotb F. et Brogliato B. Modeling, stability and control of biped robots a general framework [Revue]. - [s.l.] : Automatica, 2004. - 40.

Jalili N. Piezoelectric-Based Vibration Control, From Macro to Micro-Nano Scale Systems [Livre]. - [s.l.] : Springer, 2009.

Juang , P.A et Tsai C.C. Characterization of one-wheeled actuator driven by one piezoelectric element [Revue]. - [s.l.] : Measurement , 2009. - 42.

Khoei A.R. et Nikbakht M. Contact friction modeling with the extended finite element method (X-FEM) [Revue]. - Iran : Journal of materials processing technology, 2006.

Li Y. et Liu Z. Dynamic contact problem for viscoelastic piezoelectric materials with normal damped response and friction [Revue]. - China : Journal of Mathematical Analysis and Applications, 2011. - 373.

Loh B.G. et Ro P.I. An object transport system using flexural ultrasonic progressive waves generated by two modes excitation [Revue] // IEEE transaction on ultrasonic, ferroelectrics, and frequency control. - 2000. - pp. 994-999.

Mazeika D. et Vasiljev P. Linear inertial piezoelectric motor with bimorph disc [Revue]. - [s.l.] : Mechanical Systems and Signal Processing, 2012.

Meziane A., Baillet L. et Laulagnet B. Experimental and numerical investigation of friction-induced vibration of a beam-on-beam in contact with friction [Revue]. - France : Applied acoustics, 2010. - 71.

Pop N., Cioban H. et Horvat-Marc A. Finite element method used in contact problems with dry friction [Revue]. - [s.l.] : Computaional materials science, 2011. - 50.

Rofooei F.R. et Nikkhoo A. Application of active piezoelectric patches in controlling the dynaic response of a thin rectangular plate under a moving mass [Revue]. - Iran : International jounral of solids and structures, 2009. - 46.

Sashida T. et Kenjo T. An introduction to ultrasonic motors [Livre]. - Oxford : Clarendon Press, 1993.

Senturia Stephen Microsystem Design [Livre]. - [s.l.] : Kluwer academic publishers , 2002.

Stavroulakis G.E., Antes H. et Panagiotopoulos P.D. Transient elastodynamics around cracks including contact and friction [Revue]. - [s.l.] : Computer methodes in applied mechanics and engineering , 1999. - 177.
Suybangdum P., Smithmaitrie P. et Laoratanakul P. Dual piezoelectric actuators for the traveling wave ultrasonic linear motor [Revue] // Fourth International Conference on Experimental Mechanics. - 18-20 November 2009.
Wriggers P. Finite element methods for contact problems with friction [Revue]. - [s.l.] : Tribology international , 1969. - 8 : Vol. 29.